THE UNIVERSITY of ADELAIDE

MESO-CENOZOIC INTRAPLATE MAGMATISM ALONG THE AUSTRALIAN SOUTHERN MARGIN

by

Fun Julie Ellen Meeuws

Earth Sciences

School of Physical Sciences

University of Adelaide

This thesis is submitted in fulfilment of the requirements for the degree of Doctor of Philosophy

JULY, 2019

Abstract

The eastern and south-eastern Australian passive continental margins host a series of Cenozoic basins preserved in onshore and offshore Victoria, Tasmania and South Australia. Deposition in these basins was concurrent with the Cenozoic Magmatic Province that extends along the Australian eastern and south-eastern Australian passive continental margin. Although classified as a 'non-volcanic' passive margin, a large record of igneous rocks is preserved within the Cretaceous to Miocene syn- and post-rift successions of the offshore basins. Previous studies have mainly focussed on onshore magmatic activity and resulting geodynamic models have proposed on mantle plumes or edge-driven convection. Offshore 2D and 3D seismic reflection datasets in the Bass and Gippsland Basins analysed in this thesis have shown that the magmatism in these areas occurred during the Late Cretaceous, Eocene to Oligocene and Miocene to Recent times. The majority of magmatism significantly post-dates continental break-up and basin rifting related to the separation of Australia and Antarctica, which started around 85 Ma.

This thesis presents major and trace element and isotope geochemistry of Cenozoic igneous rocks in onshore Tasmania and in the offshore Gippsland and Bass Basins. The data presented suggest that magmas have formed over a thermal upwelling with a long time-integrated high $^{238}U/^{204}Pb$ or μ (HIMU) signature that traversed a Pacific Mid-Ocean Ridge Basalt (MORB) -like asthenosphere and interacted with the mantle lithosphere. Tasmanian lavas formed at different depths with shallow silica-oversaturated melts undergoing larger degrees of melting than deeper silica-undersaturated melts (> 20 kbar). These shallow melts have then mixed with a remnant source of Ferrar Jurassic magma, related to Gondwana break-up, residing in the lithosphere. Magmas formed in the Gippsland and Bass Basins formed under similar conditions as the shallow silica-oversaturated melts with varying Oceanic Island Basalt (OIB) to Upper Continental Crust (UCC) trace element signatures.

Regional 3D seismic mapping of the Gippsland Basin reveals a laterally (>40 km) and vertically extensive magmatic plumbing system comprising more than 186 intrusions. This network of sills shallows from the central part of the basin towards the basin-bounding faults at the northern margin, where magmas were ultimately extruded onto the palaeo-surface

during the Late Cretaceous. A second style of magmatic activity occurred during the Middle Eocene, resulting in a volcanic cone complex in the centre of the basin, which has likely been fed through vertical to near-vertical dykes or via faults. Palynology of surrounding sediments intersected by petroleum wells indicates that magmatic activity in the Bass Basin is generally younger than that of the Gippsland Basin with activity being most abundant during the Miocene. Cretaceous to Eocene magmatic activity mainly occurred at major normal faults near the basin margins, while Miocene magmatism is focussed in the centre of the Cape Wickham Sub-basin of the Bass Basin. In contrast to the Gippsland Basin, the main direction of magma transport through the upper crust was more vertically through dykes and/or faults. This phase of Miocene magmatic activity is characterised by a southward younging trend similar to the southward younging trends of the hotspot trails observed on the Australian mainland. Although the Gippsland and Bass Basin are adjoining basins, the magmatic plumbing styles observed differ significantly. These results provide insights into the origin, cause and plumbing into intraplate magmatism occurring along the Australian south-eastern margin and magma transport through sedimentary basins, in general.

Table of contents

List of publications

Meeuws, F., Holford, S., Foden, J., 2015. Geophysical and geochemical constraints on Cretaceous-Cenozoic magmatism along the southern Australian margin. ASEG Extended Abstracts, 2015(1): 1-4.

Meeuws, F., Reynolds, P., Holford, S., Foden, J., Schofield, N., 2016. Characterising extrusive and intrusive magmatism at the Kipper Field, Gippsland Basin, using 3D seismic data. ASEG Extended Abstracts, 2016(1): 1-7.

Meeuws, F.J.E., Foden, J.D., Holford, S.P., Forster, M.A., 2019. Geochemical constraints on Cenozoic intraplate magmatism and their relation to Jurassic dolerites in Tasmania, using Sr-Nd-Pb isotopes. Chemical Geology, 506: 225-273.

Meeuws, F.J.E., Holford, S.P., Foden, J.D., Schofield, N., 2016. Distribution, chronology and causes of Cretaceous – Cenozoic magmatism along the magma-poor rifted southern Australian margin: Links between mantle melting and basin formation. Marine and Petroleum Geology, 73: 271-298.

Statement of originality

I, Fun Julie Ellen Meeuws, certify that this work contains no material which has been accepted for the award of any other degree or diploma in my name in any university or other tertiary institution and, to the best of my knowledge and belief, contains no material previously published or written by another person, except where due reference has been made in the text. In addition, I certify that no part of this work will, in the future, be used in a submission in my name for any other degree or diploma in any university or other tertiary institution without the prior approval of the University of Adelaide and where applicable, any partner institution responsible for the joint award of this degree.

The author acknowledges that copyright of published works contained within this thesis resides with the copyright holder(s) of those works.

I give permission for the digital version of my thesis to be made available on the web, via the University's digital research repository, the Library Search and also through web search engines, unless permission has been granted by the University to restrict access for a period of time.

I acknowledge the support I have received for my research through the provision of an Australian Government Research Training Program Scholarship.

Fun Julie Ellen Meeuws **Date**

Acknowledgements

Finally, I have travelled the long road of writing a thesis to completion. This would not have been possible without the help of many people and institutions.

Thank you to the **Australian Society of Exploration Geophysics** (ASEG) for their funding (ASEG Research Foundation project RF14P05) that enabled me to do all the necessary geochemical analyses and present my research at both national and international conferences. Thank you to the University of Adelaide to award me the **Eric Rudd Memorial Scholarship**. This allowed me to visit Nick Schofield in Aberdeen, Scotland. **Geoscience Australia** is thanked for providing the three dimensional seismic data used in this thesis. **IHS** are thanked for access to seismic interpretation software The Kingdom Suite. **Foster-Findlay Associates'** is thanked for the use of the GeoTeric software.

Firstly, I would like to thank my supervisors, **John Foden** and **Simon Holford**, for taking me on board and giving me the opportunity to do this PhD. **John Foden**, thank you for sharing your geochemical knowledge and removing my leeches after our quest for the Laughing Jack Marsh melilitites. **Simon Holford**, thank you for your many detailed feedback sessions and helping me get funding to go to Scotland. **Nick Schofield**, thank you for showing me your tips and tricks and increasing my confidence in seismic interpretation.

Thank you to my small little research group, **Chris Wawryk** and **Ben Cooke**. Sharing an office with you was a delight and your support has been invaluable. A big thank you to **David Bruce** for help in the clean- and TIMS-lab, and **Ian West** for the many IT-related issues I have encountered over the years. **Ian**, I have definitely missed you these last months!

Thank you to my fellow PhD students, some of you have become good friends. **Morgan Blades**, thank you for being my buddy and for loving Robin as much as you do. **Stephanie Wikantyiasning Wijaya**, **Nigel Rees**, **Kam Bhowany**, **Dan Lane**, **Tess Lane**, thank you for inviting us to your many delicious curry nights, and immersing us in your multicultural happenings. We definitely have not been hungry since! **Lachy Richards** and **Donnelly Archibald**, thank you for being lovely housemates when we first arrived to Australia. **Claire Wade**, it has been lovely to share our breastfeeding-friendly office and sharing the academic mum struggles. **Katie Howard**, thank you for your support in the lab and especially for your

great kindness when things were a bit rough. **Diana Plavsa**, thank you for being our friend since we arrived in Australia and sharing the academic mum journey with me.

Last but definitely not least, I would like to thank our little family. My partner, **Stijn Glorie**, thank you for being there for me, supporting me and taking leave so I could have some extra days to work on the PhD. My son, **Robin Glorie**, thank you for being your wonderful self and dragging me away from my computer to play with your trains and duplo blocks. PhD-life has definitely changed immensely after you arrived. Thank you for showing me that life continues during PhD and showing me that there are more important things in life than the PhD!

Chapter 1

Introduction and thesis outline

Introduction

The southern Australian passive margin hosts one of the classic examples of intraplate volcanic provinces, the Eastern Australian Magmatic Province, despite being classified as a non-volcanic margin (e.g. Sayers et al., 2001). This region extends over 4400 km from northern Queensland to southern Tasmania and extends westwards into Victoria and southeast South Australia along the passive southern margin of the Australian continent. To date, studies in this area have mainly focussed on onshore volcanism, and several models such as mantle plumes (Davies et al., 2015; Knesel et al., 2008; Sutherland et al., 2012), structural controls of pre-existing lithospheric structures (Cas et al., 2017; Lesti et al., 2008) and/or edge-driven convection (Demidjuk et al., 2007; Meeuws et al., 2016b) have been proposed to account for the origin of this intraplate magmatism. This thesis however, shows that a large part of the volcanism is located offshore and remains undescribed and unaccounted for in the proposed models for the area.

Forming part of the Eastern Australian Magmatic Province (Fig. 1), the Cenozoic magmatism along the eastern and south-eastern margin of Australia has been divided into three categories; the central volcanoes, the leucitite suite and the lava fields (Wellman and McDougall, 1974). As the Australian continent is moving northwards, both the central volcanoes and leucitite suite define several age-progressive tracks that become younger towards the south at a rate of 65 ± 3 mm/year from 32 Ma to the present (Duncan and Mcdougall, 1989; Wellman and McDougall, 1974), covering central Queensland to Victoria, located to the west and east of the Great Dividing Range and offshore eastern Australia (Davies et al., 2015; Sutherland et al., 2012; Wellman and McDougall, 1974). The current locations of the proposed plume-heads are estimated to be situated beneath the Bass Strait, between Victoria and Tasmania (Davies et al., 2015), to the east of Flinders Island (Sutherland et al., 2012) and to the south of the Tasmantid seamount chain . The third category and equally abundant type of magmatism (Wellman and McDougall, 1974), the lava fields, do not show a similar age trend and are therefore not readily explained by the aforementioned hot-spot mechanisms (Meeuws et al., 2016b; Vasconcelos et al., 2008). In particular, the Cenozoic magmatism in Tasmania, classified as lava field magmatism, lies south of the proposed plume-

heads (Fig. 1) and shows no clear age trend in activity, with the youngest activity present in the north of the island (8.5 ± 0.1 Ma: Baillie, 1986). Additionally, the Pb-isotopic composition of the Tasmanian Cenozoic igneous rocks seems to be quite distinct from any other lava field provinces situated in mainland Australia, with increased $^{206}Pb/^{204}Pb$ ratios (Nasir et al., 2010).

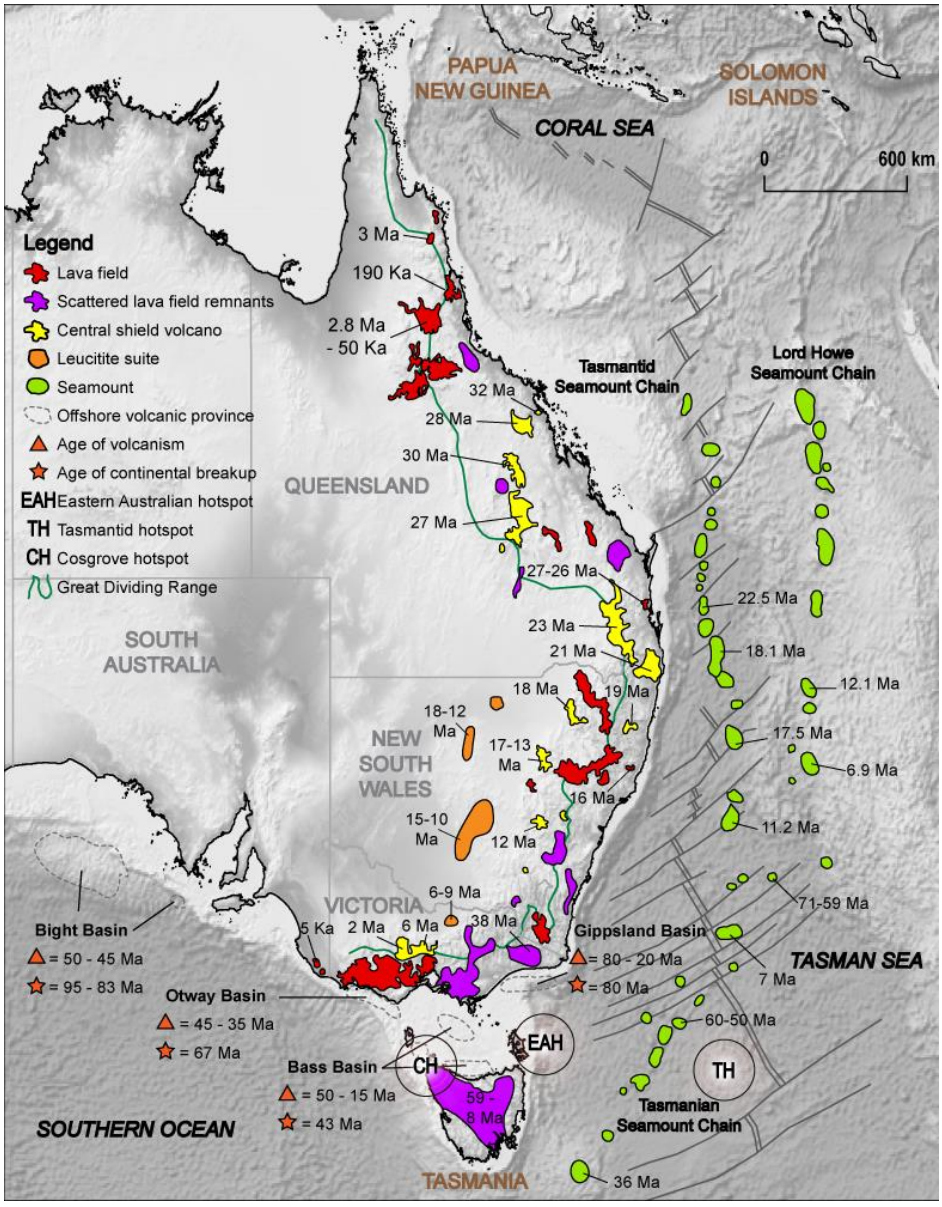

Figure 1: Overview of the Eastern Australian Magmatic Province, stretching along the eastern (Queensland to New South Wales) and south-eastern (Victoria to eastern South Australia) Australian margin, with different categories of magmatic types and ages of each smaller province portrayed as separate blobs (modified from Meeuws et al., 2016b). These ages show the southward trends observed in the central shield volcanoes, leucitite suites and lack of age trend in the lava fields. Tasmania and the Bass and Gippsland Basin do not fit these southward younging trends and are located south of proposed plume-activity (TH: Tasmantid hotspot (Johnson, 1989), EAH: Eastern Australian hotspot (Sutherland et al., 2012), CH: Cosgrove hotspot (Davies et al., 2015)).

The Bass Strait, located offshore between Victoria and Tasmania, hosts several basins which have preserved igneous rocks in their Cretaceous to Cenozoic sedimentary successions (Blevin et al., 2005; Holford et al., 2012; Holford et al., 2017; O'Brien et al., 2008; O'Halloran and Johnstone, 2001; Reynolds et al., 2018b). This magmatic activity is often overlooked in geodynamic models which try to explain Cenozoic magmatism along the Australian eastern and southern margin (e.g. Conrad et al., 2011; Davies et al., 2015; Sutherland et al., 2012) as up until now only a small number of the available seismic datasets have been studied in detail. Preliminary 2D and 3D seismic data interpretation has shown that the age of magmatic activity in these sedimentary basins significantly postdates continental break-up (Fig. 1) and so cannot be readily ascribed to decompressional melting processes associated with continental break-up.

The presence of igneous rocks in petroliferous basins, such as the Gippsland and Bass Basins, represents a key exploration uncertainty that nonetheless must be quantified due to the significant effects that magmatic activity poses to source and reservoir rock quality (e.g. Holford et al., 2012; Planke et al., 2005; Rateau et al., 2013; Rohrman, 2007; Schofield et al., 2016; Schutter, 2003). To date our understanding of magmatic processes in sedimentary basins has generally been restricted to field and geochemical studies of exhumed basins with limited exposure, though the increasing availability of 3D seismic data has provided a powerful means by which the processes that transport magma through sedimentary basins can be better understood (e.g. Cartwright and Hansen, 2006; Schofield et al., 2012; Schofield et al., 2015; Thomson and Hutton, 2004). Recent 3D seismic studies have challenged traditional views that 'magmatic plumbing systems' in sedimentary basins tend to be vertically stacked (Fig. 2 - Scenario 1), instead proposing a greater role for lateral transport of magma over significant horizontal distances through networks of sills and dykes (Fig. 2 - Scenario 2) (Cartwright and Hansen, 2006; Magee et al., 2016; Schofield et al., 2015). Such systems are likely to have multiple impacts, both positive and negative, on petroleum systems (Holford et al., 2012). For example, impermeable networks of intrusive bodies may compartmentalize source and reservoir sequences thereby reducing migration efficiencies, whilst focussed fluid flow associated with sills and dykes may reduce reservoir quality and puncture sealing horizons (Holford et al., 2013; Holford et al., 2012; Holford et al., 2017). On the other hand, intrusion into shallow source rocks may increase levels of maturity, and saucer-shaped sills

emplaced within reservoirs can create attractive traps with four-way closures through forced folding (Aarnes et al., 2011; Holford et al., 2012). Cretaceous-Cenozoic igneous rocks are common within the basins of the southern Australian margin (Meeuws et al., 2016b), including the Ceduna Basin where multiple sills and dykes intrude reservoirs within the Hammerhead Supersequence (Jackson, 2012; Reynolds et al., 2017a; Reynolds et al., 2017b; Reynolds et al., 2018a; Schofield and Totterdell, 2008), in the Bass Basin where a Miocene volcano overlies the Yolla Gas Field (Holford et al., 2017; Reynolds et al., 2018b; Watson et al., 2019), and in the Gippsland Basin where the Kipper Gas Field is partially sealed by Campanian basalts (Birch, 1987; Meeuws et al., 2016a; O'Halloran and Johnstone, 2001; Sloan et al., 1992).

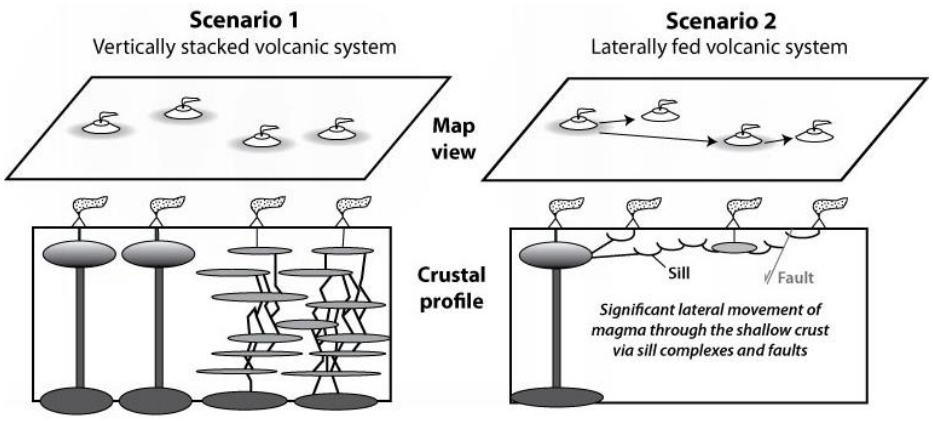

Figure 2: Different scenarios of volcanic systems. Scenario 1 depicts the most common view of systems, with volcanoes stacked vertically above a network of sills and dykes. Scenario 2 presents a volcanic system where magma travels significant distances, both vertically and horizontally, before finally extruding onto the paleosurface (modified from Magee et al. (2016)).

The central aim of this thesis is to provide an overview and further insights into both on- and offshore magmatism occurring along the south-eastern Australian margin with focus on Tasmania and the Bass and Gippsland Basins. To achieve this, several objectives have been defined:

1. Accurately constrain the distribution and chronology of Cenozoic intraplate magmatism in the Bass and Gippsland Basins. This is achieved through detailed mapping of 3D and 2D seismic reflection data available within the aforementioned basins and tying this to palynological data available from petroleum wells.

2. Determine the nature of upper crustal subvolcanic 'plumbing systems' and provide insights into the modes of Cenozoic magma transport in south-eastern Australia using 3D seismic data mapping and application of novel visualisation techniques such as opacity rendering and frequency decomposition. The combination of these techniques will reveal additional information that regular seismic amplitude data visualisation cannot provide.
3. Explain the geodynamic origins of anomalous Cenozoic intraplate magmatism in south-eastern Australia at basin-to-mantle scales. The use of major and trace element and isotope geochemistry allows for a regional scale characterisation of Cenozoic magmatism and local melting conditions of magmatism in Tasmania and Gippsland and Bass Basins.

Thesis outline

Chapter 2

Distribution, chronology and causes of Cretaceous – Cenozoic magmatism along the magma-poor rifted southern Australian margin: Links between mantle melting and basin formation. Published in Marine and Petroleum Geology (March 2016).

South-eastern Australia contains a number of passive margins formed during Gondwana break-up that host Cretaceous-Cenozoic basins. These basins are coincident with the Eastern Australian Magmatic Province that extends along the Australian eastern and south-eastern passive continental margin. Geodynamic models explaining the magmatism have relied on mantle plumes (Davies et al., 2015; Knesel et al., 2008; Sutherland et al., 2012) or edge-driven convection (Demidjuk et al., 2007), however the construction of tectonic subsidence plots and comparison with classic examples of hotspots suggests that the igneous activity along the Australian southern margin cannot be solely contributed to a classic plume model. This chapter provides an extensive overview of the regional geological evolution of the Australian southern margin and phases of intraplate magmatic activity in the region, illustrated using seismic reflection cross-sections and forms the first step towards a better understanding of igneous activity along the southern margin, by providing more insights into the origin, cause and plumbing into intraplate magmatism in general and how petroleum exploration is affected by magmatism in this region.

Chapter 3

Geochemical constraints on Cenozoic intraplate magmatism and their relation to Jurassic dolerites in Tasmania, using Sr-Nd-Pb isotopes. Published in Chemical Geology (February 2019).

Within the Eastern Australian Magmatic Province, the Tasmanian basalts are anomalous. Even though their major element geochemistry is similar to the Cenozoic volcanism in the rest of the lava field provinces, their trace element and isotope geochemistry is significantly different, with Sr- and Nd-isotope ratios spanning a large range ($^{87}Sr/^{86}Sr$: 0.702681 - 0.705544,

$^{143}Nd/^{144}Nd$: 0.512635 - 0.513013) and increased $^{206}Pb/^{204}Pb$ (19.04 – 19.58) with regards to Cenozoic magmatism in mainland Australia (Nasir et al., 2010). Both asthenospheric (Adam and Green, 2011) and subcontinental lithospheric mantle (Sun et al., 1989) source depths have been proposed. In this paper we present a new dataset of major and trace element and Sr-Nd-Pb isotope geochemistry and $^{39}Ar/^{40}Ar$ geochronology of Cenozoic magmatism in Tasmania. This paper demonstrates the different melting and fractionation controls on the composition of the Cenozoic Tasmanian igneous rocks and proposes a mixing model between different lithospheric and asthenospheric mantle end-members to explain their large range in isotopic compositions.

Chapter 4

Characterising extrusive and intrusive magmatism at the Kipper Field, Gippsland Basin, using 3D seismic data and geochemistry. Intended for submission to Australian Journal of Earth Sciences.

The Gippsland Basin is one of Australia's most important economic hydrocarbon producing basins and hosts a world-class hydrocarbon province containing both oil and gas fields (Featherstone et al., 1991; O'Brien et al., 2008; Rahmanian et al., 1990; Sloan et al., 1992). Although its petroleum system has been well studied, a large part of its geology is often overlooked. The Gippsland Basin hosts and extensive network of both intrusive and extrusive mafic igneous rocks of Campanian to Eocene age, which have a large effect, both positive and negative, on hydrocarbon plays in the basin. The Kipper Field is a prime example where volcanic rocks have benefited the hydrocarbon play by forming a seal for a 328 m gross gas column and 14 m oil leg (O'Halloran and Johnstone, 2001; Sloan et al., 1992). Detailed mapping of intrusive and extrusive rocks near the Kipper Field using 3D seismic data has revealed a vertically and laterally extensive network of sills through which magma transported from the centre towards major fault systems in the north and south of the basin. Major and trace element geochemistry of cutting and core samples of igneous rocks intersected by petroleum wells suggest an age progressive change in trace element signature from Upper Continental Crust to Oceanic Island Basalt, similar to the Jurassic and Cenozoic igneous rocks found in

onshore Tasmania. Geochemical analyses suggests that Gippsland Basin magmas have been formed at similar shallow depths and similar high degrees of melting as the basalt and basaltic andesite groups of the Tasmanian Cenozoic igneous rocks.

Chapter 5

Geochemical signatures and seismic expression of Cretaceous-Cenozoic magmatic plumbing systems in the Bass Basin.

Knowledge of magmatic plumbing systems in the Bass Basin is still not fully understood as previous studies have been largely local in nature, focussing mainly on the Miocene magmatism in the Yolla 3D and Labatt 3D seismic surveys. As the effect of magmatism on hydrocarbon systems can be both detrimental and beneficial, knowledge of subvolcanic plumbing systems is key in petroliferous basins such as the Bass Basin. This chapter reveals a large number if igneous features of Late Cretaceous to Cenozoic age preserved in the Paleocene syn-rift and Oligocene-Miocene post-rift successions of the Bass Basin. Seismic interpretation has suggested that magma is transported through dykes to form sills and volcanic vents. Magmatism is not synchronous and at least 10 episodes of magmatic activity have been identified, with Cretaceous to Eocene magmatic activity mainly occurring at major faults near the basin edges and subsequent Miocene magmatic activity exhibiting a southward age-progression in the centre of the Cape Wickham Sub-basin. Major and trace element geochemistry data on igneous drill cutting samples intersected by petroleum wells is used to compare the magmas with those from the nearby Gippsland Basin, Tasmania and Victoria (Newer and Older Volcanic Provinces). Geochemical analysis demonstrates that Bass and Gippsland Basin magmas have formed under similar shallow partial melting conditions and underwent similar amounts of fractionation.

References

Aarnes, I., Svensen, H., Polteau, S., Planke, S., 2011. Contact metamorphic devolatilization of shales in the Karoo Basin, South Africa, and the effects of multiple sill intrusions. Chemical Geology, 281(3–4): 181-194.

Adam, J., Green, T., 2011. Trace element partitioning between mica- and amphibole-bearing garnet lherzolite and hydrous basanitic melt: 2. Tasmanian Cainozoic basalts and the origins of intraplate basaltic magmas. Contributions to Mineralogy and Petrology, 161(6): 883-899.

Baillie, P.W., 1986. Radiometric ages for Circular Head and the Green Hills basalt, north-western Tasmania, Tasmania Department of Mines.

Birch, G.F., 1987. Igneous rocks of the Gippsland Basin. Esso Australia Ltd.

Blevin, J.E., Trigg, K.R., Partridge, E.D., Boreham, C.J., Lang, S.C., 2005. Tectonostratigraphy and potential source rocks of the Bass Basin. APPEA Journal, 45: 601-622.

Cartwright, J., Hansen, D., 2006. Magma transport through the crust via interconnected sill complexes. Geology, 34(11): 929-932.

Cas, R.A.F., van Otterloo, J., Blaikie, T.N., van den Hove, J., 2017. The dynamics of a very large intra-plate continental basaltic volcanic province, the Newer Volcanics Province, SE Australia, and implications for other provinces, Geological Society Special Publication, pp. 123-172.

Conrad, C., Bianco, T., Smith, E., Wessel, P., 2011. Patterns of intraplate volcanism controlled by asthenospheric shear. Nature Geoscience, 4(5): 317-321.

Davies, D.R., Rawlinson, N., Iaffaldano, G., Campbell, I.H., 2015. Lithospheric controls on magma composition along Earth/'s longest continental hotspot track. Nature, 525(7570): 511-514.

Demidjuk, Z. et al., 2007. U-series isotope and geodynamic constraints on mantle melting processes beneath the Newer Volcanic Province in South Australia. Earth and Planetary Science Letters, 261(3-4): 517-533.

Duncan, C.E., Mcdougall, I., 1989. Volcanic time-space relationships. In: Johnson, R.W. (Ed.), Intraplate volcanism in Eastern Australia and New Zealand. Cambridge University Press, Cambridge, pp. 43-54.

Featherstone, P., Aigner, T., Brown, L., King, M., Leu, W., 1991. Stratigraphic modelling of the Gippsland Basin. The APEA journal, 31(part 1): 105-114.

Holford, S.P. et al., 2013. Impacts of igneous intrusions on source and reservoir potential in prospective sedimentary basins along the western Australian continental margin. In: Keep, M., Moss, S.J. (Editors), The Sedimentary Basins of Western Australia IV, Perth.

Holford, S.P., Schofield, N., Macdonald, J.D., Duddy, I.R., Green, P.F., 2012. Seismic analysis of igneous systems in sedimentary basins and their impacts on hydrocarbon prospectivity: examples from the southern Australian margin. APPEA Journal, 52: 229-252.

Holford, S.P., Schofield, N., Reynolds, P., 2017. Subsurface fluid flow focused by buried volcanoes in sedimentary basins: Evidence from 3D seismic data, Bass Basin, offshore southeastern Australia. Interpretation, 5(3): SK39-SK50.

Jackson, C., 2012. Seismic reflection imaging and controls on the preservation of ancient sill-fed magmatic vents. Journal of the Geological Society, 169(5): 503-506.

Johnson, R.W. (Ed.), 1989. Intraplate volcanism in eastern Australia and New Zealand. Intraplate volcanism in eastern Australia and New Zealand. Cambridge University Press, in association with Australian Academy of Science.

Knesel, K., Cohen, B., Vasconcelos, P., Thiede, D., 2008. Rapid change in drift of the Australian plate records collision with Ontong Java plateau. Nature, 454(7205): 754-U75.

Lesti, C., Giordano, G., Salvini, F., Cas, R., 2008. Volcano tectonic setting of the intraplate, Pliocene-Holocene, Newer Volcanic Province (southeast Australia): Role of crustal fracture zones. Journal of Geophysical Research: Solid Earth, 113(B7): B07407.

Magee, C. et al., 2016. Lateral magma flow in mafic sill complexes. Geosphere, 12(3): 809-841.

Meeuws, F., Reynolds, P., Holford, S., Foden, J., Schofield, N., 2016a. Characterising extrusive and intrusive magmatism at the Kipper Field, Gippsland Basin, using 3D seismic data. ASEG Extended Abstracts, 2016(1): 1-7.

Meeuws, F.J.E., Holford, S.P., Foden, J.D., Schofield, N., 2016b. Distribution, chronology and causes of Cretaceous – Cenozoic magmatism along the magma-poor rifted southern Australian margin: Links between mantle melting and basin formation. Marine and Petroleum Geology, 73: 271-298.

Nasir, S.J., Everard, J.L., McClenaghan, M.P., Bombardieri, D., Worthing, M.A., 2010. The petrology of high pressure xenoliths and associated Cenozoic basalts from Northeastern Tasmania. Lithos, 118(1–2): 35-49.

O'Brien, G.W. et al., 2008. First order sealing and hydrocarbon migration processes, Gippsland Basin, Australia: implications for CO2 geosequestration, Eastern Australian Basins Symposium III. Petroleum Exploration Society of Australia, Sydney Convention and Exhibition Centre, NSW, Australia, pp. 1-28.

O'Halloran, G., Johnstone, E., 2001. Late Cretaceous rift volcanics of the Gippsland Basin, SE Australia - New insights from 3D seismic. In: Hill, K.C., Bernecker, T. (Editors), Eastern Australasian Basins Symposium: a refocussed energy perspective for the future. Petroleum Exploration Society of Australia, Melbourne, Victoria, pp. 353-361.

Planke, S., Rasmussen, T., Rey, S., Myklebust, R., 2005. Seismic characteristics and distribution of volcanic intrusions and hydrothermal vent complexes in the Vøring and Møre basins, Geological Society, London, Petroleum Geology Conference series. Geological Society of London, pp. 833-844.

Rahmanian, V.D., Moore, P.S., Mudge, W.J., Spring, D.E., 1990. Sequence Stratigraphy and the Habitat of Hydrocarbons, Gippsland Basin Australia. Classic Petroleum Provinces, 50: 525-544.

Rateau, R., Schofield, N., Smith, M., 2013. The potential role of igneous intrusions on hydrocarbon migration, West of Shetland. Petroleum Geoscience, 19(3): 259-272.

Reynolds, P., Holford, S., Schofield, N., Ross, A., 2017a. The shallow depth emplacement of mafic intrusions on a magma-poor rifted margin: An example from the Bight Basin, southern Australia. Marine and Petroleum Geology, 88: 605-616.

Reynolds, P., Holford, S., Schofield, N., Ross, A., 2017b. Three-Dimensional Seismic Imaging of Ancient Submarine Lava Flows: An Example From the Southern Australian Margin. Geochemistry, Geophysics, Geosystems, 18(11): 3840-3853.

Reynolds, P., Holford, S., Schofield, N., Ross, A., 2018a. The importance of subsurface lithology in controlling magma storage v. eruption: an example from offshore southern Australia. Journal of the Geological Society.

Reynolds, P., Schofield, N., Brown, R.J., Holford, S.P., 2018b. The architecture of submarine monogenetic volcanoes – insights from 3D seismic data. Basin Research, 30: 437-451.

Rohrman, M., 2007. Prospectivity of volcanic basins: Trap delineation and acreage de-risking. AAPG Bulletin, 91(6): 915-939.

Sayers, J., Symonds, P.A., Direen, N.O., Bernardel, G., 2001. Nature of continent-ocean transition on the non volcanic rifted margin of the central Great Australian Bight. In: Wilson, R.C.L., Whitmarsh, R.B., Taylor, B., Froitzheim, N. (Eds.), Non-volcanic rifting of oceanic margins; a comparison of evidence from land and sea. Geological Society of London, pp. 51-76.

Schofield, A., Totterdell, J., 2008. Distribution, timing and origin of magmatism in the Bight and Eucla Basins. Geoscience Australia, Record 2008/4: 19.

Schofield, N. et al., 2012. Seismic imaging of 'broken bridges': linking seismic to outcrop-scale investigations of intrusive magma lobes. Journal of the Geological Society, 169(4): 421-426.

Schofield, N. et al., 2015. Regional magma plumbing and emplacement mechanisms of the Faroe-Shetland Sill Complex: implications for magma transport and petroleum systems within sedimentary basins. Basin Research: n/a-n/a.

Schofield, N. et al., 2016. Sills in Sedimentary Basins and Petroleum Systems. In: Breitkreuz, C., Rocchi, S. (Eds.), Physical Geology of Shallow Magmatic Systems: Dykes, Sills and Laccoliths. Springer International Publishing, Cham, pp. 273-294.

Schutter, S., 2003. Hydrocarbon occurrence and exploration in and around igneous rocks. In: Petford, N., McCaffrey, K. (Eds.), Hydrocarbons in crystalline rocks. Geological Society London, London, pp. 7-33.

Sloan, M.W., Moore, P.S., McCutcheon, A., 1992. Kipper - A unique oil and gas discovery, Gippsland Basin, Australia. The APPEA Journal, 32(1): 1-8.

Sun, S.S., McDonough, W.F., Ewart, A., 1989. Four component dynamic model for East Australian basalts. In: Johnson, R.W. (Ed.), Intraplate volcanism in Eastern Australia and New Zealand. Cambridge University Press, pp. 333-347.

Sutherland, F.L., Graham, I.T., Meffre, S., Zwingmann, H., Pogson, R.E., 2012. Passive-margin prolonged volcanism, East Australian Plate: outbursts, progressions, plate controls and suggested causes. Australian Journal of Earth Sciences, 59(7): 983-1005.

Thomson, K., Hutton, D., 2004. Geometry and growth of sill complexes: insights using 3D seismic from the North Rockall Trough. Bulletin of Volcanology, 66(4): 364-375.

Vasconcelos, P., Knesel, K., Cohen, B., Heim, J., 2008. Geochronology of the Australian Cenozoic: a history of tectonic and igneous activity, weathering, erosion, and sedimentation. Australian Journal of Earth Sciences, 55(6-7): 865-914.

Watson, D., Holford, S., Schofield, N., Mark, N., 2019. Failure to predict igneous rocks encountered during exploration of sedimentary basins: A case study of the Bass Basin, Southeastern Australia. Marine and Petroleum Geology, 99: 526-547.

Wellman, P., McDougall, I., 1974. Cainozoic igneous activity in eastern australia. Tectonophysics, 23(1–2): 49-65.

Chapter 2

Distribution, chronology and causes of Cretaceous – Cenozoic magmatism along the magma-poor rifted southern Australian margin: Links between mantle melting and basin formation

Statement of Authorship

Title of Paper	Distribution, chronology and causes of Cretaceous – Cenozoic magmatism along the magma-poor rifted southern Australian margin: Links between mantle melting and basin formation.
Publication Status	☑ Published ☐ Accepted for Publication ☐ Submitted for Publication ☐ Unpublished and Unsubmitted work written in manuscript style
Publication Details	Meeuws, F.J.E., Holford, S.P., Foden, J.D., Schofield, N., 2016. Distribution, chronology and causes of Cretaceous – Cenozoic magmatism along the magma-poor rifted southern Australian margin: Links between mantle melting and basin formation. Marine and Petroleum Geology 73, 271-298.

Principal Author

Name of Principal Author (Candidate)	Fun Julie Ellen Meeuws		
Contribution to the Paper	Gathered all data, constructed subsidence plots, wrote manuscript, acted as corresponding author.		
Overall percentage (%)	80		
Certification:	This paper reports on original research I conducted during the period of my Higher Degree by Research candidature and is not subject to any obligations or contractual agreements with a third party that would constrain its inclusion in this thesis. I am the primary author of this paper.		
Signature		Date	2/07/2019

Co-Author Contributions

By signing the Statement of Authorship, each author certifies that:

i. the candidate's stated contribution to the publication is accurate (as detailed above);

ii. permission is granted for the candidate in include the publication in the thesis; and

iii. the sum of all co-author contributions is equal to 100% less the candidate's stated contribution.

Name of Co-Author	Associate Professor Simon Holford		
Contribution to the Paper	Supervised development of work, helped in data interpretation and manuscript evaluation.		
Signature		Date	2/07/2019

Name of Co-Author	Emeritus Professor John Foden		
Contribution to the Paper	Helped to evaluate and edit the manuscript.		
Signature		Date	2/07/2019

Name of Co-Author	Dr Nick Schofield		
Contribution to the Paper	Helped with seismic data interpretation and helped to evaluate and edit the manuscript.		
Signature		Date	2/07/2019

Please cut and paste additional co-author panels here as required.

Marine and Petroleum Geology 73 (2016) 271–298

Contents lists available at ScienceDirect

Marine and Petroleum Geology

journal homepage: www.elsevier.com/locate/marpetgeo

Review article

Distribution, chronology and causes of Cretaceous – Cenozoic magmatism along the magma-poor rifted southern Australian margin: Links between mantle melting and basin formation

Fun J.E. Meeuws [a, *], Simon P. Holford [b], John D. Foden [a], Nick Schofield [c]

[a] Centre for Tectonics, Resources and Exploration (TRaX), University of Adelaide, Adelaide, SA 5005, Australia
[b] Australian School of Petroleum, Centre for Tectonics, Resources and Exploration (TRaX), University of Adelaide, Adelaide, SA 5005, Australia
[c] Department of Geology and Petroleum Geology, University of Aberdeen, AB24 3UE, UK

ARTICLE INFO

Article history:
Received 1 September 2015
Received in revised form
8 February 2016
Accepted 1 March 2016
Available online 7 March 2016

Keywords:
Intraplate magmatism
Australia
Cenozoic
Magma-poor margin
Bight Basin
Otway-Sorell Basin
Bass Basin
Gippsland Basin

ABSTRACT

The eastern, south-eastern and southern Australian passive margins host a series of Cenozoic basins preserved in current onshore and offshore records in Victoria, Tasmania and South Australia. These basins are coeval with the mantle-derived, Cenozoic Magmatic Province that extends along the Australian eastern and southern passive continental margin. This igneous activity, as emphasised in this review, hosts a wide range of intrusive and extrusive bodies that developed in an intraplate setting. To date, research on this province has mainly focussed on the onshore magmatic record and several models such as mantle plumes or edge-driven convection have been proposed to account for the origin of this magmatism. This review however, shows that a vast and largely undescribed record of magmatic activity exists offshore along the Australian southern margin. Preliminary seismic studies of the offshore magmatic activity have shown that the majority of this magmatism occurred at Eocene to Oligocene and Miocene to Recent times, therefore significantly post-dating continental break-up and basin rifting related to the separation of Australia and Antarctica, which started around 85 Ma. Additionally, magmatism preserved onshore and basin events indicated by large unconformities observed offshore appear to be synchronous. Together with the analyses of tectonic subsidence plots and comparison with classic examples of hotspots, these factors suggest that igneous activity along the Australian southern margin cannot be solely contributed to a classic plume model. Instead, the distribution and timing of the magmatism is more likely to be related to edge-driven convection at least in some places like the Bight Basin. This review forms part of the first step towards a better understanding of igneous activity along the southern margin, intraplate magmatism in general and the effects on petroleum exploration along this petroliferous margin.

Contents

* Corresponding author.
E-mail address: fun.meeuws@adelaide.edu.au (F.J.E. Meeuws).

http://dx.doi.org/10.1016/j.marpetgeo.2016.03.003
0264-8172/

1. Introduction

Traditionally the cause of almost all mantle-derived terrestrial magmatism is ascribed to well-established plate boundary processes or to the influence of upwelling of thermally anomalous asthenosphere. That said there are clear global examples where plate tectonics theory does not sufficiently account for the origin of intraplate, typically basaltic, volcanic provinces. Examples are the Hawaiian volcanic chain in the Pacific plate, the Yellowstone volcanic field which is part of the Columbia River Large Igneous Province (LIP) in North America, the Auckland volcanic province in New Zealand, the Cameroon line in West Africa, the East African Rift in East Africa, the Eastern Cenozoic Magmatic Province in Australia, the Central, Rhenish and Bohemian Massif in Europe and Marie Byrd seamounts in Antarctica to name a few. Such magmatic provinces are widely distributed across our planet and are typically situated away from plate boundaries (Bryan and Ferrari, 2013; Conrad et al., 2011; Johnson, 1989). They occur both within continental settings (Coffin and Eldholm, 1994, 2005; Demidjuk et al., 2007) or appear as seamounts on the seabed (Coffin and Eldholm, 1994, 2005; Forsyth et al., 2006; Kerr, 2014).

The Australian eastern and southern margins host one of the classic examples of intraplate volcanic provinces, the Cenozoic Magmatic Province, which extends throughout south and eastern Australia (Johnson, 1989). This region extends over 4400 km from northern Queensland to southern Tasmania and extends westwards into Victoria and southeast South Australia along the passive southern margin of the Australian continent (Fig. 1). This magmatic province covers a surface area of 1.6 million km^2 and comprises a chain of basaltic lava fields and shield volcanoes, ranging in age between 70 Ma and 5 Ka (Johnson, 1989). Generally, passive margins can be classified as 'volcanic' or magma-rich and 'non-volcanic' or magma-poor passive margins (Franke, 2013). So-called volcanic margins, such as the northeast Atlantic margin, are associated with Large Igneous Provinces (LIPs), Seaward Dipping Reflectors (SDR) in the seismic record and large volumes of magmatic activity with up to 6–7 km of melt and are believed to originate due to the decompression of asthenosphere whose temperatures are 100–200 °C above the normal mantle adiabat (White and McKenzie, 1989). These small rises in temperature have been modelled based on pressure and temperature relationships and are found to be sufficient to generate the amount of decompressional melting observed along these volcanic margins (White and McKenzie, 1989) The Australian southern margin however, is classified as a 'non-volcanic' or 'magma-poor' rifted passive margin (e.g. Sayers et al. (2001)), although occurrences of scattered magmatism have been reported in the offshore Bight, Otway, Sorell, Bass and Gippsland Basins along the Australian southern margin, in addition to the onshore magmatic activity (Holford et al., 2012; Schofield and Totterdell, 2008). These reports of offshore magmatism have used a number of offshore 2D and 3D seismic reflection surveys and have revealed both volcanic and sub-volcanic features of Eocene age in the Bight and Otway basins and Oligocene and Miocene ages in the Sorell and Bass basins and Torquay sub-basin and of Cretaceous to mid-Eocene age in the Gippsland Basin (Birch, 1987; Hill et al., 1997; Holford et al., 2012). Extension and continental break-up phases, related to the separation of Australia and Antarctica however, occurred at 90 and 83 Ma in the Bight Basin, at 67 Ma in the Otway Basin, at 55 Ma in the Sorell Basin and at 83 Ma in the Gippsland Basin (Gibson et al., 2012; Krassay et al., 2004; Krassay and Totterdell, 2003; Rahmanian et al., 1990). Both on- and offshore magmatism is therefore much younger than the rift or break-up phases along the Australian southern margin, hence arguing against a direct link between rifting (and thus decompressional melting) and the distribution of Cenozoic intraplate magmatism in the sedimentary basins of south-eastern Australia.

The cause of intraplate magmatism along the Australian southern margin is subject of on-going debate. Models include; the role of stationary hotspots beneath the northward moving Australian plate (Davies et al., 2015; Knesel et al., 2008; Sutherland et al., 2012), the role of lithospheric stress changes due to far-field tectonic effects related to the opening of the Southern Ocean and Tasman Sea during the late Cretaceous (Price et al., 2003), the potential role for small-scale mantle convection driven by motion of steps in lithospheric thickness (Demidjuk et al., 2007) or rapid shear due to mantle convection (Conrad et al., 2011) and a combination by triggering of the edge-driven convection model and passing of the mantle plume which caused the Cosgrove track

which extends from Cape Hillsborough in Queensland to Cosgrove in Victoria (Davies et al., 2015). However, no consensus has been reached on the origin and emplacement of Australian Cenozoic Magmatic Province and earlier proposed models have not incorporated the observed offshore magmatic activity described in this paper (Conrad et al., 2011; Davies et al., 2015; Sutherland et al., 2012).

This investigation focuses on the definition of the record of Cenozoic magmatism preserved in the predominantly offshore sedimentary basins along the Australian southern margin. This approach anticipates that the sedimentary record in these basins is a sensitive reflection of the lithospheric stress state and its changes and that correlation with magmatic intervals will provide key evidence for the nature of asthenosphere-lithosphere interaction. This analysis applies new interpretation of seismic reflection data providing new insight into the stratigraphic position of magmatism and of sub-surface plumbing and magma trajectories through the sedimentary succession. Along the Australian southern margin, post-rift magmatic features are shallow and easily recognized in seismic reflection data. By contrast, the record of syn-rift magmatism is typically structurally more complex and more likely to be buried beneath post-rift sequences, complicating identification of intrusive and extrusive magmatic features and their trajectory from mantle through the sedimentary successions.

This paper provides with an extensive overview of the age, distribution, magmatic styles and petrological signatures of the on- and offshore volcanic activity along the Australian southern margin. Fully understanding the magmatic evolution of this margin calls for an incorporation of the offshore magmatism and will provide more insights such as origin, cause and plumbing into intraplate magmatism in general. Additionally, constraining the temporal and spatial distribution of magmatic features will provide

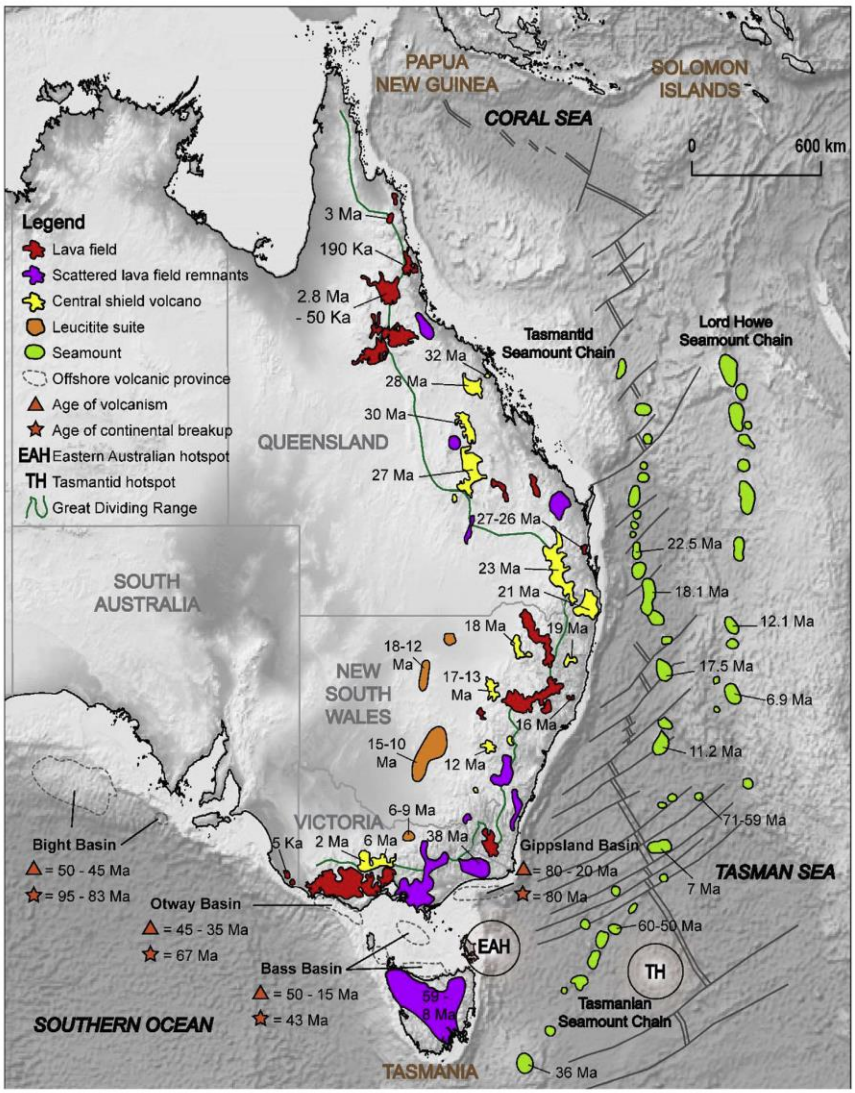

Fig. 1. Cenozoic intraplate magmatism in south-eastern Australia (modified from Blewett (2012); Cohen et al. (2008); Gaina et al. (2000)).

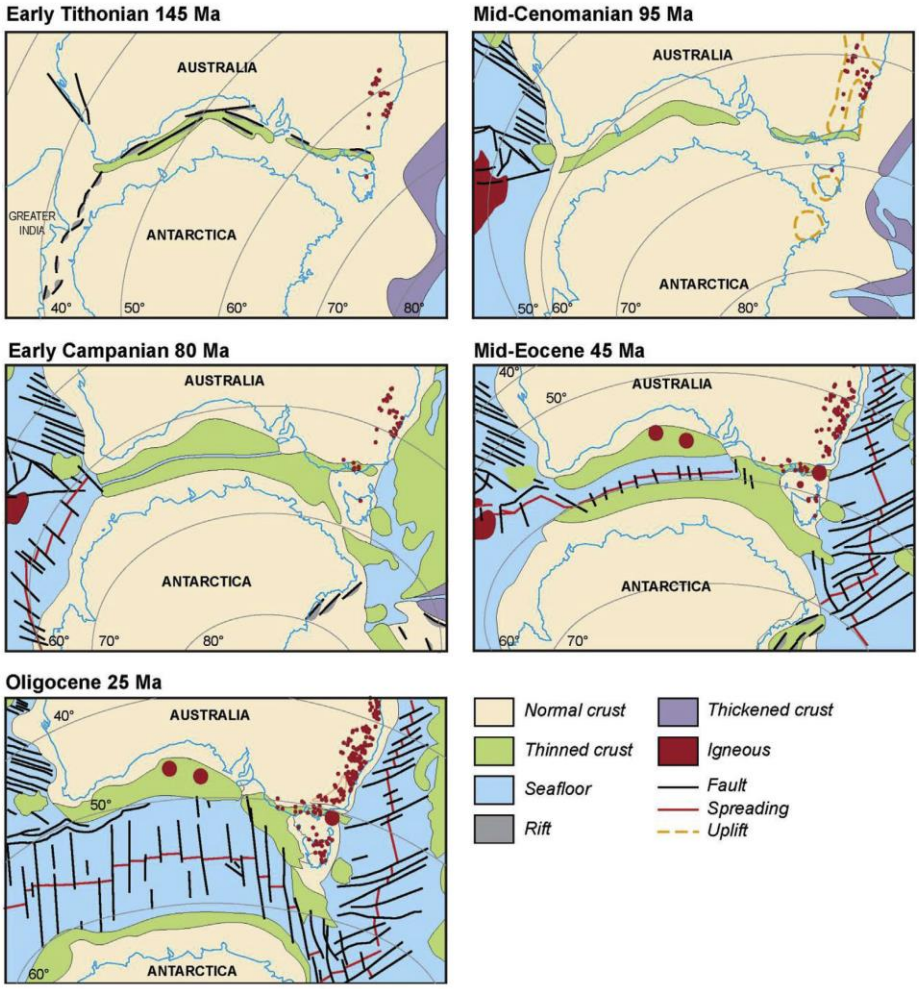

Fig. 2. Plate tectonic reconstructions for the southern Australia–Antarctica conjugate margin (modified from Norvick (2005)). Please note that the representation of igneous rocks is cumulative over time.

for a more accurate risk-assessment in further petroleum exploration along this already prolific margin and in similar magma-poor passive margins around the world.

2. Geological setting of the Southern Rift System

The Bight, Otway, Sorell, Gippsland and Bass basins all find their existence in the break-up of eastern Gondwana (Fig. 2), where Antarctica began to separate from the supercontinent's southern margin and formed the Southern Rift System, now located along Australia's present-day southern coastline (Stagg et al., 1990). Although the Sorell Basin has not undergone as much hydrocarbon exploration compared to other basins, leading to a less well known geological history, it is assumed to be very similar to that of the Otway Basin as the Sorell Basin is a continuation of the Otway Basin.

As has been summarized by Blevin and Cathro (2008), the Australian southern margin underwent three rift phases and one transitional rift phase during the middle Jurassic to late Cretaceous (phases 1–4 in Fig. 3) followed by thermal subsidence throughout most of the Cenozoic, which was interrupted by pulses of uplift and inversion (phase 6, Fig. 3) (Holford et al., 2014).

2.1. Early Cretaceous extension (non-marine to fluvio-lacustrine sedimentation) – phase 1

The first phase of rifting mainly affected the Bight Basin, was NW–SE directed, starting in the Callovian and lasting until the early Berriasian (~166–145 Ma, phase 1 Fig. 3, green arrows Fig. 4) (Blevin and Cathro, 2008). These first stages of rifting had little associated volcanism and the first sediments to fill the rift basin mainly consisted of fluvio-lacustrine sandstone, siltstone and shale with minor coal for the Bight Basin (Sea Lion and Minke Supersequences) (Krassay and Totterdell, 2003). Although extension had not yet started in the Otway Basin, carbonaceous lacustrine shales and minor interbedded basalts and sandstone were deposited as a far-field response to Bight Basin extension (lower part of the Crayfish Supersequence or Casterton Formation) (Blevin and Cathro, 2008; Krassay et al., 2004; Ryan et al., 1995).

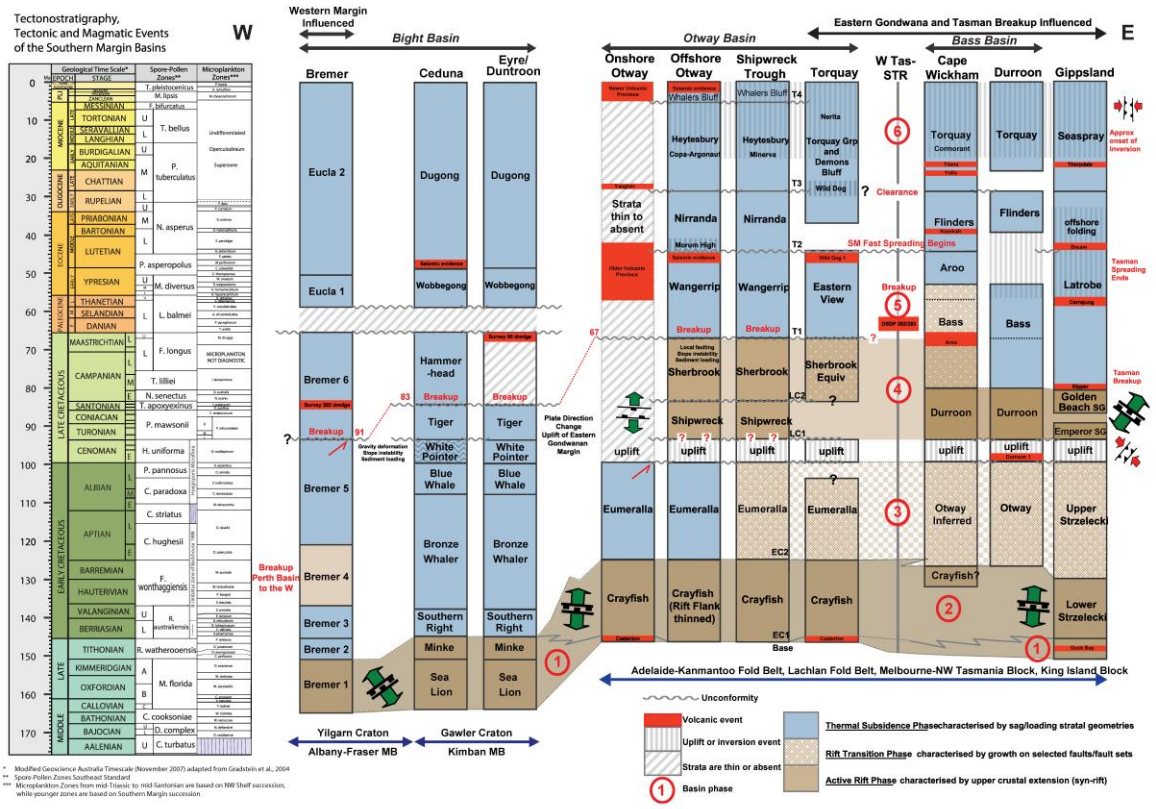

Fig. 3. Mesozoic to recent tectonostratigraphic chart for the southern margin basins with indications of magmatic intervals (modified from Blevin and Cathro (2008)).

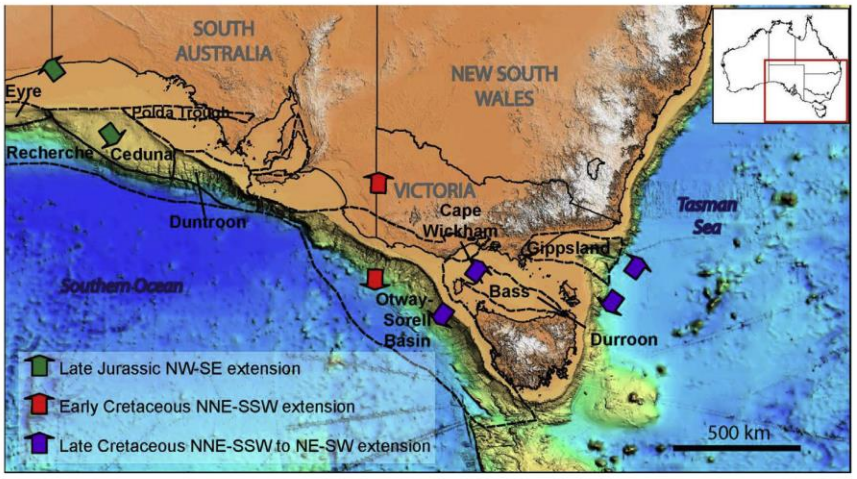

Fig. 4. Geological setting: Digital Elevation Model of the study area with location of basins and sub-basins discussed in this paper and the orientation of extension. Green arrows indicate Late Jurassic (Callovian to early Berriasian), NW-directed extension. Red arrows indicate Early Cretaceous (early to mid-Berriasian to latest Barremian), NNE-directed extension. Purple arrows indicate Late Cretaceous (Turonian to Mid-Campanian), NNE- to NE- directed extension in the Gippsland and Bass Basins and Turonian to Late Maastrichtian, NNE- to NE-directed extension in the Otway, Sorell and Bass Basin (modified from Blevin and Cathro (2008)).

2.2. Early Cretaceous thermal subsidence in the west and extension in the east (transition to coastal plain sedimentation) – phase 2

Following this first phase of rifting, the Bight Basin underwent slow thermal subsidence throughout the Early Cretaceous, resulting in the mainly non-marine Berriasian Southern Right and Valanginian to mid-Albian Bronze Whaler Supersequences which consist of fluvio-lacustrine sandstone and siltstone and a thick fine-grained lacustrine succession respectively (Krassay and Totterdell, 2003). In the eastern basins however, this first extensional phase was followed by a second extensional phase during the early to mid-Berriasian to the latest Berriasian (~146-142 Ma, red arrows Fig. 4), which caused NNE-SSW-directed extension (phase 2, Fig. 3) (Blevin and Cathro, 2008). This second phase has been expressed in the Otway, Sorell, Bass and Gippsland basins and is more or less concurrent with the cessation of upper crustal extension in the Bight Basin, shifting the locus of rifting eastwards and allowing thermal subsidence in the Bight Basin (Blevin and Cathro, 2008). As extension progressed during this second rift phase, significant accommodation space was created and was filled by amalgamated, fluvio-lacustrine syn-rift facies of the Crayfish Supersequence in the Otway Basin (Krassay et al., 2004).

2.3. Thermal subsidence or transitional rift phase (fluvial to floodplain sedimentation) – phase 3

In the latest Barremian, the onshore parts of the Otway Basin and much of its offshore sections experienced thermal subsidence, whereas the Bass Strait region comprising the Otway, Bass and Gippsland Basins, continued into a transitional rift phase during the Aptian to Albian (phase 3, Fig. 3) (Blevin and Cathro, 2008). Although described as a post-rift phase by Norvick and Smith (2001), syn-tectonic growth continued on selected faults in the Bass Basin, Shipwreck Trough, Torquay Sub-basin and Gippsland Basin during this period, making transitional rift phase a preferred term for these tectonically active regions since this period is not yet fully understood (Blevin and Cathro, 2008). During this transitional phase, the Eumeralla, Otway and Upper Strzelecki Supersequences were deposited in the Otway, Bass and Gippsland Basins respectively (Blevin and Cathro, 2008). These sequences consist mainly of volcanoclastic material, dominated by mudstone in the Eumeralla Supersequence, volcanoclastic, fluvial sands with thin, coaly overband-floodplain shales in the Otway Supersequence and non-marine arkoses and fluvial volcanoclastic sediments in the Upper Strzelecki Supersequence (Blevin et al., 2005; Krassay et al., 2004; Rahmanian et al., 1990).

2.4. Middle albian flooding and deepening in the west – Late Cretaceous uplift in the east

Coincident with accelerated subsidence in the Bight Basin during the Middle Albian, initial major marine flooding occurred. This resulted in deposition of a thick deltaic, marginal marine and marine sequence consisting of the Blue Whale, White Pointer and Tiger Supersequences in the central Ceduna sub-basin (Krassay and Totterdell, 2003) and was followed by deposition of the Hammerhead Delta, which is unconformably overlain by Cenozoic carbonate-dominated sediments of the Eucla Basin (Wobbegong and Dugong Supersequences) (Krassay and Totterdell, 2003). In the eastern basins however, Cenomanian uplift due to NW–SE compression created the Otway Ranges and ridges separating the Otway, Bass and Gippsland Basins and eroded most of the Cenomanian deposits and top of the Eumeralla and equivalent Supersequences (Krassay et al., 2004; Rahmanian et al., 1990).

2.5. Late Cretaceous extension and final break-up – phase 4

The last phase of Late Cretaceous rifting in the eastern basins was coincident with continental break-up in the Bight Basin to the west around 83 Ma (phase 4, Fig. 3) (Krassay and Totterdell, 2003). This rift phase can be subdivided into two NE–SW directed phases for the Otway Basin (purple arrows Fig. 4); Turonian to latest Santonian (Shipwreck Supersequence) and Campanian to late Maastrichtian (Sherbrook Supersequence). As fault activity and sea level started to increase, accommodation space was filled with the Shipwreck Supersequence, consisting of thick non-marine interbeds of sands, silts and shales and rare coal interbeds and abruptly changing to marine mudstones of the Sherbrook Supersequence as marine influence increased (Krassay et al., 2004). In the offshore part of the Otway Basin, the end of rifting is indicated by break-up and onset of seafloor spreading at 67 Ma (Maastrichtian - Palaeocene, phase 5, Fig. 3) (Krassay et al., 2004), previously interpreted as Cenomanian (Boult and Hibburt, 2002) or mid-Eocene (43 Ma; Norvick and Smith (2001)). As spreading continued southwards, the Sorell Basin has seen continental break-up at 55 Ma and subsequent progressive subsidence, resulting in the deposition of thick prograding shelf margin sequences in the Otway and Sorell Basins (Gibson et al., 2012; Hill and Exon, 2013). Similar to the Otway Basin, the Gippsland and Bass Basin show two pulses of NNE-SSW to NE–SW directed rifting related to Tasman Sea extension (phase 4, Fig. 3; purple arrows Fig. 4), with deposition of the Emperor Group (earliest pulse) and Golden Beach Group (second pulse) in the Gippsland Basin and the Durroon Supersequence in the Bass Basin (Bernecker and Partridge, 2005; Blevin et al., 2005). In the Durroon sub-basin of the Bass Basin, the Durroon Supersequence is separated from the Otway Supersequence by a 36 m thick package of basaltic lava flows (Blevin, 2003).

Lithospheric extension stopped in the Durroon sub-basin around Campanian times and thermal subsidence allowed for the deposition of the Bass, Flinders and Torquay Supersequences (Blevin et al., 2005). Although tectonic activity continued in the western parts of the basin and the Cape Wickham sub-basin, the Bass Basin did not extend to continental break-up as the locus of extensional stresses and accommodation progressively moved away from the Bass Basin (Blevin et al., 2005). This caused a wide variation in facies, environment and thickness of sediments in the Bass Supersequence, which is subdivided into the Furneaux (mid-Campanian to latest Maastrichtian interbedded fluvio-deltaic sandstones and freshwater lacustrine shales to delta plain shales and coals), Tilana (latest Maastrichtian to late Late Palaeocene fluvio-deltaic sandstones, floodplain shales and coals) and Narimba Sequences (latest Paleocene to late Early Eocene fluvio-deltaic to delta plain sandstones and shales and thin coals to lacustrine mudstone with shoreface and prograding deltaic sandstones and minor coal) (Blevin, 2003). Of these three sequences, the Furneaux and Tilana Sequences are heavily intruded by igneous material and associated fluids (Blevin et al., 2005). In the Gippsland Basin, this phase of Late Cretaceous rifting created the major depocentre of the Central Deep and deposition of the Latrobe Supersequence (phase 5, Fig. 3) (Rahmanian et al., 1990). Along the basin margins, this resulted in sandstones and conglomerates of braided streams and alluvial fans and in finer grained fluvial deposits in the Central Deep (Emperor subgroup) (Bernecker and Partridge, 2005). Separated from the underlying Emperor subgroup by the Longtom Unconformity, the Golden Beach subgroup consists of coastal plain sandstone and shale, marine deeper-water siltstone, mudstone and sandstone, is heavily intruded by basaltic intrusions and is terminated by basaltic lava flows and the Seahorse unconformity (related to Tasman Sea break-up) near the top (Bernecker and Partridge, 2005). As break-up of the Tasman Sea was quite early

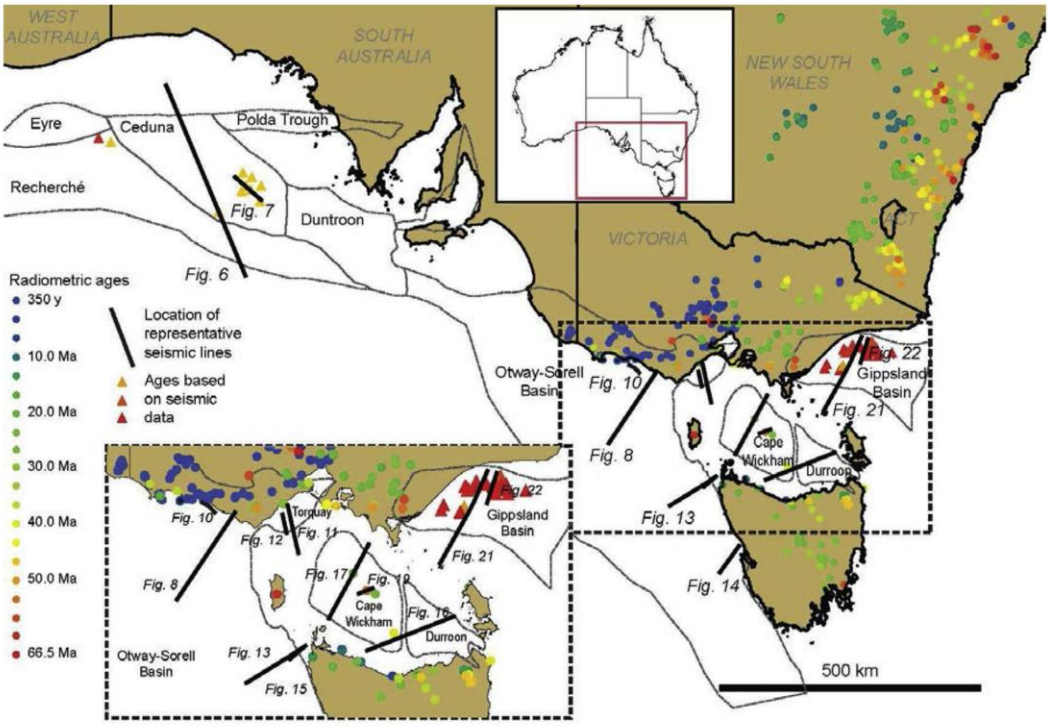

Fig. 5. Distribution of Cenozoic volcanic rocks along the Australian southern margin with locations of colour-coded age-dated samples (compiled from Vasconcelos et al. (2008), Gibson (2007), O'Brien et al. (2008)) and location of representative seismic lines discussed further in the text.

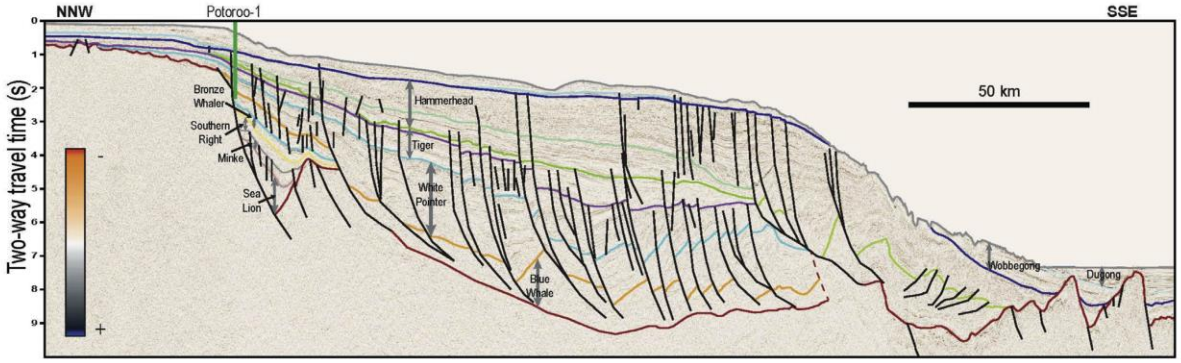

Fig. 6. Seismic line 199-08 and 199-11 (reverse SEG polarity). Regional cross-section of the Bight Basin, interpretation modified from Bradshaw et al. (2003). Location of seismic line is shown in Fig. 5.

(80–83 Ma), post-rift subsidence occurred in the mid-Campanian, which was then followed by the end of the last extensional phase in the Bass/Gippsland Basin. While the stresses in the eastern Bass and Gippsland Basins are related to the break-up of eastern Gondwana with opening of the Tasman Sea, the stresses in the Otway/Bass basin are associated with the final stages of separation between Australia and Antarctica and opening of the Southern Ocean, prolonging extensional stresses in the western Bass Basin until the Early Eocene. Although the early phase of Late Cretaceous extension is coincident in these south-eastern basins (Turonian to mid-Campanian), the stresses associated with extension in these basins have different tectonic origins.

2.6. Palaeocene thermal subsidence

From the Paleocene onwards, the whole southern margin was subject to thermal subsidence with deposition of increasingly more marine sediments (phase 6, Fig. 3). These sediments consist of the Late Maastrichtian to Eocene Wangerrip (siliciclastic deltaic sediments) and Eastern View Supersequences in the Otway Basin, the

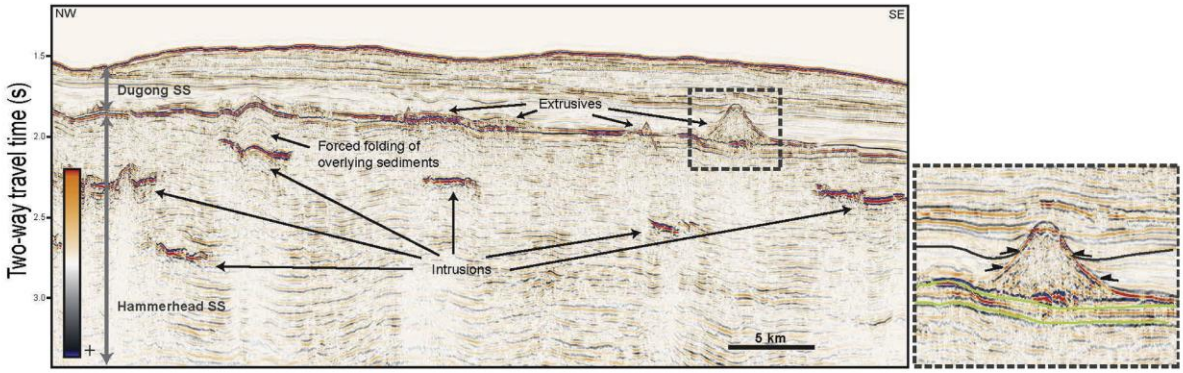

Fig. 7. Part of seismic line w00fdw0087 (reverse SEG polarity). Examples of magmatic features in the Ceduna sub-basin of the Bight Basin. Location of seismic line is shown in Fig. 5.

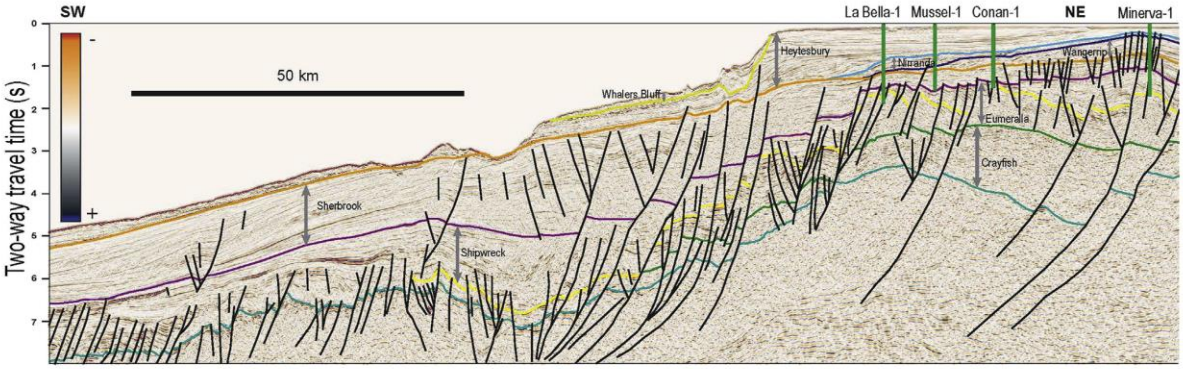

Fig. 8. Seismic line 137-09 (reverse SEG polarity). Eastern Otway regional cross-section, interpretation modified from Krassay et al. (2004). Location of seismic line is shown in Fig. 5.

Early to Middle Eocene Aroo Supersequence (interbedded silt and shale, tidal sand deposits, coal seams and abundant channel sandstones) in the Cape Wickham sub-basin of the Bass Basin and the upper part of the Turonian to Late Eocene Latrobe Supersequence (coastal plain to shallow marine) in the Gippsland Basin (Blevin et al., 2005; Krassay et al., 2004; Rahmanian et al., 1990). As spreading rates increased in the Middle Eocene, local inversions and erosion separated the Wangerrip Supersequence

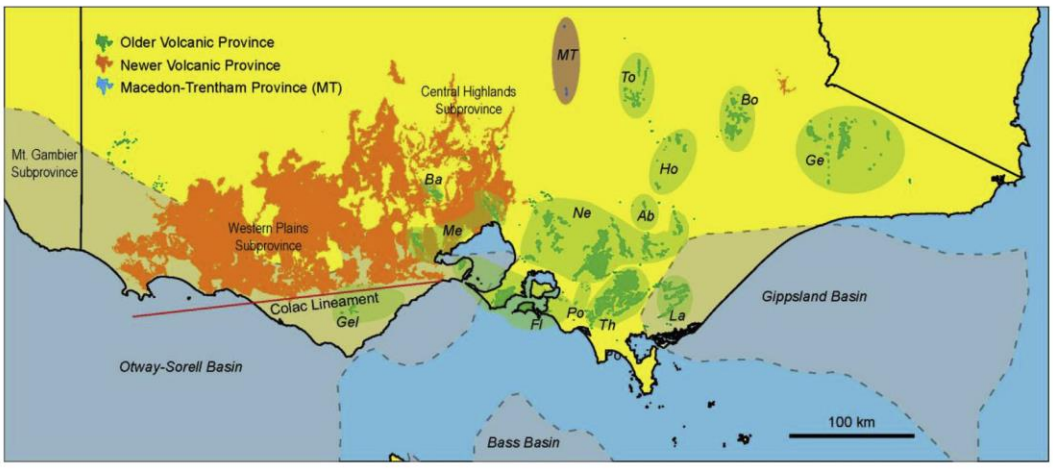

Fig. 9. Otway basin onshore volcanic provinces: Newer Volcanic Province, Macedon-Trentham Province (MT) and the Older Volcanic Province: Gelantipy (Ge), Bogong (Bo), Toombullup (To), Howitt (Ho), Aberfeldy (Ab), Neerim (Ne), Latrobe (La), Thorpdale (Th), Poowong (Po), Flinders (Fl), Melbourne (Me), Ballan Graben or Bacchus Marsh (Ba) and Gellibrand (Gel), modified from Price et al. (2014).

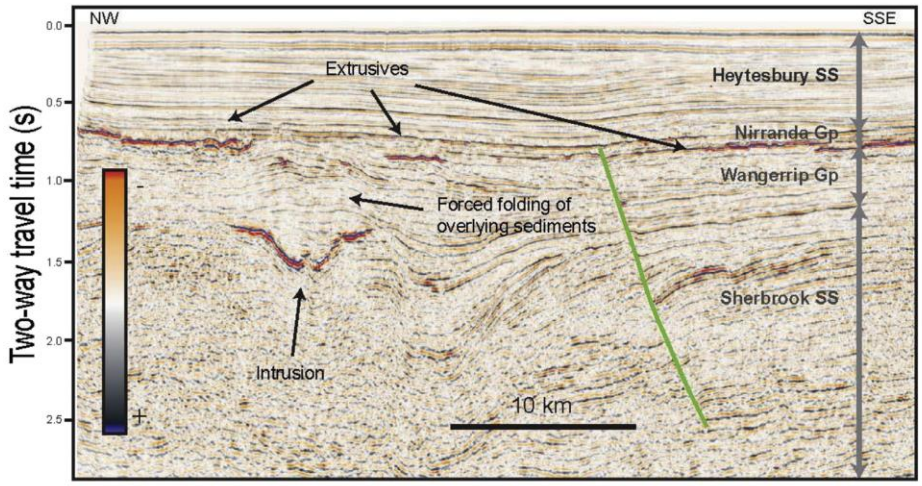

Fig. 10. Examples of magmatic features in the Otway Basin. Location of seismic line in the Champion–Hercules 3D survey is shown in Fig. 5. Note the reverse SEG polarity.

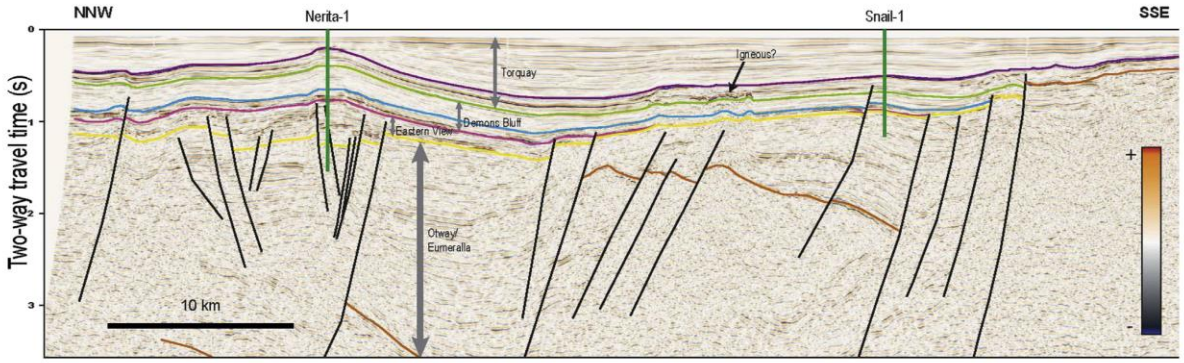

Fig. 11. Seismic line 040-12 (normal SEG polarity). Regional cross-section of the Torquay sub-basin, interpretation modified from Messent et al. (1999), location of seismic line is shown in Fig. 5. The high amplitude feature near Snail-1 is likely an igneous feature; however its intrusive/extrusive character cannot be determined without 3D seismic reflection data.

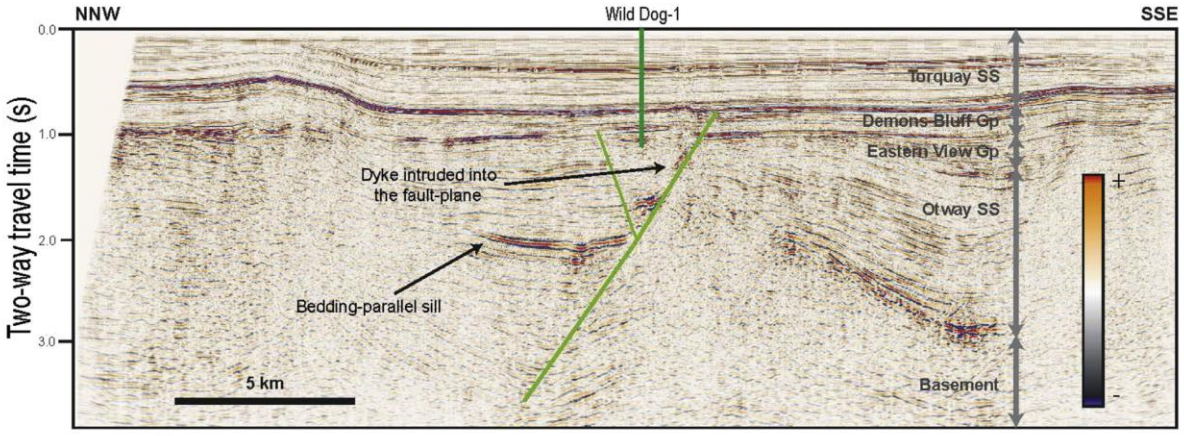

Fig. 12. Seismic line OS90A-13 (normal SEG polarity). Examples of magmatic features in the Torquay sub-basin of the Otway Basin, location of seismic line is shown in Fig. 5.

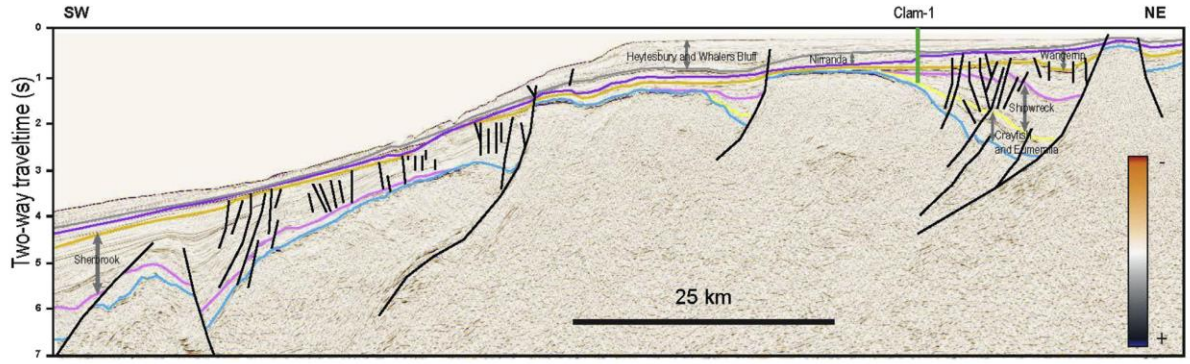

Fig. 13. Seismic line ds01-138 (reverse SEG polarity). Regional cross-section of the Sorell Basin, King Island and Sandy Cape Sub-basins, interpretation modified from Stacey et al. (2013). Location of seismic line is shown in Fig. 5.

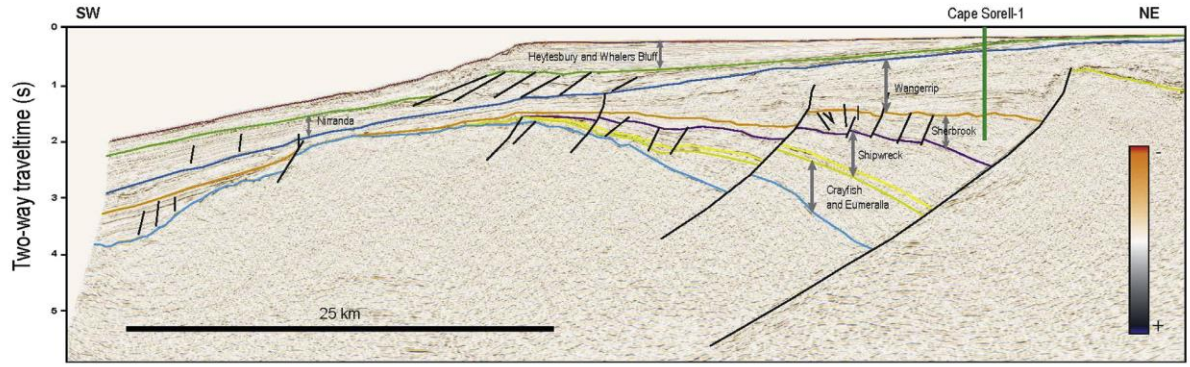

Fig. 14. Seismic line ss04-001 (reverse SEG polarity). Regional cross-section of the Sorell Basin, Strahan Sub-basin, interpretation modified from Stacey et al. (2013). Location of seismic line is shown in Fig. 5.

from the overlying Nirranda Supersequence, consisting of prograding near-shore to offshore marine clastic and carbonate sediments, followed by the cool-water carbonates of the Heytesbury and Whalers Bluff Supersequences (Krassay et al., 2004). This increase in spreading rates caused two transgressive–regressive cycles in the Middle Eocene to Early Oligocene Flinders Supersequence in the Bass Basin, depositing a thick sandstone unit (Boonah Sandstone), a shallow bay siltstone to shale facies

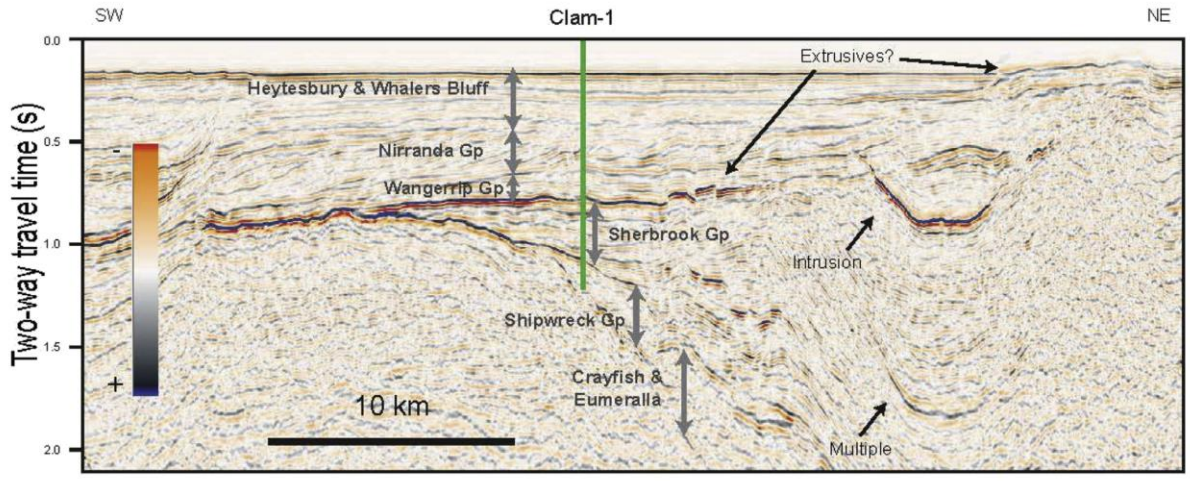

Fig. 15. Part of seismic line 078-05 (reverse SEG polarity). Examples of magmatic features in the Sorell Basin. Location of seismic line is shown in Fig. 5.

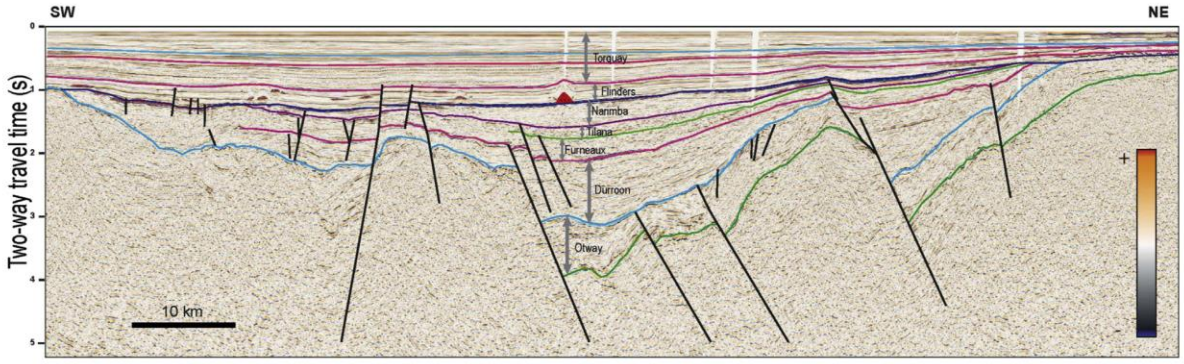

Fig. 16. Seismic line 82–302 (normal SEG polarity). Bass Basin, Durroon sub-basin regional cross-section, note the high amplitude features indicated in red and in the SW of the profile. Interpretation modified from Blevin et al. (2005). Location of seismic line is shown in Fig. 5.

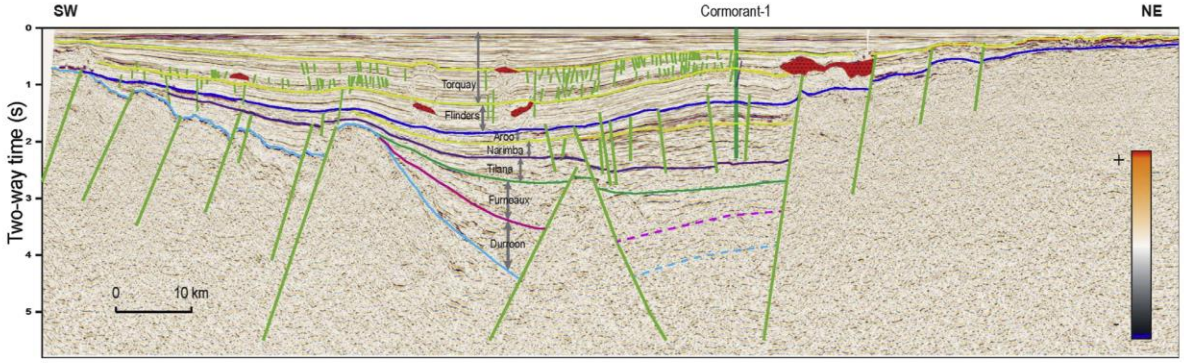

Fig. 17. Seismic line 90-27 (normal SEG polarity). Bass Basin – Cape Wickham sub-basin regional cross-section, with igneous features indicated in red. Interpretation modified from Blevin et al. (2005). Location of seismic line is shown in Fig. 5.

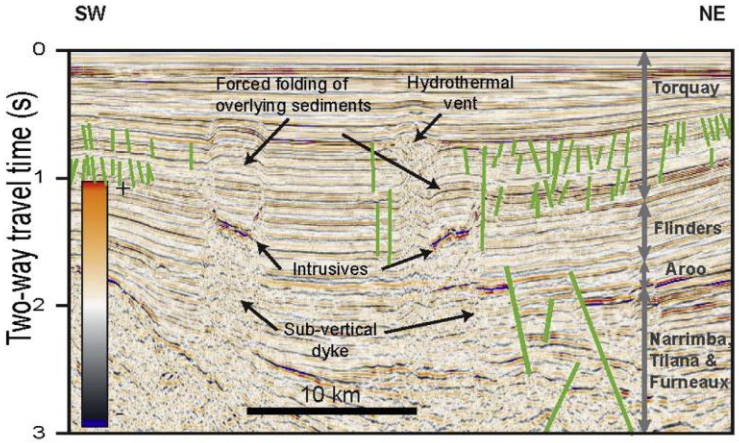

Fig. 18. Example of magmatic features in the Bass Basin, Cape Wickham Sub-basin, close-up from regional cross-section (seismic line 90-27, normal SEG polarity).

(Anglesea Formation), a second sandstone unit (Squid Sandstone) and finally marine carbonates of the Middle Oligocene Torquay Supersequence (Blevin et al., 2005). In the Gippsland Basin, the end of the Latrobe Supersequence is marked by the Latrobe Unconformity, and is followed by the deposition of the Seaspray Supersequence, consisting of increasingly marine carbonates

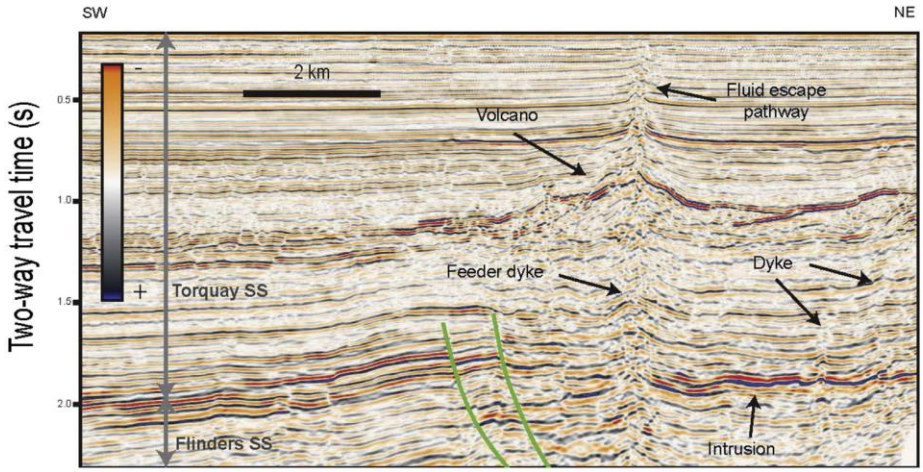

Fig. 19. Example of magmatic features in the Bass Basin near the Yolla Field. Location of seismic line from Yolla 3D survey (reverse SEG polarity) is shown in Fig. 5.

(Rahmanian et al., 1990).

3. Data and methods

This review is based on existing studies, combined with our own seismic interpretations and tectonic subsidence analyses. A comprehensive age-database of Cenozoic volcanism was compiled from Vasconcelos et al. (2008), Gibson (2007) and O'Brien et al. (2008) and maps were constructed showing the age of Cenozoic magmatism in south-eastern Australia. Similarly, an age database was constructed for Tasmanian Cenozoic magmatism and a kernel density plot was constructed using *Densityplotter* (Vermeesch, 2012). It is noted that most of the absolute ages are obtained using the K-Ar dating technique, which is generally less precise than the Ar–Ar dating technique due to analytical procedures and possible masking of retained excess $^{40}Ar^{*}$(Mcdougall and Harrison, 1999; Verati and Jourdan, 2013). Several 2D and 3D seismic reflection survey datasets were used which cover an area of ~134,000 km^2.

Bio-stratigraphic and lithological data from 12 wells located in the Bass Basin (Seal-1, Toolka-1A, Cormorant-1, Koorkah-1, Bass-1, Aroo-1, Yolla-1, Tilana-1, Bass-2, Tarook-1, Squid-1, Flinders-1 and Chat-1) and 3 wells in the Gippsland Basin (Perch-1, Admiral-1 and Kipper-1) were used to calculate tectonic subsidence plots in order to investigate the effect of magmatism on sedimentary infill of the basins (Fig. 24). A backstripping technique based on the method of Watts and Ryan (1976) was used to construct one dimensional (1D), tectonic subsidence and separate it from the effects of water and sediment loading. The tectonic subsidence was predicted assuming Airy isostasy (Jarvis and McKenzie, 1980). The backstripping procedure consists of decompacting each sedimentary layer and removing its load. This process was done twice, with and without correction for relative global sea level changes (Haq et al., 1988). As these global sea level changes were found to enhance artefacts seen in the subsidence plots, plots without global sea level corrections were preferred.

4. Magmatism along the Australian southern margin

Magmatism along the Australian southern margin is widespread and varies through time within the various sedimentary basins. This next section will therefore give an extensive overview of the timing, distribution and type of magmatism per basin, followed with a discussion of the likely causal models in section 5.

4.1. Cenozoic magmatism in eastern Australia

The Australian Cenozoic Magmatic Province is a classic example of an extensive region of mainly mafic intraplate magmatism (Johnson, 1989). With an area of 1.6 million km^2, the region runs parallel to the Australian margin and extends over 4400 km from northern Queensland to southern Tasmania and westwards into Victoria and southeast South Australia (Johnson, 1989). As emphasised in this paper these Cenozoic eruptions were both subaerial and simultaneously into nearby offshore, submarine basins. It is noted by Johnson (2009) that Cenozoic onshore magmatic activity in Eastern Australia mainly occurred in isolated patches following the line of the Great Dividing Range or eastern Highlands – the continental break-up escarpment stretching from north-eastern Queensland through New South Wales into Victoria (Fig. 1).

Within the Australian Cenozoic Magmatic Province, three categories of magmatic features can be recognised; central shield volcanoes, lava-field provinces and leucitite provinces (Wellman and McDougall, 1974). The first category, central shield volcanoes (yellow, Fig. 1), comprises predominantly basaltic flows which give rise to large volcanoes (diameter of 30–100 km, over 2 km high) and are distinguished by the presence of some felsic flows and felsic and mafic intrusions, which were fed from a central vent or clusters of vents. The composition of the shield volcanoes generally consists of slightly undersaturated olivine basalt or hawaiite, and less commonly tholeiitic basalt, mugearite, trachybasalts and trachyte. Igneous rocks of the central shield volcano type occur both east and west of the Great Dividing Range, are generally younger than 35 Ma and show a distinct southward rate of progression of 65 ± 3 mm/year (Wellman and McDougall, 1974). The second type of volcanic feature, the lava-field provinces (red and purple, Fig. 1), consists of thick, mainly basaltic lava flows forming extensive fields or lava piles up to 1 km thick, which are thought to be produced by eruptions of central vents where some are aligned along basement fractures (e.g. Mt Eccles centre, Victoria) (Johnson, 1989). This type of volcanic activity occurred mostly on, or to the east of the Great Dividing Range (green line, Fig. 1) and consists of basaltic lava ranging from strongly silica-undersaturated to saturated tholeiitic lava. This category of feature occurred since 70 Ma and does not

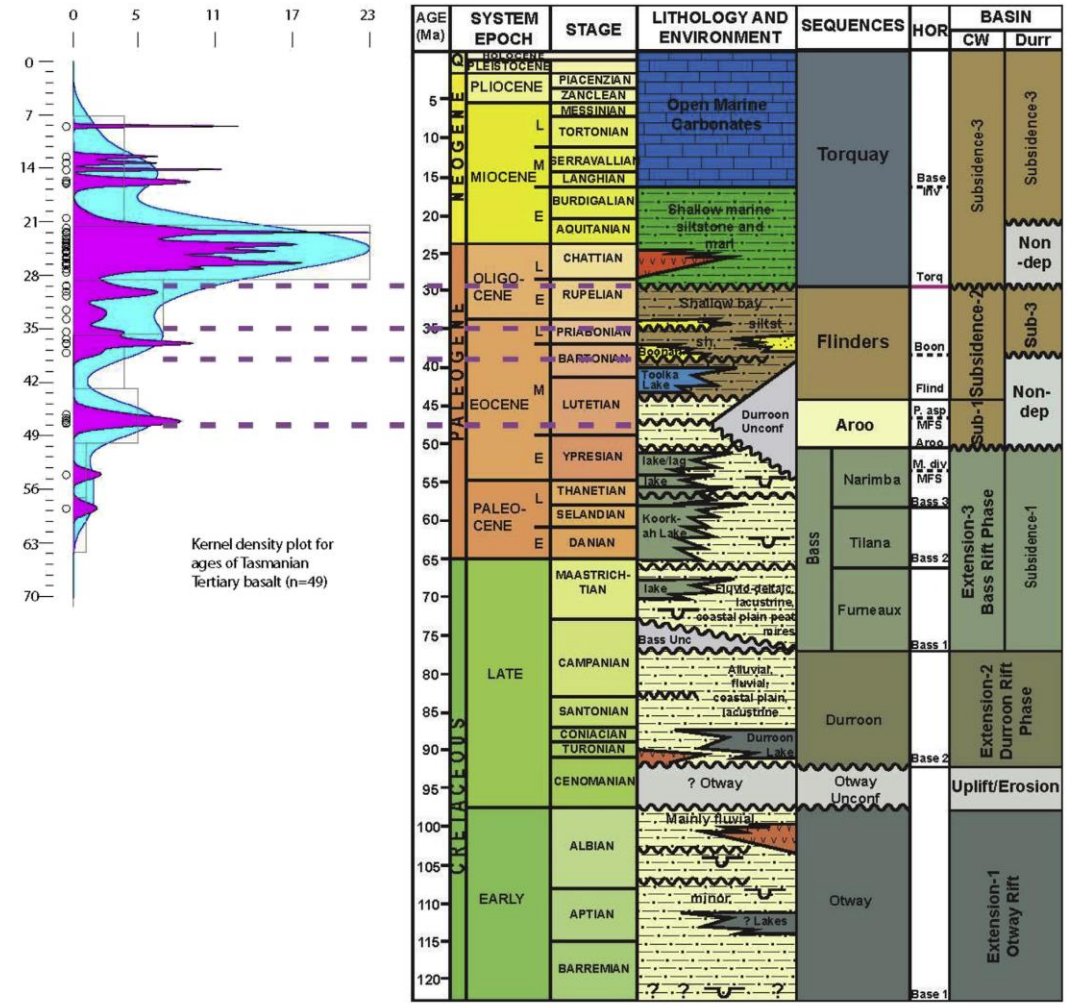

Fig. 20. Right: Generalised stratigraphy of the Bass Basin (after Blevin et al. (2005)). Left: Kernel density plot showing the ages of Tasmanian Tertiary basalt (compiled from Vasconcelos et al. (2008), Gibson (2007), modelled with *Densityplotter* by Vermeesch (2012)).

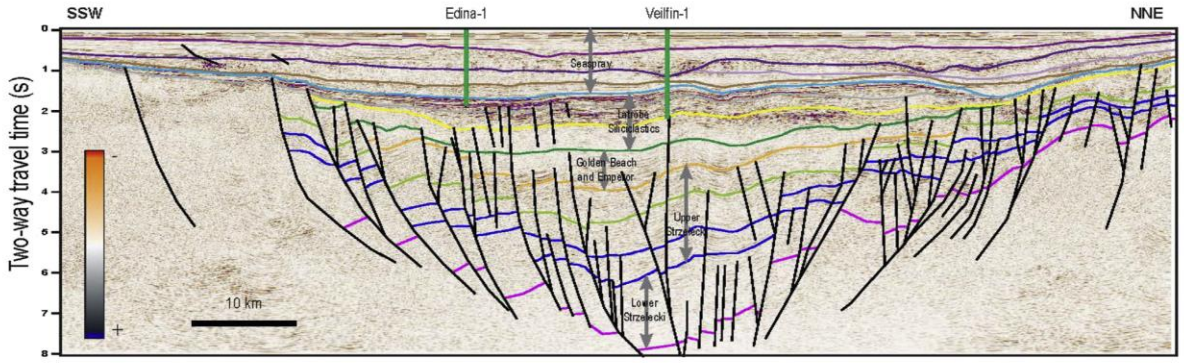

Fig. 21. Seismic line 90-07 (reverse SEG polarity). Regional cross-section of the Gippsland Basin, interpretation modified from Power et al. (2001). Location of seismic line is shown in Fig. 5.

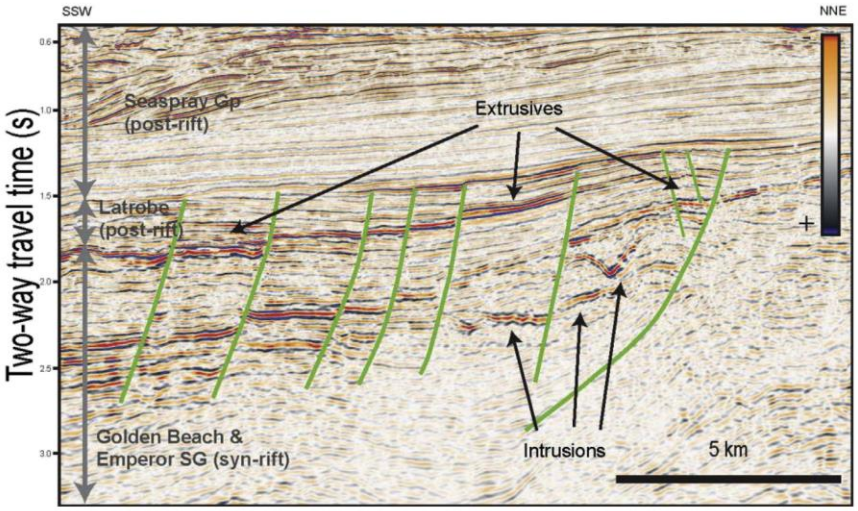

Fig. 22. Examples of magmatic features in the Gippsland Basin near the Kipper Field. Location of seismic line in 3D survey g01a (reverse SEG polarity) is shown in Fig. 5.

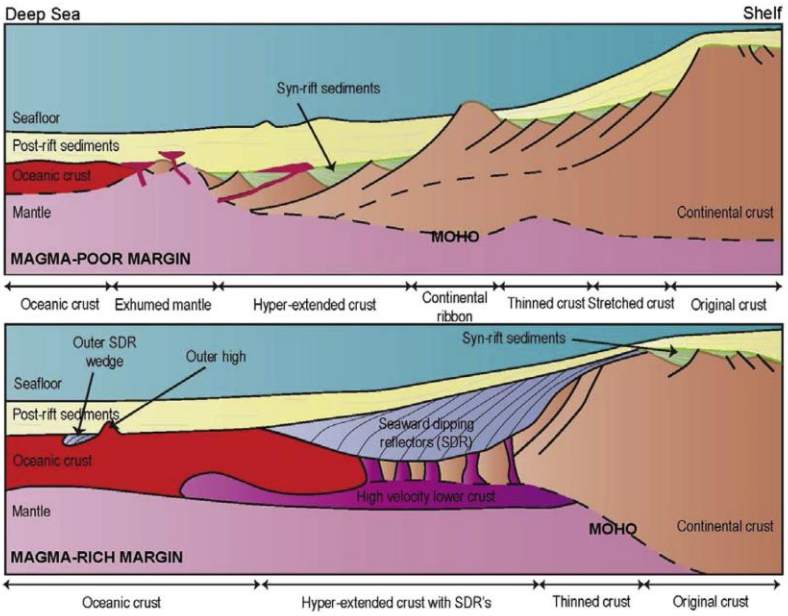

Fig. 23. Schematic comparison of magma-rich and magma-poor margins (modified from Franke (2013); Zalan (2014)).

show any clear temporal–distribution relationship with the youngest rocks occurring both in the north (north Queensland: 50 Ka) and south (South Australia: 5 Ka) of the volcanic belt (Wellman and McDougall, 1974). The third type, the less extensive leucitite suite (orange, Fig. 1), consists of mafic rocks that are very potassium-rich and which contain phlogopite, magnophorite or leucite as crystals or pseudomorphs (Wellman and McDougall, 1974). This category of features was confined to small vents that erupted only once, emplacing mainly lava flows and domes with minor scoria deposits and two volcanic plugs (Cundari, 1973). The leucitite provinces have been emplaced between 18 and 6.77 Ma and show a similar southward younging trend and rate as the central volcano category (Cohen et al., 2008; Wellman and McDougall, 1974).

In addition to the onshore magmatic activity, three distinct seamount chains (green, Fig. 1) can be recognized offshore eastern Australia. The first seamount chain is the Tasmanian Seamount Chain, which has an east–west orientation on the Lord Howe Rise and a northeast-southwest orientation on the Australian side of the Tasman Sea spreading ridge (Fig. 1). It contains the oldest dated seamounts in the Tasman Sea, the Zeehan and Heemskirk Seamounts, which span an age range between 71.3 and 59.1 Ma

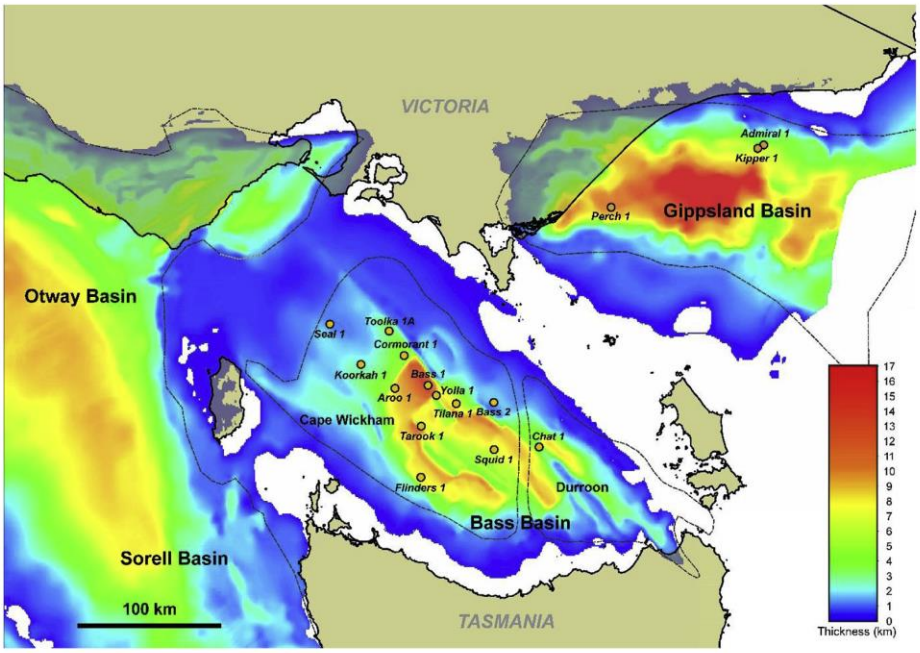

Fig. 24. Location of wells used for subsidence analyses in the Bass and Gippsland Basin. Coloured background represents the sediment thickness as calculated from SEEBASE (Teasdale, 2004).

(Jenkins et al., 1992). These seamounts consist of basalt and together with subsequent seamounts dated at 60–50 Ma and 36 Ma, form part of the Tasmanian Seamount Chain (Jenkins et al., 1992). Although not many ages are available for the Lord Howe Rise section, this seamount chain shows a younging trend towards the south-west in the Australian section of the chain. Further northwards in the Tasman Sea, the second seamount chain or Tasmantid Seamounts or Guyots extend over 1300 km along a north-south directed line of submarine volcanoes. They are situated on top of and post-date oceanic lithosphere that formed 80–50 Ma ago during the spreading of the Tasman Sea. These seamounts show a clear age progression, with the oldest in the north (Queensland Seamount; K-Ar: 20.9 Ma, Ar–Ar: 24.3 Ma) and the youngest in the south (Gascoyne Seamount; K-Ar: 6.4 Ma, Ar–Ar: 6.9–7.2 Ma) (McDougall and Duncan, 1988). These seamounts exhibit an average rate of southward younging of 67 ± 5 mm/year, similar to the onshore central volcanoes and leucitite provinces (McDougall and Duncan, 1988). A third seamount chain, parallel eastwards to the Tasmantid Seamount Chain, is the Lord Howe Seamount Chain which shows a similar north-south trend and overlies thinned lithosphere of the Lord Howe Rise. This chain stretches over 1000 km northwards from Lord Howe Island which consists of alkaline basalts aged 6.9–6.4 Ma (McDougall et al., 1981). With the additional dating of a trachyandesite (although classified as trachyte by present authors) of the Middleton Reef seamount at 12.1 Ma, a rate of 57 mm/year was assigned to the southward motion of magmatic activity of the Lord Howe Chain (Mortimer et al., 2010). This rate is again very similar to the rate of the Tasmantid Seamount Chain for the Miocene (Gaina et al., 2000). It is noted that further to the east of the Lord Howe Rise, similar volcanic chains such as the Norfolk Ridge and the Loyalty Chain have been observed towards New Zealand (Exon et al., 2004), these will however not be discussed here. It is worth nothing that in addition to these seamount chains a Large Igneous Province exists along the eastern Australian plate margin, called the Whitsunday LIP (Ernst, 2014). This LIP is of Early Cretaceous age, is more than 2500 km long and consists of silicic-dominated pyroclastic volcanic rocks (Bryan and Ferrari, 2013). The emplacement of the LIP preceded the start of large-scale continental rifting in the middle Cretaceous, which scattered the remains of the LIP and leaving only part of the province intact (Bryan and Ferrari, 2013).

Several models have been proposed towards the formation of the Eastern Australian Cenozoic Magmatic Province which will be discussed in section 5.3.

4.2. Cenozoic magmatism in the Bight Basin

The Bight Basin is a large (>800,000 km^2), east–west to northeast-southwest trending, mostly offshore basin, off the coast of West and South Australia. The basin extends 400 km onshore to the north from the present-day coastline and is bounded to the north by a major continental basement fault and monocline that marks the northern limit of thick Mesozoic strata (Bradshaw et al., 2003). To the south, where water depths can reach >5 km, the basin is bounded by ultramafic rocks, seafloor basalts and oceanic sediments of the Southern Ocean, which are thought to represent the continent-ocean boundary (COB) (Totterdell and Bradshaw, 2004). The basin contains five depocentres; the Ceduna, Duntroon, Recherché, Eyre, Bremer and Denmark sub-basins (Fig. 5), which formed during Middle-Late Jurassic to Early Cretaceous NS to NW–SE upper crustal extension related to break-up of eastern Gondwana (Totterdell and Bradshaw, 2004) which resulted in continental break-up at 83 Ma (Sayers et al., 2001). Following the major extensional phase in this basin, large amounts of sand and shale accumulated during Late Cretaceous deltaic progradation which in turn caused gravity-driven extensional and compressional

deformation along the basins southern margin (Holford et al., 2011). A regional cross-section of the Bight Basin is shown in Fig. 6.

Volcanic rocks in the Bight Basin were first recorded by Fraser and Tilbury (1979) as they interpreted mounds showing strong reflectors in early seismic studies and have later been confirmed by dredging of alkali basalt lava by Davies et al. (1989). Subsequent reporting (Jackson, 2012; Magee et al., 2013b; Schofield and Totterdell, 2008) has shown that volcanism mainly occurs in a northwest southeast oriented igneous field in the Ceduna sub-basin, called the Bight Basin Igneous Complex (BBIC), which covers a 130 km wide area of 10,000 km^2 (Schofield and Totterdell, 2008). Additional smaller incursions of apparently similar ages have been recognized in the Eyre and Duntroon sub-basins, extending the potential width of the province to over 650 km (Schofield and Totterdell, 2008). Additionally, Holford et al. (2012) noted that new seismic data of the deep-water parts of the western Bight Basin (the Recherché sub-basin) show evidence for extensive intrusive and intrusive activity, some of which is exploiting large compressional thrust-faults of the deep-water fold-thrust belt at the toe of the late Cretaceous Ceduna delta system, as opposed to the habitual extensional normal faults.

In the Ceduna sub-basin, more than 30 sills, laccoliths, dykes, volcanic cones and lava flows have been documented (Jackson, 2012; Schofield and Totterdell, 2008). Volcanic cones have been recognized both in seismic and in bathymetry data, ranging from less than 2 km–11 km in base diameter and up to 500 m high (Jackson, 2012; Schofield and Totterdell, 2008). Dredge samples of volcanic cones which protrude from the ocean floor have shown that they consist of amygdaloidal, possibly pillowed, basalts (Davies et al., 1989) and based on seismic velocity studies, they are believed to consist of a mixture of igneous and sedimentary material, rather than pure igneous material (Jackson, 2012; Magee et al., 2013b). However, previous studies (Faustmann, 1995) of seismic velocities in the Bass Basin have shown that significant variability of seismic velocities in volcanic complexes can be attributed to facies changes going from basalt to pyroclastic products such as scoria or tuff. It has been proposed that the volcanic vents have been fed by underlying sills or normal faults acting as magma conduits (Jackson, 2012) and are associated with large lava flow aprons, however, fissure-style eruptions, independent of volcanoes, also occur (Schofield and Totterdell, 2008). Sills and dykes range in morphologies from common simple sheet-like or tabular structures to domal and 'saucer' shaped morphologies (Schofield and Totterdell, 2008). These sills and dykes have intruded various levels of the late Santonian – Maastrichtian (~83–66 Ma) Hammerhead Supersequence and some at the top Turonian – Santonian (~91–83 Ma) Tiger Supersequence, implying a post-Maastrichtian age of intrusion (Schofield and Totterdell, 2008). Similarly, a Middle Eocene age has been implied for the extrusive features in this area, as they all have their basal contact on the unconformity at the base of the Middle Eocene to Pleistocene Dugong Supersequence (Schofield and Totterdell, 2008). Examples of magmatic features and forced folding structures, used to date intrusive sills, in the Ceduna sub-basin of the Bight Basin are shown in Fig. 7.

As noted by Schofield and Totterdell (2008), timing of volcanic activity is broadly coincident with a series of important tectonic reconfigurations in the region that occurred during the mid-Eocene. These include the cessation of spreading in the Tasman Sea and along the Wharton Basin Ridge in the Indian Ocean; the onset of accelerated seafloor spreading in the Southern Ocean, which began at 43 Ma (Holford et al., 2011; Veevers et al., 1991); a kink in the Emperor-Hawaii seamount chain; and the India-Eurasia collision and plate rearrangements in New Zealand creating the Challenger Rift System (Veevers, 2000). Schofield and Totterdell (2008) conclude the magmatic drivers to be of a 'tertiary' hotspot as described by Courtillot et al. (2003) since the magmatic features are located within 300 km of the margin of the Gawler Craton and the NW distribution of features parallels this margin. These 'tertiary' hotspots possess a superficial origin, caused by tensile stresses in the lithosphere and decompression melting (Courtillot et al., 2003). The combined effect of the topographic step at the base of the Australian plate and the fast northward movement of the plate may have caused edge-driven convection cells in the upper mantle. As discussed in section 5.3, the existence of similar edge-driven convection cells has been invoked to explain the origin of the Newer and Older Volcanic Provinces in Victoria (Demidjuk et al., 2007; Price et al., 2014).

4.3. Cenozoic magmatism in the Otway Basin

The Otway Basin is a large, broadly NW–SE trending basin, containing both onshore and offshore parts of South Australia and Victoria and extends into Tasmanian waters (Fig. 1). Covering an area of 150,000 km^2, it originated by N–S Late-Jurassic extension, associated with the opening of the Southern Ocean and has seen break-up at 67 Ma (Krassay et al., 2004; Stagg et al., 1990). The Basin contains five major depocentres: the mainly onshore inner Otway Basin, the offshore Morum, Nelson and Hunter Sub-basins and eastern Torquay Sub-basin. The basin overlies deformed Cambrium-Ordovician basement rocks, is bounded by Palaeozoic and Proterozoic basement rocks in the north, northeast and east, and continues into the Sorell Basin to the southeast (Moore et al., 2000). A comprehensive overview of the tectonostratigraphy has been given in section 2 and a regional cross-section of the eastern Otway Basin is shown in Fig. 8.

4.3.1. Cenozoic magmatism in the onshore Otway Basin

Volcanic activity onshore the eastern Otway Basin is widespread and ranges from Jurassic to Recent age (4600 years) (Fig. 5) (Price et al., 2014). Evidence for Jurassic to Early Cretaceous (210–90 Ma, McDougall and Wellman (1976)) volcanic activity exists in surface outcrops in western Victoria (Price et al., 2014), a breccia pipe in central Victoria and alkali dykes in central and eastern Victoria (Price et al., 2014). Volcanic activity of this age is thought to be directly related to the early rifting caused by separation of Antarctica from Gondwana (Holford et al., 2012). Subsequent volcanic activity started around 95 Ma, continued through the Cenozoic with major breaks from 77 to 52 Ma and 18 to 7 Ma with the youngest rocks emplaced about 5000 years ago (Gray and McDougall, 2009; Price et al., 2014; Vasconcelos et al., 2008). The volcanism in this area has been subdivided into three groups: the Older Volcanics (95–19 Ma), the Newer Volcanics (7.8 Ma – 4500 years) and the Macedon – Trentham group (10–4.6 Ma) (Edwards et al., 2004; Gray and McDougall, 2009; Wellman and McDougall, 1974).

The Older Volcanics group (green, Fig. 9) is distributed as monogenetic lava fields, across eastern and central Victoria, and as shallow dykes, plugs and sills in the western part of Victoria (Price et al., 2014). Based on their geographical distribution, geochronology and petrology, they have been divided into a number of provinces and sub-provinces, each representing a geographic entity comprising lava-field remnants, monogenetic cones and/or shallow intrusions (Gelantipy, Bogong, Toombullup, Howitt, Aberfeldy, Neerim, Latrobe, Thorpdale, Poowong, Flinders, Melbourne, Ballan Graben and Gellibrand; Price et al. (2014)). As described by Price et al. (2003), their composition varies from nephelinites, SiO_2-undersaturated basanites, basalts and hawaiites through transitional basalts to hypersthene and quartz normative tholeiites. Although some provinces have become more alkaline or increasingly fractioned during their lifespan, no clear relationship exists between

their composition and their age or location.

The Newer Volcanics group (orange, Fig. 9) is part of the previously described lava-field type and primarily occurs in western Victoria with the exception of a basalt outcrop of estimated 4 to 2 Ma age in eastern Victoria (Wellman, 1974). From east to west, the Newer Volcanics Province (NVP) can be subdivided into the Central Highlands (covering Palaeozoic metasediments and granite), Western Plains (covering Otway Basin fill) and Mt. Gambier subprovinces (covering Gambier Embayment sediments, metasediments of the Delamerian Orogeny and Otway Basin sediments) (Boyce et al., 2014). The southern margin of the NVP is marked by the Colac Lineament (Gambier-Gabon Lineament of Carey, 1986) and is controlled by faulting (Price et al., 1997). More than 416 volcanic centres have been recognized, with 54% located in the Central Highlands, 42% in the Western Plains and 6% in the Mt Gambier area (Boyce et al., 2014). These eruption centres consist of small scoria cones, lava shields, maars, ash cones and domes, and more complex larger edifices with multiple overlapping eruption points and volcanic complexes combining aforementioned features (Boyce et al., 2014). Lithologies range from primitive nephelinites and picrobasalts in the Mt. Gambier region (Foden et al., 2002), to scattered occurrences of basanites, sodic and potassic trachybasalts, alkali basalts and more evolved tholeiites, basaltic trachyandesites and phonotephrites (Van Otterloo et al., 2014). Studies in the South Australian Quaternary Basalt province (SAQB; Holt et al. (2013)) combining geochemical and reflection seismic data have shown that the magma that fed the SAQB was generated by adiabatic decompressional melting at pressures from about 4 to 3 GPa, corresponding to the uppermost asthenosphere, cooled 200 °C and underwent 34–41% fractional crystallisation during its ascent.

The Macedon-Trentham group (blue, Fig. 9) is located in the western highlands and consists of a group of small flows, domes and small intrusions of differentiated rocks, which underlie the NVP. These rocks range in composition from hawaiite through mugearite to trachyte and nepheline-bearing equivalents and are closer in geochemistry to the central type volcanic provinces located in New South Wales and Queensland and include the presence of a major component of felsic intrusions (Paul et al., 2005). K-Ar whole rock and potassium feldspar ages and Rb-Sr whole rock ages range between 10 and 4.6 Ma (Wellman, 1974).

4.3.2. Cenozoic magmatism in the offshore Otway Basin

Offshore volcanic features in the Otway Basin have been recognised and described by Holford et al. (2012). Examples of magmatic features in the Otway Basin are shown in Fig. 10. It has been found that igneous features occur diffusely throughout the basin, with the greatest concentration ca. 160 km off the coast between Portland and Cape Otway. Based on the interpretation of seismic reflection data, they identified lava aprons, small sills and possible hydrothermal vents. Many of the extrusive features occur in the latest Maastrichtian to Middle Eocene Wangerrip Group or near the top Wangerrip Group, intra-Lutetian age conformity, while sills have mostly intruded into the Wangerrip Group and some larger sills into the Upper Cretaceous Sherbrook Group, suggesting an early to mid-Eocene age (Holford et al., 2012; Schneider et al., 2004). This timing is largely consistent with peaks in onshore Otway Basin volcanism reported earlier occurring between 45 and 37 Ma (Price et al., 2003). Offshore, about 30 km south-west from Cape Otway, submerged volcanoes have been described based on bathymetry and recovery of basalt boulders by Gill and Segnit (1986) and have been confirmed by grab-samples of olivine basalt on the later BMR Cruise 67 (Exon et al., 1992). No absolute ages exist for these submerged volcanoes, however, based on petrological and geochemical similarities with the onshore Newer Volcanic Province, a probable age of Upper Pliocene has been proposed (Gill and Segnit, 1986).

4.3.3. Cenozoic magmatism in the Torquay sub-basin

The Torquay sub-basin is primarily located offshore and forms part of the eastern Otway Basin (Trupp et al., 1994). It extends from the Otway Ranges in the west and north to the King Island – Mornington Peninsula High in the east, which separates it from the Bass Basin to the southeast (Trupp et al., 1994). Its infill is mainly dominated by typical Otway Group volcanoclastic sediments, however, the regional mid-Cretaceous unconformity is overlain by a Cretaceous – Tertiary section equivalent to that of the Bass Basin (Trupp et al., 1994). A regional cross-section for the Torquay Sub-basin is shown in Fig. 11.

Within the Torquay sub-basin, volcanic features are recognized as part of the Angahook Member in the Demon's Bluff Formation and they are exposed in coastal cliffs and platforms extending from Airey's Inlet to Urquharts Bluff (Cas et al., 1993). Volcanic features in this area comprise remnants of the Airey's Inlet Volcanic Complex which consists of intrusive and extrusive basalts, hyaloclastites, pyroclastic lapilli-tuffs, tuffs and locally agglomerate and mass-flow resedimented and reworked volcanic sediments (Cas et al., 1993). Basalts have been dated by K-Ar (25.7 ± 0.4 Ma and 27.6 ± 0.6 Ma; Abele and Page (1973)) and $^{40}Ar/^{39}Ar$ isotope systems (28.7 ± 0.2 Ma; McLaren et al. (2009)), indicating mid-Oligocene volcanic activity. Both intrusive and extrusive rocks have been recognized in the offshore part of the sub-basin and are thought to be of early Oligocene age (Messent et al., 1999), which is consistent with onshore ages. Some of the sills show saucer-shaped geometries and have large diameters (up to 5 km in diameter), causing overlying sediments to fold (Holford et al., 2012). One of the largest intrusions is observed near the Wild Dog-1 well (Holford et al., 2012). As shown on Fig. 12, it intrudes the Lower Cretaceous Eumeralla Group sediments and consists of a concave upwards saucer-shaped sill, which transforms into an inclined dyke as it intersects and exploits a large northwest-dipping fault as a conduit (Holford et al., 2012).

4.4. Cenozoic magmatism in the Sorell Basin

The Sorell Basin is located offshore along the margin of western Tasmania and is the least explored basin along the Australian southern margin, with only three hydrocarbon exploration wells drilled to date. It comprises a series of north-northwest trending transtensional depocentres: King Island, Sandy Cape, Strahan, Port Davey, Toogee and two unnamed sub-basins. Sediment thicknesses vary significantly between these sub-basins and are thought to reach more than 6.5 km in the Strahan sub-basin (Boreham et al., 2002). Similar to the other Mesozoic basins of the Australian southern margin, the Sorell Basin initiated as part of the Southern Rift System in the Late Jurassic to Early Cretaceous (Boreham et al., 2002). While break-up occurred around 83 Ma in the Bight Basin (Sayers et al., 2001), the Otway-Sorell region only started spreading in the early Middle Eocene, creating a narrow, restricted seaway along western Tasmania during the Middle to Late Eocene (Boreham et al., 2002). A regional cross-section of the Sorell Basin is shown in Figs. 13 and 14.

Although seismic data is sparse in the Sorell Basin, magmatic features have been recognized on seismic data and have been dredged during several cruises in the area (Exon et al., 1994, 1992, 1995). Igneous intrusions within the lower part of the Upper Cretaceous Shipwreck Supersequence and Sherbrook Supersequence (Fig. 15) and Palaeocene flows in the King Island Subbasin have been interpreted as being formed coevally with Maastrichtian-Palaeocene strike-slip faulting along the west Tasmanian margin (Hill et al., 1997). However, a younger, more

extensive phase of basaltic magmatism is recognized as widespread flows in a shallow Late Cenozoic section, which have been correlated to the extensive basaltic fields occurring onshore north-west Tasmania (Hill et al., 1997). Towards the central and southern part of the Sorell Basin, igneous intrusions have been found to invade presumed continental blocks adjacent to the continent-ocean boundary (COB) and presumed basaltic flows are found in the Late Tertiary section beneath the shelf near the Strahan and Port Davey Sub-basins (Hill et al., 1997). It is noted that south of the Sorell Basin, along the southern Tasmanian margin, numerous (>100) volcanic cones (500–600 m high) of presumed Tertiary age based on affinities with Tertiary Tasmanian basalts, have been identified in the Tasmanian Seamounts Marine Protected Area (Hill et al., 2001).

4.5. Cenozoic magmatism in the Bass Basin and onshore Tasmania

4.5.1. Cenozoic magmatism in the offshore Bass Basin

The Bass Basin is located offshore between the mainland of Australia and Tasmania and includes the Tamar Graben, and spans an area of 42,000 km^2 (Fig. 1). It is separated by two basement structural highs from the Otway Basin to the west and northwest by the King Island High, and separated from the Gippsland Basin to the northeast by Flinders Island and the Bassian Rise.

In contrast to the Otway and Gippsland basins, the Bass Basin has not seen any continental break-up or seafloor spreading due to an abrupt shift in the locus of extension to the south of Tasmania, preventing it from progressing into a passive margin basin (Blevin et al., 2005). The overall structural style of the Bass Basin ranges from a graben to half-graben structure, with tilted Palaeozoic and Proterozoic basement blocks, showing large scale offset along NE and SW dipping normal faults (Blevin et al., 2005). Based on this structural style, the Bass Basin can be sub-divided into two sub-basins; the Durroon Sub-basin in the eastern part and the Cape Wickham Sub-basin in the western part of the Bass Basin. The tectonostratigraphy of the Bass Basin has been addressed by several studies (Blevin, 2003; Blevin et al., 2005; Smith, 1986; Veevers et al., 1991) and is presented in Fig. 3 and a regional cross-section through both depocentres are shown in Figs. 16 and 17.

The presence of igneous rocks in the offshore Bass Basin has been reported by several authors (Baillie and Brown, 1984a, b; Blevin, 2003; Holford et al., 2012), with many of the offshore wells penetrating both intrusive and extrusive rocks, particularly in the southern and western parts of the basin. Bass-1 for example, one of the first wells drilled in the offshore Bass Basin was intended to target a carbonate reef, however, intersected a volcano (Blevin, 2003). These wells show that the basin has seen several phases of volcanism, associated with large-scale faults and accommodation zones (Blevin, 2003). The earliest presence of volcanic rocks is expressed as Early Cretaceous volcaniclastic sediments (Otway Megasequence, Fig, 3), which have been suggested to be derived from ignimbritic volcanoes in the Whitsunday Volcanic Province (Bryan et al., 1997; Bryan and Ferrari, 2013). This unit is comparable to the Otway Group and Strzelecki Group in the Otway and Gippsland basins respectively, illustrating the large volume of volcanic sediment input into the Bass Strait region (Norvick and Smith, 2001). Over 100 m of Middle Cretaceous Volcanics (Otway and Durroon Megasequence, Fig. 3) have been intersected in the Durroon-1 well, consisting of highly weathered, amygdaloidal basalt, interbedded with sediments of Aptian age (Blevin, 2003). Middle Cretaceous Volcanics are expressed as flows, mounds, and cones, associated with large normal faults, suggesting an origin related to the onset of rifting in the Tasman Basin (Blevin, 2003). They are mainly situated in the Durroon sub-basin, however, the extent of these features is poorly constrained to the west of the Durroon sub-basin, due to lack of well control and poor seismic resolution (Blevin, 2003). A subsequent phase of volcanism of Late Cretaceous to Palaeocene age (Bass Megasequence, Fig 3), has been demonstrated with lavas recovered from Aroo-1, Bass-2, Chat-1, Tilana-1, Yolla-1 and Yolla-2 wells and intrusive rocks from Cormorant-1 in the central and northeastern parts of the Bass Basin (Fig. 18). The spatial extent of this volcanic phase is poorly constrained due to the presence of overlying coals in the Bass Megasequence, hindering the interpretation of seismic reflections (Blevin, 2003). The composition of the mostly amygdaloidal basaltic flows range from alkali olivine basalt, to basanite and picrite and have undergone varying degrees of alteration, challenging their absolute dating (Blevin, 2003). However, Dunlap (2003) was able to date whole rock and mineral separates from limited samples in Chat-1, Aroo-1, Koorkah-1, Yolla-1 and Tilana-1 wells (73–18 Ma; Table 1), which corroborates with dating of palynofloras from within the volcanic suite have placed the volcanics to constrain the volcanics as late Cretaceous to Palaeocene (Baillie, 1993).

The most extensive and most recent period of volcanism during the Oligocene to Miocene (Torquay Megasequence) was coincident with strike-slip reactivation and inversion within the Bass Basin and is expressed as volcanic mounds, vents, lava flows and intrusive sills and dykes (Blevin, 2003; Cummings et al., 2004; Lennon et al., 1999). Faustmann (1995) reported several large Miocene volcanic mounds in the vicinity of Bass-1, Yolla-1 and Cormorant-1 wells, located along active faults that acted as feeder conduits. Based on in-depth seismic analysis, he deduced that they consist of scoria cones and maar volcanoes, analogous to extrusive complexes such as Mt. Eccles and Tower Hill found onshore. Additionally, Faustmann (1995) observed significant variability in seismic velocities in the large Oligocene-Miocene volcanic complex overlying the Yolla Field (Fig. 19) and attributed them to facies changes from basalt to scoria to tuff. Several mafic intrusions of Miocene age have been intersected by a number of wells and are assumed to have fed the shallower volcanics present in Eocene units (Cummings et al., 2004). Magma transport along these faults is indicated to have taken place along some of the reactivated Palaeocene faults, but most of the volcanic material was extruded along north-south trending Late Oligocene fault systems (Lennon et al., 1999).

4.5.2. Cenozoic magmatism in onshore Tasmania

Onshore, south of the Bass Basin, the Cenozoic Tasmanian igneous rocks form the southern insular end of the Australian

Table 1
Radiometric ages of igneous rocks in the Bass Basin.

Well name and sample depth	Age	Comments
Chat-1 (3030 m)	>167 Ma	Eruption age
Aroo-1 (3596.91 m)	63–73 Ma	
Koorkah-1 (2098–2128 m)	32–40 Ma	
Yolla-1 (2597–2624 m)	24.2 Ma	Some alteration of biotite is possible
Tilana-1 (2172–2193 m)	17.9 Ma	Possibly older than 22 Ma
Peejay-1 (2083–2086 m)	42.46 Ma	Whole rock K-Ar age

Cenozoic volcanic belt. These volcanic rocks are dominantly basaltic lavas and are widespread in Tasmania, covering 6% of the Tasmanian land surface, equivalent to 40,000 km^2 (Sutherland et al., 2004). They are exposed over the biggest part of the mainland of Tasmania (Fig. 1), with the greatest density in the northwest, and are absent in south-western Tasmania, where older basement rocks surface (Sutherland et al., 2004). Together with the offshore Bass Basin basaltic intervals, the north-western part of Tasmania holds the most important basaltic extrusion in the wider Tasmanian province. Radiometric ages range from 8.5 Ma (Baillie, 1986a, b) to 62 Ma (Sutherland et al., 2002), but the age distribution cannot be readily ascribed to any plume or hotspot beneath the northward-moving Australian plate as ages are randomly distributed rather than showing a clear younging direction from north to south. The north-western part of Tasmania is dominated by a remnant lava plain with stepped margins and protruding peaks of underlying basement rocks (Collins et al., 1981). Here, ancient valley terrains are in-filled with lava which can reach thicknesses of up to 360 m with many of these valleys extending into the Bass Strait (Sutherland et al., 2004). These marine–lava interactions create many aquagene volcanic intervals similar to the marine–lava interactions observed within Bass Basin sequences (Sutherland, 1980). East of the Tamar Graben, northern Tasmania, northward draining river courses are in-filled with confined lavas, now visible as narrow strips on the land surface (Sutherland et al., 2004). Further to the east, the basalts extend over sediments in flat valley floors in the northern Midlands, while in the southern Midlands, limited flows form inverted caps accompanied by numerous small intrusions, associated with narrow rift structures (Forsyth, 1984, 1989). The lavas in central Tasmania were erupted onto the central plateau and form a source for extensive flows that descended south into the Derwent drainage and into the Great Lake (Sutherland et al., 1973). In south-eastern Tasmania, the sequences are thinner and wider and occupy low lying rifted troughs (Leaman, 1976). Elsewhere, the basalts consist of limited flows, capping underlying sediments and often creating inverted relief and include numerous necks and intrusive bodies (Sutherland et al., 2004). In addition to the Cenozoic volcanic features, a small portion of Cretaceous igneous rocks exists, which consist of small dykes, related sub-volcanic intrusions and occasional flow remnants with very different geochemistry than their Cenozoic equivalents (Bottrill et al., 2014). The Large Igneous Province containing the Jurassic dolerites in Tasmania will not be discussed here (Ernst, 2014; Storey et al., 2013).

There appears to be a timing relationship between the ages of the Tasmanian Cenozoic basalts and unconformities in the basin evolution of the Bass Basin. Fig. 20 demonstrates this link by showing the timing of unconformities in the Bass Basin (Blevin et al., 2005) and peaks in Tasmanian Cenozoic igneous activity. At first sight, periods of peak magmatic activity seem to follow the reported unconformities in the Bass Basin. However, more detailed research is needed into the cause and timing of these unconformities to be able to explain the link with magmatism onshore Tasmania.

4.6. Meso-Cenozoic magmatism in the Gippsland Basin

The Gippsland Basin is located 200 km east of the city of Melbourne, spans an area of 46,000 km^2 and is located for two thirds offshore (Figs. 4–5). It is bounded to the north by Palaeozoic basement of the Eastern Uplands, to the west by uplifted Lower Cretaceous fault-blocks and to the southwest by the Bassian Rise. The basin initiated as a result of rifting and subsidence along the southern margins of Australia during the Jurassic to Early Cretaceous and was affected by a renewed period of incomplete rifting of a branch of the Tasman Sea (Ollier, 1995). As a consequence, it shows an east–west trend, similar to the basins to the west (Norvick and Smith, 2001). The initial architecture of the basin during the Early Cretaceous consisted of a rift valley complex, which broadened into the Central Deep by continued rifting into the Late Cretaceous, flanked by fault-bounded platforms and terraces to the north and south (Fig. 21) (Power et al., 2001). After a period of post-rift subsidence, a compressional event started during the late Eocene and peaked during the middle Miocene, giving rise to a series of northeast to east-northeast-trending anticlines and which resulted in partial basin inversion (Power et al., 2001). An overview of the tectonostratigraphy of the Gippsland Basin is provided in Fig. 3.

Spreading of the Tasman Sea (between ~90 and 80 Ma) is believed to be responsible for a phase of intrusive and extrusive activity in the Gippsland Basin, which is still preserved within the syn-rift sediments of the Golden Beach and Emperor subgroups (O'Halloran and Johnstone, 2001). The discovery of the Kipper gas field, which is sealed by a basaltic lava flow, drew interest in the igneous rocks of the Gippsland Basin (Birch, 1987; McPhail, 2000). Offshore, these igneous rocks are mainly located along the northern and southern basin-bounding fault systems, with minor occurrences near the Bream Field, the Remora-Sunfish, Whiting-Wirrah and Tuna areas (Birch, 1987). Magmatic features occurring along the eastern end of the northern basin-bounding faults appear to be most extensive and mainly consists of multi-layered anastomosing, aggregated flows (Fig. 22), whereas other areas consist of single or double igneous intervals, with a single volcanic cone of about 100 m high, hosted in the Bream area (Birch, 1987). Both intrusive and extrusive features have been recognized and they are believed to be of olivine basalt or dolerite composition based on seismic velocities and petrography of recovered rock, but tuffaceous or rhyolitic compositions are also possible (Birch, 1987; McPhail, 2000).

Since most samples that were investigated have undergone significant alteration, the igneous bodies were not suitable for absolute dating techniques available at that time (Birch, 1987; McPhail, 2000). However, stratigraphic relationships have indicated ages ranging from 87 to 49 Ma with the majority being of Late Cretaceous (Campanian) age (Birch, 1987; McPhail, 2000). The oldest features are located in the north-eastern part of the basin, getting younger along the fault system towards the west, with the youngest features, interpreted as intrusives, located in the Bream area (Birch, 1987). Occurrences of Late Cretaceous igneous rocks in the onshore part of the Gippsland Basin are limited to a number of small enigmatic basalt, dolerite and gabbroic dykes in the area between Korumburra and Inverloch (Duddy and Green, 1992; Edwards, 1934).

O'Halloran and Johnstone (2001) conducted a detailed study of the igneous rocks in the vicinity of the Kipper Field. They identified a range of extrusive and intrusive volcanic bodies using the G99a Kipper 3D seismic survey and illustrated that volcanic intervals intersected in numerous wells tie to high impedance reflectors in the seismic data. These reflectors thicken across west to northwest trending growth faults and are generally concordant with stratigraphy. Samples taken from volcanic intervals in wells, show that these intervals consist of variably altered, fine-grained, glassy basaltic lavas and tuffs (McPhail, 2000). Some of the lava flows studied by O'Halloran and Johnstone (2001) show prograding geometries in the seismic data, which may record lava deltas building out into standing bodies of water. Additionally, O'Halloran and Johnstone (2001) interpreted a circular feature, located on a fault junction south of the South Kipper Fault, as an eroded scoria cone, and several smaller, and less obvious amplitude anomalies, which may represent cinder and spatter cones. O'Halloran and Johnstone

Table 2
Summary of discussed basins with their extrusive and intrusive styles, age of magmatism and timing relative to rifting of the basins.

Basin/Sub-basin	Extrusive styles	Intrusive styles	Age	Post-rift/ Syn-rift
Bight Basin/Ceduna sub-basin	Volcanic cones and lava flows	Sills, laccoliths and dykes	Extrusives: Mid-Eocene (~45 Ma) Intrusives: post-Maastrichtian (<66 Ma)	Post-rift
Otway Basin (onshore)	Monogenetic lava fields, scoria cones, lava shields, maars, ash cones and domes	Shallow intrusions	Older Volcanic Province: 95-19 Ma Macedon-Trentham Province: 10–4.6 Ma Newer Volcanic Province: 4.6 Ma – 4500 years	Post-rift
Otway Basin (offshore)	Lava aprons, hydrothermal vents	Sills	Extrusives & intrusives: early to mid Eocene (55-40 Ma)	Post-rift
Torquay sub-basin	Hyaloclastite, pyroclastic lapilli-tuff	Sills and dykes	Extrusives & intrusives: early to mid Oligocene (34-27 Ma)	Post-rift
Sorell Basin	Lava flows	Sills	Extrusives: Maastrichtian to Palaeocene (~70-55 Ma) Intrusives: post Late Cretaceous (<83 Ma)	Post-rift
Bass Basin	Volcanoes, lava flows, mounds, vents and cones	Sills and dykes	Extrusives: Middle Cretaceous, Late Cretaceous to Palaeocene, Oligocene to Miocene Intrusives: Oligocene to Miocene	Post-rift
Tasmania (onshore)	Lava flows	Sills, necks and dykes	Extrusives & intrusive: 62–8.5 Ma	Post-rift
Gippsland Basin	Lava flows, various cones such as scoria, cinder and spatter cones	Sills, dykes and cone sheet?	Extrusives & intrusive: Late Cretaceous to Eocene (87-49 Ma)	Syn- and post-rift

(2001) suggest that these scoria cones are fissure-fed and are feeding the basaltic lava flows. In addition to the extrusive bodies, they also recognized irregular, ring-like intrusive features cross-cutting stratigraphy located along the major fault zones and classified them as cone sheets which fed overlying eruptive centres.

5. Discussion

Although the Australian southern margin has been classified as a non-volcanic or magma-poor rifted margin, it has been demonstrated in section 4 that magmatic activity is quite widespread in this area, making a magma-poor rifted margin the preferred term. All rifted basins along the Australian margin have been shown to have seen some magmatic activity during their evolution and this magmatic activity is preserved in the post-rift and syn-rift sequences of their sedimentary successions. Table 2 summarizes the extrusive and intrusive styles encountered in the sedimentary basins, their age and timing with regards to rifting of the basins.

5.1. Comparison of magmatic styles along the Australian southern margin and volcanic passive margins

Generally, two end-members exist in passive margins: volcanic or magma-rich margins and non-volcanic or magma-poor margins (Fig. 23) (Franke, 2013). Examples of volcanic margins are: the eastern and western margins of Greenland, the east coast of South America, the west coast of southern Africa, the East-African rift, western Australia, southwest coast of India and Antarctica directly south of Africa (Geoffroy, 2005). These volcanic or magma-rich margins are typically linked to Large Igneous Provinces (e.g. Menzies (2002), White and McKenzie (1989)). As summarized by several studies (e.g. Zalan (2014), Menzies (2002), White and McKenzie (1989)) volcanic or magma-rich margins are characterized by (from onshore to offshore direction): (1) unstretched continental crust covered by extensive basaltic lava flows (pre-rift volcanism), (2) a zone of thinned continental crust (20 km instead of 40 km) where deep grabens may develop (up to 20 km thick), (3) thinned to hyper-extended crust covered by grabens entirely filled with volcanic material showing Seaward Dipping Reflectors (SDR) which consist of sub-aerial basaltic lava flows (up to 15 km thick) that are interbedded with volcaniclastic material and (4) oceanic crust (Fig. 23). Volcanic margins generally entrain a zone of high seismic velocity (Vp > 7.3 km/s) in the lower crust, seaward of the margin, and as thinning occurs only along a small distance, the continent-ocean transition (COT) is quite abrupt and occurs in the vicinity of the SDR's (either landward or seaward) (Franke, 2013). In contrast, magma-poor or non-volcanic rifted margins are characterized by (from onshore to offshore direction): (1) original unstretched continental crust (thickness 30–40 km), (2) stretched but not thinned continental crust, with few minor grabens, (3) thinned and stretched continental crust with several major deep grabens and aborted necked regions (H-blocks) are preserved as aulacogens, (4) final stretch of continental crust where hyper-extension dominates, and where both the upper elastic and lower plastic crust are deformed by brittle processes due to their extreme thinning, (5) exhumed mantle, under the form of a belt of varying width up to several tens of km and (6) oceanic crust (Zalan, 2014) (Fig. 23).

Typically, volcanic margins will host several types of magmatic features. Next to the sub-aerial lava-flows showing SDR's, they are often associated with Large Igneous Provinces (LIP's), where a large volume of magma is extruded over a short time span (2 Ma) (Franke, 2013; Menzies, 2002; White and McKenzie, 1989). With regards to the rifting stages, magmatism along volcanic passive margins can occur during pre-rift (expressed as plateau-basalts), syn-rift (SDR's, high velocity zones in the lower crust and intrusions in the transitional crust) or during post-rift continental break-up (thicker than normal oceanic crust including oceanic SDR and high velocity zones) (Geoffroy, 2005).

Magmatism along the Australian southern margin and non-volcanic passive margins in general, mainly show magmatic activity during post-rift stages and is less voluminous than activity occurring along volcanic margins. As has been summarized earlier, magmatic features in the Bight Basin have been interpreted to be of post-Maastrichtian and Middle Eocene age, occurring in the post-rift Hammerhead and Tiger Supersequences (Schofield and Totterdell, 2008) and are therefore emplaced post-dating the rifting events in the basin. Similarly, Cenozoic magmatic activity in the offshore Otway Basin is of presumed early to mid-Eocene age, indicating post-rift activity (Holford et al., 2012). Onshore magmatic activity in the Otway Basin ranges from Jurassic to Recent age, with Jurassic and Cretaceous activity being directly related to rifting between Australia and Antarctica (Holford et al., 2012). As subsequent activity picked up again from ~52 Ma (Price et al., 2014), this activity post-dates rifting in the Otway Basin. Magmatic activity in the Torquay Sub-basin is interpreted to be of mid-Oligocene age and Palaeocene lava flows in the Sorell Basin therefore also post-date rifting (Hill et al., 1997; Messent et al., 1999). The

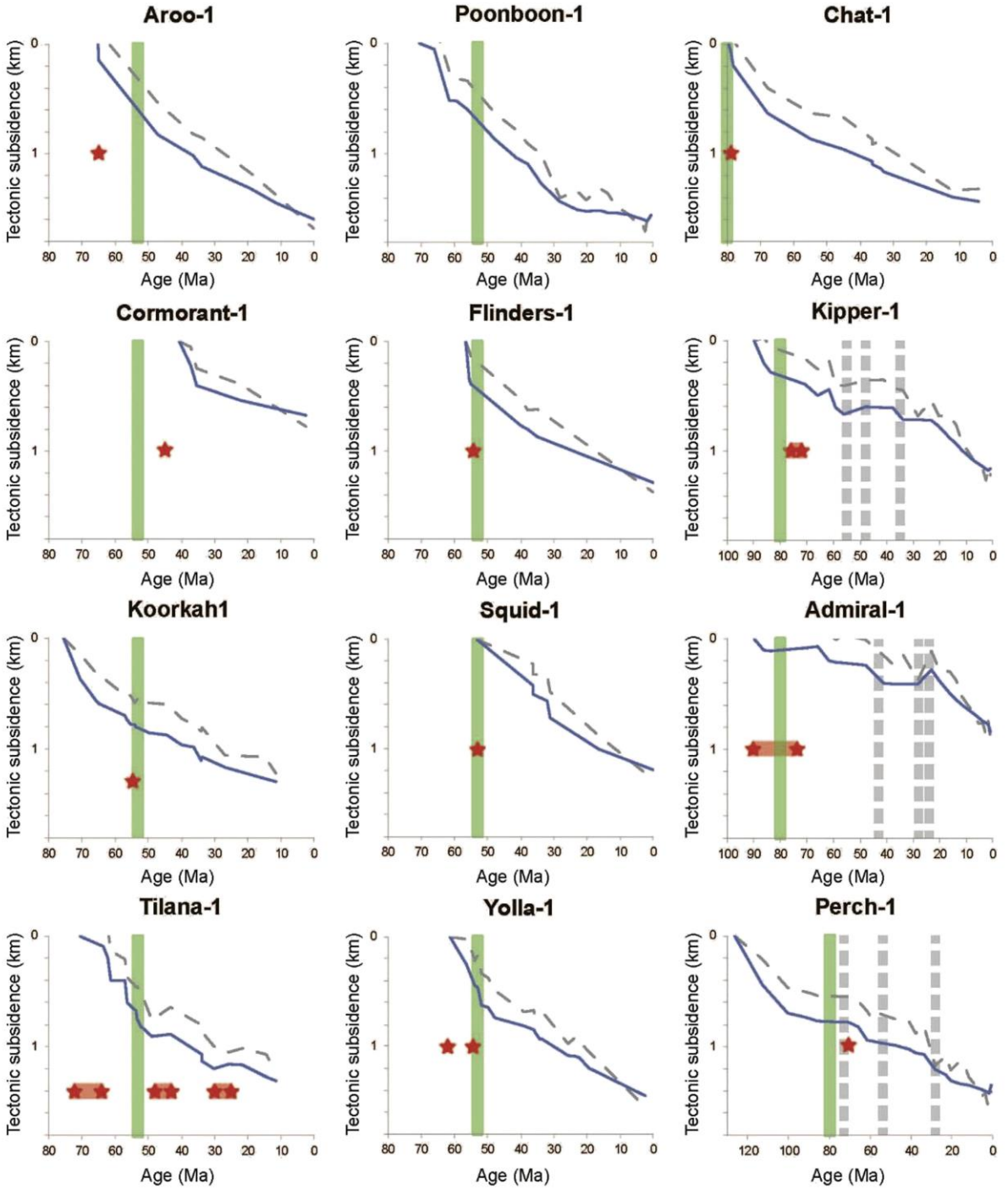

Fig. 25. Tectonic subsidence plots corrected for global sea level changes (grey dashed curves) and without corrections (blue curves) for global sea level changes (Haq et al., 1988) for selected wells in the Bass and Gippsland Basins. Red stars indicate the location of igneous rocks in the succession. Green bars indicate the start of post-rift sedimentation. Grey dashed bars indicate unconformities in the Gippsland Basin. Note the different time scale bar for the Gippsland Basin wells.

Bass Basin has seen several phases of magmatic activity in the Middle Cretaceous (directly related to the onset of Tasman Sea spreading), Late Cretaceous to Palaeocene (syn- and post-rift) and Oligocene to Miocene (post-rift), which coincides with onshore Tasmanian activity (Blevin, 2003; Cummings et al., 2004; Sutherland et al., 2002). Similarly to the Bass Basin, magmatic activity in the Gippsland Basin (87–49 Ma; Birch (1987); McPhail (2000)) occurred during both syn- and post-rift phases of the basin.

5.2. Influence of magmatism on sedimentary infill along the southern margin

Volcanic margins often show uplift due to underplating (e.g. the North Atlantic Igneous Province LIP along the North Atlantic margin) (Jones et al., 2001). In order to investigate the impact of magmatism on vertical motions or subsidence and sedimentary infill of the sedimentary basins of the southern Australian margin, tectonic subsidence plots were constructed based on biostratigraphic and lithological data for selected wells in the Bass and Gippsland Basin (Figs. 24 and 25). Most of the wells in the Bass Basin did not intersect or do not have enough data on syn-rift sediments (Durroon and Otway Sequences (Blevin et al., 2005)), so mainly post-rift successions have been portrayed here. These post-rift sequences started around 53 Ma in the Cape Wickham sub-basin and around 80 Ma in the Durroon sub-basin and the Gippsland Basin (Blevin and Cathro, 2008). Tectonic subsidence has been calculated with and without corrections for global sea level changes (with corrections: grey dashed curve; without corrections: continuous blue curve, Fig. 25). Tectonic subsidence plots for the Bass Basin show the expected negative exponential response to thermal relaxation following ductile extension of the lithosphere (Fig. 25). As the Bass Basin never evolved to break-up, it is regarded as a failed rift and stretch factors are expected to be quite low ($\beta < 1.5$). In general, magmatic activity does not seem to have an effect on the tectonic subsidence in these wells. However, in some wells, such as Tilana-1, still-stands (when eustasy equals subsidence) or uplift is observed in the subsidence following igneous rocks in the succession. These layers are of quite substantial thickness (>200 m) in Tilana-1, however, whether this is caused by the magmatic activity is unclear. Gippsland Basin wells show similar thermal sag subsidence in the post-rift sequence. As magmatic activity is believed to be related to rifting in the Gippsland Basin, no major impact is expected in this basin.

In comparison to a volcanic margin such as the North Atlantic margin, transient uplift in the Faroe-Shetland and the Porcupine Basin, has been attributed to mantle convection of the Iceland plume associated with the NAIP LIP (Champion et al., 2008; Jones et al., 2001). This period of Early Eocene transient uplift has been observed in an area extending over 1000 km from the continental margin, including the Faroe-Shetland Basin, the northern North Sea Basin, Ireland and the Celtic Sea basins south of Ireland (Jones et al., 2001). Uplift in these areas was short-lived, grew and decayed within 2–3 Ma, suggesting changes in dynamic support generated by mantle convection (Champion et al., 2008). Along the Australian southern margin however, similar transient uplift has not been observed in the produced subsidence plots, therefore rendering a plume origin unlikely for Cenozoic magmatic activity along this magma-poor margin. This however does imply that substantial amount of magmatism is possible without any significant uplift.

5.3. Possible causes of magmatism along the Australian southern margin

To this date, the origin of magmatism in south-eastern Australia has not yet been fully unravelled and over time, several theories have been proposed, however, large scale models do not include the offshore magmatic features found along the Australian southern margin. Sutherland (1981) suggested that when you plot the onshore central-volcanic and offshore seamount chain provinces back in time to the start of the Southern Ocean spreading (taken at 53 Ma), it plots across the former Coral Sea - Louisiade Trough spreading system, which he suggests to mark a long-lived thermal anomaly in the mantle. This allowed him to develop a similar model (Sutherland, 1981, 1983, 1989, 1991, 2003) containing both central and lava-field volcanism which suggests that this volcanic activity is related to similar extinct spreading zones such as the North Tasman Rift (65 Ma) and the Central Tasman Rift (95 Ma). These rifts then initiated the 'East Australian Plume System', over which the Australian plate moved northward. However, as Richards (2014) points out for the offshore seamount chains, magmatic chains that are located so close to each other (locally $\leq$ 350 km) are hard to reconcile with whole-mantle convection models. Instead, deep plumes are expected to coalesce rapidly which is more energetically favourable, most likely implying a shallower origin than the deep mantle. The latest model in this line of thinking (Sutherland et al., 2014) adds the numerous young felsic events (<10 Ma) in southeast Australia. Another theory, postulated by (O'Reilly and Zhang, 1995) is that partial melting for the lava-field volcanism in eastern Australia is likely to have been initiated by upwelling of an abnormally hot, deep mantle region, rather than a hot-spot. They proposed that this region could have been a delayed effect of regional extension induced by the opening of the Tasman Sea and/or the Southern Ocean during the late Mesozoic and which may in turn have weakened the sub-continental lithospheric mantle (SCLM). This weakening of the SCLM could then have resulted in a weak spot where the later central-volcano magmatism, triggered by an independent mantle plume, could have made its way through. On the other hand, Pilger (1982) suggests that the southward younging of the central shield volcanism is due to changes in stress regimes from tensional to east–west compressional stress during the last 35 Ma. However, new lava-field volcanic ages do not seem to support this model (Cohen et al., 2013; Sutherland, 2003; Vasconcelos et al., 2008).

Finn et al. (2005) suggested that eastern Australian volcanism is related to a major diffuse alkaline magmatic province (DAMP). This province is located in the southwest Pacific and covers a vast area from eastern Australia, over the Tasman Sea to New Zealand, south over the Campbell Plateau and parts of East Antarctica and offshore islands of West Antarctica. Igneous rocks from this province are characterised by a distinctive isotopic composition, interpreted to result from both depleted and high μ (HIMU) components in the mantle source (Price et al., 2003). This province is believed to have originated from mantle flow induced by slab detachment and mantle upwelling, without strong rift or deep plume inputs (Finn et al., 2005). However, it is not entirely clear how the magmatic activity along the southern margin fits this model.

For the Bight Basin, Schofield and Totterdell (2008) have discussed several possibilities in trying to pinpoint the cause of magmatism observed in the Ceduna sub-basin (Bight Basin Igneous Complex, BBIC). They conclude that rifting and subsequent melting due to mantle decompression during rifting was not likely to be a driver for magmatism in the area as they had not observed any significant upper crustal extension at that time. Additionally, they conclude that a migratory Hawaiian-style form of hotspot activity ('primary' plumes of Courtillot et al. (2003)) is inconsistent with the approximate NW–SE distribution of the BBIC, the short-lived activity and the known hotspot tracks in the area (Davies et al., 2015), however, a hotspot-like model reflective of edge-driven convection cells in the mantle seems to be more likely (Schofield and Totterdell, 2008). These convection cells are set up between

continental and oceanic crust or younger crust and cratonic root zones, and correspond to the 'tertiary' hotspots of Courtillot et al. (2003). As the BBIC is located within 300 km of the margin of the Gawler Craton, and the distribution of igneous rocks in the BBIC parallels the craton margin, this might be a plausible explanation.

Similar models have been put forward for the Newer Volcanic Province in the Otway Basin by several authors (Davies and Rawlinson, 2014; Demidjuk et al., 2007; Holt et al., 2013). These models are supported by both geochemical (Demidjuk et al., 2007; Holt et al., 2013) and geophysical studies (Aivazpourporgou et al., 2015; Davies and Rawlinson, 2014). Based upon U-series isotopes, Demidjuk et al. (2007) were able to prove dynamic melting in an upwelling mantle at a rate (1.5 cm/year) which is slower than would be expected for mantle plumes. They therefore hypothesize that this upwelling takes the form of secondary convection cells driven by edge effects in topography in the base of the Australian plate. Based on enriched Sr-Nd isotopes, they conclude that melting in this case is caused by the presence of hydrous mantle, originating from inherited previous enrichment phases or entrainment of lithospheric mantle. The depth of melt segregation was further refined by geothermobarometry to 3–4 GPa, corresponding to upper asthenosphere (Holt et al., 2013). Upwelling rates (1.5 cm/year) and depth of melting (4 GPa) were confirmed by Davies and Rawlinson (2014) using 3D teleseismic tomography and 2D and 3D geodynamic modelling. They conclude that shallow and localized upwelling is causing magmatism in the NVP. Additionally, they conclude that next to edge-driven convection, shear-driven upwelling is an equally important process which causes increase in upwelling rates, and places convection in the upper asthenosphere. A more recent model combines one of the longest recognized hotspot tracks in Australia, the Cosgrove track, with the edge-driven convection model (Davies et al., 2015). They state that the edge-driven convection cells must have been long-lived but were only triggered by the passing of the Cosgrove hotspot track <50 km to the east of the NVP around 6.5 to 5 Ma. Additionally, this study highlights a strong correlation between lithospheric thickness and geochemical composition of the magmatism: a lithospheric thickness of less than 110 km allows for basaltic compositions, whereas gaps in volcanism occur in regions with lithospheric thicknesses exceeding 150 km and intermediate lithospheric thicknesses allow for low volume, leucitite-bearing volcanism.

Based on the tectonic subsidence plots discussed in section 5.1, the authors do not favour linking the offshore magmatic activity to mantle convection of a plume such as the Iceland plume. Instead, a model of edge-driven convection, as has been proposed for the Newer Volcanic Province in Victoria (Demidjuk et al., 2007; Price et al., 2014), seems to be more likely. However, further research on the geochemistry of both intrusive and extrusive rocks in the offshore basins is needed. This will aid in unravelling the source of the magmatism and its trajectory towards the surface and allow for testing of the proposed models. This will provide further insight in possible mechanisms and causes for intraplate magmatism in general.

5.4. Effects on hydrocarbon exploration

The Australian southern margin hosts several prolific, hydrocarbon producing basins such as the Gippsland, Bass and Otway Basin. However, large, under-explored areas still exist which have great potential for hydrocarbon generation if source rocks are present (Bradshaw et al., 2003). Although this margin is classified as a non-volcanic margin, magmatic activity is present along the Australian southern margin and has affected hydrocarbon exploration both positively and negatively. This section will therefore briefly discuss the possible effects of magmatism on hydrocarbon exploration and exploitation in the study area. For a more thorough analysis of the positive and negative consequences of igneous activity on hydrocarbon plays, the reader is redirected to Schutter (2003) and Ernst (2014). Although less relevant for the Australian southern margin, Rohrman (2007) has evaluated prospect delineation in sub-basalt plays, by giving an example of using filtered gravity and magnetic data together with possible low-frequency seismic and seismic velocity analysis to better delineate and de-risk volcanic basin plays along the North Atlantic volcanic margin and the Deccan traps, offshore western India.

5.4.1. Difficulties in seismic imaging and interpretation

Sub-basalt seismic imaging has always been a hurdle caused by internal physical heterogeneities of intrusive and extrusive igneous rocks (Rohrman, 2007). These heterogeneities cause the formation of strong multiples and attenuation of the seismic signal, acting as low frequency pass filters in the seismic data (Rohrman, 2007). Although sub-basaltic plays are not present along the southern margin, several exploration wells are interpreted to have failed due to the presence of igneous rocks. For example in the Bass Basin, Bass-1, Aroo-1, Flinders-1 and Tasmanian Devil-1 were all plugged and abandoned after the high amplitude primary drilling objective was found to be volcanic rock (Trigg et al., 2003). Additionally in the Bass Basin, Faustmann (1995) has shown that the variation in seismic velocities within the Miocene volcanic pile may be related to facies changes going from basalt to pyroclastic products such as scoria or tuff, within the volcanic pile. This variation poses a significant complication for the correction of seismic pull-up and push-down for depth conversion and the accurate interpretation of exploration targets beneath the volcanic units and intrusive bodies.

5.4.2. Reservoirs, seals, traps and migration pathways

Although many examples exist of both intrusive and extrusive igneous rocks with primary (associated with vesicles in extrusive rocks) or secondary porosity (due to alteration and fracturing) acting as good reservoir rocks (e.g. the Jatibarang Field on the northwest coast of Java is hosted in andesitic volcanics), there have been few discoveries of commercial accumulations in igneous rocks in offshore passive margin basins (Schutter, 2003). However, igneous rocks acting as seals have been reported more regularly (e.g. the Kipper Field in the Gippsland Basin (O'Halloran and Johnstone, 2001)). Additionally, as has been illustrated in the Bass, Torquay and Gippsland Basin, intrusive rocks often use existing faults as conduits and can therefore induce fault-seal when juxtaposed against a reservoir (Holford et al., 2012).

Perhaps more relevant than igneous rocks forming reservoir rocks or sealing units, are the effects of compartmentalisation on hydrocarbon migration pathways (Fig. 26). Previous studies offshore the Norwegian coast (Cartwright and Hansen, 2006) have illustrated that shallow sills are fed by deeper sills and that sill complexes can transport melt from lower-mid crustal levels to shallow near-surface depths over distances greater than 10 km, both vertically and laterally. These intrusions have the tendency of exploiting and intruding particular stratigraphic horizons such as ductile and/or over-pressured shales (Thomson, 2007) or pre-existing structural discontinuities such as faults (Holford et al., 2012; Magee et al., 2013a). If these intrusions do not possess any secondary permeability caused by processes such as cooling joints or tectonic fracturing (Rateau et al., 2013), compartmentalisation of large volumes of source or reservoir rock may occur and hydrocarbon migration pathways may be compromised. Additionally, as pointed out by Holford et al. (2013), significant under-compaction of sediments may occur due to the intrusive network acting as a rigid framework during rapid burial of sediments by possible coeval igneous extrusive deposits. Depending on sealing capacities of the

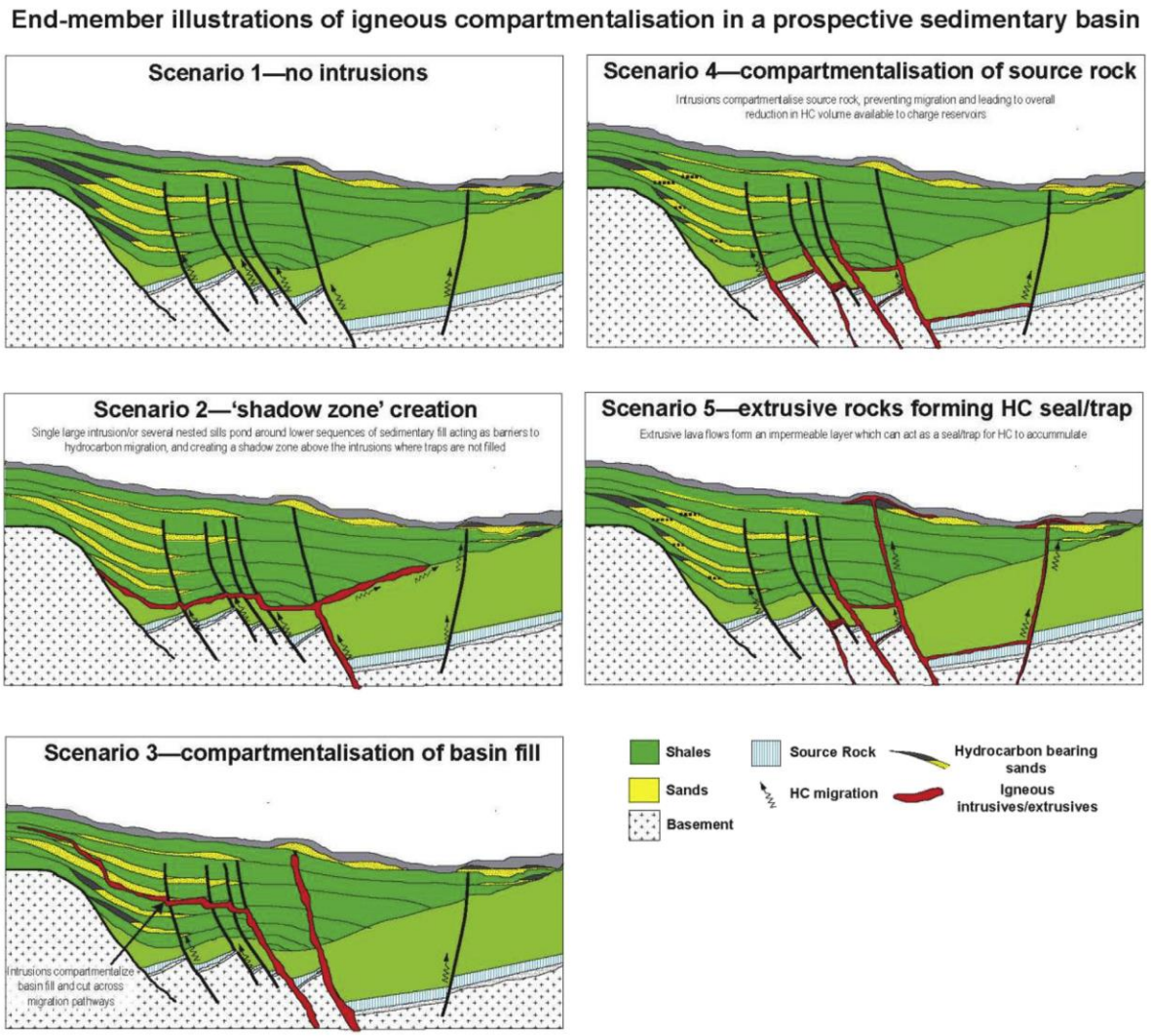

Fig. 26. Conceptual diagrams of potential end-member impacts of igneous intrusions and extrusions on hydrocarbon plays in sedimentary basins. Modified from Holford et al. (2012).

intrusions, lateral pressure changes may develop within a reservoir body bound by intrusive rocks, which may pose a significant hazard during drilling of sub-igneous plays. This risk may exist in the Ceduna sub-basin, where networks of closely-spaced sills and dykes have been reported in the late Cretaceous-Eocene Hammerhead Supersequence which hosts a potential reservoir rock (Schofield and Totterdell, 2008).

Degassing of igneous rocks can result in a significant CO_2 charge and even flood the whole structure (e.g. northern Kaiparowitz Basin in southern Utah) (Schutter, 2003). Along the Australian southern margin, degassing of Newer Volcanic magmas has been attributed to varying levels of CO_2 accumulations in the Otway Basin (e.g. Mt Burr volcanics and the Ladbroke Grove-1 well in the western Otway Basin, Mt Gambier and Mt Schank volcanics near the Caroline-1 well and Port Campbell-1 well in the Port Campbell Embayment in the eastern Otway Basin) (Watson et al., 2003).

Trap-formation may also occur caused by igneous activity. Although considered rare along the Australian southern margin, intrusive rocks may be dome-shaped and create traps. More applicable to the region of interest is deformation or forced folding of overlying sediments caused by intrusion of igneous rocks and four-way closure of the reservoir, similar to fault sealing, caused by networks of dykes or sills feeding overlying extrusives. These types of structures have mainly been reported in the upper Hammerhead, Wobbegong and Dugong Supersequences in the Ceduna sub-basin and similar traps have been reported in reservoir sequences in the Otway and Torquay sub-basins (Holford et al., 2012; Jackson et al., 2013; Totterdell et al., 2008).

5.4.3. Hydrothermal circulation systems

Direct thermal effect of intrusive bodies on source rocks has been proven minimal, with thermal aureoles ranging from half to 5

times the intrusion thickness (e.g. Schutter (2003) and references therein). However, when multiple igneous intrusions create a dense network, i.e. when multiple, thick intrusive sills (>100 m thick) intrude organic-rich sediments simultaneously (Aarnes et al., 2011) or when previous igneous activity has raised the background geothermal gradient (e.g. Taranaki Basin of New Zealand, Schutter (2003)), greater influence is to be expected. These effects are dependant of the composition (and thus melting temperature) of the intrusions, and thermal conductivity, state of compaction, pore-water volume and degree of maturation of host rock lithologies at the time of intrusion (Rohrman, 2007). Next to direct thermal effects, heating by convective and/or advective processes have been indicated to play an equal or even greater part in influencing source rock maturation by creating hydrothermal systems due to heating of pore-water in porous sedimentary rocks (Rohrman, 2007). In the Bass Basin for example, hydrothermal activity is common and occurs in relation to igneous activity in the basin. This hydrothermal activity has been attributed to altering quartz grains and cementing quartz sandstone reservoir rocks adjacent to igneous rocks, compromising porosity and permeability as a consequence (Blevin, 2003). In the Torquay sub-basin, elevated palaeotemperatures in the Boonah Formation and Eastern View Group sandstones in the Wild Dog-1 well may be attributed to hydrothermal systems driven by igneous intrusions (Holford et al., 2012). Additionally, the presence of hydrothermal vents or gas chimneys can be indicative of active gas seepage, migration pathways or hydrocarbon reservoirs themselves and can potentially result in breaching of sealing sequences (Holford et al., 2012). Gas chimneys occur both onshore and offshore in the Gippsland Basin and several examples exist of gas seepage, e.g. near Flathead-1 well, near the Sunfish-Tuna field and west of the Wahoo-1 well on the offshore Northern Terrace (Nourollah et al., 2010).

6. Conclusions

We highlight that although the Australian southern margin is classified as 'non-volcanic', its sedimentary basins do indeed host an under recognised archive of magmatic activity. This magmatism is part of the intraplate magmatism which occurs onshore along the Australian south-eastern margin. Over time several models have been proposed to explain the onshore activity. However, none of these models have incorporated the offshore magmatic record observed along the Australian southern margin. The coupled observation of basin dynamics and sedimentology and mantle melt generation episodes provide a potentially powerful tool in understanding the causes of this enigmatic magmatism. For instance, based on tectonic subsidence plots for the Bass Basin which do not show any significant uplift, we discount a model of mantle convection due to a plume such as the Iceland plume as the cause of magmatism. Additionally, with break-up occurring at 83, 67 and 55 Ma in the Bight, Otway and Sorell Basin respectively and no break-up occurring in the Bass Basin, the offshore magmatism is significantly younger than periods of rifting. Evidence for magmatism is recorded in post-rift sedimentary sequences and has mid-Eocene extrusive and post-Maastrichtian intrusive ages for the Bight Basin, early to mid-Eocene extrusive and intrusive ages for the Otway Basin, early to mid-Oligocene ages in the Torquay sub-basin, Maastrichtian to Palaeocene extrusive and post Late Cretaceous ages for the Sorell Basin and Middle Cretaceous, Late Cretaceous to Palaeocene and Oligocene to Miocene ages in the Bass Basin. This therefore rules a first order causal link out between rifting and the observed magmatism. In contrast, magmatism in the Gippsland Basin is believed to be related to rifting as break-up and magmatism are coeval and occurs in syn- to post-rift sedimentary sequences.

The authors believe that further research on the magmatic processes within these sedimentary basins, their sub-surface plumbing and trajectories through the sedimentary successions will provide further insights into this enigmatic magmatic activity. Investigating the time-constrained geochemistry of the offshore intrusive and extrusive rocks will further constrain possible mechanisms and will allow for testing of existing models in the area, such as the edge-driven convection models proposed for the Newer Volcanic Province.

Acknowledgements

The authors would like to thank David Taylor and Richard Ernst for their detailed and constructive review. This research forms part of a PhD project supported by the ASEG Research Foundation (RF14P05) for which funding is greatly acknowledged. The authors would also like to thank the University of Adelaide for scholarship funding, IHS for access to the Kingdom Suite, GA and PGS for access to the used seismic data and the S^3 research group for support. This paper forms TRaX record 341.

References

Aarnes, I., Svensen, H., Polteau, S., Planke, S., 2011. Contact metamorphic devolatilization of shales in the Karoo Basin, South Africa, and the effects of multiple sill intrusions. Chem. Geol. 281, 181–194.
Abele, C., Page, R.W., 1973. Stratigraphic and Isotopic Ages of Tertiary Basalts at Maude and Airey's Inlet, Victoria, Australia, Record 1973/002. Bureau of Mineral Resources, Geology and Geophysics, Canberra.
Aivazpourporgou, S., Thiel, S., Hayman, P., Moresi, L., Heinson, G., 2015. Decompression melting driving intraplate volcanism in Australia: evidence from magnetotelluric sounding. Geophys. Res. Lett. 42, 346–354.
Baillie, P.W., 1986a. A Radiometric Age for the Moriarty Basalt, North-western Tasmania. Unpublished report. Tasmania Department of Mines.
Baillie, P.W., 1986b. Radiometric Ages for Circular Head and the Green Hills Basalt, North-western Tasmania. Unpublished report. Tasmania Department of Mines.
Baillie, P.W., 1993. Regional geology. In: Maung, T.U., Miyazaki, S., Baillie, P.W., Lavering, I.H., Vuckovic, V., Stephenson, A.E., Williamson, P.E., Staunton, J., Radke, S.G., West, B.W., Gippespie, R.G., Resiak, E., Temple, P.R. (Eds.), Eastern Bass Basin Petroleum Prospectivity Bulletin. Bureau of Resource Sciences.
Baillie, P.W., Brown, A.V., 1984a. Igneous Rocks from Squid #1. Unpublished report. Tasmania Department of Mines.
Baillie, P.W., Brown, A.V., 1984b. Igneous Rocks from Tasmanian Devil #1. Unpublished report. Tasmania Department of Mines.
Bernecker, T., Partridge, A.D., 2005. Approaches to palaeogeographic reconstructions of the Latrobe Group, Gippsland Basin, southeastern Australia. APPEA J. 45, 581–599.
Birch, G.F., 1987. Igneous Rocks of the Gippsland Basin. Esso Australia Ltd.
Blevin, J.E., 2003. Petroleum Geology of the Bass Basin, Interpretation Report, an Output of the Western Tasmanian Regional Minerals Program. Geoscience Australia Record 2003/19.
Blevin, J.E., Cathro, D.L., 2008. Australian Southern Margin Synthesis, Project GA707. Client Report to Geoscience Australia by FrOG Tech Pty Ltd.
Blevin, J.E., Trigg, K.R., Partridge, E.D., Boreham, C.J., Lang, S.C., 2005. Tectonostratigraphy and potential source rocks of the Bass Basin. APPEA J. 45, 601–622.
Blewett, R., 2012. Shaping a Nation: a Geology of Australia. Geoscience Australia and ANU E Press, Canberra.
Boreham, C.J., Blevin, J.E., Duddy, I.R., Newman, J., Liu, K., Middleton, H., MacPhail, M.K., Cook, A.C., 2002. Exploring the potential for oil generation, migration and accumulation in Cape Sorell-1, Sorell Basin, offshore West Tasmania. APPEA J. 42, 405–437.
Bottrill, R.S., Everard, J.L., Taheri, J., 2014. Cretaceous igneous rocks. In: Corbett, K.D., Quilty, P.G., Calver, C.R. (Eds.), Geological Evolution of Tasmania. Geological Society of Australia (Tasmania Division), pp. 453–462.
Boult, P.J., Hibburt, J.E., 2002. Petroleum geology of South Australia. 1: Otway Basin South Australia, second ed. Department of Primary Industries and Resources.
Boyce, J., Nicholls, I., Keays, R., Hayman, P., 2014. Victoria erupts: the Newer Volcanics Province of south-eastern Australia. Geol. Today 30, 105–109.
Bradshaw, B.E., Rollet, N., Totterdell, J.M., Borissova, I., 2003. A Revised Structural Framework for Frontier Basins on the Southern and Southwestern Australian Continental Margin. Geoscience Australia Record 2003/03.
Bryan, S.E., Constantine, A.E., Stephens, C.J., Ewart, A., Schön, R.W., Parianos, J., 1997. Early Cretaceous volcano-sedimentary successions along the eastern Australian continental margin: implications for the break-up of eastern Gondwana. Earth Planet. Sci. Lett. 153, 85–102.
Bryan, S.E., Ferrari, L., 2013. Large Igneous Provinces and Silicic Large Igneous Provinces: progress in our understanding over the last 25 years. Geol. Soc. Am. Bull. 125, 1053–1078.

Cartwright, J., Hansen, D., 2006. Magma transport through the crust via interconnected sill complexes. Geology 34, 929–932.
Cas, R., Simpson, C., Sato, H., 1993. In: Australia, G. (Ed.), Newer Volcanics Province – Processes and Products of Phreatomagmatic Activity.
Champion, M.E.S., White, N.J., Jones, S.M., Lovell, J.P.B., 2008. Quantifying transient mantle convective uplift: an example from the Faroe-Shetland basin. Tectonics 27.
Coffin, M.F., Eldholm, O., 1994. Large igneous provinces: crustal structure, dimensions, and external consequences. Rev. Geophys. 32, 1–36.
Coffin, M.F., Eldholm, O., 2005. Large igneous provinces. In: Selley, R.C., Cocks, R., Plimer, I.R. (Eds.), Encyclopedia of Geology. Elsevier, Oxford, pp. 315–323.
Cohen, B., Knesel, K., Vasconcelos, P., Thiede, D., Hergt, J., 2008. $^{40}Ar/^{39}Ar$ constraints on the timing and origin of Miocene leucitite volcanism in southeastern Australia. Aust. J. Earth Sci. 55, 407–418.
Cohen, B.E., Knesel, K.M., Vasconcelos, P.M., Schellart, W.P., 2013. Tracking the Australian plate motion through the Cenozoic: constraints from 40Ar/39Ar geochronology. Tectonics 32, 1371–1383.
Collins, P.L.F., Gulline, A.B., Williams, E., 1981. Geological Survey Explanatory Report. Geological Atlas 1 Mile Series. Sheet 44 (8014N). Mackintosh. Tasmania Department of Mines.
Conrad, C., Bianco, T., Smith, E., Wessel, P., 2011. Patterns of intraplate volcanism controlled by asthenospheric shear. Nat. Geosci. 4, 317–321.
Courtillot, V., Davaille, A., Besse, J., Stock, J., 2003. Three distinct types of hotspots in the Earth's mantle. Earth Planet. Sci. Lett. 205, 295–308.
Cummings, A.M., Hillis, R.R., Tingate, P.R., 2004. New perspectives on the structural evolution of the Bass Basin: implications for petroleum prospectivity. In: Boult, P.J., Johns, D.R., Lang, S.C. (Eds.), Eastern Australian Basins Symposium II. PESA Special Publication, pp. 133–149.
Cundari, A., 1973. Petrology of the leucite-bearing lavas in New South Wales. J. Geol. Soc. Aust. 20, 465–492.
Davies, D.R., Rawlinson, N., 2014. On the origin of recent intraplate volcanism in Australia. Geology 43, 367–368.
Davies, D.R., Rawlinson, N., Iaffaldano, G., Campbell, I.H., 2015. Lithospheric controls on magma composition along Earth/'s longest continental hotspot track. Nature 525, 511–514.
Davies, H.L., Clarke, J.D.A., Stagg, H.M.J., McGowran, B., Alley, N.F., Willcox, J.B., 1989. Maastrichtian and Younger Sediments from the Great Australian Bight. Bureau of Mineral Resources, Australia.
Demidjuk, Z., Turner, S., Sandiford, M., George, R., Foden, J., Etheridge, M., 2007. U-series isotope and geodynamic constraints on mantle melting processes beneath the Newer Volcanic Province in South Australia. Earth Planet. Sci. Lett. 261, 517–533.
Duddy, I.R., Green, P.F., 1992. Tectonic development of the Gippsland Basin and environs: identification of key episodes using apatite fission track analysis (AFTA). Energy, economics and environment. In: Proc. Gippsland Basin Symposium, Melbourne, 1992, pp. 111–120.
Dunlap, J., 2003. 40Ar/39Ar Dating of Minerals and Whole Rock from the Bass Basin. Research School of Earth Sciences, Australian National University for Geoscience Australia.
Edwards, A.B., 1934. Tertiary Dykes and Volcanic Necks of South Gippsland, Victoria, vol. 47. Royal Society of Victoria, pp. 112–132.
Edwards, J., Cayley, R.A., Joyce, E.B., 2004. Geology and geomorphology of the Lady Julia Percy Island volcano, a Late Miocene submarine and subaerial volcano off the coast of Victoria, Australia. Proc. R. Soc. Vic. 116, 15–35.
Ernst, R.E., 2014. Large Igneous Provinces. Cambridge University Press.
Exon, N.F., Hill, P.J., Royer, J.-Y., Muller, D.R., Whitmore, G.P., Belton, D., Dutkiewicz, A., Ramel, C., Rollet, N., Wellington, A., 1994. In: Organisation, A.G.S. (Ed.), AGSO Cruise 125 Report: TASMANTE Swath-mapping and Reflection Seismic Cruise off Tasmania Using R.V. L'Atalante.
Exon, N.F., Lee, C., Felton, E.A., Heggie, D., McKirdy, D., Penney, C., Shafik, S., Stephenson, A., Wilson, C., 1992. BMR Cruise 67: Otway Basin and West Tasmanian Sampling. Australian Goverment Publishing Service.
Exon, N.F., Marshall, J.F., McCorkle, D.C., Alcock, M., Chaproniere, G.C.H., Connell, R., Dutton, S.J., Elmes, M., Findlay, C., Robertson, L., Rollet, N., Samson, C., Shafik, S., Whitmore, G.P., 1995. AGSO Cruise 147 Report – Tasman Rises Geological Sampling Cruise of Rig Seismic: Stratigraphy, Tectonic History and Palaeoclimate of the Offshore Tasmanian Region.
Exon, N.F., Quilty, P.G., Lafoy, Y., Crawford, A.J., Auzende, J.M., 2004. Miocene volcanic seamounts on northern Lord Howe Rise: lithology, age and origin. Aust. J. Earth Sci. 51, 291–300.
Faustmann, C., 1995. The Seismic Expression of Volcanism in the Bass Basin Referring to Western Victorian Analogues. University of Adelaide unpublished.
Finn, C.A., Müller, R.D., Panter, K.S., 2005. A Cenozoic diffuse alkaline magmatic province (DAMP) in the southwest Pacific without rift or plume origin. Geochem. Geophys. Geosyst. 6.
Foden, J., Song, S.H., Turner, S., Elburg, M., Smith, P.B., Van der Steldt, B., Van Penglis, D., 2002. Geochemical evolution of lithospheric mantle beneath SE South Australia. Chem. Geol. 182, 663–695.
Forsyth, D.W., Harmon, N., Scheirer, D.S., Duncan, R.A., 2006. Distribution of recent volcanism and the morphology of seamounts and ridges in the GLIMPSE study area: implications for the lithospheric cracking hypothesis for the origin of intraplate, non-hot spot volcanic chains. J. Geophys. Res. Solid Earth 111.
Forsyth, S.M., 1984. Geological Survey Explanatory Report. Geological Atlas 1: 50,000 Series. Sheet 68 (8313S). Tasmania Department of Mines, Oatlands.
Forsyth, S.M., 1989. Geological Survey Explanatory Report. Geological Atlas 1: 50,000 Series. Sheet 61 (8313N). Tasmania Department of Mines, Interlaken.
Franke, D., 2013. Rifting, lithosphere breakup and volcanism: comparison of magma-poor and volcanic rifted margins. Mar. Pet. Geol. 43, 63–87.
Fraser, A.R., Tilbury, L.A., 1979. Structure and stratigraphy of the Ceduna Terrace region, Great Australian Bight Basin. APEA J. 19, 53–65.
Gaina, C., Dietmar Müller, R., Cande, S.C., 2000. Absolute Plate Motion, Mantle Flow, and Volcanism at the Boundary between the Pacific and Indian Ocean Mantle Domains since 90 MA, the History and Dynamics of Global Plate Motions. American Geophysical Union, pp. 189–210.
Geoffroy, L., 2005. Volcanic passive margins. Comptes Rendus Geosci. 337, 1395–1408.
Gibson, D., 2007. Potassium-argon Ages of Late Mesozoic and Cainozoic Igneous Rocks of Eastern Australia, p. 53. CRC Leme Open File Report 193.
Gibson, G.M., Totterdell, J.M., Morse, M.P., Goncharov, A., Mitchell, C.H., Stacey, A., 2012. Basement Structure and its Influence on the Pattern and Geometry of Continental Rifting and Breakup along Australia's Southern Rift Margin. Geoscience Australia Record 2012/47.
Gill, E.D., Segnit, E.R., 1986. Submerged volcanoes off Cape Otway, S.E. Australia. Search 17, 151–152.
Gray, C.M., McDougall, I., 2009. K-Ar geochronology of basalt petrogenesis, Newer Volcanic Province, Victoria. Aust. J. Earth Sci. 56, 245–258.
Haq, B.U., Hardenbol, J., Vail, P.R., 1988. Mesozoic and Cenozoic chronostratigraphy and cycles of sea-level change. In: Wilgus, C.K., Hastings, B.S., Kendall, C.G.S.C., Posamentier, H.W., Ross, C.A., Van Wagoner, J.C. (Eds.), Sea-level Changes; an Integrated Approach. Economic Paleontologists and Mineralogists, pp. 72–108. Special Publication.
Hill, P.J., Exon, N.F., 2013. Tectonics and Basin Development of the Offshore Tasmanian Area Incorporating Results from Deep Ocean Drilling, the Cenozoic Southern Ocean: Tectonics, Sedimentation, and Climate Change between Australia and Antarctica. American Geophysical Union, pp. 19–42.
Hill, P.J., Meixner, A.J., Moore, A.M.G., Exon, N.F., 1997. Structure and development of the west Tasmanian offshore sedimentary basins: results of recent marine and aeromagnetic surveys. Aust. J. Earth Sci. 44, 579–596.
Hill, P.J., Rollet, N., Symonds, P.A., 2001. Seafloor mapping of the south-east marine region and adjacent waters. AUSTREA final report Lord Howe Island, South-east Australian Margin (Includes Tasmania and South Tasman Rise) and Central Great Australian Bight. Australian Geological Survey Organisation, Canberra.
Holford, S.P., Hillis, R.R., Duddy, I.R., Green, P.F., Stoker, M.S., Tuitt, A.K., Backé, G., Tassone, D.R., MacDonald, J.D., 2011. Cenozoic post-breakup compressional deformation and exhumation of the southern Australian margin. APPEA J. 51, 613–638.
Holford, S.P., Schofield, N., Jackson, C.A.L., Magee, C., Green, P.F., Duddy, I.R., 2013. Impacts of Igneous Intrusions on Source and Reservoir Potential in Prospective Sedimentary Basins along the Western Australian Continental Margin. In: Keep, M., Moss, S.J. (Eds.). The Sedimentary Basins of Western Australia IV, Perth.
Holford, S.P., Schofield, N., Macdonald, J.D., Duddy, I.R., Green, P.F., 2012. Seismic analysis of igneous systems in sedimentary basins and their impacts on hydrocarbon prospectivity: examples from the southern Australian margin. APPEA J. 52, 229–252.
Holford, S.P., Tuitt, A.K., Hillis, R.R., Green, P.F., Stoker, M.S., Duddy, I.R., Sandiford, M., Tassone, D.R., 2014. Cenozoic deformation in the Otway Basin, southern Australian margin: implications for the origin and nature of post-breakup compression at rifted margins. Basin Res. 26, 10–37.
Holt, S.J., Holford, S.P., Foden, J., 2013. New insights into the magmatic plumbing system of the South Australian Quaternary Basalt province from 3D seismic and geochemical data. Aust. J. Earth Sci. 60, 797–817.
Jackson, C., 2012. Seismic reflection imaging and controls on the preservation of ancient sill-fed magmatic vents. J. Geol. Soc. 169, 503–506.
Jackson, C.A.-L., Schofield, N., Golenkov, B., 2013. Geometry and controls on the development of igneous sill–related forced folds: a 2-D seismic reflection case study from offshore southern Australia. Geol. Soc. Am. Bull. 125, 1874–1890.
Jarvis, G.T., McKenzie, D.P., 1980. Sedimentary basin formation with finite extension rates. Earth Planet. Sci. Lett 48, 42–52.
Jenkins, C.J., Packham, G.H., Hubble, T.C., Quilty, P.G., Adams, C.J., 1992. Trace of the Balleny hot-spot in the Tasman Sea and Southern Ocean from 70 Ma to present. In: First Australian Marine Sciences Association Meeting, Canberra.
Johnson, D., 2009. The Geology of Australia, second ed.
Johnson, R.W., 1989. Intraplate Volcanism in Eastern Australia and New Zealand, Intraplate Volcanism in Eastern Australia and New Zealand. Cambridge University Press, in Association with Australian Academy of Science.
Jones, S.J.M., White, N., Lovell, B., 2001. Cenozoic and Cretaceous transient uplift in the Porcupine Basin and its relationship to a mantle plume. Geol. Soc. Lond. Spec. Publ. 188, 345–360.
Kerr, A.C., 2014. Oceanic plateaus. In: Rudnick, R. (Ed.), The Crust (Treatise on Geochemistry, 2nd edn.). Elsevier, Amsterdam.
Knesel, K., Cohen, B., Vasconcelos, P., Thiede, D., 2008. Rapid change in drift of the Australian plate records collision with Ontong Java plateau. Nature 454, 754–U775.
Krassay, A.A., Cathro, D.L., Ryan, D.J., 2004. A regional tectonostratigraphic framework for the Otway Basin. In: Boult, P.J., Johns, D.R., Lang, S.C. (Eds.), Eastern Australian Basins Symposium II. Petroleum Exploration Society of Australia, Special Publication, Adelaide, South Australia, pp. 97–116.
Krassay, A.A., Totterdell, J.M., 2003. Seismic stratigraphy of a large, Cretaceous shelf-margin delta complex, offshore southern Australia. AAPG Bull. 87, 935–963.

Leaman, D.E., 1976. Geological Survey Explanatory Report. Geological Atlas 1:50,000 Series. Sheet 82 (8312S). Tasmania Department of Mines, Hobart.

Lennon, R.G., Suttill, R.J., Guthrie, D.A., Waldron, A.R., 1999. The renewed search for oil and gas in the Bass Basin: results of Yolla-2 and White Ibis-1. APPEA J. 39, 248–262.

Magee, C., Briggs, F., Jackson, C.A.L., 2013a. Lithological controls on igneous intrusion-induced ground deformation. J. Geol. Soc. Lond. 170, 853–856.

Magee, C., Hunt-Stewart, E., Jackson, C.A.L., 2013b. Volcano growth mechanisms and the role of sub-volcanic intrusions: insights from 2D seismic reflection data. Earth Planet. Sci. Lett. 373, 41–53.

McDougall, I., Duncan, R.A., 1988. Age progressive volcanism in the Tasmantid Seamounts. Earth Planet. Sci. Lett. 89, 207–220.

McDougall, I., Embleton, B.J.J., Stone, D.B., 1981. Origin and evolution of Lord Howe Island, Southwest Pacific Ocean. J. Geol. Soc. Aust. 28, 155–176.

Mcdougall, I., Harrison, T.M., 1999. Geochronology and Thermochronology by the $^{40}Ar/^{39}Ar$ Method. Oxford University Press, Oxford.

McDougall, I., Wellman, P., 1976. Potassium-argon ages for some Australian Mesozoic igneous rocks. J. Geol. Soc. Aust. 23, 1–9.

McLaren, S., Wallace, M.W., Gallagher, S.J., Dickinson, J.A., McAllister, A., 2009. Age constraints on Oligocene sedimentation in the Torquay Basin, southeastern Australia. Aust. J. Earth Sci. 56, 595–604.

McPhail, A., 2000. A Petrographic and Geochemical Study of Gippsland Basin Volcanics (BSc Honours thesis). University of Adelaide. unpublished.

Menzies, M.A., 2002. Volcanic Rifted Margins. Geological Society of America.

Messent, B.E., Collins, G.I., West, B.G., 1999. Hydrocarbon Prospectivity of the Offshore Torquay Sub-basin, Victoria: Gazettal Area V99-1. Victorian Initiative for Minerals and Petroleum Report 60. Department of Natural Resources and Environment.

Moore, A.M.G., Stagg, H.M.J., Norvick, M.S., 2000. Deep-water Otway Basin: a new assessment of the tectonics and hydrocarbon prospectivity. APEA J. 40, 66–85.

Mortimer, N., Gans, P.B., Palin, J.M., Meffre, S., Herzer, R.H., Skinner, D.N.B., 2010. Location and migration of Miocene–Quaternary volcanic arcs in the SW Pacific region. J. Volcanol. Geoth Res. 190, 1–10.

Norvick, M.S., 2005. Plate Tectonic Reconstructions of Australia's Southern Margins. Geoscience Australia. Record 2005/007.

Norvick, M.S., Smith, M.A., 2001. Mapping the plate tectonic reconstruction of southern and southeastern Australia and implications for petroleum systems. APPEA J. 41, 15–35.

Nourollah, H., Keetley, J., O'Brien, G., 2010. Gas chimney identification through seismic attribute analysis in the Gippsland Basin, Australia. Lead Edge 29, 896–901.

O'Brien, G.W., Tingate, P.R., Goldie Divko, L.M., Harrison, M.L., Boreham, C.J., Liu, K., Arian, N., Skladzien, P., 2008. First order sealing and hydrocarbon migration processes, Gippsland Basin, Australia: implications for CO_2 geosequestration. In: Eastern Australian Basins Symposium III. Petroleum Exploration Society of Australia, Sydney Convention and Exhibition Centre, NSW, Australia, pp. 1–28.

O'Halloran, G., Johnstone, E., 2001. Late Cretaceous rift volcanics of the Gippsland Basin, SE Australia – new insights from 3D seismic. In: Hill, K.C., Bernecker, T. (Eds.), Eastern Australasian Basins Symposium: a Refocussed Energy Perspective for the Future. Petroleum Exploration Society of Australia, Melbourne, Victoria, pp. 353–361.

O'Reilly, S.Y., Zhang, M., 1995. Geochemical characteristics of lava-field basalts from eastern Australia and inferred sources: connections with the subcontinental lithospheric mantle? Contrib. Mineral. Petrol. 121, 148–170.

Ollier, C.D., 1995. Tectonics and landscape evolution in Southeast Australia. Geomorphology 12, 37–44.

Paul, B., Hergt, J.M., Woodhead, J.D., 2005. Mantle heterogeneity beneath the Cenozoic volcanic provinces of central Victoria inferred from trace-element and Sr, Nd, Pb and Hf isotope data. Aust. J. Earth Sci. 52, 243–260.

Pilger, R.H., 1982. The origin of hotspot traces: evidence from eastern Australia. J. Geophys. Res. Solid Earth 87, 1825–1834.

Power, M.R., Hill, K.C., Hoffman, N., Bernecker, T., Norvick, M.S., 2001. The structural and tectonic evolution of the Gippsland Basin; results from 2D section balancing and 3D structural modelling. In: Hill, K.C., Bernecker, T. (Eds.), Eastern Australasian Basin Symposium, a Refocused Energy Perspective for the Future. Petroleum Exploration Society of Australia, pp. 373–384. Special Publication, 1.

Price, R.C., Gray, C.M., Frey, F.A., 1997. Strontium isotopic and trace element heterogeneity in the plains basalts of the Newer Volcanic Province, Victoria, Australia. Geochim. Cosmochim. Acta 61, 171–192.

Price, R.C., Nicholls, I.A., Day, A., 2014. Lithospheric influences on magma compositions of late Mesozoic and Cenozoic intraplate basalts (the Older Volcanics) of Victoria, south-eastern Australia. Lithos 206–207, 179–200.

Price, R.C., Nicholls, I.A., Gray, C.M., 2003. Cainozoic igneous activity. In: Birch, W.D. (Ed.), Geology of Victoria. Geological Society of Australia, pp. 361–375.

Rahmanian, V.D., Moore, P.S., Mudge, W.J., Spring, D.E., 1990. Sequence stratigraphy and the Habitat of hydrocarbons, Gippsland Basin Australia. Geol. Soc. Spec. Publ. 50, 525–544.

Rateau, R., Schofield, N., Smith, M., 2013. The potential role of igneous intrusions on hydrocarbon migration, West of Shetland. Pet. Geosci. 19, 259–272.

Richards, F., 2014. The origin, structural evolution and potential field signatures of the Tasmantid Seamount Chain. Unpublished Master thesis. Oxford University.

Rohrman, M., 2007. Prospectivity of volcanic basins: trap delineation and acreage de-risking. AAPG Bull. 91, 915–939.

Ryan, S.M., Knight, L.A., Parker, G.J., 1995. The stratigraphy and structure of the Tyrendarra Embayment. Geological Survey of Victoria, Otway Basin, Victoria.

Sayers, J., Symonds, P.A., Direen, N.O., Bernardel, G., 2001. Nature of continent-ocean transition on the non volcanic rifted margin of the central Great Australian Bight. In: Wilson, R.C.L., Whitmarsh, R.B., Taylor, B., Froitzheim, N. (Eds.), Non-volcanic Rifting of Oceanic Margins; a Comparison of Evidence from Land and Sea. Geological Society of London, pp. 51–76.

Schneider, C.L., Hill, K.C., Hoffman, N., 2004. Compressional growth of the Minerva Anticline, Otway Basin, Southeast Australia – evidence for oblique rifting. APPEA J. 44, 463–480.

Schofield, A., Totterdell, J., 2008. Distribution, Timing and Origin of Magmatism in the Bight and Eucla Basins, p. 19. Geoscience Australia Record 2008/4.

Schutter, S., 2003. Hydrocarbon occurrence and exploration in and around igneous rocks. In: Petford, N., McCaffrey, K. (Eds.), Hydrocarbons in Crystalline Rocks. Geological Society London, London, pp. 7–33.

Smith, G., 1986. Bass Basin Geology and Petroleum Exploration.

Stacey, A., Mitchell, C.H., Struckmeyer, H.I.M., Totterdell, J.M., 2013. Geology and Hydrocarbon Prospectivity of the Deepwater Otway and Sorell Basins, Offshore Southeastern Australia. Geoscience Australia. Record 2013/02.

Stagg, H.M.V., Cockshell, C.D., Willcox, J.B., Hill, A.J., Needham, D.V.L., Thomas, B., O'Brien, G.W., Hough, L.P., 1990. Basins of the Great Australian Bight region, geology and petroleum potential. In: Bureau of Mineral Resources, A. (Ed.), Continental Margins Program, Folio 5.

Storey, B.C., Vaughan, A.P.M., Riley, T.R., 2013. The links between large igneous provinces, continental break-up and environmental change: evidence reviewed from Antarctica. T Roy. Soc. Edin-Earth 104, 17–30.

Sutherland, F.L., 1980. Aquagene volcanism in the Tasmanian Tertiary in relation to coastal areas and river systems. Pap. Proc. R. Soc. Tasman. 114, 177–199.

Sutherland, F.L., 1981. Migration in relation to possible tectonic and regional controls in eastern Australian volcanism. J. Volcanol. Geoth Res. 9, 181–213.

Sutherland, F.L., 1983. Timing, trace and origin of basaltic migration in eastern Australia. Nature 305, 123–126.

Sutherland, F.L., 1991. Cainozoic volcanism, eastern Australia: a predictive model based on migration over multiple 'hotspot' magma sources. In: Williams, M.A.J., de Decker, P., Kershaw, A.P. (Eds.), Cenozoic of the Australian Region; a Reappraisal of the Evidence. Special Publication of the Geological Society of Australia,, pp. 15–43.

Sutherland, F.L., 2003. 'Boomerang' migratory intraplate Cenozoic volcanism, eastern Australian rift margins and the Indian-Pacific mantle boundary. Geol. Soc. Am. Spec. Pap. 372, 203–221.

Sutherland, F.L., Ewart, A., Raynor, L.R., Hollis, J.D., McDonough, W.F., 1989. Tertiary basaltic magmas and the Tasmanian lithosphere. In: Burrett, C.F., Martin, E.L. (Eds.), Geology and Mineral Resources of Tasmania. A Bicentennial Volume. Special Publication of the Geological Society of Australia, pp. 386–398.

Sutherland, F.L., Forsyth, S.M., Zwingmann, H., 2002. Bassian basalts: dating, Cenozoic biogeohistory and a new model for Tasmanian volcanism. Geol. Soc. Aust. Abstr. 67.

Sutherland, F.L., Graham, I.T., Everard, J.L., Forsyth, S.M., Zwingmann, H., 2004. Cenozoic Basalts, Tasmania: Landscapes, Exposures, Ages, Petrography, Geochemistry, Entrainments and Petrogenesis. Field Guide A5. Geological Society of Australia.

Sutherland, F.L., Graham, I.T., Hollis, J.D., Meffre, S., Zwingmann, H., Jourdan, F., Pogson, R.E., 2014. Multiple felsic events within post-10 Ma volcanism, Southeast Australia: inputs in appraising proposed magmatic models. Aust. J. Earth Sci. 1–27.

Sutherland, F.L., Graham, I.T., Meffre, S., Zwingmann, H., Pogson, R.E., 2012. Passive-margin prolonged volcanism, East Australian Plate: outbursts, progressions, plate controls and suggested causes. Aust. J. Earth Sci. 59, 983–1005.

Sutherland, F.L., Green, D.C., Wyatt, B.W., 1973. Age of the Great Lake basalts, Tasmania, in relation to Australian Cainozoic volcanism. J. Geol. Soc. Aust. 20, 85–93.

Teasdale, J., April 2004. Southern Australian Margin SEEBASE® Compilation. Geoscience Australia, Canberra.

Thomson, K., 2007. Determining magma flow in sills, dykes and laccoliths and their implications for sill emplacement mechanisms. Bull. Volcanol. 70, 183–201.

Totterdell, J.M., Bradshaw, B.E., 2004. The structural framework and tectonic evolution of the Bight Basin. In: Boult, P.J., Johns, D.R., Lang, S.C. (Eds.), Eastern Australian Basins Symposium II. PESA Special Publication, pp. 41–61.

Totterdell, J.M., Struckmeyer, H.I.M., Boreham, C.J., Mitchell, C.H., Monteil, E., Bradshaw, B.E., 2008. Mid-Late Cretaceous organic-rich rocks from the eastern Bight Basin: implications for prospectivity. In: Blevin, J.E., Bradshaw, B.E., Uruski, C. (Eds.), Eastern Australian Basins Symposium III. Petroleum Exploration Society of Australia, pp. 137–158. Special Publication.

Trigg, K.R., Blevin, J.E., Boreham, C.J., 2003. In: Australia, G. (Ed.), An Audit of Petroleum Exploration Wells in the Bass Basin 1965–1999.

Trupp, M.A., Spence, K.W., Gidding, M.J., 1994. Hydrocarbon prospectivity of the Torquay sub-basin, offshore Victoria. APEA J. 34.

Van Otterloo, J., Raveggi, M., Cas, R.A.F., Maas, R., 2014. Polymagmatic activity at the monogenetic Mt Gambier volcanic complex in the newer volcanics province, SE Australia: new insights into the occurrence of intraplate volcanic activity in Australia. J. Pet. 55, 1317–1351.

Vasconcelos, P., Knesel, K., Cohen, B., Heim, J., 2008. Geochronology of the Australian Cenozoic: a history of tectonic and igneous activity, weathering, erosion, and sedimentation. Aust. J. Earth Sci. 55, 865–914.

Veevers, J.J., 2000. Change of tectono-stratigraphic regime in the Australian plate during the 99 Ma (mid-Cretaceous) and 43 Ma (mid-Eocene) swerves of the Pacific. Geology 28, 47–50.

Veevers, J.J., Powell, C.M., Roots, S.R., 1991. Review of sea-floor spreading around

Australia .1. Synthesis of the Patterns of spreading. Aust. J. Earth Sci. 38, 373–389.
Verati, C., Jourdan, F., 2013. Modelling Effect of Sericitization of Plagioclase on the 40K/40Ar and 40Ar/39Ar Chronometers: Implication for Dating Basaltic Rocks and Mineral Deposits. Geological Society, London. Special Publications 378.
Vermeesch, P., 2012. On the visualisation of detrital age distributions. Chem. Geol. 312–313, 190–194.
Watson, M.N., Zwingmann, N., Lemon, N.M., Tingate, P.R., 2003. Onshore Otway Basin carbon dioxide accumulations: CO_2-induced diagenesis in natural analogues for underground storage of greenhouse gas. APPEA J. 43, 637–653.
Watts, A.B., Ryan, W.B.F., 1976. Flexure of the lithosphere and continental margin basins. Tectonophysics 36, 25–44.
Wellman, P., 1974. Potassium-argon ages on the Cainozoic volcanic rocks of Eastern Victoria, Australia. J. Geol. Soc. Aust. 21, 359–376.
Wellman, P., McDougall, I., 1974. Cainozoic igneous activity in eastern australia. Tectonophysics 23, 49–65.
White, R., McKenzie, D., 1989. Magmatism at rift zones – the generation of volcanic continental margins and flood basalts. J. Geophys. Res. Solid Earth Planets 94, 7685–7729.
Zalan, P., 2014. Comparisons between the deep crustal structure of magma-poor and volcanic passive margins. In: 4th Atlantic Conjugate Margins Conference, Saint John's, Newfoundland, Canada.

Chapter 3

Geochemical constraints on Cenozoic intraplate magmatism and their relation to Jurassic dolerites in Tasmania, using Sr-Nd-Pb isotopes

Statement of Authorship

Title of Paper	Geochemical constraints on Cenozoic intraplate magmatism and their relation to Jurassic dolerites in Tasmania, using Sr-Nd-Pb isotopes.
Publication Status	☑ Published ☐ Accepted for Publication ☐ Submitted for Publication ☐ Unpublished and Unsubmitted work written in manuscript style
Publication Details	Meeuws, F.J.E., Foden, J.D., Holford, S.P., Forster, M.A., 2019. Geochemical constraints on Cenozoic intraplate magmatism and their relation to Jurassic dolerites in Tasmania, using Sr-Nd-Pb isotopes. Chemical Geology 506, 225-273.

Principal Author

Name of Principal Author (Candidate)	Fun Julie Ellen Meeuws		
Contribution to the Paper	Project fieldwork, performed analyses on all samples, interpreted data, wrote manuscript and acted as corresponding author.		
Overall percentage (%)	80%		
Certification:	This paper reports on original research I conducted during the period of my Higher Degree by Research candidature and is not subject to any obligations or contractual agreements with a third party that would constrain its inclusion in this thesis. I am the primary author of this paper.		
Signature		Date	2/07/2019

Co-Author Contributions

By signing the Statement of Authorship, each author certifies that:

i. the candidate's stated contribution to the publication is accurate (as detailed above);

ii. permission is granted for the candidate in include the publication in the thesis; and

iii. the sum of all co-author contributions is equal to 100% less the candidate's stated contribution.

Name of Co-Author	Emeritus Professor John Foden		
Contribution to the Paper	Guidance in the field, supervised development of work, helped in data interpretation and manuscript evaluation.		
Signature		Date	2/07/2019

Name of Co-Author	Associate Professor Simon Holford		
Contribution to the Paper	Helped to evaluate and edit the manuscript.		
Signature		Date	2/07/2019

Name of Co-Author	Dr Marnie Forster		
Contribution to the Paper	Sample preparation for Ar-analysis, collection and interpretation of Ar-data.		
Signature		Date	2/07/2019

Please cut and paste additional co-author panels here as required.

Chemical Geology 506 (2019) 225–273

Contents lists available at ScienceDirect

Chemical Geology

journal homepage: www.elsevier.com/locate/chemgeo

Geochemical constraints on Cenozoic intraplate magmatism and their relation to Jurassic dolerites in Tasmania, using Sr-Nd-Pb isotopes

Fun J.E. Meeuws[a,*], John D. Foden[a], Simon P. Holford[b], Marnie A. Forster[c]

[a] Centre for Tectonics, Resources and Exploration (TRaX), University of Adelaide, Adelaide, SA 5005, Australia
[b] Australian School of Petroleum, Centre for Tectonics, Resources and Exploration (TRaX), University of Adelaide, Adelaide, SA 5005, Australia
[c] Research School of Earth Sciences, The Australian National University, Canberra 0200, Australia

ARTICLE INFO

Editor: Catherine Chauvel

Keywords:
Tasmania
Sr-Nd-Pb isotopes
Cenozoic basalts
$^{39}Ar/^{40}Ar$
Jurassic dolerite

ABSTRACT

Tasmania hosts two prominent Meso-Cenozoic mafic magmatic provinces: abundant Jurassic dolerites that belong to the Ferrar Magmatic Province that formed during Gondwana break-up; and Cenozoic, mainly basaltic volcanics, which represent intraplate magmatism, post-Gondwana break-up. The origin of the Cenozoic volcanics is still controversial, in that the detailed role of competing asthenospheric and lithospheric sources remains unclear. This study presents new geochemical and isotopic data which is used to identify and contrast the magmatic sources and their relationship to Jurassic and Cenozoic magmas. The compositions of the Cenozoic lavas span a wide range from highly silica-undersaturated olivine melilitites and nephelinites to basanites, nehawaiites, olivine basalts and quartz-tholeiites. New Sr-Nd-Pb isotopic data combined with major and trace element geochemistry show that the most silica-undersaturated rocks are most enriched in incompatible elements and also have the least radiogenic Sr and most radiogenic Nd. Sr-Nd-Pb isotope ratios for the most silica-rich lavas trend towards values for the Ferrar Jurassic dolerite source. More generally, Sr, Nd and Pb isotopes in the Cenozoic lavas can be modelled by a three component mixture of Pacific Mid-Ocean Ridge Basalts (MORB), HIMU-like (characterized by high time-integrated μ ($^{238}U/^{204}Pb$)) and Jurassic dolerite sources. Pb isotope values confirm the HIMU-like component in the array. Various degrees of melting during decompression melting has also contributed to the wide range of compositions observed, with most silica-undersaturated rocks originating at the highest pressures (> 20 kbar) and by the smallest percentages of melting. We suggest that this process, combined with variable interaction of MORB and HIMU-like asthenospheric sources with lithospheric mantle containing remnant Jurassic signatures, resulted in the wide range of Cenozoic lava compositions observed today.

1. Introduction

Dominantly basaltic, intra-plate magmatic provinces are distributed globally (e.g. Hawaii, Réunion, Heard Islands and Ontong Java, Columbia River, Hikurangi and Caribbean flood basalt provinces). The most typical explanation for their occurrence involves upwelling mantle plumes (e.g. Coffin and Eldholm, 1994; Morgan, 1971; Morgan, 1972; Richards et al., 1989). This model is premised on stationary plumes that are thermal driven and deeply sourced. Although successful in explaining linear, age progressive, volcano chains, not all intraplate volcanism conforms to this pattern. Linked to this problem is the identification of the source regions of intraplate magmas. This includes, the detailed roles of competing asthenospheric and lithospheric mantle sources and the factors that generate melting in each of these domains remain a source of on-going debate (e.g. Anderson, 1998; Clouard and Bonneville, 2001; Courtillot et al., 2003; Morgan, 1971; Morgan, 1972; Pettke et al., 2018).

Cenozoic magmatism in Tasmania is an example of an intraplate magmatic province where no clear age-relationship exists with plate motions. It forms part of one of the world's largest intraplate magmatic provinces: the mainly basaltic Eastern Australian Magmatic Province (EAMP) (Appendix Fig. A1). The latter, has been attributed to several hotspot-tracks (e.g. Davies et al., 2015; Sutherland, 1981; Sutherland et al., 2006; Wellman and McDougall, 1974). Cenozoic magmatism in Tasmania, however, lies south of the plume-head of the Eastern Australian hotspot (Appendix Fig. A1), which is proposed to be situated beneath the Bass Strait, between Victoria and Tasmania. Unlike Cenozoic magmatism on mainland Australia, it shows no southward age-trend in activity (Fig. 1), with youngest basalts occurring in the north of the island (Baillie, 1986b). Although geochemically quite similar, the

* Corresponding author.
E-mail address: fun.meeuws@adelaide.edu.au (F.J.E. Meeuws).

https://doi.org/10.1016/j.chemgeo.2018.12.025
Received 24 April 2018; Received in revised form 20 November 2018; Accepted 20 December 2018
Available online 04 January 2019

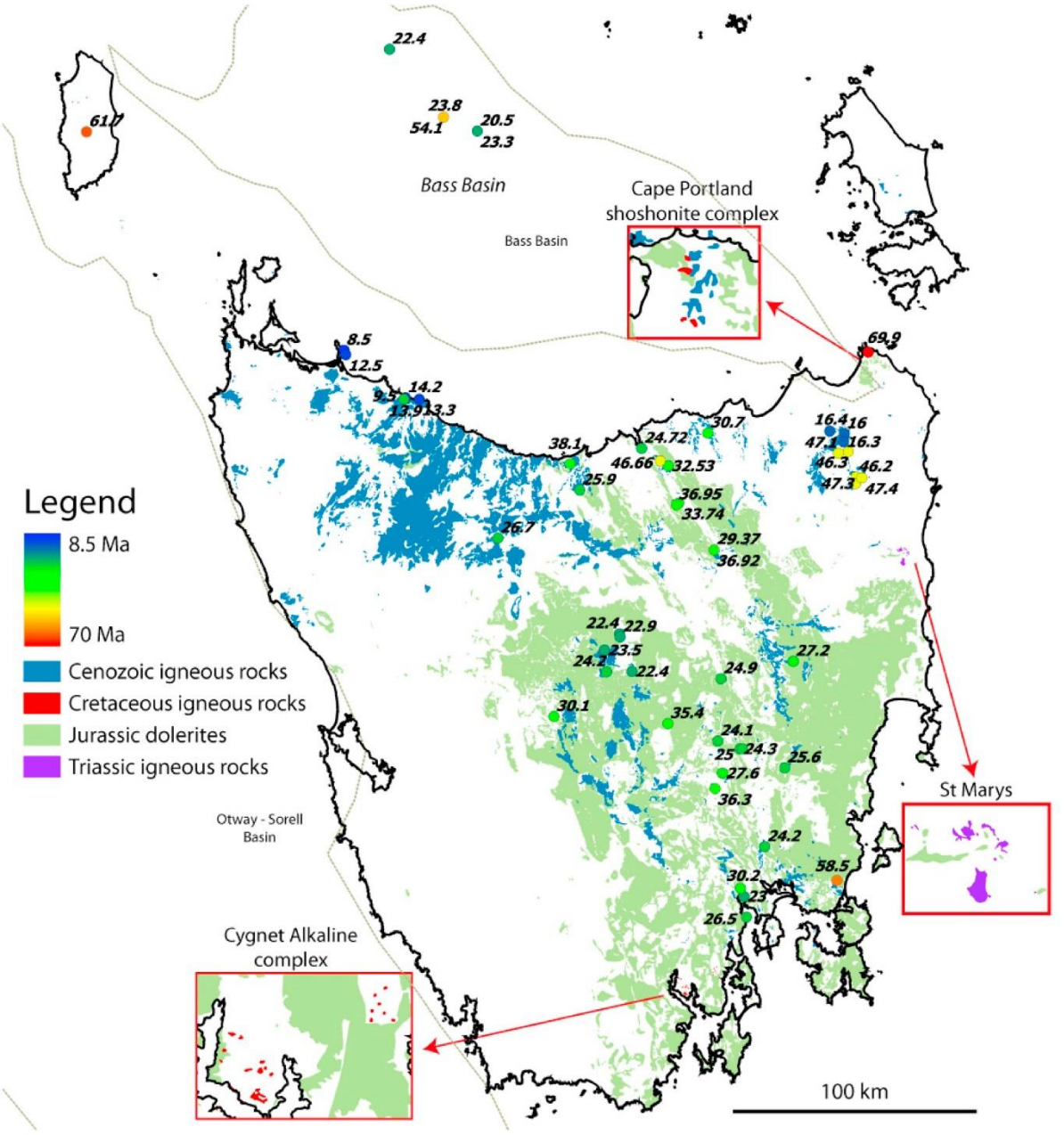

Fig. 1. Absolute ages of Meso- and Cenozoic igneous rocks in Tasmania (compiled from Gibson (2007); Vasconcelos et al. (2008)).

Pb-isotopic composition of the Tasmanian Cenozoic igneous rocks seems to be quite distinct from any other lava field provinces situated in mainland Australia (Nasir et al., 2010). Both asthenospheric (Adam and Green, 2011) and subcontinental lithospheric mantle (SCLM) (Sun et al., 1989) source depths have been proposed.

The origin of Cenozoic lava field magmatism in eastern Australia, and Tasmania in particular, is still controversial. One of the proposed models is a 'plume swathe' model whereby passive mantle upwelling or upwelling of abnormally hot, elongated deep mantle material is related to regional extension triggered by Tasman Sea opening and/or Gondwana break-up (Lister and Etheridge, 1989; O'Reilly and Zhang, 1995). A second stream of thoughts relates the Tasmanian volcanism to one or several hotspots that link the offshore Tasmanian seamounts (Sutherland et al., 2006) and Balleny plume (Lanyon et al., 1993) to the magmatism onshore.

An extensive number of samples of Cenozoic volcanic rocks in

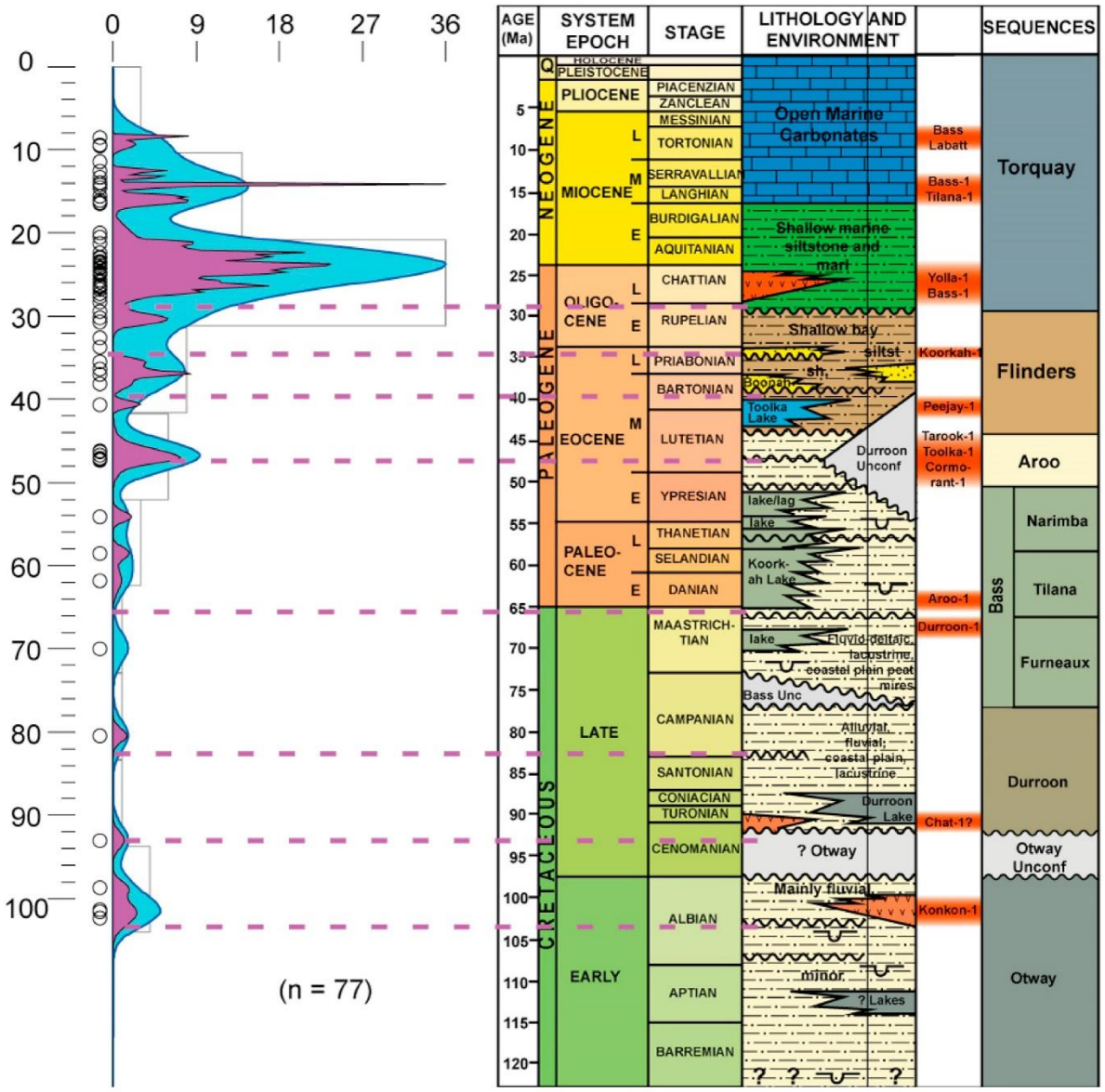

Fig. 2. Left: Kernel density plot showing the ages of Cenozoic volcanism onshore Tasmania (compiled from Corbett et al. (2014); Gibson (2007); Vasconcelos et al. (2008)), modelled with Densityplotter by Vermeesch (2012)). Right: Generalised stratigraphy of the Bass Basin with indication of magmatic events (after Blevin et al. (2005)).

Tasmania have been analysed by several authors (e.g. Adam (1990); Adam and Green (2011); Everard et al. (2007); Frey et al. (1978); Lanyon et al. (1993); McDonough et al. (1985); Nasir et al. (2010); Sutherland (1973); Sutherland (1974); Sutherland et al. (1989); Sutherland et al. (2004); Sutherland and Hale (1970)), however, almost no Pb isotopes (except for a few published by Ewart et al. (1988), two olivine tholeiites from the Great Lake area (Sutherland, 2003), and xenoliths analysed by Nasir et al. (2010)) and little Nd isotope data are available in the published data (Adam and Green, 2011; Everard et al., 1997; Ewart et al., 1988; Matthews et al., 1996; McDonough et al., 1985; Nasir et al., 2010; Sutherland, 2003). In this paper, we present a new dataset of major, minor and trace elements, and of Sr-Nd-Pb isotopes for Cenozoic igneous rocks in Tasmania. Also included is a smaller sub-set of data for the Tasmanian Jurassic dolerites. This information is used to assess models of origin (including the competing roles of continental lithosphere, asthenosphere and plume sources) for Tasmanian Cenozoic magmas.

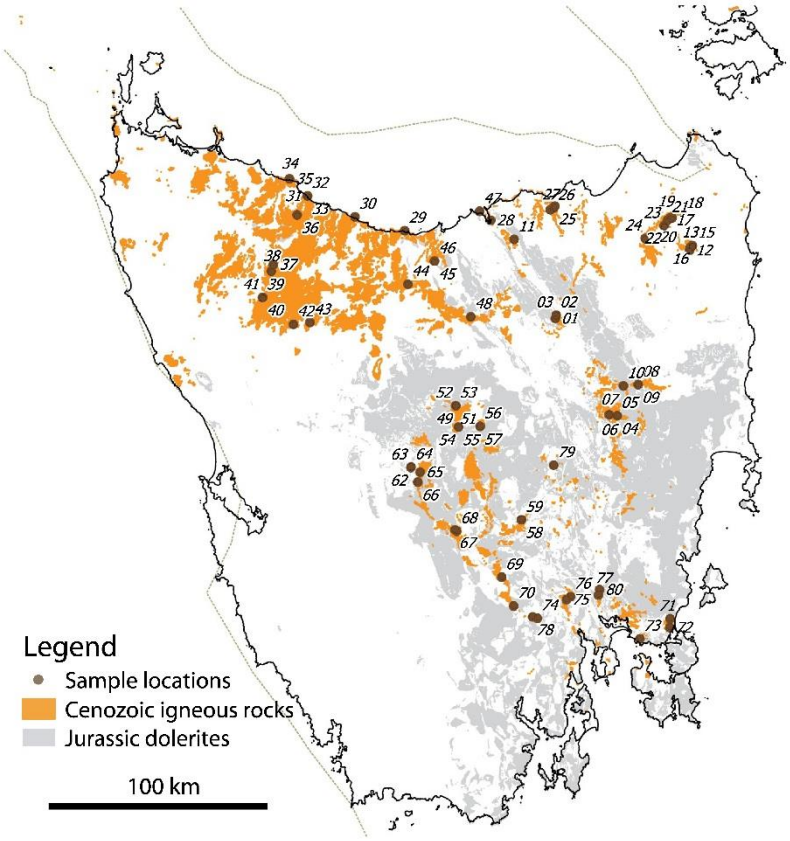

Fig. 3. Location map of samples taken. Orange indicates the location of Cenozoic igneous rocks, grey indicates the location of Jurassic igneous rocks.

2. Geological setting

2.1. Tasmania

Tasmania is part of the Australian continent, and has a complex Early Palaeozoic history of accretion of Neoproterozoic terrains and plate margin activity. Pre-Mesozoic geology of Tasmania can be divided into eastern terrane and western terranes, separated by the Tamar Lineament, situated beneath the Tamar Graben (Seymour et al., 2013). The western terrane consists of Mesoproterozoic and Neoproterozoic cratonic crust (Seymour et al., 2013). The eastern terrane on the other hand is younger, with Ordovician–Lower Devonian turbiditic sandstone and mudstone assumed to overlie oceanic crust (Seymour et al., 2013). The eastern terrane was substantially separated from the western terrane and was joined during the Middle Devonian Tabberaberan orogeny (Seymour et al., 2013). The intrusion of enormous volumes of Early Jurassic low Ti tholeiite dolerite heralded Gondwana break-up (Hergt et al., 1989). These intrusions occur mainly as sills intruding the Tasmania Basin and form part of the vast Ferrar Magmatic Province (Hergt et al., 1989), ultimately extending across Antarctica to the Karoo Large Igneous Province in Southern Africa (Encarnación et al., 1996). Further rifting of Gondwana and the separation of Australia and Antarctica continued into the Cretaceous, resulting in the sedimentary rift basins along the Australian southern margin and opening of the Southern Ocean. This rifting eventually evolved to complete continental break-up, in the Otway and Sorell Basins, whereas the Bass Basin never saw break-up (Meeuws et al., 2016 and references therein). Break-up of the Tasman Sea to the east of Tasmania (80–83 Ma) accelerated subsidence in the Bass Basin and caused break-up adjacent to the Gippsland Basin. As spreading continued west of Tasmania along a major transform fault in the Sorell Basin, major NW-SE directed graben faulting occurred (e.g. Tamar Graben) in onshore Tasmania, giving rise to the modern topography. Scattered, mainly alkaline igneous activity occurred during the middle to late Cretaceous, followed by a major episode of Cenozoic volcanism which occurred both onshore in Tasmania and offshore in the Bass, Sorell, South Tasman Rise and East Tasman Plateau (Everard, 2014).

2.2. Meso-Cenozoic volcanism in Tasmania

The Tasmanian Cenozoic Province forms the southernmost extension of the Eastern Australian Cenozoic Magmatic Province ((Meeuws et al., 2016: Appendix Fig. A1). The Tasmanian province is dominated by mafic lavas with widely varying compositions from highly

Table 1
Major element concentrations in weight% of Tertiary and Jurassic Tasmanian mafic rocks and their locations in GDA94.

Sample	latitude	longitude	height	L.O.I.%	LOI XRF (%)	Sum of conc (%)	SiO_2	TiO_2	Al_2O_3	Fe_2O_3*	MnO	MgO	CaO	Na_2O	K_2O	P_2O_5	SO_3	Cl	Mg#	FeO*
TAS14-01	−41.53188	147.19110	187	1.0973	−0.03	100.03	47.80	1.933	14.63	11.86	0.1642	10.01	9.14	2.767	1.233	0.446	0.0345	36	66.29	10.67623504
TAS14-02	−41.51807	147.19562	215	0.8714	−0.42	100.42	48.34	2.280	16.72	11.24	0.1635	6.03	9.66	4.322	1.151	0.495	−0.0045	43	55.55	10.11743004
TAS14-03	−41.51788	147.19652	202	0.8144	−0.59	100.59	49.03	2.093	15.58	11.44	0.1623	8.00	8.84	3.776	1.210	0.451	0.0000	49	61.96	10.29514982
TAS14-04	−41.94075	147.54247	222	0.6156	−0.15	100.15	52.74	1.681	14.62	11.22	0.1350	6.62	9.37	2.939	0.532	0.256	0.0240	52	57.87	10.0994331
TAS14-05	−41.94075	147.54247	222	0.7138	0.50	99.50	53.29	1.762	15.24	10.24	0.1259	5.08	9.83	3.074	0.541	0.269	0.0465	41	53.65	9.211284082
TAS14-06	−41.93642	147.49646	198	0.6828	0.15	99.85	54.22	1.877	15.46	8.97	0.1200	6.02	9.23	3.153	0.600	0.208	−0.0060	13	60.98	8.07252767
TAS14-07b	−41.93642	147.49646	198	0.4402	−0.19	100.19	53.70	1.857	15.29	9.39	0.1295	6.32	9.43	3.141	0.670	0.264	−0.0060	30	61.06	8.449113651
TAS14-08	−41.80980	147.66116	212	−0.1369	−0.13	100.13	51.99	1.693	14.07	11.74	0.1522	7.77	8.83	2.899	0.669	0.248	0.0585	106	60.66	10.56240439
TAS14-09	−41.81006	147.66083	211	0.7653	−0.08	100.08	52.12	1.704	14.08	11.55	0.1489	7.57	9.02	2.879	0.666	0.250	0.0920	88	60.43	10.38963376
TAS14-10	−41.81552	147.57721	207	2.1533	0.16	99.84	43.32	2.530	10.73	14.15	0.2347	12.81	8.43	4.466	1.459	1.608	0.0410	595	67.85	12.73283542
TAS14-11	−41.19670	146.95755	91	0.5530	−0.63	100.63	49.09	2.167	15.50	11.26	0.1647	7.20	9.90	3.689	1.222	0.428	0.0100	67	59.86	10.12777828
TAS14-12	−41.24369	147.95317	497	1.2996	−0.19	100.19	45.13	2.148	15.32	11.88	0.1949	10.45	10.42	3.277	0.807	0.537	0.0335	69	67.21	10.6870332
TAS14-13	−41.23146	147.95534	580	1.6810	−0.11	100.11	45.80	2.068	15.60	11.18	0.1950	10.13	10.28	2.934	1.394	0.526	−0.0035	58	67.86	10.05849006
TAS14-14	−41.22365	147.96770	655	0.7490	−0.50	100.50	45.98	2.076	15.75	11.50	0.1870	8.81	10.44	4.237	0.827	0.661	−0.0050	340	64.10	10.35004049
TAS14-15	−41.22349	147.96840	642	0.7592	−0.91	100.91	45.25	2.017	14.65	12.21	0.1909	11.76	9.80	3.248	1.200	0.569	−0.0020	178	69.18	10.98938181
TAS14-16	−41.22358	147.96886	652	1.5663	−0.26	100.26	46.15	2.112	15.75	11.60	0.1909	9.45	10.66	3.046	0.615	0.640	0.0270	166	65.49	10.43867543
TAS14-17	−41.10601	147.85313	217	2.3733	0.02	99.98	42.55	2.662	11.79	13.99	0.2018	12.40	11.35	2.984	1.017	1.030	0.0035	183	67.38	12.58526051
TAS14-18	−41.10482	147.84399	222	0.2398	0.02	99.98	42.73	2.627	11.76	13.56	0.2241	12.35	10.46	3.894	1.445	0.890	0.0025	287	67.98	12.20462521
TAS14-19	−41.11495	147.82747	256	0.4192	−0.66	100.66	42.67	2.621	11.58	13.86	0.1981	12.56	10.63	4.063	1.507	0.897	0.0540	208	67.87	12.47008009
TAS14-20	−41.11494	147.82735	260	0.4662	−1.23	101.23	42.92	2.625	11.69	13.85	0.1987	12.68	10.60	4.088	1.585	0.902	0.0655	300	68.09	12.46378116
TAS14-21	−41.11497	147.82727	260	0.1740	−0.60	100.60	39.97	2.915	10.59	15.21	0.2210	13.14	11.07	4.591	1.532	1.305	0.0340	314	66.81	13.68667327
TAS14-22	−41.13737	147.80992	238	0.4479	−0.67	100.67	40.54	2.813	10.72	14.93	0.2205	13.56	11.04	4.189	1.369	1.234	0.0345	202	67.91	13.43381625
TAS14-23	−41.13965	147.80853	216	1.0945	0.00	100.00	40.58	2.837	10.78	14.99	0.2042	13.01	11.08	3.983	1.272	1.252	0.0160	166	66.92	13.48465761
TAS14-24	−41.19257	147.70021	251	1.0895	−0.82	100.82	46.04	2.443	12.57	12.96	0.1745	11.78	10.05	2.792	1.336	0.651	0.0175	104	67.93	11.65841807
TAS14-25	−41.05572	147.18843	96	0.5428	0.63	99.37	51.94	1.780	14.23	10.51	0.1645	7.39	9.66	2.966	0.369	0.225	0.1315	31	62.10	9.457842167
TAS14-26	−41.06406	147.18091	97	−0.1916	0.83	99.17	49.21	1.976	13.36	12.80	0.1708	9.23	8.65	2.981	0.463	0.317	0.0165	68	62.69	11.51399262
TAS14-27	−41.07141	147.16277		−0.2370	0.41	99.59	52.21	1.573	13.52	11.27	0.1531	9.26	8.50	2.640	0.287	0.183	−0.0005	22	65.70	10.13722667
TAS14-28	−41.11585	146.82452	11	0.1109	−0.57	100.57	49.19	2.165	14.03	13.31	0.1650	8.50	8.44	3.418	0.945	0.399	0.0080	39	59.83	11.97336453
TAS14-29	−41.15998	146.33623	6	0.1320	0.14	99.86	50.62	1.830	13.63	12.09	0.1624	8.86	8.74	3.048	0.568	0.257	0.0435	72	63.07	10.87915054
TAS14-30	−41.10120	146.05423	4	1.1615	−0.98	100.98	45.71	2.157	13.99	12.83	0.1935	11.32	9.80	3.205	1.265	0.448	0.0400	293	67.27	11.54593719
TAS14-31	−41.01318	145.78427	12	1.1154	−0.62	100.62	43.99	2.614	13.38	12.79	0.1747	12.04	9.01	4.027	1.861	0.682	0.0235	269	68.68	11.51084316
TAS14-32	−41.01236	145.78578	11	0.6506	−0.16	100.16	43.73	2.595	13.35	12.77	0.1755	11.88	9.17	4.211	1.555	0.690	0.0190	200	68.44	11.48699721
TAS14-33	−41.01236	145.78578	11	0.6535	−0.48	100.48	44.17	2.603	13.37	12.74	0.1736	12.37	8.97	4.306	1.082	0.673	0.0110	87	69.35	11.46495096
TAS14-34	−40.93953	145.68269	54	0.6337	−28.89	128.89	45.64	2.106	14.29	13.324	0.1786	9.722	8.634	3.771	1.569	0.640	0.0030	86	62.97	11.98956177
TAS14-35	−40.93953	145.68269	54	0.6423	−0.36	100.36	45.80	2.140	14.38	13.43	0.1822	9.72	8.66	3.772	1.611	0.661	−0.0025	135	62.78	12.08224602
TAS14-36	−41.09302	145.72609	255	1.3463	−0.25	100.25	47.13	1.932	15.31	12.78	0.1799	9.58	8.80	2.785	1.337	0.400	0.0180	29	63.58	11.50319446
TAS14-37	−41.30416	145.59056	581	0.9144	−0.65	100.65	47.77	2.218	13.75	12.58	0.1831	10.66	9.15	2.622	1.285	0.422	0.0010	41	66.38	11.32187528
TAS14-38	−41.33179	145.57985	600	0.7232	−0.56	100.56	50.04	1.728	14.50	12.40	0.1785	9.23	8.40	2.961	0.865	0.245	−0.0060	29	63.43	11.16215243
TAS14-39	−41.44316	145.52948	571	3.8596	0.92	99.08	48.80	1.632	14.48	12.72	0.1724	8.31	8.75	3.060	0.860	0.234	0.0770	46	60.35	11.44425448
TAS14-40	−41.44255	145.53099	587	1.2531	−0.43	100.43	51.98	1.815	14.61	12.39	0.2133	6.80	8.14	2.948	1.214	0.283	0.0320	55	56.13	11.14595519
TAS14-41	−41.44292	145.53088	602	0.6770	−0.48	100.48	52.70	1.906	15.04	10.99	0.1410	6.80	8.31	3.036	1.244	0.299	0.0100	43	59.05	9.890218663
TAS14-42	−41.55696	145.70523	729	0.2630	−25.08	125.08	50.34	1.781	14.46	11.639	0.1515	8.560	8.519	3.146	0.873	0.271	0.0090	13	63.15	10.47331954
TAS14-43	−41.54843	145.79926	742	1.1287	−0.67	100.67	45.29	2.306	13.57	13.97	0.1949	10.58	9.94	2.843	1.274	0.685	0.0070	110	63.83	12.57491226
TAS14-44	−41.38691	146.35432	282	0.5728	−0.35	100.35	47.40	1.879	14.31	12.43	0.1796	10.27	9.00	3.115	1.337	0.407	0.0155	30	65.82	11.18734815
TAS14-45	−41.28900	146.50558	182	−0.1877	−0.49	100.49	46.79	2.243	13.85	12.62	0.1724	10.64	8.65	3.555	1.460	0.499	0.0055	66	66.28	11.35202016
TAS14-46	−41.28893	146.50568	182	−0.1880	−0.31	100.31	47.32	2.341	14.43	12.01	0.1647	9.51	8.38	3.779	1.748	0.581	0.0370	97	64.86	10.80986232
TAS14-47	−41.07824	146.76164	2	0.2851	−0.43	100.43	48.66	2.354	14.03	13.60	0.1668	8.34	8.26	3.470	1.097	0.446	0.0035	36	58.82	12.24151894
TAS14-48	−41.52486	146.71147	252	1.8844	−0.26	100.26	48.47	1.838	14.80	12.07	0.1739	9.28	9.57	2.754	0.946	0.321	0.0340	13	64.18	10.86430307

(*continued on next page*)

Table 1 (*continued*)

Sample	latitude	longitude	height	LOI%	LOI XRF (%)	Sum of conc (%)	SiO_2	TiO_2	Al_2O_3	Fe_2O_3*	MnO	MgO	CaO	Na_2O	K_2O	P_2O_5	SO_3	Cl	Mg#	FeO*
TAS14-49	−41.89893	146.62675	1106	0.2313	−0.49	100.49	52.19	1.614	14.30	11.98	0.1578	7.86	8.84	2.821	0.524	0.210	0.0045	16	60.46	10.77746783
TAS14-50	−41.89893	146.62675	1108	−0.1071	−0.46	100.46	47.49	2.283	13.77	13.45	0.1824	9.83	9.17	2.833	1.068	0.391	−0.0060	38	63.01	12.10024296
TAS14-51	−41.89877	146.62558	1110	2.4225	0.12	99.88	47.80	2.163	14.05	13.17	0.1849	10.24	8.25	2.621	1.008	0.393	0.0000	33	64.43	11.85143526
TAS14-52	−41.89877	146.62558	1110	1.9967	−0.31	100.31	47.61	2.251	13.84	13.49	0.1790	10.51	8.47	2.510	1.060	0.393	−0.0030	27	64.48	12.13623684
TAS14-53	−41.89877	146.62558	1110	0.0797	−0.47	100.47	51.64	1.562	14.92	11.36	0.1563	8.13	9.21	2.782	0.504	0.198	0.0005	16	62.52	10.22451183
TAS14-54	−41.98798	146.64182	1018	0.0699	−0.74	100.74	52.55	1.747	13.98	12.16	0.1606	7.72	8.83	2.787	0.549	0.222	0.0205	25	59.68	10.94348961
TAS14-55	−41.98798	146.64182	1018	0.0420	−0.85	100.85	52.68	1.756	14.57	11.76	0.1547	7.22	9.02	2.889	0.554	0.226	0.0180	16	58.85	10.58400072
TAS14-56	−41.98545	146.76479	1062	−0.1637	−24.29	124.29	51.66	1.620	14.48	11.232	0.1479	8.086	8.517	2.880	0.938	0.232	0.0480	54	62.65	10.1070818
TAS14-57	−41.98537	146.76413	1058	1.2720	−0.46	100.46	52.05	1.671	14.45	12.56	0.1668	6.94	8.56	2.913	0.898	0.239	0.0190	50	56.28	11.3011788
TAS14-58	−42.37547	146.99854	356	0.7712	−0.52	100.52	52.14	1.749	14.15	13.57	0.1923	6.35	8.48	3.013	0.614	0.241	0.0055	31	52.17	12.21362368
TAS14-59	−42.37570	146.99960		0.8192	−1.06	101.06	46.41	2.587	13.58	14.21	0.1768	9.80	9.71	2.782	1.258	0.538	0.0135	48	61.64	12.78457662
TAS14-60	−42.15754	146.37141	707	0.0350	−0.92	100.92	38.15	2.634	9.75	14.22	0.2239	16.40	12.96	3.872	1.334	1.279	0.0715	305	72.88	12.79492486
TAS14-61	−42.15758	146.37138	734	0.1078	−0.15	100.15	37.83	2.625	9.74	14.16	0.2226	16.10	12.98	3.765	1.382	1.274	0.0555	261	72.60	12.73958427
TAS14-62	−42.15740	146.37114	715	0.2524	−0.17	100.17	37.74	2.675	9.89	14.28	0.2246	15.75	13.01	3.841	1.399	1.304	0.0305	293	71.99	12.84846576
TAS14-63	−42.15759	146.37151	733	0.0682	−0.77	100.77	38.12	2.635	9.78	14.21	0.2230	16.15	13.11	3.785	1.357	1.278	0.0830	293	72.59	12.79087555
TAS14-64	−42.15583	146.37263	726	0.8760	−0.21	100.21	54.87	0.758	16.44	10.71	0.1737	4.06	9.79	2.209	1.065	0.117	0.0225	0	46.87	9.64006119
TAS14-65	−42.17685	146.42426	647	−0.3298	−1.17	101.17	51.17	1.662	14.59	12.51	0.1670	8.19	9.08	2.824	0.709	0.215	0.0395	57	60.41	11.26068568
TAS14-66	−42.21818	146.41115	663	−0.3374	−0.22	100.22	46.98	2.254	13.26	13.81	0.1877	9.74	9.27	3.067	1.156	0.472	0.0070	48	62.18	12.42868712
TAS14-67	−42.41754	146.62228	332	0.4461	−0.45	100.45	51.72	1.551	14.56	12.16	0.1599	7.52	9.33	2.802	0.421	0.220	0.0145	68	59.03	10.94034014
TAS14-68	−42.42284	146.63138	262	−0.2373	−0.07	100.07	51.55	1.601	13.74	11.77	0.1623	8.73	8.94	2.712	0.580	0.251	0.0395	46	63.35	10.5911995
TAS14-69	−42.61444	146.88727	206	0.0404	0.12	99.88	53.95	0.604	15.03	9.59	0.1625	7.00	10.92	1.724	0.810	0.092	−0.0065	3	62.97	8.629083056
TAS14-70	−42.73384	146.95436	23	−0.2747	−0.63	100.63	51.14	1.637	14.47	12.16	0.1614	8.11	9.17	2.924	0.548	0.227	0.0625	93	60.86	10.93989022
TAS14-71	−42.78634	147.84196	154	0.2764	−0.44	100.44	54.46	0.627	15.09	9.82	0.1684	6.71	10.81	1.871	0.800	0.098	0.0040	5	61.42	8.832448484
TAS14-72	−42.82283	147.83951	95	−0.1404	−0.81	100.81	48.69	1.242	15.06	12.49	0.1777	10.25	9.56	2.766	0.282	0.274	0.0050	65	65.65	11.24133897
TAS14-73	−42.86903	147.67082	21	3.2305	−0.18	100.18	48.69	2.758	15.31	12.85	0.1594	5.02	8.18	4.596	1.748	0.822	0.0235	336	47.64	11.5594349
TAS14-74	−42.78444	147.08943	14	4.9986	0.18	99.82	41.58	2.949	13.53	16.81	1.3992	5.23	11.24	4.378	1.460	1.177	0.0435	247	42.01	15.13047782
TAS14-75	−42.70780	147.25406	57	−0.0574	−0.16	100.16	52.17	1.716	14.27	11.25	0.1498	7.68	8.73	2.939	0.922	0.247	0.0775	58	61.40	10.12687843
TAS14-76	−42.69538	147.27740	72	3.3175	−0.75	100.75	52.73	1.616	14.48	11.10	0.1654	6.00	10.68	2.950	0.640	0.227	0.1620	50	55.73	9.987402142
TAS14-77	−42.68861	147.43546	39	1.5114	−0.81	100.81	49.28	1.785	14.12	13.06	0.1707	8.34	10.03	3.081	0.554	0.343	0.0550	44	59.82	11.75065239
TAS14-78	−42.77850	147.06274	45	−0.0037	−0.43	100.43	52.04	1.686	14.15	11.48	0.1509	8.15	8.66	2.916	0.880	0.247	0.0685	68	62.31	10.3329434
TAS14-79	−42.14832	147.18185	841	0.5651	−0.62	100.62	54.55	0.635	15.08	9.86	0.1703	6.77	10.74	1.868	0.846	0.098	0.0055	17	61.55	8.870242059
TAS14-80	−42.66618	147.44180	53	2.5876	−0.56	100.56	48.56	1.825	13.96	12.66	0.1691	9.65	9.79	3.083	0.452	0.373	0.0425	59	63.97	11.39476289
Estimated uncertainty							0.1	0.005	0.03	0.02	0.0005	0.01	0.01	0.005	0.002	0.001	0.0005	5		

Table 2
XRF trace element analyses in ppm for Cenozoic and Jurassic mafic rocks in Tasmania.

Sample	Ag	As	Ba	Bi	Br	Cd	Ce	Cl	Co	Cr	Cs	Cu	Ga	Ge	Hf	I	La	Mo	Nb	Nd
TAS14-01 Agate mill	< 5	< 3	254	5	< 3	< 5	46	36	48	258	< 10	50	21	< 3	< 10		< 10	31	< 3	33
TAS14-02 Agate mill	7	< 3	216	< 5	< 3	< 5	54	43	32	136	< 10	38	20	< 3	< 10		< 10	24	< 3	33
TAS14-03 Agate mill	< 5	< 3	273	< 5	< 3	< 5	51	49	37	164	< 10	28	23	< 3	< 10		< 10	28	< 3	30
TAS14-04 Agate mill	6	< 3	130	< 5	< 3	< 5	< 20	52	37	203	< 10	45	18	< 3	< 10		< 10	< 20	< 3	14
TAS14-05 Agate mill	< 5	< 3	475	< 5	< 3	< 5	32	41	41	216	< 10	48	22	3	< 10		< 10	29	< 3	16
TAS14-06 Agate mill	< 5	< 3	135	< 5	< 3	< 5	22	13	29	249	< 10	41	21	< 3	< 10		< 10	28	< 3	17
TAS14-07 Agate mill	< 5	< 3	128	< 5	< 3	< 5	27	30	37	244	< 10	51	21	< 3	< 10		< 10	< 20	< 3	16
TAS14-08 Agate mill	< 5	< 3	95	< 5	< 3	< 5	27	106	49	217	< 10	49	21	< 3	< 10		< 10	29	< 3	14
TAS14-09 Agate mill	6	< 3	102	< 5	< 3	< 5	< 20	88	45	184	< 10	50	22	< 3	< 10		< 10	< 20	< 3	13
TAS14-10 Agate mill	6	5	708	< 5	< 3	< 5	213	595	55	481	< 10	36	25	< 3	14		< 10	107	7	121
TAS14-11 Agate mill	7	< 3	260	5	< 3	< 5	61	67	38	220	16	20	22	< 3	< 10		< 10	40	< 3	28
TAS14-12 Agate mill	6	< 3	330	< 5	< 3	< 5	65	69	51	315	< 10	65	17	< 3	< 10		< 10	51	< 3	57
TAS14-13 TC mill	7	< 3	383	< 5	< 3	< 5	70	58	55	333	< 10	55	18	3	< 10		< 10	54	< 3	61
TAS14-14 TC mill	6	3	374	< 5	< 3	< 5	76	340	62	266	< 10	50	19	< 3	< 10		< 10	45	< 3	61
TAS14-15 TC mill	5	3	326	< 5	< 3	< 5	83	178	51	359	< 10	65	19	< 3	< 10		< 10	52	< 3	51
TAS14-16 TC mill	6	< 3	314	< 5	< 3	< 5	94	166	53	266	< 10	58	17	< 3	< 10		< 10	38	< 3	62
TAS14-17 TC mill	8	< 3	298	< 5	< 3	< 5	116	183	59	306	< 10	47	20	< 3	< 10		< 10	53	5	76
TAS14-18 Agate mill	5	3	301	< 5	< 3	< 5	58	287	58	322	< 10	60	22	< 3	< 10		< 10	58	7	73
TAS14-19 TC mill	7	4	242	< 5	< 3	< 5	109	208	67	305	< 10	45	20	< 3	11		< 10	37	7	74
TAS14-20 Agate mill	8	< 3	282	< 5	< 3	< 5	91	300	58	309	< 10	45	21	< 3	< 10		< 10	32	7	74
TAS14-21 Agate mill	6	4	232	< 5	< 3	< 5	164	314	56	343	< 10	39	23	< 3	< 10		< 10	80	< 3	106
TAS14-22 Agate mill	< 5	3	271	< 5	< 3	< 5	136	202	55	322	< 10	52	24	< 3	14		< 10	76	< 3	101
TAS14-23 TC mill	8	4	235	< 5	< 3	< 5	127	166	71	350	< 10	53	25	3	11		< 10	89	< 3	102
TAS14-24 TC mill	5	< 3	260	< 5	< 3	< 5	68	104	62	218	< 10	41	21	< 3	< 10		< 10	43	4	49
TAS14-25 Agate mill	< 5	< 3	94	6	< 3	< 5	< 20	31	54	221	< 10	47	21	< 3	< 10		< 10	21	< 3	11
TAS14-26 Agate mill	< 5	< 3	144	< 5	< 3	< 5	< 20	68	49	217	< 10	45	21	3	< 10		< 10	21	< 3	18
TAS14-27 Agate mill	< 5	< 3	79	< 5	< 3	< 5	27	22	39	287	11	40	20	< 3	< 10		< 10	< 20	< 3	8

(continued on next page)

Table 2 (*continued*)

Sample	Ag	As	Ba	Bi	Br	Cd	Ce	Cl	Co	Cr	Cs	Cu	Ga	Ge	Hf	I	La	Mo	Nb	Nd
TAS14-28 Agate mill	8	< 3	182	< 5	< 3	< 5	< 20	39	51	200	< 10	51	25	< 3	< 10		< 10	24	< 3	24
TAS14-29 Agate mill	8	< 3	143	< 5	< 3	< 5	< 20	72	55	211	11	44	20	< 3	< 10		< 10	< 20	< 3	16
TAS14-30 Agate mill	< 5	< 3	351	< 5	< 3	< 5	35	293	49	288	< 10	63	19	< 3	< 10		< 10	38	< 3	39
TAS14-31 TC mill	5	< 3	323	< 5	< 3	< 5	66	269	66	325	< 10	50	21	< 3	< 10		< 10	45	3	55
TAS14-32 TC mill	7	< 3	335	< 5	< 3	< 5	86	200	65	331	< 10	49	22	< 3	< 10		< 10	48	4	56
TAS14-33 Agate mill	8	3	314	< 5	< 3	< 5	72	87	70	357	< 10	53	21	< 3	< 10		< 10	37	< 3	55
TAS14-34 Agate mill	7	< 3	125	< 5	< 3	< 5	66	86	47	207	< 10	64	25	< 3	< 10		< 10	40	< 3	39
TAS14-35 Agate mill	7	< 3	126	< 5	< 3	< 5	48	135	51	206	< 10	65	25	< 3	< 10		< 10	42	4	41
TAS14-36 Agate mill	< 5	< 3	163	5	< 3	< 5	38	29	51	181	< 10	55	19	< 3	< 10		< 10	< 20	< 3	25
TAS14-37 Agate mill	6	< 3	251	< 5	< 3	< 5	36	41	50	248	< 10	45	21	< 3	< 10		< 10	< 20	< 3	35
TAS14-38 Agate mill	6	< 3	183	< 5	< 3	< 5	45	29	55	219	< 10	40	21	< 3	< 10		< 10	< 20	< 3	18
TAS14-39 Agate mill	< 5	< 3	179	< 5	< 3	< 5	27	46	49	248	< 10	39	19	< 3	< 10		< 10	< 20	< 3	12
TAS14-40 Agate mill	6	< 3	186	< 5	< 3	< 5	< 20	55	49	248	14	29	21	< 3	< 10		< 10	22	< 3	17
TAS14-41 Agate mill	6	< 3	187	< 5	< 3	< 5	35	43	41	199	< 10	35	20	< 3	< 10		< 10	< 20	< 3	18
TAS14-42 Agate mill	< 5	< 3	175	< 5	< 3	< 5	20	13	54	204	< 10	45	20	< 3	< 10		< 10	< 20	< 3	16
TAS14-43 Agate mill	7	< 3	226	< 5	< 3	< 5	62	110	63	253	< 10	50	22	< 3	< 10		< 10	36	< 3	38
TAS14-44a Agate mill	6	< 3	225	< 5	< 3	< 5	47	30	52	251	16	60	19	< 3	< 10		< 10	< 20	< 3	29
AS14-44b TC mill	6	< 3	208	< 5	< 3	< 5	47	30	63	252	< 10	57	20	< 3	< 10		< 10	< 20	< 3	29
TAS14-45a Agate mill	5	3	120	< 5	< 3	< 5	42	66	57	269	< 10	56	24	3	< 10		< 10	21	4	34
AS14-45b TC mill	< 5	< 3	134	< 5	< 3	< 5	58	66	74	277	14	52	23	< 3	< 10		< 10	29	4	34
TAS14-46 Agate mill	8	< 3	143	< 5	< 3	< 5	74	97	56	228	< 10	63	24	< 3	< 10		< 10	42	4	40
TAS14-47 Agate mill	< 5	< 3	213	< 5	< 3	< 5	54	36	51	196	< 10	52	22	< 3	< 10		< 10	20	< 3	27
TAS14-48 Agate mill	7	< 3	173	< 5	< 3	< 5	22	13	48	257	< 10	47	20	< 3	< 10		< 10	< 20	< 3	22
TAS14-49 Agate mill	6	< 3	108	< 5	< 3	< 5	< 20	16	43	175	< 10	37	20	< 3	< 10		< 10	30	< 3	11
TAS14-50 Agate mill	6	< 3	245	< 5	< 3	< 5	39	38	49	178	12	57	21	< 3	< 10		< 10	< 20	< 3	27
TAS14-51 Agate mill	8	< 3	186	< 5	< 3	< 5	33	33	52	197	< 10	47	20	< 3	< 10		< 10	< 20	< 3	25
TAS14-52 Agate mill	8	< 3	189	< 5	< 3	< 5	40	27	58	190	< 10	47	18	< 3	< 10		< 10	21	< 3	26
TAS14-53	6	< 3	105	< 5	< 3	< 5	22	16	48	151	< 10	43	20	< 3	< 10		< 10	< 20	< 3	12

(*continued on next page*)

Table 2 (*continued*)

Sample	Ag	As	Ba	Bi	Br	Cd	Ce	Cl	Co	Cr	Cs	Cu	Ga	Ge	Hf	I	La	Mo	Nb	Nd
Agate mill																				
TAS14-54	6	< 3	103	< 5	< 3	< 5	< 20	25	51	142	< 10	26	21	< 3	< 10		< 10	< 20	< 3	11
Agate mill																				
TAS14-55	< 5	< 3	118	< 5	< 3	< 5	23	16	45	122	< 10	27	22	< 3	< 10		< 10	< 20	< 3	11
Agate mill																				
TAS14-56	< 5	< 3	121	< 5	< 3	< 5	30	54	48	199	< 10	34	21	3	< 10		< 10	< 20	< 3	16
Agate mill																				
TAS14-57	6	< 3	149	< 5	< 3	< 5	< 20	50	47	168	12	31	22	4	< 10		< 10	< 20	< 3	16
Agate mill																				
TAS14-58	6	< 3	111	5	< 3	< 5	24	31	51	177	12	41	21	< 3	< 10		< 10	< 20	< 3	13
Agate mill																				
TAS14-59	< 5	< 3	279	< 5	< 3	< 5	59	48	50	226	< 10	53	22	< 3	< 10		< 10	32	< 3	35
Agate mill																				
TAS14-60	< 5	5	454	< 5	< 3	< 5	168	305	64	370	< 10	56	16	< 3	< 10		< 10	95	< 3	102
Agate mill																				
TAS14-61	< 5	5	457	< 5	< 3	< 5	159	261	67	382	< 10	58	18	< 3	< 10		< 10	90	< 3	105
Agate mill																				
TAS14-62	< 5	5	334	< 5	< 3	< 5	162	293	68	340	< 10	58	19	< 3	< 10		< 10	93	< 3	104
Agate mill																				
TAS14-63	< 5	5	676	< 5	< 3	< 5	131	293	62	371	< 10	59	17	< 3	< 10		< 10	100	< 3	105
Agate mill																				
TAS14-64	6	< 3	258	< 5	< 3	< 5	25	0	38	12	< 10	132	20	3	< 10		< 10	31	< 3	6
Agate mill																				
TAS14-65	< 5	< 3	103	< 5	< 3	< 5	< 20	57	49	208	< 10	45	21	3	< 10		< 10	< 20	< 3	14
Agate mill																				
TAS14-66	7	< 3	253	< 5	< 3	< 5	59	48	60	208	< 10	50	24	< 3	< 10		< 10	29	< 3	36
Agate mill																				
TAS14-67	< 5	< 3	123	< 5	< 3	< 5	< 20	68	45	193	16	43	20	< 3	< 10		< 10	22	< 3	12
Agate mill																				
TAS14-68	5	< 3	103	< 5	< 3	< 5	< 20	46	52	256	< 10	40	21	< 3	< 10		< 10	22	< 3	14
Agate mill																				
TAS14-69	6	< 3	198	< 5	< 3	< 5	< 20	3	38	105	13	63	16	< 3	< 10		< 10	< 20	< 3	5
Agate mill																				
TAS14-70	< 5	< 3	99	< 5	< 3	< 5	< 20	93	47	202	< 10	46	20	< 3	< 10		< 10	< 20	< 3	12
Agate mill																				
TAS14-71	5	< 3	185	< 5	< 3	< 5	34	5	42	96	< 10	63	17	< 3	< 10		< 10	< 20	< 3	6
Agate mill																				
TAS14-72	7	< 3	187	< 5	< 3	< 5	57	65	60	340	< 10	67	18	< 3	< 10		< 10	< 20	< 3	15
Agate mill																				
TAS14-73	9	< 3	453	< 5	< 3	< 5	107	336	42	97	< 10	26	25	< 3	< 10		< 10	66	< 3	57
Agate mill																				
TAS14-74	7	5	622	< 5	< 3	< 5	181	247	112	191	< 10	40	22	3	< 10		< 10	101	5	98
TC mill																				
TAS14-75	5	< 3	142	< 5	< 3	< 5	21	58	49	213	< 10	33	18	< 3	< 10		< 10	23	< 3	17
Agate mill																				
TAS14-76	< 5	< 3	106	< 5	< 3	< 5	25	50	61	188	< 10	35	19	< 3	< 10		< 10	< 20	< 3	13
TC mill																				
TAS14-77	< 5	< 3	229	< 5	< 3	< 5	40	44	72	222	< 10	46	22	3	< 10		< 10	27	< 3	20
TC mill																				
TAS14-78	8	< 3	130	< 5	< 3	< 5	< 20	68	49	215	< 10	32	19	< 3	< 10		< 10	< 20	< 3	16
Agate mill																				
TAS14-79	6	< 3	215	< 5	< 3	< 5	37	17	38	95	11	65	17	< 3	< 10		< 10	< 20	< 3	5
Agate mill																				

(*continued on next page*)

Table 2 (*continued*)

Sample	Ag	As	Ba	Bi	Br	Cd	Ce	Cl	Co	Cr	Cs	Cu	Ga	Ge	Hf	I	La	Mo	Nb	Nd
TAS14-80 TC mill	8	< 3	178	< 5	< 3	< 5	37	59	67	236	< 10	48	20	< 3	< 10		< 10	25	< 3	21
Detection limit	5	3	20	5	3	5	20	5	5	5	10	3	3	3	10		10	20	3	3

Sample	Ni	Pb	Rb	Sb	Sc	Se	Sm	Sn	Sr	Ta	Te	Th	Tl	U	V	Y	Yb	Zn	Zr	Mill head
TAS14-01	122	< 5	22	< 10	14	< 3	< 15	< 5	648	< 10	< 10	13	8	7	156	20	< 15	96	161	Agate mill
TAS14-02	24	< 5	19	< 10	12	< 3	< 15	< 5	756	< 10	< 10	15	< 5	9	199	20	< 15	80	159	Agate mill
TAS14-03	52	< 5	29	11	14	< 3	< 15	< 5	768	< 10	< 10	11	6	8	166	20	< 15	81	157	Agate mill
TAS14-04	115	< 5	22	< 10	16	< 3	< 15	< 5	308	< 10	< 10	11	< 5	5	142	22	< 15	94	117	Agate mill
TAS14-05	125	< 5	20	11	19	< 3	< 15	< 5	328	< 10	< 10	11	6	5	142	55	< 15	94	125	Agate mill
TAS14-06	66	< 5	22	< 10	21	< 3	< 15	< 5	317	< 10	< 10	12	5	6	146	21	< 15	96	132	Agate mill
TAS14-07	91	< 5	23	< 10	19	< 3	< 15	< 5	314	< 10	< 10	13	< 5	6	146	23	< 15	89	127	Agate mill
TAS14-08	120	< 5	24	< 10	17	< 3	< 15	< 5	290	< 10	< 10	12	< 5	6	139	21	< 15	105	116	Agate mill
TAS14-09	114	< 5	23	< 10	11	< 3	< 15	< 5	289	< 10	< 10	10	7	5	122	21	< 15	98	116	Agate mill
TAS14-10	423	< 5	56	< 10	10	< 3	25	< 5	1467	< 10	< 10	26	< 5	17	103	44	< 15	161	623	Agate mill
TAS14-11	19	< 5	24	< 10	14	< 3	< 15	< 5	595	< 10	< 10	13	10	6	176	21	< 15	65	166	Agate mill
TAS14-12	153	< 5	18	11	19	< 3	< 15	< 5	640	< 10	< 10	15	< 5	6	179	25	< 15	74	218	Agate mill
TAS14-13	142	< 5	38	11	17	< 3	< 15	< 5	649	< 10	< 10	14	< 5	7	191	25	< 15	77	247	TC mill
TAS14-14	118	< 5	22	< 10	22	< 3	< 15	< 5	750	< 10	< 10	14	6	9	188	25	< 15	76	256	TC mill
TAS14-15	238	< 5	38	< 10	20	< 3	< 15	< 5	751	< 10	< 10	14	< 5	6	171	23	< 15	73	212	TC mill
TAS14-16	138	< 5	29	< 10	18	< 3	< 15	< 5	782	< 10	< 10	16	6	9	187	24	< 15	80	246	TC mill
TAS14-17	208	< 5	24	13	8	< 3	< 15	< 5	1381	< 10	< 10	17	6	16	151	23	< 15	114	274	TC mill
TAS14-18	213	< 5	20	< 10	10	< 3	< 15	< 5	950	< 10	< 10	17	< 5	9	172	26	< 15	103	259	Agate mill
TAS14-19	211	< 5	21	< 10	8	< 3	< 15	< 5	942	< 10	< 10	18	6	10	176	25	< 15	113	258	TC mill
TAS14-20	214	< 5	21	13	15	< 3	< 15	< 5	964	< 10	< 10	17	< 5	14	175	25	< 15	112	258	Agate mill
TAS14-21	225	< 5	19	12	10	< 3	< 15	< 5	1292	< 10	< 10	21	< 5	15	179	30	< 15	143	364	Agate mill
TAS14-22	224	< 5	17	< 10	10	< 3	< 15	< 5	1187	< 10	< 10	19	< 5	13	170	28	< 15	132	349	Agate mill
TAS14-23	249	< 5	18	< 10	11	< 3	< 15	< 5	1434	< 10	< 10	21	< 5	16	180	28	< 15	140	359	TC mill
TAS14-24	164	< 5	24	< 10	9	< 3	< 15	< 5	688	< 10	< 10	15	< 5	10	157	21	< 15	106	180	TC mill
TAS14-25	211	< 5	10	15	13	< 3	< 15	< 5	282	< 10	< 10	12	9	< 3	144	22	< 15	106	116	Agate mill
TAS14-26	145	< 5	11	< 10	13	< 3	< 15	< 5	371	< 10	< 10	12	6	5	147	23	< 15	102	150	Agate mill
TAS14-27	115	< 5	8	< 10	16	< 3	< 15	< 5	247	< 10	< 10	10	5	5	142	19	< 15	100	93	Agate mill
TAS14-28	127	< 5	15	13	16	< 3	< 15	6	441	< 10	< 10	12	6	< 3	154	22	< 15	118	170	Agate mill
TAS14-29	119	< 5	14	< 10	14	< 3	< 15	< 5	322	< 10	< 10	12	< 5	4	144	21	< 15	101	125	Agate mill
TAS14-30	178	< 5	23	< 10	18	< 3	< 15	< 5	629	< 10	< 10	13	9	8	183	20	< 15	86	166	Agate mill
TAS14-31	215	< 5	27	< 10	13	< 3	< 15	< 5	808	< 10	< 10	15	6	8	166	19	< 15	105	240	TC mill
TAS14-32	200	< 5	25	< 10	10	< 3	< 15	< 5	842	< 10	< 10	16	5	9	172	19	< 15	105	245	TC mill
TAS14-33	240	< 5	20	< 10	10	< 3	< 15	< 5	877	< 10	< 10	14	7	7	175	20	< 15	99	240	Agate mill
TAS14-34	131	< 5	18	11	12	< 3	< 15	< 5	796	< 10	< 10	13	< 5	6	143	19	< 15	98	196	Agate mill
TAS14-35	135	< 5	19	< 10	10	< 3	< 15	< 5	873	< 10	< 10	14	< 5	6	140	19	< 15	98	207	Agate mill
TAS14-36	137	< 5	23	< 10	10	< 3	< 15	< 5	510	< 10	< 10	14	< 5	8	160	21	< 15	90	164	Agate mill
TAS14-37	140	< 5	23	13	11	< 3	< 15	< 5	476	< 10	< 10	13	< 5	6	162	20	< 15	80	161	Agate mill
TAS14-38	140	< 5	20	< 10	16	< 3	< 15	< 5	273	< 10	< 10	11	< 5	< 3	144	20	< 15	96	116	Agate mill
TAS14-39	101	< 5	17	15	14	< 3	< 15	< 5	307	< 10	< 10	10	6	< 3	155	17	< 15	96	110	Agate mill
TAS14-40	105	< 5	27	< 10	13	< 3	< 15	< 5	354	< 10	< 10	13	< 5	4	152	20	< 15	87	151	Agate mill
TAS14-41	61	< 5	28	< 10	13	< 3	< 15	< 5	364	< 10	< 10	12	< 5	4	160	21	< 15	230	159	Agate mill
TAS14-42	125	< 5	16	< 10	15	< 3	< 15	< 5	341	< 10	< 10	12	5	6	149	20	< 15	99	128	Agate mill
TAS14-43	151	< 5	25	11	13	< 3	< 15	< 5	802	< 10	< 10	14	5	7	175	22	< 15	109	224	Agate mill
TAS14-44a	131	< 5	26	< 10	17	< 3	< 15	< 5	530	< 10	< 10	13	< 5	5	185	22	< 15	88	154	Agate mill
AS14-44b	143	< 5	24	< 10	17	< 3	< 15	< 5	517	< 10	< 10	14	7	6	180	21	< 15	93	153	TC mill
TAS14-45a	161	< 5	18	11	12	< 3	< 15	< 5	734	< 10	< 10	14	6	6	188	19	< 15	94	192	Agate mill

(*continued on next page*)

Table 2 (*continued*)

Sample	Ni	Pb	Rb	Sb	Sc	Se	Sm	Sn	Sr	Ta	Te	Th	Tl	U	V	Y	Yb	Zn	Zr	Mill head
AS14-45b	170	< 5	18	< 10	7	< 3	< 15	< 5	732	< 10	< 10	12	< 5	7	192	18	< 15	97	192	TC mill
TAS14-46	135	< 5	21	13	9	< 3	< 15	< 5	682	< 10	< 10	12	6	5	176	20	< 15	98	220	Agate mill
TAS14-47	129	< 5	21	11	13	< 3	< 15	< 5	480	< 10	< 10	12	< 5	6	154	22	< 15	117	189	Agate mill
TAS14-48	86	< 5	18	< 10	16	< 3	< 15	< 5	461	< 10	< 10	12	< 5	4	160	19	< 15	77	125	Agate mill
TAS14-49	83	< 5	13	11	13	< 3	< 15	< 5	252	< 10	< 10	11	6	4	125	19	< 15	86	104	Agate mill
TAS14-50	109	< 5	24	< 10	14	< 3	15	< 5	487	< 10	< 10	14	< 5	< 3	163	22	< 15	93	172	Agate mill
TAS14-51	132	< 5	21	< 10	15	< 3	< 15	< 5	370	< 10	< 10	11	6	4	141	21	< 15	97	162	Agate mill
TAS14-52	147	< 5	23	< 10	12	< 3	< 15	< 5	419	< 10	< 10	12	5	3	154	21	< 15	102	167	Agate mill
TAS14-53	72	< 5	14	< 10	13	< 3	< 15	< 5	274	< 10	< 10	12	6	4	133	19	< 15	94	109	Agate mill
TAS14-54	56	< 5	13	< 10	18	< 3	< 15	< 5	236	< 10	< 10	12	< 5	< 3	133	22	< 15	94	115	Agate mill
TAS14-55	49	< 5	14	12	13	< 3	< 15	< 5	244	< 10	< 10	12	7	3	127	22	< 15	91	115	Agate mill
TAS14-56	77	< 5	24	< 10	14	< 3	< 15	< 5	302	< 10	< 10	11	7	3	132	20	< 15	91	124	Agate mill
TAS14-57	103	< 5	23	< 10	13	< 3	< 15	< 5	297	< 10	< 10	13	8	5	131	21	< 15	89	124	Agate mill
TAS14-58	148	< 5	21	12	21	< 3	< 15	< 5	258	< 10	< 10	13	7	6	137	23	< 15	108	116	Agate mill
TAS14-59	126	< 5	32	< 10	10	< 3	< 15	< 5	693	< 10	< 10	15	< 5	6	167	23	< 15	103	210	Agate mill
TAS14-60	301	< 5	29	< 10	13	< 3	< 15	< 5	1324	< 10	< 10	23	< 5	13	206	27	< 15	112	261	Agate mill
TAS14-61	299	< 5	38	16	11	< 3	< 15	< 5	1629	< 10	< 10	24	< 5	16	217	29	< 15	111	271	Agate mill
TAS14-62	264	< 5	34	< 10	14	< 3	< 15	< 5	1183	< 10	< 10	22	6	14	212	29	< 15	110	266	Agate mill
TAS14-63	295	< 5	33	12	14	< 3	< 15	< 5	1495	< 10	< 10	21	< 5	16	219	27	< 15	112	267	Agate mill
TAS14-64	11	< 5	40	11	24	< 3	< 15	< 5	144	< 10	< 10	14	< 5	< 3	175	24	< 15	70	113	Agate mill
TAS14-65	83	< 5	18	11	14	< 3	< 15	< 5	264	< 10	< 10	13	< 5	3	148	21	< 15	99	109	Agate mill
TAS14-66	120	< 5	28	< 10	13	< 3	< 15	< 5	566	< 10	< 10	14	< 5	5	163	23	< 15	100	193	Agate mill
TAS14-67	101	< 5	11	< 10	14	< 3	< 15	< 5	266	< 10	< 10	12	7	4	147	28	< 15	102	93	Agate mill
TAS14-68	129	< 5	14	< 10	17	< 3	< 15	< 5	280	< 10	< 10	11	< 5	3	150	19	< 15	105	104	Agate mill
TAS14-69	48	< 5	31	11	31	< 3	24	< 5	117	< 10	< 10	14	< 5	5	225	20	< 15	64	86	Agate mill
TAS14-70	95	< 5	12	< 10	18	< 3	< 15	< 5	277	< 10	< 10	13	6	5	144	20	< 15	101	102	Agate mill
TAS14-71	44	< 5	29	< 10	27	< 3	< 15	< 5	120	< 10	< 10	12	7	< 3	193	21	< 15	64	92	Agate mill
TAS14-72	172	< 5	7	12	18	< 3	< 15	< 5	316	< 10	< 10	10	< 5	< 3	155	21	< 15	82	88	Agate mill
TAS14-73	69	< 5	37	11	10	< 3	< 15	< 5	944	< 10	< 10	16	< 5	8	104	26	< 15	124	335	Agate mill
TAS14-74	107	< 5	50	< 10	10	< 3	20	< 5	1027	< 10	< 10	20	7	11	163	32	< 15	143	381	TC mill
TAS14-75	75	< 5	28	< 10	16	< 3	< 15	< 5	292	< 10	< 10	13	5	< 3	153	20	< 15	97	125	Agate mill
TAS14-76	117	< 5	21	< 10	8	< 3	< 15	< 5	284	< 10	< 10	11	7	< 3	121	18	< 15	100	106	TC mill
TAS14-77	163	< 5	15	< 10	16	< 3	16	< 5	428	< 10	< 10	14	8	6	140	19	< 15	102	119	TC mill
TAS14-78	79	< 5	27	11	13	< 3	< 15	< 5	290	< 10	< 10	10	< 5	3	135	19	< 15	92	120	Agate mill
TAS14-79	40	< 5	34	< 10	24	< 3	< 15	< 5	159	< 10	< 10	11	< 5	3	192	20	< 15	61	91	Agate mill
TAS14-80	130	< 5	11	< 10	14	< 3	< 15	< 5	407	< 10	< 10	10	< 5	< 3	141	19	< 15	106	126	TC mill
Detection limit	3	5	5	10	5	3	15	5	3	10	10	5	5	3	10	3	15	5	3	

undersaturated alkali basalts through basanites to quartz tholeiites. They cover an area of 40,000 km^2, concentrated in the northwest and north, and continuing through the centre towards the south-east (Sutherland et al., 2004). Based on existing K–Ar dating, volcanic activity occurred from 69.9 Ma (Corbett et al., 2014) to 8.5 Ma (Baillie, 1986a; Baillie, 1986b), with most voluminous activity occurring between 30 and 20 Ma (Figs. 1–2). The province consists of lava flows and "inverted" caps accompanied by numerous small intrusions, confined in narrow rift zones (Forsyth, 1984; Forsyth, 1989) and larger necks or plugs (Sutherland et al., 2004).

The Tasmanian Cenozoic volcanism followed earlier phases of mafic magmatism during the Cretaceous, Jurassic and Triassic. The Cretaceous event was volumetrically small, preserved as scattered, mainly (but not exclusively) mafic lava flows, sills and dykes (Bottrill et al., 2014), while the Jurassic episode was highly voluminous, mainly occurring as extensive, thick sills of low Ti tholeiite dolerite (Hergt et al., 1989). They mainly intrude the flat-lying Carboniferous to Triassic strata of the Tasman Basin. The Tasmanian Jurassic dolerites are part of the very extensive Ferrar Magmatic Province, which extends from southern Australia (Hergt et al., 1989) into Antarctica (Elliot and Fleming, 2004; Kyle, 1980; Kyle, 1981) and New Zealand (Mortimer et al., 1995). The distinct major, trace and isotope geochemistry of the Tasmanian dolerites is attributed to re-enrichment of a depleted mantle source region by a small proportion of subducted upper crustal material (Hergt and Brauns, 2001). Remnants of Triassic volcanic activity are found as basalts in the St. Marys area (e.g. Turner and Calver, 1987 and references therein) and poorly welded ash-fall tuffs of rhyolitic to rhyodacitic composition near Bicheno (Bacon and Everard, 1981).

2.2.1. Related Cenozoic tectonic history

2.2.1.1. Offshore Bass Basin. The Eastern Australian Cenozoic Magmatic Province extends off-shore to the Bight, Otway, Bass and Gippsland Basins along the Australian southern margin (Holford et al., 2012; Meeuws et al., 2016; Schofield and Totterdell, 2008). These occurrences are mostly of Cenozoic age and consist of both volcanic and sub-volcanic features of Eocene age in the Bight and Otway basins and Oligocene and Miocene ages in the Sorell and Bass basins and Torquay sub-basin and of Cretaceous to mid-Eocene age in the Gippsland Basin (Birch, 1987; Hill et al., 1997; Holford et al., 2012; Meeuws et al., 2016). The Bass Basin directly north of Tasmania, shows direct correlation with the timing of Tasmanian onshore magmatism. Peaks in magmatic activity onshore Tasmania directly coincide with major and minor unconformities in the Bass Basin (Fig. 2). In particular the Oligocene peak in volcanism coincides with a major unconformity, followed by several episodes of offshore volcanism in the basin during the Miocene (Holford et al., 2017; Reynolds et al., 2018). There may also be correlations with Middle and Late Eocene events.

3. Data and analytical methods

During our sampling campaign in March 2014, eighty samples were taken at key localities where published ages are available, ensuring a spread of samples over Tasmania (Fig. 3). Following removal of weathered surfaces, samples were crushed using a tungsten-carbide jaw-crusher and powdered in either a tungsten-carbide or agate ring mill at the University of Adelaide. These powders have been analysed for major and trace elements using X-ray fluorescence (XRF) at the Commonwealth Scientific and Industrial Research Organisation (CSIRO), Adelaide (Table 1–2). Major elements have been analysed on XRF fused discs using a lithium tetra-borate flux and trace elements have been analysed on pressed powders mixed with a binding wax. Contamination due to the use of a tungsten carbide mill head was only observed for W. Thirty-one samples were selected based on a range of magnesium-numbers for analyses using solution Inductively Coupled Plasma Mass Spectrometry (ICP-MS) at Bureau Veritas, Adelaide. Several standards such as BCR-2, BHVO-2 and the in-house TASBAS have been included as unknowns in the analyses (Table 3). Additionally, as per the method of Eggins (2003), fused discs used earlier for XRF analyses were cut and glued onto glass plates and have been analysed for trace elements using a New Wave UP-213 laser ablation system connected to an Agilent 7500cx inductively coupled mass spectrometer (LA-ICP-MS) at the University of Adelaide. A total of three spots were analysed per sample for 90 s, ensuring homogeneity of the discs (Table 4). Appropriate standards such as BCR-1 and BHVO-1 underwent the same procedure and analyses for trace elements are indistinguishable from published reference values except for As, Pr and W. Some samples (TAS14-34B, TAS14-42B and TAS14-56B) have been duplicated a few months later to check for possible effects on the timing and degrading of fused discs, but no differences in data have been observed. XRF values of CaO wt% were used as internal standards to normalise the ICP-MS results to. Data reduction procedures were done using Glitter V3.0 (Van Achterbergh et al., 2001) with a drift correction applied to the unknowns between the bracketing NIST SRM 612 calibrations assuming linear drift through the analysis sequence. A subset of thirteen samples was prepared for Sr, Sm–Nd and Pb isotope analysis. For each of the thirteen samples, a representative sub-sample of 0.05–0.4 g of rock powder was spiked with an in-house ^{147}Sm–^{150}Nd mixed spike. These powders were then dissolved using a mixture of HF and HNO_3. Sr, Sm and Nd were separated by ion chromatography using 2 ml AG 50 W-X8 200–400 mesh resin in Polyprep columns. The Sr separate was further purified using a 50 g Eichrom Sr Resin SPS, 50-100 µ. Sm and Nd are further separated by 1 ml of Eichrom Ln Resin SPS. For Pb isotope analyses, a separate sub-sample of powder was dissolved using a mixture of HF and HNO_3. Samples were then redissolved in 0.6 M HBr and Pb was separated with Dowex 1-X8 anion exchange resin. Isotopic compositions (Table 5) were measured at 1200 °C using an IsotopX Phoenix Thermal Ionization Mass Spectrometer (TIMS) at the University of Adelaide. Fractionation-corrected Pb isotopic compositions and internal errors were obtained by a closed-form linear double-spike deconvolution (Johnson and Beard, 1999) using the Southampton-Brest-Lead 207-204 (SBL74) double spike developed at the University of Southampton (Ishizuka et al., 2003). Procedural blanks are 366 pg (< 1.2E−3%) for Sr, 84 pg (< 1.2E−3%) for Nd, 4 pg (< 2.2E−4%) for Sm, and 68 pg (< 0.1%) for Pb, rendering blank values insignificant so no blank corrections need to be applied.

For six samples, plagioclase was separated and analysed using the furnace step-heating diffusional experiments technique at the ANU RSES Argon Laboratory. Irradiation of samples for ^{40}Ar/^{39}Ar analysis was undertaken at the University of California Davis MNRC, California, USA. Biotite (GA 1550) has been used as the Flux Monitor (Spell and Mcdougall, 2003). The ^{40}Ar/^{39}Ar analysis procedures are as described by Mcdougall and Brown (2006) with updated procedures (Forster and Lister, 2009). The samples were analysed on the Thermofisher VG1200 as diffusion experiments with the numbers of steps defined by the mineral type and character (see Table 6). Two or more isothermal steps are analysed throughout the schedule, with temperatures of the overall schedule rising from 450 °C to 1450 °C (Lovera et al., 1989). The furnace was decontaminated prior to each sample at 1450 °C for 15 min three times. The gases from the furnace cleaning process during analysis as required were pumped away and not included in the analysis. ^{40}K abundances and decay constants are taken from standard values recommended by the IUGS subcommission on Geochronology (Steiger and Jager, 1977). Stated precisions for ^{40}Ar/^{39}Ar ages include all uncertainties in the measurement of isotope ratios and are quoted at the 2 sigma level.

Table 3
ICP-MS trace element analyses in ppm for Cenozoic and Jurassic mafic rocks in Tasmania. BCR-2* and BHVO-2* are certified and recommended reference values (Wilson, 1997a and 1997b)

Sample	Be	Co	Ni	Cu	Zn	Ga	As	Se	Rb	Sr	Y	Zr	Nb	Mo	Ag
TAS14-01	2	46	195	51	104	17	< 1	< 5	18	572	17.9	144	29	2	< 0.2
TAS14-02	2	34	60	46	108	19.4	< 1	< 5	15.4	685	18.1	150	39	1	< 0.2
TAS14-07	1.5	33	130	52	108	19.6	< 1	< 5	20.8	303	22.9	130	16.5	2	< 0.2
TAS14-08	1	46	180	58	116	19.4	< 1	< 5	21.8	286	21.3	113	13	1.5	< 0.2
TAS14-10	5	54	510	40	202	24.4	3	< 5	50.6	1410	43	667	201	10	< 0.2
TAS14-15	2	56	300	70	92	16.4	< 1	< 5	32	687	22.2	202	57	3	< 0.2
TAS14-17	4	54	265	51	154	19.6	< 1	< 5	17	1320	23.1	262	78.5	7.5	< 0.2
TAS14-21	6	54	295	43	166	21.4	< 1	< 5	12	1220	26.6	342	96	4	< 0.2
TAS14-26	1.5	54	240	51	128	20.4	< 1	< 5	8.8	326	22.2	171	56	4	< 0.2
TAS14-29	1	50	175	49	110	17.8	2	< 5	11	288	19.3	119	15.5	1.5	< 0.2
TAS14-31	3	58	285	54	120	19.4	< 1	< 5	21.8	762	18.2	222	59.5	4	< 0.2
TAS14-36	2	49	195	56	108	19.4	< 1	< 5	20	472	20.2	167	26.5	3	< 0.2
TAS14-41	2	42	110	38	212	20.8	2	< 5	26.8	346	21.3	160	17.5	2.5	< 0.2
TAS14-42	1.5	49	175	47	106	17.8	< 1	< 5	13.6	298	19.1	119	15	1.5	< 0.2
TAS14-46	3	53	195	61	122	21.4	< 1	< 5	16.4	613	18.5	205	42	5.5	< 0.2
TAS14-47	2	49	190	59	140	21	< 1	< 5	18	424	22.1	181	21.5	2	< 0.2
TAS14-48	1.5	46	145	49	106	15.4	< 1	< 5	13.2	402	18	128	23	2	< 0.2
TAS14-50	2	54	190	54	134	18.2	< 1	< 5	19.2	440	20.2	238	29	7	< 0.2
TAS14-54	1	42	90	33	104	17.6	< 1	< 5	12	207	20.9	114	12.5	1	< 0.2
TAS14-59	2.5	58	210	58	140	21.6	< 1	< 5	29.2	672	23	220	36	3	< 0.2
TAS14-61	3.5	59	370	58	130	16.4	< 1	< 5	30.2	1440	25.6	264	98	1	< 0.2
TAS14-64	1	41	45	136	84	17	< 1	< 5	36.8	136	24.3	115	7	1	< 0.2
TAS14-67	1	46	150	43	116	17.2	< 1	< 5	8.8	246	28.3	88	11	1	< 0.2
TAS14-68	1	45	170	42	106	18	< 1	< 5	11	258	18	98	13	1.5	< 0.2
TAS14-69	1	38	80	71	68	13.6	< 1	< 5	27	104	18.6	82	5	1	< 0.2
TAS14-71	1	38	75	74	70	14	2	< 5	25.6	106	19.6	87	5	1	< 0.2
TAS14-72	1	51	230	70	90	15.4	< 1	< 5	4.4	282	20.3	82	15.5	1	< 0.2
TAS14-75	2	43	125	42	112	19	< 1	< 5	26.6	274	20.5	121	16.5	2	< 0.2
TAS14-78	1.5	43	130	41	106	17.4	< 1	< 5	24.4	264	19.6	118	15.5	2	< 0.2
TAS14-79	1	40	85	76	76	14.4	< 1	< 5	31	150	20.5	90	5	1	< 0.2
TAS14-80	1	60	205	54	124	18.2	< 1	< 5	8	397	19.1	126	21.5	2	< 0.2
TASBAS	4.5	53	170	58	136	23.2	2	< 5	14.4	864	17.7	246	52	7.5	< 0.2
BCR-2	3	37	25	22	144	22	< 1	< 5	41.4	293	31.6	172	11	222	< 0.2
BCR-2	3	39	25	24	152	24	< 1	< 5	43.4	310	33	169	11	221	< 0.2
BCR-2	3	39	25	27	156	23.6	< 1	< 5	46	331	34.5	186	10	229	< 0.2
*BCR-2**		*37*		*19*	*127*	*23*			*48*	*346*	*37*	*188*		*248*	
BHVO-2	1.5	44	130	133	116	20.8	< 1	< 5	8.6	347	23	164	16.5	4.5	< 0.2
BHVO-2	1	50	145	148	130	24.2	< 1	< 5	9.2	385	25.7	165	13	4	< 0.2
BHVO-2	1	48	145	145	132	22.8	< 1	< 5	9	386	24.1	166	21	4.5	< 0.2
*BHVO-2**		*45*	*119*	*127*	*103*	*21.7*			*9.8*	*389*	*26*	*172*			
Detection limit	0.5	1	5	1	2	0.2	1	5	0.2	0.5	0.1	1	0.5	0.5	0.2

Sample	Cd	In	Sn	Sb	Te	Cs	Ba	La	Ce	Pr	Nd	Sm	Eu	Gd	Tb
TAS14-01	< 0.5	< 0.05	1.5	0.3	< 0.2	0.2	227	22.5	51.9	5.8	25	5.4	1.8	5	0.68
TAS14-02	< 0.5	< 0.05	1.7	0.2	< 0.2	0.3	204	22.1	51.8	5.85	25	5.6	1.9	5	0.68
TAS14-07	< 0.5	< 0.05	1.9	0.2	< 0.2	1	128	14.6	33.6	4.6	21.1	5.45	1.85	5.6	0.86
TAS14-08	< 0.5	0.1	1.7	0.2	< 0.2	0.8	101	10.5	26.9	3.4	15.8	4.6	1.55	5	0.76
TAS14-10	< 0.5	0.1	6.5	0.5	< 0.2	0.8	664	95.2	214	24.1	101	20.6	6.15	15.8	2
TAS14-15	< 0.5	< 0.05	1.6	0.2	< 0.2	0.4	300	33	70.5	7.85	31.5	6.15	2.1	5.6	0.76
TAS14-17	< 0.5	0.1	2.2	0.3	< 0.2	0.3	264	48	106	11.5	47.1	9.7	3.2	8.6	1.12
TAS14-21	< 0.5	0.1	2.5	0.3	< 0.2	0.2	194	67.1	149	15.9	69.9	13	4.4	11.6	1.34
TAS14-26	< 0.5	0.1	1.8	0.2	< 0.2	0.3	114	13.8	36.1	4.35	20.5	5.35	1.85	5.8	0.8

(*continued on next page*)

Table 3 (*continued*)

Sample	Cd	In	Sn	Sb	Te	Cs	Ba	La	Ce	Pr	Nd	Sm	Eu	Gd	Tb
TAS14-29	< 0.5	< 0.05	1.4	0.2	< 0.2	0.4	135	12.1	29	3.6	16.3	4.6	1.5	4.6	0.68
TAS14-31	< 0.5	< 0.05	2.1	0.2	< 0.2	0.5	288	31.8	71.6	8.25	34.6	6.95	2.3	6	0.78
TAS14-36	< 0.5	< 0.05	1.6	0.2	< 0.2	0.5	151	17.3	43.1	5.2	22.4	5.2	1.8	5.2	0.74
TAS14-41	< 0.5	0.1	1.9	0.2	< 0.2	2.3	186	16.7	40.5	4.65	21.6	5.15	1.6	5	0.7
TAS14-42	< 0.5	< 0.05	1.4	0.2	< 0.2	0.2	148	12.2	29.8	3.7	16.7	4.3	1.5	4.4	0.66
TAS14-46	< 0.5	< 0.05	2.1	0.3	< 0.2	0.5	132	25.4	60.7	6.55	29.5	6.5	2.15	5.6	0.78
TAS14-47	< 0.5	0.1	2	0.2	< 0.2	0.2	199	18.5	43.2	5.45	24.3	6.4	2.25	6.2	0.86
TAS14-48	< 0.5	< 0.05	1.3	0.2	< 0.2	0.3	155	15	35.2	4.3	18.5	4.45	1.55	4.4	0.58
TAS14-50	< 0.5	0.1	2.3	0.2	< 0.2	0.2	210	17.8	43.2	5.15	24.4	5.7	1.95	5.6	0.78
TAS14-54	< 0.5	< 0.05	1.6	< 0.1	< 0.2	0.4	93	9.2	23.5	2.9	14	4.15	1.45	4.6	0.72
TAS14-59	< 0.5	0.1	2.3	0.2	< 0.2	0.4	259	25	61.8	7.4	31.4	7.5	2.6	7	0.94
TAS14-61	< 0.5	0.1	2.7	0.3	< 0.2	0.7	356	68.4	148	16.2	63.4	12.2	3.8	9.4	1.16
TAS14-64	< 0.5	< 0.05	1.3	0.2	< 0.2	1.3	224	12.2	30.5	3.5	15.5	3.9	1.05	4	0.64
TAS14-67	< 0.5	< 0.05	1.3	0.2	< 0.2	0.5	109	11.1	23.8	3.25	15.2	4.1	1.45	4.8	0.7
TAS14-68	< 0.5	0.1	1.2	0.2	< 0.2	0.4	99.5	10.4	25.4	3.3	15.3	4.05	1.5	4.6	0.68
TAS14-69	< 0.5	< 0.05	1.1	0.2	< 0.2	1.1	167	9	22.7	2.55	12	2.85	0.8	2.8	0.46
TAS14-71	< 0.5	< 0.05	1.3	0.5	< 0.2	0.9	167	9.5	24	2.75	12.4	2.9	0.8	3	0.5
TAS14-72	< 0.5	< 0.05	0.9	0.2	< 0.2	< 0.1	145	13	26.9	3.05	13.7	3.4	1.2	3.8	0.58
TAS14-75	< 0.5	0.1	1.6	0.2	< 0.2	1.1	138	12.1	29.4	3.8	17.1	4.35	1.5	4.6	0.68
TAS14-78	< 0.5	0.1	1.5	< 0.1	< 0.2	1	132	11.8	29.2	3.6	16.2	4.4	1.45	4.4	0.64
TAS14-79	< 0.5	< 0.05	1.1	0.2	< 0.2	1.7	178	10	25.6	2.9	12.8	3.3	0.85	3.2	0.56
TAS14-80	< 0.5	< 0.05	1.4	< 0.1	< 0.2	0.2	171	18.1	45.9	5.2	24.3	5.8	1.95	5.4	0.74
TASBAS	< 0.5	< 0.05	2.4	0.3	0.2	1	165	36.2	79.6	8.95	36.6	7.4	2.4	6.4	0.82
BCR-2	< 0.5	0.1	2.1	0.4	< 0.2	1.1	587	20.9	49.1	5.95	25.6	5.95	1.9	6.2	0.92
BCR-2	< 0.5	0.1	2	0.4	< 0.2	1.1	627	21.1	50.3	6.15	27.1	6.4	1.9	6.2	1
BCR-2	< 0.5	0.1	2.3	0.4	< 0.2	1.2	643	21.1	52.5	6.5	28.2	6.85	2.0	6.6	1.02
*BCR-2**						*1.1*	*683*	*25*	*53*	*6.8*	*28*	*6.7*	*2.0*	*6.8*	
BHVO-2	< 0.5	0.1	2	0.3	< 0.2	< 0.1	119	12.9	35.7	4.7	22	5.95	2.05	5.8	0.86
BHVO-2	< 0.5	0.1	1.8	0.2	< 0.2	< 0.1	122	13.4	37	5.3	24.2	6.4	2.15	6.2	0.9
BHVO-2	< 0.5	0.1	2.2	0.2	< 0.2	< 0.1	133	13	37.9	5.25	23.8	6.4	2.1	6	0.94
*BHVO-2**							*130*	*15*	*38*		*25*	*6.2*			*0.9*
Detection limit	0.5	0.05	0.1	0.1	0.2	0.1	0.5	0.1	0.1	0.05	0.05	0.05	0.05	0.2	0.02

Sample	Dy	Ho	Er	Tm	Yb	Lu	Hf	Ta	W	Re	Tl	Pb	Bi	Th	U
TAS14-01	4.15	0.72	1.9	0.25	1.45	0.26	3.2	1.4	< 0.5	< 0.1	< 0.1	3	< 0.1	4.5	1.3
TAS14-02	4.05	0.76	1.95	0.25	1.55	0.26	3.4	3.2	< 0.5	< 0.1	< 0.1	3	< 0.1	3.1	0.8
TAS14-07	5.25	0.96	2.5	0.3	1.95	0.3	3.2	1.2	1	< 0.1	< 0.1	3	< 0.1	3.1	1.1
TAS14-08	4.7	0.86	2.3	0.25	1.8	0.28	2.8	0.8	< 0.5	< 0.1	< 0.1	2	< 0.1	2.3	0.9
TAS14-10	10.2	1.74	3.8	0.4	2.25	0.32	14.4	5.6	2.5	< 0.1	< 0.1	7	< 0.1	13.9	4.1
TAS14-15	4.75	0.92	2.45	0.3	2	0.32	4.2	3.7	30	< 0.1	< 0.1	2	< 0.1	4.7	1.3
TAS14-17	5.9	0.98	2.3	0.25	1.5	0.24	5.2	4.1	22	< 0.1	< 0.1	3	< 0.1	6.4	2.5
TAS14-21	7.05	1.18	2.55	0.3	1.5	0.22	6.8	5.6	< 0.5	< 0.1	< 0.1	4	< 0.1	8.7	3.5
TAS14-26	5	0.9	2.35	0.25	1.65	0.28	4.4	5.8	2	< 0.1	< 0.1	2	< 0.1	2.2	0.6
TAS14-29	4.35	0.82	2.05	0.25	1.55	0.26	3	0.9	< 0.5	< 0.1	< 0.1	2	< 0.1	2.3	0.7
TAS14-31	4.3	0.78	1.8	0.25	1.25	0.2	4.8	3.5	34	< 0.1	< 0.1	3	< 0.1	4.1	1.3
TAS14-36	4.45	0.88	2.3	0.25	1.8	0.28	3.6	1.8	< 0.5	< 0.1	< 0.1	2	< 0.1	2.4	0.8
TAS14-41	4.35	0.82	2.3	0.3	1.8	0.3	3.8	1.1	1	< 0.1	< 0.1	3	0.3	3.2	0.9
TAS14-42	3.85	0.74	2	0.25	1.5	0.26	2.8	0.9	< 0.5	< 0.1	< 0.1	2	< 0.1	2.4	0.6
TAS14-46	4.45	0.76	1.95	0.25	1.4	0.22	4.4	2.6	< 0.5	< 0.1	< 0.1	2	< 0.1	3.2	1.3
TAS14-47	5.15	0.88	2.2	0.25	1.5	0.22	4.4	1.3	< 0.5	< 0.1	< 0.1	2	< 0.1	2.4	0.7
TAS14-48	3.7	0.74	1.95	0.25	1.55	0.26	2.8	1.3	< 0.5	< 0.1	< 0.1	2	< 0.1	2.3	0.6
TAS14-50	4.6	0.86	2.1	0.25	1.6	0.24	5.6	1.9	2.5	< 0.1	< 0.1	2	< 0.1	3	0.8
TAS14-54	4.5	0.86	2.25	0.3	1.8	0.28	2.8	0.7	< 0.5	< 0.1	< 0.1	2	< 0.1	2	0.5

(*continued on next page*)

Table 3 (*continued*)

Sample	Dy	Ho	Er	Tm	Yb	Lu	Hf	Ta	W	Re	Tl	Pb	Bi	Th	U
TAS14-59	5.4	0.9	2.3	0.25	1.55	0.22	5	1.9	< 0.5	< 0.1	< 0.1	2	< 0.1	3.4	1
TAS14-61	6.6	1.06	2.4	0.3	1.55	0.26	5.4	9.5	< 0.5	< 0.1	< 0.1	4	< 0.1	10.3	2.9
TAS14-64	4.6	0.94	2.85	0.4	2.65	0.46	2.8	0.5	1	< 0.1	0.2	7	< 0.1	4.3	1.1
TAS14-67	4.45	0.9	2.4	0.3	1.8	0.28	2.4	0.6	< 0.5	< 0.1	< 0.1	2	< 0.1	1.9	0.5
TAS14-68	4.15	0.8	2.05	0.25	1.65	0.26	2.6	0.8	< 0.5	< 0.1	< 0.1	2	< 0.1	1.9	0.5
TAS14-69	3.4	0.74	2.3	0.3	2.1	0.34	2.2	0.5	< 0.5	< 0.1	0.2	5	< 0.1	3.3	0.9
TAS14-71	3.85	0.78	2.3	0.3	2.15	0.36	2.2	0.4	< 0.5	< 0.1	0.2	5	< 0.1	3.3	0.9
TAS14-72	4	0.8	2.25	0.3	1.9	0.3	2	0.8	< 0.5	< 0.1	< 0.1	2	< 0.1	2	0.5
TAS14-75	4.25	0.8	2.1	0.25	1.65	0.26	2.8	0.9	< 0.5	< 0.1	< 0.1	4	< 0.1	2.5	1.2
TAS14-78	4.3	0.78	2.05	0.25	1.55	0.28	2.8	0.8	< 0.5	< 0.1	< 0.1	3	< 0.1	2.4	1.2
TAS14-79	3.75	0.8	2.4	0.35	2.2	0.34	2.2	0.4	< 0.5	< 0.1	0.2	6	< 0.1	3.5	0.9
TAS14-80	4.5	0.84	2	0.25	1.55	0.24	3	1.3	45.5	< 0.1	< 0.1	2	< 0.1	2.5	0.7
TASBAS	4.3	0.76	1.7	0.2	1.2	0.18	5	3.2	43.5	< 0.1	< 0.1	5	< 0.1	4.6	1.7
BCR-2	6.1	1.26	3.45	0.5	3.15	0.5	4.4	0.6	2	< 0.1	0.3	10	< 0.1	5.9	1.5
BCR-2	6.15	1.3	3.6	0.45	3.1	0.54	5	0.6	2.5	< 0.1	0.3	10	< 0.1	5.7	1.6
BCR-2	6.75	1.34	3.85	0.5	3.5	0.52	5.2	0.5	2	< 0.1	0.3	10	< 0.1	6	1.7
*BCR-2**		*1.33*		*0.54*	*3.5*	*0.51*	*4.8*					*11*		*6.2*	*1.69*
BHVO-2	5	0.96	2.5	0.3	1.85	0.3	4.4	1.3	1	< 0.1	< 0.1	2	< 0.1	1.2	0.5
BHVO-2	5.4	1.06	2.65	0.3	2.05	0.34	4.8	0.7	1	< 0.1	< 0.1	2	< 0.1	1.2	0.5
BHVO-2	5.6	1.02	2.6	0.3	1.9	0.28	4.6	2	1	< 0.1	< 0.1	2	< 0.1	1.3	0.5
*BHVO-2**		*1.04*			2	*0.28*	*4.1*	*1.4*						*1.2*	
Detection limit	0.05	0.02	0.05	0.05	0.05	0.02	0.2	0.1	0.5	0.1	0.1	1	0.1	0.1	0.1

4. Results

4.1. Major and trace element compositions

Major element compositions are given in Table 1. Three sets of trace element data are given in Tables 2–4. Due to the lower detection limit of the LA-ICP-MS technique, these values are preferred and used in following plots.

4.1.1. Cenozoic samples

All our samples roughly overlap the major element data of Tasmanian Cenozoic basalts available as published data (e.g. Adam (1990); Adam and Green (2011); Everard et al. (2007); Frey et al. (1978); Lanyon et al. (1993); McDonough et al. (1985); Nasir et al. (2010); Sutherland (1973); Sutherland (1974); Sutherland et al. (1989); Sutherland et al. (2004); Sutherland and Hale (1970)). According to the TAS diagram by Le Bas et al. (1986), the Cenozoic Tasmanian samples (Table 1) span a range from foidite, to tephrite, trachy-basalt, basalt and to basaltic andesite (Fig. 4). On a normative basis the Tasmanian suites range from highly undersaturated olivine melilitite and nephelinite to basanite, *ne*-hawaiite, olivine basalt and *Q*-tholeiite. SiO_2 content ranges between 37.7 wt% at the most silica-undersaturated end of the spectrum to 54.2 wt% in somewhat fractionated *Q*-normative suites (Fig. 5). Normative nepheline content in undersaturated rocks ranges from 0.88 to 21.04 wt% (Fig. 5). Of these highly undersaturated rocks, TAS14-60 to 63, sampled at Laughing Jack Marsh, are classified as melilitites and contain normative larnite. There is a general positive correlation between the degree of SiO_2-undersaturation and total alkalis, MgO, TiO_2, CaO, K_2O, P_2O_5 and FeO^{total} (Fig. 4). The most undersaturated magmas not only have the highest total alkalis and MgO, but also have the highest TiO_2. Over the entire suite, mg# values range from 0.70 to 0.38 and increasingly SiO_2-undersaturated samples tend to have increasing mg# values.

Trace element values are listed in Table 2–4. The Cenozoic samples analysed show a wide spread in trace element concentrations (Fig. 6). The most undersaturated lavas not only have the highest MgO and compatible trace element content (Sc, Cr, Ni) but also have the highest incompatible trace elements (e.g. Sr, Y, Zr, Ba, Hf and LREE).

Mantle-normalized incompatible element diagrams (Fig. 7) show that the alkaline Cenozoic samples have a typical OIB-like trace element signature. They are relatively enriched in the LREE and incompatible elements such as Rb, Ba, Th, U, Nb, and show significant relative depletions in K and Rb, which is also seen in HIMU end member patterns (Willbold and Stracke, 2006).

Amongst the Cenozoic samples, the transition of *Q*-tholeiites to olivine melilitite is marked by increasing LREE and increasing negative K_N anomalies. Like the Eu/Eu*, K/K* is calculated using the extrapolated value for K based on the normalized values for Ta and La. In this case however, Nb_N and La_N have been used as not all published data had Ta reported. The olivine melilitites and nephelinites have lower HREE and Y (e.g. Lu = 0.198–0.274 ppm, Y = 27.4–29.7 ppm) compared to the SiO_2-saturated to oversatured basalt and have significantly higher La/Y (2.5–3 or $(La/Y)_N$ = 16–20) and La/Lu (263–388 or $(La/Lu)_N$ = 27–40) ratios.

4.1.2. Jurassic samples

For comparison with the Cenozoic samples, some of the Jurassic dolerites were also sampled (TAS14–64, 69, 70, 71, 79). The Jurassic samples are more siliceous (SiO_2 between 51.1 and 54.8 wt%) and classified as basaltic andesite on the TAS diagram (Le Bas et al., 1986) or as low Ti tholeiites (Hergt and Brauns, 2001). MgO values range between 4 and 8.1 wt%, with mg# values between 0.47 and 0.63. They have significantly higher K_2O/Na_2O ratios than the Cenozoic lavas, lower CaO and FeO_t and have much lower TiO_2 and Na_2O.

Jurassic samples have trace element signatures more like those of the upper continental crust (Rudnick and Gao, 2003; Taylor and

Table 4
LA-ICP-MS trace element analyses in ppm for Cenozoic and Jurassic mafic rocks in Tasmania. BCR-2* and BHVO-2* are certified and recommended reference values (Wilson, 1997a and 1997b).

Sample	Be	Ca	Sc	Ti	V	Cr	Mn	Co	Ni	Cu	Zn	Ga	As	Rb	Sr	Y	Zr
TAS14-01_01	< 9.27	65352.27	22.64	8336.39	180.31	309.43	1192.92	48.50	207.83	49.77	98.80	18.39	1.33	17.65	633.95	19.22	151.63
TAS14-01_02	< 9.68	65352.27	24.78	8906.99	194.17	332.04	1252.75	52.38	220.47	51.32	104.86	19.83	< 0.83	19.08	669.17	20.24	161.63
TAS14-01_03	< 5.65	65352.27	21.84	8235.23	177.84	308.64	1187.17	50.66	205.86	44.63	102.44	17.71	0.95	17.64	620.82	18.69	148.49
TAS14-02_01	< 9.92	69068.70	25.88	10555.57	222.28	167.30	1279.51	38.83	56.29	42.71	103.33	21.72	1.54	16.91	823.48	21.84	170.32
TAS14-02_02	< 7.28	69068.70	24.80	10277.03	219.77	154.53	1217.19	36.90	48.32	40.04	99.94	21.64	< 1.03	16.11	781.71	21.23	161.83
TAS14-02_03	< 8.34	69068.71	24.09	9931.61	210.47	152.97	1212.14	37.45	50.61	48.94	95.71	21.34	< 1.23	15.63	764.65	20.20	156.97
TAS14-03_01	< 7.06	63190.30	25.06	9423.82	212.39	254.64	1233.79	43.88	112.07	25.88	101.37	21.23	< 1.44	24.00	772.52	20.51	159.67
TAS14-03_02	< 6.10	63190.30	23.65	9472.81	208.51	251.03	1234.69	42.55	104.93	26.15	107.26	20.85	< 0.90	24.10	776.73	20.54	156.97
TAS14-03_03	< 6.53	63190.29	24.46	9302.95	208.64	249.13	1229.90	41.98	108.01	27.38	103.31	20.77	< 0.78	23.58	771.82	20.21	159.67
TAS14-04_01	5.10	66996.08	25.50	7236.85	168.18	265.86	971.73	38.47	141.37	44.25	98.89	18.46	1.67	19.62	308.12	22.36	117.62
TAS14-04_02	< 5.74	66996.08	26.67	7828.62	182.69	291.32	1044.46	40.43	153.44	47.85	108.94	20.08	< 1.09	20.36	329.44	23.11	123.74
TAS14-04_03	< 7.21	66996.08	25.71	7580.72	175.96	262.75	997.67	39.88	156.76	46.42	104.44	19.60	1.76	20.17	317.66	22.41	119.23
TAS14-05_01	6.05	70226.53	26.76	8049.31	184.60	302.83	989.34	40.36	136.61	48.66	113.32	22.31	< 1.05	19.02	353.12	58.40	131.07
TAS14-05_02	< 5.32	70226.53	26.30	7972.27	182.13	307.84	963.61	39.84	137.74	46.88	114.65	22.23	< 0.81	17.73	346.35	57.41	128.25
TAS14-05_03	3.36	70226.53	27.08	8039.77	179.55	308.00	962.62	40.91	138.40	46.25	125.58	22.17	< 1.02	17.86	343.63	57.28	125.01
TAS14-06_01	< 4.01	65938.32	25.63	8100.88	175.96	325.37	954.01	33.50	125.74	47.60	106.10	20.42	0.88	20.61	321.20	23.13	126.38
TAS14-06_02	< 6.50	65938.33	25.94	8075.09	177.55	322.05	946.87	33.42	122.88	50.60	118.39	20.92	1.40	20.73	317.16	22.74	124.61
TAS14-06_03	5.91	65938.33	26.48	8194.54	177.83	327.40	973.11	33.31	127.80	47.54	116.25	20.55	< 0.91	20.47	321.18	23.80	127.19
TAS14-07_01	< 6.98	67374.87	27.63	8317.40	182.02	335.97	974.22	34.80	126.15	48.01	115.60	21.52	1.56	23.47	328.71	23.74	128.91
TAS14-07_02	3.90	67374.87	26.05	8143.12	175.94	323.17	960.79	33.43	125.09	51.27	113.01	21.16	1.19	20.30	313.76	22.40	122.08
TAS14-07_03	< 6.54	67374.87	27.37	8395.49	183.90	332.81	1001.92	35.86	131.99	52.61	107.81	22.40	< 0.95	22.44	339.98	24.08	132.29
TAS14-08_01	< 4.42	63122.39	24.55	7581.21	160.32	267.43	1156.80	47.21	180.00	51.62	116.08	19.33	< 0.86	21.63	300.24	21.62	115.46
TAS14-08_02	< 4.41	63122.39	24.32	7410.96	158.60	267.88	1166.60	47.25	173.27	54.95	127.28	20.17	< 0.98	20.92	290.48	20.73	112.27
TAS14-08_03	< 3.39	63122.39	23.77	7461.47	159.08	256.10	1139.17	47.88	174.46	53.11	119.85	20.33	0.83	21.24	286.50	20.48	111.20
TAS14-09_01	< 5.22	64498.19	23.64	7421.78	158.13	253.53	1133.73	48.00	175.09	57.86	114.40	19.86	1.17	20.94	299.61	20.65	117.73
TAS14-09_02	< 5.19	64498.19	24.34	7541.80	159.97	248.66	1123.65	47.54	174.98	58.24	115.97	19.89	< 0.85	20.24	297.57	21.24	115.58
TAS14-09_03	< 4.02	64498.19	25.58	7905.40	169.76	269.13	1177.74	49.80	186.87	60.02	125.13	20.18	< 1.21	21.37	310.36	22.11	124.49
TAS14-10_01	< 5.04	60256.45	17.36	10615.44	106.88	556.12	1728.39	53.78	523.17	32.62	181.49	28.69	3.77	48.09	1497.25	42.36	608.02
TAS14-10_02	5.84	60256.44	17.18	10665.98	110.34	571.21	1773.96	54.53	518.67	38.62	196.28	28.98	3.76	49.59	1549.31	42.95	611.84
TAS14-10_03	4.78	60256.44	17.76	10903.06	113.37	583.78	1815.97	56.46	536.55	39.38	195.48	29.06	2.87	49.31	1529.84	43.25	614.32
TAS14-11_01	< 5.20	70719.67	25.27	9401.28	222.09	274.66	1216.32	38.59	51.88	23.79	96.49	20.99	1.13	19.70	595.68	21.33	171.55
TAS14-11_02	< 4.87	70719.68	24.61	9332.50	225.82	268.28	1232.68	39.44	51.02	24.88	106.63	21.15	< 1.10	18.95	585.56	20.15	165.10
TAS14-11_03	3.76	70719.66	25.22	9643.55	230.93	284.17	1267.64	40.86	54.72	27.16	104.83	22.65	< 0.93	19.44	591.95	20.17	168.39
TAS14-12_01	< 5.31	74471.84	26.78	9642.98	230.36	389.26	1497.79	52.08	222.46	69.09	91.59	20.90	1.87	16.65	713.32	27.63	233.85
TAS14-12_02	< 6.06	85048.71	30.72	10668.69	253.92	430.07	1665.98	58.73	251.46	76.44	103.74	23.74	< 1.49	18.38	796.75	30.30	260.39
TAS14-12_03	5.08	85048.71	29.30	11060.05	261.09	438.38	1733.20	58.87	253.04	78.49	107.92	23.90	1.19	18.22	805.31	30.07	259.89
TAS14-13_01	1.52	73503.40	30.27	11941.74	214.11	405.60	1402.12	50.59	184.06	54.25	74.72	19.44	1.00	34.45	682.91	26.91	257.08
TAS14-13_02	2.13	73503.39	30.44	11845.01	211.77	417.11	1448.85	50.76	186.42	58.02	82.68	20.05	1.08	35.86	692.52	27.22	265.10
TAS14-13_03	3.02	73503.39	29.16	11768.18	210.10	402.68	1379.85	49.50	186.78	53.02	75.25	19.02	1.17	33.33	660.52	25.31	249.12
TAS14-14_01	3.05	74596.88	26.90	11918.86	200.45	294.70	1323.87	51.25	162.31	46.80	75.05	19.93	1.49	17.68	756.94	24.26	255.76
TAS14-14_02	3.29	74596.89	26.80	11841.18	200.26	294.48	1322.70	51.91	158.38	47.77	76.71	19.39	0.91	17.29	760.63	24.33	255.56
TAS14-14_03	2.76	74596.89	26.72	11933.62	202.08	300.63	1350.95	53.53	164.57	48.96	79.38	20.63	1.57	17.90	773.88	24.68	257.60
TAS14-15_01	2.26	70015.66	24.79	11311.13	186.56	426.60	1323.75	54.78	288.98	66.98	77.91	17.96	1.40	31.73	753.48	22.80	206.14
TAS14-15_02	2.34	70015.65	26.05	11576.36	191.08	447.40	1389.65	56.59	299.15	71.04	89.28	18.80	0.88	33.26	769.51	24.27	219.83
TAS14-15_03	2.42	70015.66	26.36	11893.89	200.52	461.24	1439.58	60.77	316.26	69.14	92.09	19.89	0.57	34.77	799.13	24.71	226.87
TAS14-16_01	1.98	76212.10	26.80	11672.01	197.06	316.55	1311.78	48.92	168.18	57.13	72.40	18.12	1.07	24.96	783.60	23.83	235.64
TAS14-16_02	2.24	76212.11	27.47	12211.44	206.73	331.99	1364.94	50.85	177.68	57.98	78.09	19.36	1.38	26.05	821.99	24.71	244.96
TAS14-16_03	2.80	76212.12	27.27	12211.30	206.39	332.76	1362.34	51.91	179.37	61.79	80.18	19.59	1.58	25.58	806.74	24.00	241.22
TAS14-17_01	5.00	81082.80	20.28	15141.46	176.26	361.19	1475.18	59.12	270.53	53.74	132.39	22.55	2.03	18.34	1461.04	26.72	289.55
TAS14-17_02	2.96	81082.80	20.10	15381.08	178.58	358.06	1435.40	58.63	270.54	46.08	122.71	22.08	2.62	17.87	1396.22	25.21	278.05
TAS14-17_03	4.32	81082.80	20.48	15474.21	179.35	371.32	1526.44	60.65	282.46	50.68	138.11	20.11	2.33	18.41	1438.14	26.14	288.58

(continued on next page)

Table 4 (*continued*)

Sample	Be	Ca	Sc	Ti	V	Cr	Mn	Co	Ni	Cu	Zn	Ga	As	Rb	Sr	Y	Zr
TAS14-18_01	4.17	74754.13	22.46	14966.67	188.40	385.29	1580.46	55.48	283.73	49.51	107.03	20.85	2.78	14.71	928.32	25.09	249.18
TAS14-18_02	3.78	74754.13	22.03	14964.88	190.23	388.30	1587.78	55.92	282.69	48.20	111.32	21.88	2.65	14.62	918.59	24.77	244.72
TAS14-18_03	2.14	74754.13	23.23	15230.59	194.51	396.64	1648.15	58.12	293.57	51.80	120.16	21.93	2.08	15.26	949.97	26.39	264.87
TAS14-19_01	3.59	75972.69	21.63	15139.14	185.16	343.65	1407.25	64.93	264.92	43.37	106.02	20.72	1.99	15.77	978.55	25.74	264.64
TAS14-19_02	2.24	75972.69	21.02	15096.23	183.70	342.98	1435.06	65.55	266.77	43.33	122.61	21.78	2.58	15.68	959.68	25.66	259.36
TAS14-19_03	2.15	75972.70	20.83	15035.94	185.07	340.24	1414.72	65.01	268.64	43.74	112.95	21.07	1.75	15.58	952.07	24.35	250.49
TAS14-20_01	2.33	75765.42	20.78	14899.54	182.28	340.65	1390.11	53.09	273.40	46.39	111.39	20.89	1.49	15.89	981.26	24.55	256.01
TAS14-20_02	2.39	75765.43	21.17	15126.59	185.18	343.11	1433.98	57.46	279.91	47.73	125.41	21.69	2.05	16.24	997.57	25.50	266.10
TAS14-20_03	2.39	75765.42	21.51	15083.94	186.31	347.55	1439.88	56.75	277.94	48.19	128.28	21.85	2.24	16.28	997.40	25.06	262.18
TAS14-21_01	4.81	79081.64	18.25	16752.59	173.88	428.10	1583.06	56.63	295.22	39.85	141.74	22.91	1.90	11.90	1279.58	29.02	362.69
TAS14-21_02	4.65	79081.63	18.42	16789.71	173.61	373.75	1593.23	58.05	294.26	44.08	156.25	22.80	2.18	11.95	1285.61	30.12	374.21
TAS14-21_03	2.16	79081.63	18.26	16645.65	172.87	384.83	1610.80	58.65	298.62	40.69	158.47	23.10	1.93	12.28	1281.52	29.18	361.82
TAS14-22_01	4.19	78931.55	19.26	16417.81	177.99	400.24	1580.73	58.07	313.72	56.63	140.83	22.86	2.57	11.24	1239.98	29.23	358.41
TAS14-22_02	5.11	78931.55	20.21	16505.52	181.32	422.15	1641.24	59.61	324.06	57.22	161.22	23.69	3.33	11.31	1260.85	30.37	372.67
TAS14-22_03	3.41	78931.55	19.97	16301.00	177.89	400.93	1609.39	59.08	309.63	57.29	154.75	23.01	2.68	11.54	1240.34	29.62	365.19
TAS14-23_01	3.87	79156.68	19.57	16063.17	176.69	390.46	1425.30	62.95	317.92	48.42	130.18	22.54	2.26	10.16	1400.36	28.70	349.85
TAS14-23_02	5.59	79156.68	20.18	16300.86	180.09	415.74	1508.85	67.54	321.89	52.77	162.86	24.08	2.25	10.33	1485.36	29.84	367.14
TAS14-23_03	4.95	79156.68	19.91	16285.45	179.70	410.82	1498.52	67.18	319.80	51.70	159.47	23.48	1.68	10.37	1467.69	29.48	362.48
TAS14-24_01	3.75	71791.70	19.86	13934.79	172.55	252.98	1215.89	62.22	205.86	38.34	103.84	19.88	1.85	20.21	702.85	21.30	182.28
TAS14-24_02	2.17	71791.70	20.58	13932.56	170.64	261.17	1278.35	68.02	215.04	44.37	118.73	21.01	1.45	21.33	720.31	22.25	189.52
TAS14-24_03	2.31	71791.70	19.66	13784.20	169.42	253.15	1246.93	63.60	212.15	42.21	118.70	20.33	1.39	20.72	707.31	21.35	182.86
TAS14-25_01	1.81	69032.95	25.34	10180.47	162.01	284.99	1149.74	50.78	236.50	43.99	100.48	18.32	0.56	7.54	277.95	21.72	113.25
TAS14-25_02	1.71	69032.95	25.69	10076.20	161.93	285.39	1161.68	50.62	237.88	43.10	110.36	18.41	0.28	7.57	274.78	21.96	114.04
TAS14-25_03	1.43	69032.95	25.60	10105.89	161.74	297.65	1188.43	52.76	241.97	47.37	119.45	18.99	1.00	7.59	277.54	22.59	114.65
TAS14-26_01	1.30	61814.47	24.23	11323.85	162.61	272.63	1193.03	50.70	214.50	41.24	102.48	18.65	1.03	8.38	358.15	22.02	145.11
TAS14-26_02	1.15	61814.47	23.89	11211.71	159.86	269.64	1208.15	51.50	215.75	43.36	110.98	18.95	0.96	8.51	363.99	23.26	151.47
TAS14-26_03	****	61814.46	23.92	11253.32	160.28	276.11	1241.67	52.23	217.42	42.46	121.32	18.96	0.94	8.91	360.94	23.02	151.58
TAS14-27_01	2.07	60724.55	24.93	9038.82	153.96	351.46	1070.42	44.20	161.91	31.39	90.05	16.81	0.08	5.66	242.56	18.88	90.97
TAS14-27_02	1.25	60724.56	25.29	9075.75	156.39	369.74	1106.21	45.96	163.46	34.32	104.70	17.60	0.52	5.62	242.34	19.70	94.02
TAS14-27_03	1.65	60724.56	25.71	9297.19	158.26	362.33	1135.38	45.97	168.63	35.96	108.76	18.38	0.35	5.80	244.68	19.57	94.67
TAS14-28_01	2.44	60345.76	23.21	12325.14	170.00	256.22	1168.99	52.77	195.78	49.23	113.45	21.31	0.60	12.10	443.96	22.12	170.06
TAS14-28_02	2.41	60345.76	22.66	12292.28	169.80	255.30	1157.98	52.38	190.99	48.71	105.02	20.86	0.66	11.70	442.09	21.80	168.90
TAS14-28_03	1.16	60345.76	22.59	12346.31	169.95	251.37	1174.55	53.22	191.70	48.89	120.83	21.70	0.73	12.37	452.23	21.66	168.90
TAS14-29_01	1.37	62493.45	24.12	10474.35	168.91	265.67	1156.28	40.32	173.44	43.97	94.97	19.02	1.30	11.33	326.61	21.73	128.69
TAS14-29_02	2.25	62493.45	23.31	10469.02	169.00	265.71	1136.06	48.11	170.95	44.04	95.07	18.54	1.06	10.93	318.93	20.72	123.26
TAS14-29_03	1.47	62493.45	23.95	10716.70	174.55	273.64	1181.76	50.37	179.88	45.59	101.01	19.14	1.42	11.40	331.51	21.16	125.53
TAS14-30_01	0.75	70037.11	24.18	12349.58	206.25	362.38	1390.00	55.41	264.58	67.54	91.90	20.32	0.66	21.14	667.16	21.51	177.35
TAS14-30_02	2.55	70037.12	23.98	12179.41	206.43	358.02	1378.94	55.45	262.26	63.67	93.30	20.47	1.10	20.69	659.93	20.86	170.32
TAS14-30_03	2.47	70037.12	24.16	12269.04	207.16	363.17	1375.21	56.09	262.28	64.44	95.08	20.66	1.12	20.52	654.66	21.36	171.55
TAS14-31_01	3.50	64426.72	19.13	15117.46	186.20	356.34	1215.50	59.42	275.91	51.79	92.14	21.36	3.71	21.79	840.52	19.42	234.33
TAS14-31_02	2.71	64426.72	20.43	15450.34	191.04	369.16	1252.01	60.79	278.51	48.72	103.28	22.39	2.48	22.23	859.82	20.68	250.77
TAS14-31_03	3.45	64426.71	19.25	15181.60	189.43	364.69	1217.50	58.79	280.19	49.50	98.09	21.55	2.44	21.85	835.35	18.89	231.44
TAS14-32_01	3.29	65505.91	20.05	15558.93	193.68	394.19	1238.62	59.43	341.17	47.18	104.19	22.22	1.90	20.56	867.61	19.40	239.42
TAS14-32_02	2.93	65505.91	20.77	15542.65	194.31	389.54	1266.89	61.12	341.58	47.77	104.30	22.41	1.28	21.24	886.46	20.33	250.59
TAS14-32_03	3.13	65505.91	20.17	15432.24	191.48	391.42	1254.91	60.43	339.52	47.77	105.39	22.50	1.64	20.58	889.14	20.61	254.02
TAS14-33_01	4.04	64090.81	19.70	15393.38	191.84	393.26	1233.95	65.53	304.69	50.78	98.67	21.78	2.37	14.59	894.19	18.81	232.84
TAS14-33_02	3.76	64090.81	20.42	15343.92	191.03	389.71	1248.50	65.93	298.44	49.69	109.13	26.14	1.98	14.89	902.76	19.71	242.84
TAS14-33_03	2.95	64090.80	19.39	15430.74	192.98	395.95	1248.99	65.85	303.61	50.62	106.46	21.74	2.01	15.14	906.28	18.69	231.99
TAS14-34_01	3.74	61707.28	18.82	12457.94	168.19	261.86	1287.17	50.52	201.66	55.21	112.01	22.54	0.91	15.26	799.03	18.28	192.41
TAS14-34_02	3.74	61707.28	19.32	12643.40	171.36	253.07	1323.10	51.33	205.25	63.84	115.00	22.91	0.49	13.69	807.88	18.52	196.85
TAS14-34_03	2.27	61707.28	18.59	12503.92	170.20	257.06	1299.06	50.93	202.06	56.91	120.28	22.35	0.53	13.87	803.21	18.06	190.00
TAS14-34B_01	1.56	61707.28	18.97	12067.92	164.24	252.91	1259.20	50.46	192.70	53.99	111.99	21.87	1.25	13.05	764.75	18.45	194.08
TAS14-34B_02	2.76	61707.28	18.76	12446.76	170.52	264.89	1309.99	51.92	200.02	57.46	117.44	22.81	0.97	13.65	800.51	18.43	194.70

(*continued on next page*)

Table 4 *(continued)*

Sample	Be	Ca	Sc	Ti	V	Cr	Mn	Co	Ni	Cu	Zn	Ga	As	Rb	Sr	Y	Zr
TAS14-34B_03	2.87	61707.28	18.76	12593.99	171.80	267.92	1320.03	53.00	203.62	58.58	124.41	23.58	0.76	13.61	802.38	17.98	191.56
TAS14-35_01	2.66	61878.81	19.22	12380.09	165.49	246.81	1280.10	50.01	193.39	55.64	115.46	22.08	1.29	14.07	838.03	19.06	206.58
TAS14-35_02	2.61	61878.81	18.39	12350.69	167.02	253.49	1290.78	50.79	192.82	58.33	120.98	22.37	1.47	14.34	833.56	17.69	194.67
TAS14-35_03	2.90	61878.81	18.55	12495.57	170.78	259.56	1316.63	51.61	198.38	58.95	121.34	22.60	1.39	14.61	848.59	17.95	198.13
TAS14-36_01	2.32	62879.39	23.55	11407.55	176.45	206.76	1281.77	50.85	181.28	50.89	97.29	20.21	1.28	19.10	529.84	21.80	166.46
TAS14-36_02	1.70	62879.39	22.77	11369.05	178.74	211.52	1277.62	50.09	181.11	51.49	97.41	20.23	0.70	19.38	525.29	20.90	161.21
TAS14-36_03	1.73	62879.39	22.83	11155.09	177.98	209.08	1278.58	51.17	181.04	51.62	97.88	19.99	0.93	19.44	516.23	20.05	154.34
TAS14-37_01	1.51	65427.30	22.83	12857.51	198.07	281.35	1295.50	51.12	188.61	41.44	98.29	21.12	0.73	20.19	488.27	21.26	168.56
TAS14-37_02	2.76	65427.30	21.65	12816.23	198.75	283.95	1289.82	52.17	193.03	42.73	97.69	20.94	1.13	20.17	483.86	19.83	157.72
TAS14-37_03	1.88	65427.30	21.89	13040.47	203.61	289.99	1306.81	51.57	194.81	45.65	100.90	21.97	0.96	20.42	487.97	20.48	162.42
TAS14-38_01	1.58	60017.01	23.47	10049.64	172.22	268.32	1264.35	55.22	178.98	38.35	92.92	19.36	0.94	17.63	284.30	19.73	116.17
TAS14-38_02	1.16	60017.01	23.58	10096.56	171.40	257.69	1270.39	56.03	180.40	39.13	93.24	19.57	0.31	17.87	286.57	19.77	115.78
TAS14-38_03	1.50	60017.01	23.75	10350.48	176.36	263.60	1287.28	56.88	181.72	40.19	96.87	20.16	0.68	17.87	285.74	19.91	117.39
TAS14-39_01	0.85	62504.17	23.52	9689.68	175.24	296.70	1250.22	49.89	142.23	41.71	103.48	20.52	1.20	15.57	328.24	18.74	117.64
TAS14-39_02	1.98	62504.17	22.22	9627.64	175.98	299.39	1242.40	49.64	143.23	42.26	94.31	20.08	1.26	15.66	324.87	17.38	112.77
TAS14-39_03	1.61	62504.17	21.78	9550.02	174.66	299.34	1242.76	49.51	139.45	43.97	100.86	19.95	0.88	15.28	317.63	17.07	107.35
TAS14-40_01	2.24	58205.25	22.30	10404.56	178.95	284.18	1510.95	47.91	131.26	36.79	95.94	19.99	2.48	24.12	361.93	21.64	156.10
TAS14-40_02	1.97	58205.25	21.44	10412.41	180.98	287.09	1516.63	48.71	135.37	43.90	99.85	20.13	2.54	27.27	360.48	20.30	146.74
TAS14-40_03	2.17	58205.25	21.95	10445.62	182.01	282.05	1529.80	49.33	135.96	41.60	97.81	20.18	1.69	24.04	357.21	20.23	146.11
TAS14-41_01	2.89	59366.64	23.41	11122.64	190.18	265.45	1018.45	40.95	96.65	31.98	195.67	21.34	2.05	25.73	377.98	22.28	165.77
TAS14-41_02	2.36	59366.64	23.20	11257.50	194.06	262.34	1011.69	43.17	97.97	33.64	186.56	21.56	1.91	25.94	376.47	21.00	157.96
TAS14-41_03	1.74	59366.64	23.05	11169.17	192.99	263.48	1013.40	42.48	102.99	33.74	194.95	21.58	1.85	26.25	378.53	20.93	157.98
TAS14-42A_01	2.70	60885.38	23.08	10144.91	165.61	254.26	1086.02	50.98	172.67	41.97	101.33	18.89	0.36	13.60	337.79	19.81	125.88
TAS14-42A_02	1.23	60885.38	22.81	10481.91	170.86	254.80	1104.42	52.59	169.09	44.96	102.25	19.98	0.30	13.98	351.29	19.34	123.41
TAS14-42A_03	2.10	60885.38	22.77	10261.17	170.52	257.09	1084.21	51.72	166.59	40.56	96.63	19.43	0.74	13.80	344.53	19.14	123.96
TAS14-42B_01	1.04	60885.38	23.47	10375.82	168.12	254.21	1094.62	51.19	164.02	43.71	102.52	19.41	0.96	13.64	346.77	20.49	130.91
TAS14-42B_02	1.16	60885.38	22.61	10427.03	170.24	257.28	1091.68	51.42	164.47	42.13	97.28	19.42	0.85	13.75	340.89	19.24	123.90
TAS14-42B_03	1.24	60885.38	22.83	10604.12	174.83	260.82	1100.10	51.03	169.70	44.09	98.99	19.64	0.79	13.81	345.09	19.35	125.94
TAS14-43_01	3.72	71012.70	21.93	13071.12	187.71	296.07	1397.68	60.83	210.63	50.83	123.59	23.14	2.01	20.66	825.27	23.35	234.61
TAS14-43_02	2.58	71012.70	22.48	13646.47	193.33	300.70	1414.45	61.92	215.17	51.26	122.89	23.60	0.85	20.73	845.26	23.05	232.96
TAS14-43_03	3.19	71012.70	21.74	13195.99	186.92	289.54	1397.09	59.74	206.70	49.10	130.05	22.46	1.67	19.96	804.31	22.67	231.46
TAS14-44_01	2.28	64340.95	25.81	11127.01	199.66	286.33	1304.53	51.41	197.34	54.85	89.98	18.86	16.14	22.29	538.47	20.55	151.83
TAS14-44_02	2.67	64340.95	25.18	10717.07	192.21	275.21	1274.24	50.28	193.81	56.76	92.76	18.13	1.73	21.51	526.99	20.82	152.61
TAS14-44_03	0.86	64340.96	25.85	10904.08	195.95	291.42	1304.27	52.27	198.00	55.94	97.20	23.44	1.39	22.34	539.53	21.17	155.78
TAS14-45_01	1.67	61807.35	20.21	13097.90	199.64	308.97	1228.36	56.32	214.63	46.41	102.96	21.78	1.07	13.87	735.55	17.58	185.82
TAS14-45_02	2.26	61807.34	20.55	13220.79	202.16	303.30	1251.24	56.55	222.26	47.04	98.65	21.23	1.11	13.47	727.58	17.66	183.84
TAS14-45_03	2.78	61807.34	19.88	13096.60	199.85	301.80	1237.51	56.13	216.12	47.60	101.93	21.42	0.91	13.77	734.03	17.85	187.18
TAS14-46_01	1.99	59877.65	19.27	13503.98	183.23	265.14	1170.47	52.21	192.85	54.19	100.17	22.54	1.41	16.46	683.63	20.12	212.58
TAS14-46_02	2.13	59877.65	18.69	13580.37	184.33	266.77	1191.53	53.02	193.67	57.73	105.98	22.87	0.36	16.63	681.67	19.86	212.87
TAS14-46_03	3.00	59877.65	18.33	13263.77	179.52	261.91	1183.79	52.67	192.70	57.71	102.43	22.65	1.03	16.42	685.14	19.48	211.28
TAS14-47_01	2.63	58998.57	22.62	13592.29	172.61	234.63	1210.31	52.74	180.88	50.11	123.35	23.15	1.42	18.21	483.43	23.71	194.83
TAS14-47_02	1.39	58998.57	22.05	13783.19	176.43	235.47	1201.07	51.93	182.89	48.59	119.54	23.18	1.11	18.20	487.38	23.00	191.76
TAS14-47_03	1.70	58998.57	19.45	12292.36	155.00	206.63	1075.71	47.89	163.13	44.92	108.11	19.97	0.44	16.28	431.02	20.03	166.12
TAS14-48_01	0.12	68375.45	27.05	10412.76	200.16	315.83	1230.53	46.53	139.40	44.00	91.66	17.71	0.77	14.32	469.35	20.08	136.35
TAS14-48_02	3.15	68375.45	27.56	10699.09	206.31	324.85	1270.24	48.00	145.68	49.09	96.97	18.77	1.01	14.97	481.28	20.91	140.95
TAS14-48_03	2.38	68375.45	27.15	10687.29	207.98	329.98	1268.08	48.72	143.69	49.92	94.63	20.07	0.68	14.76	470.73	19.91	133.88
TAS14-49_01	1.33	63147.41	24.74	9271.86	159.15	224.93	1112.81	43.56	118.80	37.26	84.84	18.16	0.39	11.48	260.42	20.42	109.06
TAS14-49_02	****	63147.41	26.03	9527.84	163.67	232.27	1172.27	46.01	133.65	40.41	99.60	18.91	0.31	11.94	264.72	21.73	114.42
TAS14-49_03	2.36	63147.41	25.41	9391.53	161.79	238.43	1168.66	44.82	130.74	43.12	104.41	19.25	0.68	11.92	258.22	20.80	112.51
TAS14-50_01	2.68	65530.93	22.03	13427.48	196.39	237.03	1311.59	56.59	192.49	52.11	120.69	21.74	1.44	20.43	497.61	21.85	173.18
TAS14-50_02	2.02	65530.93	23.05	13432.67	196.47	238.84	1333.83	57.44	195.75	48.09	128.07	22.07	1.45	20.34	496.88	21.94	174.50
TAS14-50_03	1.69	65530.93	22.78	13696.41	200.89	250.15	1365.58	60.13	200.76	50.69	135.92	22.94	1.44	21.75	511.73	21.99	177.69
TAS14-51_01	1.86	58973.55	23.10	12844.18	188.90	257.29	1369.61	55.56	187.05	56.48	124.59	21.56	2.64	19.76	402.65	22.41	173.86

(continued on next page)

Table 4 (*continued*)

Sample	Be	Ca	Sc	Ti	V	Cr	Mn	Co	Ni	Cu	Zn	Ga	As	Rb	Sr	Y	Zr
TAS14-51_02	1.90	58973.55	22.64	12934.35	191.23	261.10	1360.14	55.74	191.19	50.34	118.25	22.29	1.07	19.83	410.18	22.38	175.81
TAS14-51_03	2.10	58973.55	22.43	12673.72	190.98	257.77	1355.69	55.94	183.07	51.03	120.99	21.97	0.83	20.06	407.56	21.73	173.32
TAS14-52_01	1.56	60513.73	22.40	13221.44	194.95	241.64	1292.99	57.41	197.44	50.34	112.75	21.18	0.68	21.50	445.72	20.97	169.29
TAS14-52_02	2.48	60513.73	22.57	13359.61	195.78	253.42	1314.14	58.31	195.60	49.89	118.32	21.65	0.83	21.77	451.50	21.68	173.74
TAS14-52_03	0.77	60513.73	22.49	13491.87	201.18	248.20	1330.44	57.73	198.26	52.30	123.18	21.67	0.76	22.26	456.36	21.37	171.15
TAS14-53_01	1.08	65827.53	24.86	9543.12	173.89	265.06	1185.32	48.93	133.10	39.62	118.09	19.90	1.46	12.58	294.17	20.28	112.27
TAS14-53_02	1.15	65827.53	23.61	9312.40	171.56	258.53	1148.09	48.89	131.08	38.61	113.17	19.73	1.36	11.66	283.22	19.51	106.98
TAS14-53_03	2.13	65827.53	24.80	9341.15	170.26	254.25	1154.22	49.27	132.27	40.75	116.73	19.71	1.28	11.96	288.89	20.29	109.60
TAS14-54_01	2.17	63097.38	25.10	10375.69	170.40	192.61	1180.10	46.91	91.24	31.79	103.09	19.84	0.66	12.83	245.39	23.18	116.99
TAS14-54_02	1.99	63097.38	25.79	10428.10	171.58	193.32	1194.49	48.27	92.37	32.39	116.61	20.30	0.74	13.22	253.20	24.37	122.89
TAS14-54_03	1.85	63097.38	25.34	10476.85	171.29	191.45	1196.43	48.68	89.70	31.28	118.25	20.41	1.81	13.27	248.68	23.56	118.48
TAS14-55_01	1.36	64494.61	25.15	10486.65	168.04	174.77	1122.33	43.30	78.26	30.21	99.05	20.04	0.20	12.37	257.25	24.04	121.99
TAS14-55_02	1.59	64494.61	24.67	10360.33	167.05	174.61	1135.66	44.57	82.10	34.79	106.75	20.54	0.61	12.48	258.13	23.82	120.93
TAS14-55_03	1.68	64494.61	25.56	10507.38	170.68	184.21	1154.07	44.92	82.48	35.50	113.96	20.99	1.83	12.73	261.14	24.38	121.95
TAS14-56A_01	1.41	60871.08	22.56	9821.79	158.78	247.62	1114.32	47.57	132.21	36.31	97.25	21.00	1.25	22.38	324.84	20.93	128.59
TAS14-56A_02	1.73	60871.08	22.45	9624.62	155.76	243.76	1103.41	46.60	129.80	38.41	110.99	20.29	0.59	22.62	323.02	21.22	128.11
TAS14-56A_03	1.25	60871.07	22.46	9823.88	161.16	250.35	1121.90	47.15	132.99	37.27	127.61	21.11	0.30	22.73	324.46	20.52	126.42
TAS14-56B_01	1.85	60871.08	22.54	9776.49	157.15	346.42	1094.81	45.91	130.24	39.66	102.71	20.38	0.84	22.77	321.11	20.83	128.05
TAS14-56B_02	1.54	60871.08	22.41	9673.32	155.50	243.45	1098.98	45.86	129.66	39.37	109.90	19.91	1.09	22.76	317.62	20.94	127.57
TAS14-56B_03	1.20	60871.08	22.39	9684.29	157.68	247.48	1112.31	46.35	130.98	40.31	110.48	20.28	1.89	22.72	319.19	20.91	126.16
TAS14-57_01	1.87	61146.24	21.97	9779.19	154.66	236.87	1208.53	54.59	162.48	39.11	133.58	20.29	0.83	20.86	313.85	22.13	126.76
TAS14-57_02	2.34	61146.24	22.99	9977.91	160.63	243.51	1258.26	56.15	166.68	52.82	124.74	27.83	2.30	22.35	329.20	23.69	135.25
TAS14-57_03	1.96	61146.24	22.46	9745.12	157.31	233.69	1212.27	54.30	162.17	38.96	112.87	20.08	1.71	21.18	312.37	21.70	124.58
TAS14-58_01	2.33	60638.80	25.24	10486.96	165.96	220.46	1408.82	53.29	188.72	47.74	120.77	20.49	0.93	17.96	272.52	24.35	118.87
TAS14-58_02	1.48	60638.80	25.13	10337.44	162.43	216.82	1396.93	52.72	184.35	46.40	121.48	20.19	1.27	17.68	270.02	24.68	120.46
TAS14-58_03	1.94	60638.80	25.08	10385.64	165.66	219.60	1415.43	54.21	188.57	46.65	121.92	20.62	1.00	17.86	272.98	24.60	120.36
TAS14-59_01	2.86	69408.18	20.61	14936.33	190.15	279.76	1255.12	56.01	209.65	48.02	117.22	22.49	0.99	26.62	685.13	22.34	207.68
TAS14-59_02	2.67	69408.18	20.44	14679.13	187.38	275.04	1228.19	55.58	192.25	46.37	114.68	22.47	1.42	26.70	684.48	22.04	204.48
TAS14-59_03	1.70	69408.18	21.10	15373.18	198.18	286.56	1290.27	58.95	205.81	49.15	130.32	23.47	1.21	28.18	714.89	22.72	210.77
TAS14-60_01	2.98	92607.38	21.59	15651.98	221.06	476.74	1624.49	66.87	409.78	56.67	121.08	21.08	2.77	23.83	1396.47	28.56	265.92
TAS14-60_02	3.66	92607.38	21.66	15686.49	224.26	523.88	1626.60	66.00	414.18	55.63	111.07	20.35	2.22	23.21	1387.26	27.65	259.60
TAS14-60_03	3.22	92607.38	21.45	15559.77	220.06	488.97	1615.64	65.31	412.75	53.62	118.24	20.72	2.51	23.37	1373.98	27.88	258.82
TAS14-61_01	2.32	92786.05	21.25	15342.38	217.44	481.71	1578.14	64.06	385.72	52.26	118.85	19.79	2.51	29.29	1623.45	27.00	254.00
TAS14-61_02	2.69	92786.05	21.20	15413.18	220.84	487.21	1607.24	64.89	390.33	51.32	112.07	19.79	3.67	31.00	1668.98	27.65	257.95
TAS14-61_03	3.81	92786.05	21.36	15801.27	226.43	504.37	1618.53	64.87	395.75	52.21	116.19	20.75	2.95	30.29	1663.52	27.55	258.92
TAS14-62_01	3.86	92975.45	22.04	15763.99	222.10	460.25	1621.59	64.22	355.96	53.19	123.12	20.13	3.38	28.77	1275.29	29.39	277.03
TAS14-62_02	3.04	92975.45	21.65	15898.55	224.06	475.31	1645.64	64.26	358.21	53.17	118.49	20.44	3.01	28.84	1264.77	29.26	275.60
TAS14-62_03	2.97	92975.45	21.59	15871.81	224.43	471.60	1651.35	64.24	366.66	54.55	122.18	20.83	3.47	29.21	1266.03	29.20	277.27
TAS14-63_01	2.82	93668.70	21.17	15272.74	217.46	482.77	1578.12	64.62	390.76	50.78	107.03	20.90	2.61	26.19	1522.68	28.00	259.99
TAS14-63_02	4.12	93668.70	21.93	15803.00	223.83	500.48	1662.22	66.73	404.81	55.40	119.58	21.87	10.55	26.89	1552.50	28.70	267.40
TAS14-63_03	1.71	93668.70	21.55	15619.24	221.03	508.45	1659.77	66.69	405.87	54.35	124.13	25.50	3.00	30.37	1538.02	28.29	267.22
TAS14-64_01	1.75	69983.52	38.48	4588.83	230.48	18.09	1235.60	39.04	35.57	116.54	74.16	18.38	0.98	37.32	145.65	25.34	114.86
TAS14-64_02	1.04	69983.52	38.38	4571.62	229.20	18.47	1241.54	39.34	36.25	116.54	79.65	18.03	0.99	37.86	147.31	25.34	115.67
TAS14-64_03	1.95	69983.52	37.30	4483.21	223.89	18.23	1231.94	39.52	36.08	114.11	79.57	17.77	1.14	36.83	144.80	24.33	110.39
TAS14-65_01	1.43	64894.84	24.65	9514.85	164.88	252.71	1170.19	47.88	135.43	43.35	105.63	18.80	1.06	15.71	263.28	21.33	108.93
TAS14-65_02	0.78	64894.85	25.26	9828.87	167.84	257.58	1202.52	48.50	140.38	44.65	113.73	19.56	1.33	15.21	270.68	21.58	111.07
TAS14-65_03	1.72	64894.85	24.40	9580.75	164.45	257.28	1173.48	48.31	140.09	42.48	101.18	19.42	0.72	15.11	271.69	20.90	106.32
TAS14-66_01	3.29	66238.48	21.78	13134.14	180.83	240.24	1344.38	55.51	185.76	47.87	109.30	21.43	1.30	23.68	556.46	22.69	184.89
TAS14-66_02	3.16	66238.48	22.41	13502.09	185.95	239.97	1354.89	57.15	189.60	46.41	119.95	22.19	1.38	24.35	565.52	23.62	192.19
TAS14-66_03	2.57	66238.48	21.75	13241.96	184.53	253.90	1368.93	56.25	183.79	46.56	139.02	22.59	0.91	24.18	571.51	23.48	194.71
TAS14-67_01	1.33	66678.02	25.06	9896.57	168.80	247.35	1162.78	49.58	147.57	46.86	101.46	18.86	0.85	10.42	288.36	20.65	105.75
TAS14-67_02	1.60	66678.02	25.61	9833.02	166.27	245.07	1184.67	50.09	149.58	47.29	112.09	19.15	1.02	10.43	286.04	20.74	104.19
TAS14-67_03	****	66678.02	24.38	9575.75	162.17	236.59	1119.36	48.59	145.16	44.41	99.41	18.49	0.52	9.85	280.31	19.90	99.70

(*continued on next page*)

Table 4 (*continued*)

Sample	Be	Ca	Sc	Ti	V	Cr	Mn	Co	Ni	Cu	Zn	Ga	As	Rb	Sr	Y	Zr
TAS14-68_01	0.53	63887.12	23.63	8891.41	168.60	251.03	1099.69	45.02	140.63	35.94	96.65	18.40	1.25	9.04	265.26	27.68	90.83
TAS14-68_02	2.70	63887.12	24.36	8973.52	167.67	251.78	1100.71	45.93	144.96	36.82	98.83	18.28	1.18	9.19	270.85	28.22	91.93
TAS14-68_03	2.13	63887.12	23.62	8782.50	166.31	248.44	1088.98	45.55	142.66	38.22	108.10	18.01	0.90	9.10	258.89	26.53	87.45
TAS14-69_01	2.74	78077.52	28.01	11182.09	178.87	320.02	1345.47	55.65	195.26	50.93	109.73	20.50	0.81	13.07	357.74	23.12	118.37
TAS14-69_02	1.99	78077.52	29.31	11527.47	184.40	339.59	1393.85	56.61	197.73	51.82	112.90	21.81	1.59	13.42	334.14	23.27	117.35
TAS14-69_03	1.56	78077.52	29.54	11574.27	186.78	341.91	1406.72	57.01	202.45	61.96	128.25	22.07	1.37	13.85	333.34	23.14	117.68
TAS14-70_01	1.03	65548.80	34.14	3120.58	193.12	104.12	957.55	33.01	64.68	54.44	49.97	12.04	0.77	22.63	101.42	16.45	72.46
TAS14-70_02	1.33	65548.80	34.04	3040.24	193.17	102.22	957.38	33.04	62.67	53.49	49.84	12.07	0.86	22.65	95.75	15.91	69.95
TAS14-70_03	2.31	65548.80	32.72	3036.04	196.40	103.04	961.86	33.57	63.62	55.86	54.20	12.22	0.90	22.49	95.97	15.80	68.86
TAS14-71_01	1.08	77227.02	40.41	3826.74	234.71	110.25	1181.16	40.47	70.57	72.00	61.44	14.95	1.93	25.95	118.61	20.45	90.84
TAS14-71_02	0.39	77227.02	40.47	3780.07	233.19	109.99	1188.12	40.66	70.22	75.41	62.27	14.94	1.79	25.90	118.44	20.34	90.35
TAS14-71_03	2.32	77227.02	40.60	3739.22	235.22	107.09	1171.31	39.90	67.53	67.48	64.25	15.06	1.54	25.71	117.18	20.38	89.30
TAS14-72_01	2.31	68332.55	29.32	7181.83	179.13	374.60	1252.99	53.21	227.89	66.64	81.89	16.48	50.64	5.22	310.74	20.99	82.95
TAS14-72_02	1.44	68332.57	28.37	7250.06	171.92	372.15	1245.72	51.28	213.13	64.78	78.96	16.01	0.25	4.37	311.81	20.37	80.39
TAS14-72_03	1.47	68332.56	28.81	7384.98	176.73	385.90	1275.61	53.64	222.19	66.89	85.39	16.25	0.65	4.37	319.74	20.95	82.54
TAS14-73_01	2.38	58441.11	16.35	15547.51	123.23	130.74	1098.59	40.67	108.97	37.79	142.88	26.50	1.24	30.26	939.72	25.34	330.48
TAS14-73_02	1.51	58441.10	16.57	16074.91	126.55	132.38	1117.45	41.93	109.18	32.38	146.45	28.21	1.94	32.40	973.67	25.99	341.61
TAS14-73_03	3.26	58441.11	16.28	16120.22	125.97	132.59	1124.64	42.55	106.53	35.97	157.70	27.99	1.51	31.60	961.96	25.08	334.21
TAS14-74_01	4.96	80353.84	18.32	17218.32	163.03	190.11	9684.27	102.04	138.11	42.29	144.66	24.88	3.57	43.68	1089.53	33.73	386.25
TAS14-74_02	4.29	80353.84	18.36	17505.99	168.41	194.04	9983.24	105.28	139.43	42.04	145.41	24.73	4.42	44.29	1107.94	34.34	393.19
TAS14-74_03	2.79	80353.84	18.13	17521.01	165.31	199.61	9992.42	104.56	138.30	42.41	151.23	24.95	3.38	43.52	1077.62	32.61	379.01
TAS14-75_01	1.00	62357.66	22.52	9825.33	154.76	236.94	1240.98	41.94	107.04	35.58	82.90	18.70	1.19	26.63	296.99	19.26	117.76
TAS14-75_02	2.95	62357.66	23.56	10053.47	162.43	246.76	1097.91	43.03	114.73	37.57	90.02	19.20	0.70	25.31	296.17	19.81	118.57
TAS14-75_03	1.58	62357.66	23.43	10077.85	161.62	239.99	1082.01	43.95	111.55	37.02	87.37	19.15	0.42	24.70	289.14	19.30	115.80
TAS14-76_01	1.83	76330.07	24.15	9575.33	163.44	270.94	1167.85	53.95	148.07	42.09	90.68	18.48	0.83	19.23	304.39	19.30	108.49
TAS14-76_02	1.03	76330.08	23.41	9596.33	162.84	270.84	1158.46	53.59	147.85	40.79	91.17	18.92	0.74	18.51	300.72	19.10	106.26
TAS14-76_03	0.58	76330.08	23.40	9469.32	160.31	266.07	1166.76	54.14	150.25	42.68	99.23	18.56	0.24	18.61	299.68	18.84	105.96
TAS14-77_01	0.33	71648.78	23.95	10312.71	162.34	283.35	1187.12	65.62	227.39	50.25	106.90	18.59	0.70	11.25	428.83	19.74	116.91
TAS14-77_02	2.96	71648.78	24.78	10719.36	169.36	294.99	1251.31	69.56	235.46	52.26	117.11	19.92	0.80	11.58	443.91	20.23	121.24
TAS14-77_03	1.93	71648.78	23.72	10415.74	167.46	287.10	1197.93	66.18	230.68	47.55	105.15	18.99	0.75	11.06	431.39	18.91	114.07
TAS14-78_01	2.37	61878.81	23.27	10035.51	162.93	269.59	1083.60	45.20	129.04	36.67	92.36	19.18	0.58	23.68	298.33	19.62	118.50
TAS14-78_02	1.83	61878.82	22.85	9833.48	160.86	252.08	1054.02	43.43	119.69	37.39	87.78	18.63	0.88	23.07	293.06	19.06	115.65
TAS14-78_03	2.52	61878.81	23.35	9959.83	160.31	257.96	1089.79	44.03	124.46	41.84	99.89	19.35	0.68	23.91	294.24	20.03	118.64
TAS14-79_01	1.21	76723.16	40.91	3979.77	234.69	122.48	1241.45	40.35	73.17	73.10	72.31	15.39	1.01	30.94	166.62	22.10	97.21
TAS14-79_02	1.42	76723.16	40.04	3843.16	233.96	117.58	1194.93	40.11	72.46	67.47	63.30	15.36	0.83	29.76	162.76	20.56	92.53
TAS14-79_03	1.89	76723.16	40.30	3767.40	231.76	115.25	1204.02	39.45	72.29	69.81	75.18	14.94	1.33	30.47	160.30	21.03	92.53
TAS14-80_01	1.82	69947.79	24.48	10496.12	167.95	294.92	1221.29	59.33	190.02	55.51	112.67	19.01	0.92	5.02	426.13	20.46	127.50
TAS14-80_02	1.56	69947.79	22.14	10013.81	156.71	270.25	1125.40	55.81	180.61	48.95	93.21	17.68	0.92	7.55	401.69	18.78	116.68
TAS14-80_03	2.00	69947.79	24.36	10882.65	169.63	297.38	1227.39	62.03	195.53	53.18	113.97	19.61	0.55	7.90	436.57	20.42	130.79

Sample	Nb	Mo	Ag	Cd	In	Sn	Sb	Cs	Ba	La	Ce	Pr	Nd	Sm
TAS14-01_01	33.30	1.61	0.09	0.43	0.06	2.66	0.52	0.14	210.41	24.87	46.55	5.59	23.15	4.92
TAS14-01_02	34.55	1.53	0.13	0.39	0.07	1.11	0.48	0.13	221.08	26.08	48.86	5.99	24.04	5.02
TAS14-01_03	32.65	1.43	0.12	< 0.33	0.07	1.52	0.51	0.13	209.88	24.53	46.66	7.50	22.10	4.74
TAS14-02_01	36.38	0.80	0.14	0.61	0.08	1.53	0.48	0.23	217.38	26.56	49.06	5.94	24.79	5.52
TAS14-02_02	34.67	0.89	0.16	< 0.33	0.06	1.36	0.44	0.21	203.75	24.82	46.85	5.64	22.86	5.10
TAS14-02_03	33.92	0.98	0.12	< 0.37	0.06	1.37	0.43	0.22	203.47	25.05	46.37	5.65	23.27	4.74
TAS14-03_01	31.88	2.22	0.13	< 0.57	0.07	1.37	0.51	0.45	218.85	24.24	45.21	5.59	22.38	5.19

(*continued on next page*)

Table 4 (*continued*)

Sample	Nb	Mo	Ag	Cd	In	Sn	Sb	Cs	Ba	La	Ce	Pr	Nd	Sm
TAS14-03_02	32.24	5.26	0.11	0.37	0.07	2.12	0.46	0.47	224.17	24.38	46.10	5.58	22.78	5.07
TAS14-03_03	31.89	1.78	0.11	0.37	0.05	1.43	0.52	0.44	223.10	24.00	45.74	5.53	22.80	4.71
TAS14-04_01	14.55	1.54	0.12	0.35	3.29	1.43	0.47	0.59	105.75	11.98	23.32	3.15	13.88	3.65
TAS14-04_02	15.58	1.50	0.11	0.34	0.07	1.46	0.46	0.66	116.69	13.08	25.54	3.41	15.25	4.05
TAS14-04_03	14.63	1.47	0.13	< 0.40	0.06	1.32	0.54	0.61	108.98	12.42	24.77	3.31	14.73	3.96
TAS14-05_01	16.54	1.62	0.11	0.27	0.08	1.39	0.53	0.64	390.73	22.06	37.37	5.49	24.94	6.65
TAS14-05_02	16.52	1.53	0.11	< 0.47	0.06	1.43	0.43	0.56	374.79	21.51	36.33	5.36	24.42	6.69
TAS14-05_03	15.79	1.62	0.17	< 0.33	0.07	1.17	0.48	0.56	376.57	21.36	36.29	5.27	24.05	6.24
TAS14-06_01	16.62	1.66	0.15	< 0.50	0.05	1.51	0.45	0.69	113.92	15.19	28.92	4.20	18.53	4.66
TAS14-06_02	16.49	1.71	0.15	0.38	0.07	1.29	0.46	0.76	113.45	14.98	28.49	4.28	17.95	4.68
TAS14-06_03	16.84	1.72	0.14	0.41	0.06	1.78	1.47	0.75	114.72	15.25	28.60	4.14	18.42	4.68
TAS14-07_01	17.42	1.54	0.09	0.43	0.06	2.22	0.48	0.77	116.20	14.89	28.89	4.26	17.58	4.82
TAS14-07_02	16.32	1.48	0.11	0.55	0.06	1.48	0.47	0.74	111.47	14.62	28.07	4.10	17.50	4.63
TAS14-07_03	17.88	1.81	0.09	0.42	0.07	1.61	0.50	0.80	120.52	15.93	30.58	4.40	19.18	5.09
TAS14-08_01	13.73	1.73	0.16	0.43	0.06	1.29	0.50	0.71	89.31	10.52	22.34	3.00	13.27	3.60
TAS14-08_02	13.75	1.92	0.08	< 0.45	0.08	1.37	0.46	1.00	86.42	10.09	21.69	2.95	13.08	3.60
TAS14-08_03	13.54	1.58	0.08	< 0.41	0.07	1.47	0.44	0.69	89.14	10.10	21.95	2.87	12.63	3.61
TAS14-09_01	13.94	1.76	0.13	< 0.60	0.07	1.40	0.53	0.80	93.06	10.95	23.09	3.00	13.21	3.93
TAS14-09_02	13.58	1.74	0.09	< 0.47	0.07	1.43	0.50	0.81	90.44	10.79	22.52	2.86	13.83	3.82
TAS14-09_03	14.19	1.88	0.10	0.41	0.08	1.32	0.48	0.79	92.80	11.15	23.63	3.13	13.77	3.84
TAS14-10_01	126.04	9.15	0.45	1.10	0.10	3.60	0.62	0.63	584.88	94.11	174.44	20.96	82.32	16.35
TAS14-10_02	130.54	9.67	0.46	1.30	0.11	3.76	0.68	0.66	593.84	94.38	180.72	21.39	87.20	16.56
TAS14-10_03	131.85	9.27	0.48	1.21	0.11	3.87	0.67	0.68	597.11	94.98	182.08	21.42	86.50	17.13
TAS14-11_01	33.12	2.44	0.14	< 0.59	0.06	1.61	0.50	0.49	200.56	22.05	44.65	5.38	23.38	5.10
TAS14-11_02	32.80	7.65	0.11	< 0.44	0.06	1.55	0.51	0.49	197.09	21.70	43.49	5.30	22.30	5.09
TAS14-11_03	33.24	2.57	0.13	0.40	0.08	1.52	0.54	0.49	200.45	21.44	43.60	5.36	22.12	4.87
TAS14-12_01	67.74	2.85	0.23	0.82	0.06	2.14	0.50	0.38	337.31	41.34	76.61	8.86	34.38	6.55
TAS14-12_02	74.77	3.17	0.24	< 0.88	0.09	1.36	0.63	0.36	369.24	48.43	84.21	9.61	37.46	7.34
TAS14-12_03	77.30	2.97	0.24	0.61	0.09	1.59	0.71	0.36	384.12	46.41	85.90	9.61	38.93	7.23
TAS14-13_01	66.90	2.95	0.11	0.02	0.07	1.94	1.06	4.15	376.76	46.16	81.19	9.23	36.38	7.31
TAS14-13_02	68.32	3.15	0.13	****	0.08	1.84	0.67	4.44	390.96	48.24	85.22	9.51	37.07	7.21
TAS14-13_03	66.36	3.15	0.35	4.18	0.07	2.11	8.73	4.27	370.10	45.26	80.93	9.20	35.03	6.71
TAS14-14_01	65.39	3.51	0.11	0.17	0.07	1.93	0.60	0.46	364.58	45.56	81.61	9.30	36.64	6.95
TAS14-14_02	66.01	3.81	0.06	0.28	0.08	1.98	0.64	0.44	367.99	46.33	82.96	9.36	37.14	6.76
TAS14-14_03	67.68	3.43	0.09	0.27	0.07	1.98	0.57	0.41	376.23	46.05	83.93	9.68	37.41	6.92
TAS14-15_01	53.81	2.89	0.03	***	0.05	1.69	0.54	0.32	308.34	36.99	67.96	7.87	30.29	6.00
TAS14-15_02	55.85	< ****	0.06	0.50	0.09	1.97	0.60	0.33	322.09	39.43	71.21	8.20	33.14	6.44
TAS14-15_03	57.75	3.00	0.11	0.27	0.06	1.75	0.72	0.34	334.12	40.24	73.04	8.67	33.65	6.71
TAS14-16_01	61.55	3.02	0.04	0.59	0.07	1.73	0.45	0.20	304.59	43.32	76.41	8.87	33.91	6.84
TAS14-16_02	65.00	3.36	0.06	0.19	1.68	1.98	0.40	0.25	319.55	45.11	81.99	9.17	36.27	6.67
TAS14-16_03	64.09	3.73	0.05	***	0.08	1.99	0.55	0.24	315.53	44.13	81.07	9.19	35.79	6.74
TAS14-17_01	85.60	7.32	0.05	1.16	0.15	2.19	0.61	0.24	278.52	56.72	103.30	12.34	50.06	10.55
TAS14-17_02	86.52	7.32	0.05	0.32	0.10	2.11	0.66	0.25	272.31	54.80	102.81	12.09	49.16	9.93
TAS14-17_03	87.64	7.40	0.19	0.40	0.08	2.25	0.71	0.22	280.17	57.12	104.91	12.38	50.28	10.48
TAS14-18_01	76.10	6.84	< ****	0.27	0.09	2.00	0.66	0.22	252.60	50.18	89.70	10.48	43.35	9.28
TAS14-18_02	74.65	7.19	0.07	0.78	0.06	2.42	1.79	0.24	250.27	48.67	87.29	10.39	41.45	8.75
TAS14-18_03	78.69	7.14	0.08	0.48	0.10	2.52	0.73	0.23	265.00	52.95	93.53	11.33	45.79	9.36
TAS14-19_01	78.90	8.13	0.09	0.25	0.10	2.22	0.54	0.32	237.76	50.08	91.41	10.94	44.50	9.23
TAS14-19_02	76.99	8.00	0.05	0.63	0.14	2.23	0.57	0.26	233.30	49.41	89.48	10.85	44.32	9.38
TAS14-19_03	77.43	8.14	0.55	0.37	0.08	2.62	0.57	0.29	233.33	48.04	88.94	10.74	43.21	9.25
TAS14-20_01	77.87	7.87	0.10	0.67	0.10	3.76	0.57	0.27	265.23	48.55	89.46	10.59	42.83	9.26
TAS14-20_02	78.60	8.04	0.10	0.56	0.09	2.36	0.61	0.26	269.47	50.55	92.50	10.45	44.88	9.93
TAS14-20_03	78.70	7.81	0.16	0.58	0.06	2.39	0.62	0.29	268.48	50.72	91.53	10.82	44.73	9.28

(*continued on next page*)

Table 4 (*continued*)

Sample	Nb	Mo	Ag	Cd	In	Sn	Sb	Cs	Ba	La	Ce	Pr	Nd	Sm
TAS14-21_01	111.66	4.17	0.14	0.14	0.09	2.79	0.62	0.15	197.63	75.97	139.40	16.48	65.85	13.53
TAS14-21_02	112.02	4.21	0.14	0.80	0.10	3.30	0.65	< ****	199.64	77.92	142.64	16.81	67.94	13.97
TAS14-21_03	110.43	4.59	0.13	****	0.09	2.81	0.76	0.13	197.50	76.57	141.01	16.78	67.19	13.10
TAS14-22_01	110.71	3.64	0.08	0.03	0.10	2.90	0.64	0.14	216.50	72.02	132.16	15.73	63.33	12.87
TAS14-22_02	112.20	3.60	0.09	****	0.10	3.47	0.72	0.13	221.17	74.57	135.69	15.96	64.36	12.69
TAS14-22_03	110.98	3.21	0.14	****	0.11	2.73	0.58	2.52	221.88	72.99	134.96	16.01	64.10	13.40
TAS14-23_01	106.98	3.04	0.11	0.88	0.32	2.59	0.84	0.30	191.90	69.50	128.59	15.36	61.73	12.48
TAS14-23_02	111.12	3.09	0.14	****	0.14	3.48	0.74	0.27	200.11	73.60	133.23	15.69	64.89	12.96
TAS14-23_03	109.79	2.94	0.17	0.54	0.27	2.72	0.82	0.31	200.57	73.08	135.11	16.07	64.03	13.28
TAS14-24_01	51.77	4.65	0.13	0.63	0.20	1.89	0.58	0.34	227.41	33.02	60.64	7.60	30.79	6.85
TAS14-24_02	52.48	4.47	0.14	0.27	0.14	2.27	0.67	0.38	238.31	33.76	62.03	7.54	31.81	7.35
TAS14-24_03	51.73	4.01	0.10	0.03	0.11	1.98	0.53	0.42	229.55	33.45	59.90	7.47	30.62	7.08
TAS14-25_01	10.83	2.21	0.12	****	0.11	2.26	0.60	0.30	82.76	10.10	21.73	3.15	14.17	4.22
TAS14-25_02	10.55	2.27	0.04	0.10	0.09	1.25	0.75	0.23	81.29	10.25	21.44	2.94	14.39	4.17
TAS14-25_03	11.24	2.37	0.06	0.11	0.11	1.48	0.79	0.25	85.02	10.42	22.16	3.05	14.91	4.16
TAS14-26_01	18.08	1.77	0.07	0.43	0.07	1.49	0.49	0.24	113.93	15.75	31.80	4.30	19.25	5.18
TAS14-26_02	18.51	1.50	0.05	0.38	0.09	1.40	0.61	0.25	118.97	16.55	33.21	4.48	20.18	5.17
TAS14-26_03	18.94	1.67	0.15	0.52	0.10	1.62	0.61	0.23	121.09	16.44	33.57	4.57	20.80	5.76
TAS14-27_01	8.13	0.99	0.06	0.17	0.08	1.15	0.52	0.22	63.39	7.68	16.38	2.23	11.37	3.52
TAS14-27_02	7.95	1.30	0.09	****	0.06	1.00	0.51	0.18	65.50	7.76	16.40	2.39	11.50	3.42
TAS14-27_03	8.01	1.13	0.15	0.12	0.07	1.23	0.65	0.17	63.34	7.94	16.38	2.30	11.40	3.53
TAS14-28_01	24.94	2.09	0.06	0.23	0.09	1.84	0.59	0.12	169.33	19.30	38.66	5.17	23.35	6.24
TAS14-28_02	24.65	2.05	0.05	0.58	0.10	1.76	0.56	0.07	166.62	18.89	39.78	5.25	23.02	5.88
TAS14-28_03	25.36	2.12	0.42	0.58	0.10	1.72	0.55	0.06	172.08	19.54	40.02	5.26	23.63	6.27
TAS14-29_01	16.20	1.75	*****	0.13	0.09	1.21	0.50	0.35	140.93	14.22	28.53	3.77	16.45	4.72
TAS14-29_02	15.51	1.76	0.09	****	0.09	1.59	0.55	0.34	140.53	13.77	27.98	3.69	16.97	4.36
TAS14-29_03	16.12	1.60	0.04	0.17	0.10	1.46	0.63	0.41	144.00	14.36	29.23	3.87	17.13	4.44
TAS14-30_01	43.05	2.25	*****	0.61	0.12	2.56	0.56	0.28	338.13	30.30	57.31	6.94	28.98	5.92
TAS14-30_02	42.02	2.22	0.08	0.52	0.07	1.70	0.55	0.29	327.74	29.26	56.23	6.83	28.28	6.40
TAS14-30_03	42.11	2.31	0.12	0.01	0.07	1.80	0.63	0.26	335.99	29.84	57.06	6.90	28.87	6.10
TAS14-31_01	56.34	4.46	0.16	0.18	0.09	2.24	0.57	0.54	311.87	38.50	71.19	8.55	35.22	7.50
TAS14-31_02	57.90	4.41	0.10	0.32	0.08	2.09	0.54	0.53	321.81	39.65	73.60	9.08	37.62	7.94
TAS14-31_03	56.34	4.77	0.05	0.58	0.06	2.08	0.45	0.50	310.29	37.91	71.94	8.64	34.96	7.40
TAS14-32_01	58.82	4.62	0.09	0.14	0.08	2.71	0.47	0.36	315.95	38.83	73.52	8.80	35.59	7.31
TAS14-32_02	60.38	4.75	0.09	0.16	3.34	1.95	0.69	0.36	330.50	40.60	75.20	9.12	37.50	7.45
TAS14-32_03	60.13	4.66	0.09	0.36	0.10	2.05	0.55	0.40	329.30	40.83	75.03	9.03	37.11	8.05
TAS14-33_01	55.87	4.04	0.02	0.41	0.08	2.01	0.64	1.21	298.54	37.14	71.53	8.65	35.25	7.22
TAS14-33_02	56.41	3.52	0.00	0.53	0.08	2.21	0.65	1.14	297.08	38.02	70.58	8.45	35.66	7.26
TAS14-33_03	57.53	3.74	0.02	0.04	0.10	2.16	0.64	1.23	305.75	38.52	72.46	8.84	35.13	7.57
TAS14-34_01	42.35	3.48	0.08	****	0.08	1.83	0.48	0.19	121.14	32.70	62.45	7.60	30.03	6.69
TAS14-34_02	42.70	3.81	0.07	0.33	0.09	2.07	0.64	0.20	122.25	33.52	63.52	7.71	30.89	6.74
TAS14-34_03	41.78	3.41	0.09	0.10	0.08	2.02	0.57	0.22	120.18	32.86	63.09	7.48	30.17	6.23
TAS14-34B_01	39.97	3.07	0.10	0.13	0.08	1.69	0.55	0.20	114.14	32.45	60.44	7.26	31.00	6.75
TAS14-34B_02	42.55	3.40	0.10	0.05	0.07	1.74	0.65	0.21	119.47	32.58	61.75	7.41	30.52	6.86
TAS14-34B_03	42.69	3.51	0.07	0.33	0.08	1.95	0.63	0.18	120.31	32.09	62.63	7.41	30.44	6.50
TAS14-35_01	42.64	4.68	0.10	0.27	0.11	1.88	0.58	0.17	116.22	33.44	62.50	7.51	31.19	6.46
TAS14-35_02	42.09	4.55	0.10	0.54	0.06	2.16	< ****	0.17	119.39	32.58	62.50	7.42	31.30	6.42
TAS14-35_03	43.62	4.89	0.09	0.32	0.11	1.98	0.63	0.18	123.59	33.35	65.01	7.99	31.28	6.81
TAS14-36_01	25.73	2.56	0.03	0.50	0.06	1.59	0.50	0.44	158.79	21.24	41.00	5.17	22.23	4.86
TAS14-36_02	25.55	2.52	0.06	0.10	0.06	1.88	0.46	0.47	161.87	20.97	41.84	5.23	21.98	4.94
TAS14-36_03	25.43	2.62	0.06	0.16	0.06	1.70	0.56	0.45	161.73	20.89	41.67	5.16	21.59	5.10
TAS14-37_01	37.77	2.42	0.11	0.53	0.05	1.79	0.70	0.34	239.74	24.50	46.47	6.42	24.90	5.64
TAS14-37_02	38.53	2.60	*****	0.23	0.07	4.13	0.47	0.34	239.79	23.87	47.17	5.88	24.64	5.62

(*continued on next page*)

Table 4 (*continued*)

Sample	Nb	Mo	Ag	Cd	In	Sn	Sb	Cs	Ba	La	Ce	Pr	Nd	Sm
TAS14-37_03	38.96	2.42	0.03	0.03	0.10	2.38	0.54	0.34	243.32	24.30	48.09	5.93	24.74	5.50
TAS14-38_01	18.88	1.27	0.05	0.38	0.32	6.12	0.53	0.33	176.76	13.94	28.60	3.64	15.84	4.01
TAS14-38_02	18.77	1.43	0.06	****	0.08	1.15	0.43	0.31	178.43	13.85	27.98	3.48	15.92	4.09
TAS14-38_03	19.22	1.15	0.01	0.25	0.08	1.26	0.61	0.35	181.92	13.93	28.73	3.70	16.28	4.04
TAS14-39_01	12.62	1.76	0.05	****	0.07	1.17	0.63	2.84	187.97	13.33	26.13	3.45	15.10	3.84
TAS14-39_02	12.58	1.61	0.02	0.05	0.06	1.41	0.49	2.80	187.99	12.80	26.08	3.32	14.54	3.62
TAS14-39_03	12.40	1.78	0.03	0.44	0.07	1.32	0.58	2.64	183.18	12.35	25.68	3.34	14.32	3.64
TAS14-40_01	16.98	1.86	0.05	0.33	0.05	1.70	1.16	3.21	181.90	18.74	36.78	4.65	19.83	4.85
TAS14-40_02	17.00	1.84	0.04	0.70	0.08	1.58	0.59	3.20	181.88	18.23	36.90	4.54	19.60	4.58
TAS14-40_03	17.21	2.05	0.55	0.09	0.07	1.67	0.61	3.34	181.67	18.12	36.75	4.61	19.44	4.67
TAS14-41_01	17.78	2.09	0.13	****	0.10	3.89	0.59	2.11	196.10	19.40	37.61	4.85	21.43	5.27
TAS14-41_02	18.16	2.25	0.01	0.53	0.08	3.68	0.53	2.21	201.90	19.08	38.18	4.84	20.29	4.88
TAS14-41_03	18.43	1.91	0.01	****	0.10	3.86	0.60	2.16	200.96	19.06	38.39	4.88	20.85	5.02
TAS14-42A_01	15.50	2.58	0.04	0.19	0.06	1.88	0.54	2.70	153.94	14.30	27.64	3.66	16.59	4.30
TAS14-42A_02	16.16	1.84	0.14	****	0.06	1.47	0.54	0.14	160.63	14.77	29.98	3.81	17.35	4.33
TAS14-42A_03	15.82	1.72	*****	0.83	0.09	1.32	0.59	0.12	159.14	14.75	29.61	3.85	17.15	4.45
TAS14-42B_01	16.20	1.62	0.05	0.44	0.07	1.58	0.59	0.17	161.27	15.29	30.39	3.99	17.55	4.61
TAS14-42B_02	15.99	1.64	0.08	****	0.06	1.48	0.54	0.14	158.41	14.84	29.60	3.71	16.38	4.18
TAS14-42B_03	16.27	1.96	0.03	****	0.07	1.46	0.46	0.15	161.15	14.95	30.44	3.84	17.07	4.40
TAS14-43_01	40.54	3.50	****	0.73	0.07	2.01	0.60	0.17	211.27	34.91	65.20	8.14	32.88	7.73
TAS14-43_02	42.36	3.61	0.08	0.28	0.07	2.38	7.51	0.19	219.55	35.70	68.73	8.35	34.73	7.57
TAS14-43_03	40.20	3.48	0.10	****	0.09	2.01	0.70	0.20	208.71	34.33	66.04	8.09	33.48	7.72
TAS14-44_01	30.16	2.77	0.09	0.02	0.06	1.42	0.65	0.56	208.49	23.64	45.63	5.59	23.15	5.39
TAS14-44_02	29.73	2.72	0.29	0.25	0.06	1.46	0.59	0.53	206.79	23.66	45.15	5.64	23.87	5.54
TAS14-44_03	30.43	< ****	0.07	****	0.08	1.57	0.55	0.54	209.50	23.87	45.53	5.59	23.70	5.27
TAS14-45_01	34.57	5.13	*****	0.72	0.06	2.17	0.60	0.42	125.94	25.27	49.53	6.15	25.96	5.78
TAS14-45_02	34.41	4.92	0.07	0.25	0.08	1.82	0.61	0.41	127.25	25.49	50.03	6.27	25.83	5.76
TAS14-45_03	35.50	4.84	0.46	0.00	0.07	1.82	0.60	0.41	125.62	25.50	50.49	6.13	25.77	5.97
TAS14-46_01	41.39	4.89	0.07	****	0.05	2.09	0.60	0.40	139.59	29.78	58.07	6.98	29.31	6.63
TAS14-46_02	43.07	5.27	0.10	****	0.09	2.05	0.68	0.42	139.83	29.73	58.64	7.20	29.64	6.09
TAS14-46_03	41.28	5.24	0.03	0.16	3.32	2.39	0.64	0.41	139.05	29.66	57.95	7.09	29.26	6.27
TAS14-47_01	27.87	1.75	0.07	0.67	0.09	1.98	0.53	0.17	210.92	21.64	43.50	5.89	26.67	6.94
TAS14-47_02	28.57	1.83	0.03	****	0.08	2.04	0.64	0.14	211.30	21.17	44.16	5.81	26.54	6.58
TAS14-47_03	24.87	1.57	0.05	0.03	0.07	1.87	2.15	0.14	187.17	18.71	38.95	5.02	22.87	5.79
TAS14-48_01	24.74	1.80	0.01	0.04	0.07	1.30	0.56	0.24	166.70	18.73	36.67	4.69	20.07	4.58
TAS14-48_02	25.76	1.67	0.05	0.00	0.05	1.35	0.62	0.27	169.50	19.24	37.62	4.80	20.48	4.94
TAS14-48_03	25.27	1.80	0.05	0.33	0.07	1.36	0.45	0.24	167.57	18.97	37.08	4.66	20.60	4.99
TAS14-49_01	12.42	1.24	0.01	0.12	0.06	1.26	0.49	0.16	100.90	11.32	23.15	3.01	14.18	4.01
TAS14-49_02	12.58	1.26	0.09	0.33	0.08	1.23	0.64	0.18	106.72	11.88	24.59	3.24	15.18	4.24
TAS14-49_03	12.52	1.01	0.11	0.05	0.10	1.36	0.61	0.19	102.93	11.64	24.01	3.11	14.83	4.00
TAS14-50_01	29.14	2.26	0.14	0.73	0.26	1.88	0.60	0.21	224.14	21.98	45.69	5.80	25.77	6.18
TAS14-50_02	28.80	2.47	0.11	****	0.07	1.87	0.61	0.14	227.96	22.08	46.33	5.85	25.75	6.37
TAS14-50_03	29.91	2.34	*****	0.89	0.07	2.55	0.56	0.23	240.42	22.98	48.34	6.10	26.74	6.25
TAS14-51_01	29.20	1.67	0.08	0.52	0.08	1.62	0.53	0.20	191.25	22.65	46.00	5.72	25.02	6.17
TAS14-51_02	30.34	1.66	0.14	0.03	0.07	3.41	0.58	0.21	198.05	22.99	47.13	6.02	25.71	6.11
TAS14-51_03	30.35	1.63	0.00	****	0.10	1.76	0.42	0.19	195.45	22.51	47.39	5.94	25.79	5.86
TAS14-52_01	29.08	1.76	0.06	****	0.07	1.87	0.49	0.48	204.00	22.12	46.60	5.87	25.23	5.83
TAS14-52_02	29.19	1.74	0.13	****	0.07	1.71	0.60	0.48	204.04	22.15	45.92	5.79	25.09	5.58

(*continued on next page*)

Table 4 (*continued*)

Sample	Nb	Mo	Ag	Cd	In	Sn	Sb	Cs	Ba	La	Ce	Pr	Nd	Sm
TAS14-52_03	29.63	1.85	0.16	0.14	0.09	1.83	0.52	0.49	208.06	22.30	47.28	5.88	25.04	6.61
TAS14-53_01	13.07	1.12	0.01	0.44	0.08	1.30	0.67	0.47	98.47	11.71	25.03	3.28	14.62	4.16
TAS14-53_02	12.35	1.30	*****	0.18	0.07	1.27	1.28	0.47	94.64	11.25	24.38	3.16	14.49	3.90
TAS14-53_03	12.19	1.16	0.03	0.39	0.06	0.45	9.53	0.49	96.29	11.42	24.66	3.17	14.62	4.14
TAS14-54_01	11.91	1.65	0.03	0.48	0.10	< ****	0.52	0.28	99.99	11.92	25.05	3.29	15.30	4.18
TAS14-54_02	12.32	1.46	0.08	0.39	0.07	1.70	0.53	0.33	107.07	12.71	25.96	3.36	15.35	4.14
TAS14-54_03	12.17	1.46	0.04	0.01	0.09	1.49	0.52	0.31	102.61	11.66	25.07	3.32	14.86	4.46
TAS14-55_01	11.99	1.50	0.04	0.61	0.07	1.51	0.48	0.23	103.91	11.87	25.56	3.36	15.49	4.51
TAS14-55_02	12.23	1.46	0.06	****	0.10	1.72	0.61	0.26	103.18	11.65	25.41	3.27	15.35	4.33
TAS14-55_03	12.29	1.50	0.06	0.71	0.08	1.47	0.60	0.26	105.97	12.22	25.96	3.42	16.26	4.43
TAS14-56A_01	20.16	2.11	0.08	0.20	0.09	1.44	0.74	0.89	138.99	14.77	30.95	3.91	17.76	4.26
TAS14-56A_02	16.71	1.88	0.06	0.76	0.09	1.46	0.50	0.85	142.40	14.99	30.63	4.00	17.94	4.60
TAS14-56A_03	17.19	1.92	0.06	0.47	0.07	1.56	0.51	0.88	142.08	15.00	31.52	4.01	17.49	4.72
TAS14-56B_01	16.82	1.85	0.00	0.23	0.08	2.18	0.61	0.81	140.12	14.89	30.92	4.03	17.50	4.46
TAS14-56B_02	16.68	1.94	0.04	0.03	0.10	1.42	0.68	0.86	139.61	14.77	30.13	3.87	17.27	4.57
TAS14-56B_03	16.81	1.93	0.06	0.34	0.09	1.53	0.58	0.90	143.27	15.02	31.18	4.01	17.00	4.46
TAS14-57_01	17.20	2.07	0.18	0.12	0.11	3.71	0.52	0.76	147.82	15.24	31.06	4.12	17.78	4.94
TAS14-57_02	17.77	2.21	0.06	0.30	0.09	2.44	0.64	0.85	154.91	15.99	32.74	4.17	18.50	4.58
TAS14-57_03	16.97	2.12	*****	0.31	0.08	1.69	0.61	0.85	146.64	14.69	30.48	3.78	17.26	4.38
TAS14-58_01	13.16	1.41	0.06	0.23	0.12	1.99	0.57	0.49	120.16	13.45	27.50	3.62	16.67	4.67
TAS14-58_02	12.85	1.57	0.13	0.27	0.10	1.63	0.58	0.48	118.38	13.64	27.72	3.71	16.73	4.43
TAS14-58_03	12.97	1.59	0.05	0.14	0.09	2.15	0.61	0.50	118.14	13.52	28.20	3.68	16.87	4.65
TAS14-59_01	38.12	2.30	0.02	****	0.09	2.07	0.65	0.38	259.32	28.06	55.91	7.16	30.90	7.07
TAS14-59_02	38.48	2.45	0.09	0.41	0.08	2.07	1.73	0.35	256.11	27.58	55.94	7.10	30.61	7.21
TAS14-59_03	40.33	2.78	0.09	0.27	0.09	2.21	0.63	0.39	266.83	28.86	59.46	7.52	31.60	7.63
TAS14-60_01	110.13	1.27	0.07	0.39	0.07	2.38	0.60	0.39	384.60	80.94	143.07	16.72	65.47	12.74
TAS14-60_02	111.40	1.06	0.15	0.10	0.13	2.08	0.55	0.38	387.61	79.99	143.62	16.44	65.99	12.62
TAS14-60_03	110.05	1.08	9.81	0.62	0.09	2.34	1.01	0.40	379.63	79.82	141.75	16.28	63.76	11.84
TAS14-61_01	108.98	0.89	0.09	****	0.10	2.62	0.63	0.72	367.66	78.89	139.21	16.18	63.72	11.91
TAS14-61_02	111.76	0.77	0.14	0.03	0.10	2.43	0.91	0.85	381.09	80.28	142.85	16.51	64.76	12.28
TAS14-61_03	112.44	0.67	0.08	0.36	0.41	2.25	0.69	0.77	378.54	79.51	143.48	16.28	64.69	11.98
TAS14-62_01	114.35	0.87	0.07	0.22	0.09	2.47	0.66	0.67	308.87	87.42	147.47	17.01	67.61	12.75
TAS14-62_02	115.39	0.85	0.13	0.13	0.07	2.36	1.07	0.66	310.09	87.50	148.29	17.03	68.46	12.67
TAS14-62_03	117.00	0.78	0.16	0.16	0.08	2.55	0.55	0.63	309.87	87.42	150.07	17.17	68.53	12.99
TAS14-63_01	110.28	0.89	0.03	0.29	0.09	2.05	0.61	0.60	559.26	78.48	139.63	16.02	63.87	12.20
TAS14-63_02	112.40	0.97	0.02	0.34	0.09	2.46	0.68	0.62	582.48	82.09	144.40	16.80	66.27	12.49
TAS14-63_03	113.01	0.87	0.15	38.34	0.10	2.26	0.63	0.61	583.64	80.90	145.01	16.51	66.72	12.39
TAS14-64_01	5.95	0.89	0.14	0.47	3.29	1.26	0.59	1.22	227.77	14.17	29.09	3.73	15.57	3.77
TAS14-64_02	5.87	0.99	0.10	****	0.08	1.33	0.59	1.30	231.42	14.40	29.72	3.74	15.17	3.81
TAS14-64_03	5.84	0.78	0.09	0.27	0.09	3.47	0.60	1.19	226.61	14.88	28.67	3.59	14.49	3.43
TAS14-65_01	12.92	1.69	*****	0.13	0.04	1.20	0.62	0.47	98.04	11.83	24.05	3.20	14.00	4.12
TAS14-65_02	13.44	1.55	0.03	0.31	0.08	1.42	0.57	0.50	97.87	11.97	24.68	3.24	14.80	4.09
TAS14-65_03	13.42	1.74	0.01	0.29	0.11	1.37	0.57	0.46	96.69	11.76	24.32	3.29	14.43	3.92
TAS14-66_01	36.48	2.67	0.06	0.41	0.11	1.99	0.73	0.53	231.37	27.99	54.63	6.98	29.23	6.77
TAS14-66_02	37.74	2.70	*****	****	0.08	2.34	0.55	0.55	235.58	28.63	56.25	7.05	30.05	7.05
TAS14-66_03	38.38	2.55	0.26	0.24	0.10	2.12	0.70	0.55	240.03	29.16	56.61	7.12	31.83	7.46
TAS14-67_01	11.85	1.73	0.04	0.53	0.08	1.37	0.52	0.35	93.01	10.69	22.39	3.03	14.86	4.07
TAS14-67_02	11.96	1.60	0.04	0.11	0.05	1.41	0.82	0.28	92.17	10.62	22.04	2.96	14.31	4.15
TAS14-67_03	11.51	1.35	0.03	****	0.08	1.49	0.49	0.30	88.91	10.11	21.43	2.78	13.73	3.77
TAS14-68_01	11.70	1.29	0.05	0.18	0.08	6.07	0.52	0.49	110.74	12.96	22.91	3.23	14.34	4.14
TAS14-68_02	11.72	1.16	0.21	1.44	0.05	1.34	0.48	0.48	115.44	13.27	23.75	3.25	14.66	3.89
TAS14-68_03	11.33	1.61	0.08	0.30	0.06	1.61	0.52	0.47	111.68	13.40	22.80	3.15	13.81	3.70
TAS14-69_01	15.18	1.86	0.07	0.41	0.23	1.33	0.64	0.43	116.30	14.61	< ****	3.72	17.06	4.46

(*continued on next page*)

Table 4 (*continued*)

Sample	Nb	Mo	Ag	Cd	In	Sn	Sb	Cs	Ba	La	Ce	Pr	Nd	Sm
TAS14-69_02	15.85	1.97	1.08	3.09	0.08	1.36	0.61	0.44	121.77	15.19	29.45	3.89	17.60	4.96
TAS14-69_03	15.86	1.80	0.08	0.33	0.10	1.40	0.65	0.43	120.49	15.06	30.04	3.81	17.41	4.98
TAS14-70_01	3.80	0.55	0.06	0.18	0.03	1.06	0.40	0.87	141.29	8.85	17.82	2.32	9.92	2.27
TAS14-70_02	3.58	0.60	0.09	0.24	0.04	1.21	< ****	0.83	139.80	8.56	17.60	2.23	9.57	2.36
TAS14-70_03	3.57	0.40	0.01	0.13	0.04	1.77	0.47	0.85	137.91	8.50	17.65	2.18	9.35	2.17
TAS14-71_01	4.46	0.97	0.05	0.39	0.04	1.05	0.68	0.88	171.78	11.20	23.21	2.85	12.20	2.89
TAS14-71_02	4.45	0.88	0.05	0.47	0.07	1.15	0.70	0.87	173.44	11.35	23.31	3.00	12.55	2.93
TAS14-71_03	4.59	0.96	0.09	0.58	0.06	1.22	0.73	0.88	171.37	11.43	23.11	2.92	11.90	2.89
TAS14-72_01	14.31	1.09	0.03	0.50	0.09	1.45	0.55	0.13	151.65	14.45	25.78	3.12	13.40	3.31
TAS14-72_02	14.54	1.11	0.06	0.24	0.06	1.11	0.47	0.13	148.15	14.34	25.40	3.13	13.31	3.19
TAS14-72_03	15.57	0.84	0.04	0.29	0.08	0.96	0.49	0.12	153.83	14.70	26.43	3.16	13.77	3.26
TAS14-73_01	59.51	3.03	0.19	0.00	0.11	2.89	0.56	0.47	427.35	47.19	91.33	11.45	48.48	10.26
TAS14-73_02	62.05	3.14	0.12	0.12	0.08	2.90	0.54	0.45	442.55	49.21	95.46	12.02	50.34	10.38
TAS14-73_03	62.55	3.11	0.11	0.17	0.10	3.15	0.54	0.43	450.89	48.88	97.10	12.32	51.20	10.61
TAS14-74_01	104.68	5.64	0.17	0.83	0.10	2.91	0.69	1.22	564.01	84.70	157.25	18.76	74.09	13.66
TAS14-74_02	107.94	5.51	0.11	0.66	0.10	2.51	0.62	1.24	573.00	87.15	162.29	19.39	76.62	14.07
TAS14-74_03	106.53	5.65	0.06	0.62	0.10	2.58	0.65	1.18	573.35	85.78	161.08	19.15	74.81	14.03
TAS14-75_01	18.15	5.06	0.07	0.13	0.06	4.02	0.46	0.92	144.65	14.38	29.23	3.76	16.46	4.25
TAS14-75_02	16.68	1.48	0.02	0.25	0.07	1.63	0.50	1.01	140.99	13.97	28.52	3.67	15.88	4.16
TAS14-75_03	16.38	1.78	0.06	0.01	0.08	1.61	0.47	0.97	137.73	13.45	28.08	3.71	16.27	4.14
TAS14-76_01	13.54	1.57	0.05	0.04	0.06	1.57	0.45	0.75	121.61	12.06	24.56	3.23	14.39	3.85
TAS14-76_02	13.39	1.29	0.09	****	0.07	1.55	0.36	0.70	118.51	11.82	24.25	3.19	14.77	3.79
TAS14-76_03	13.45	1.59	0.09	0.23	0.07	1.75	0.59	0.70	118.97	11.67	24.33	3.16	14.40	3.89
TAS14-77_01	19.91	1.65	0.04	0.28	0.08	5.30	0.53	0.11	197.41	20.86	39.71	4.97	21.37	4.85
TAS14-77_02	20.96	1.81	0.03	0.50	0.10	1.71	0.64	0.12	209.46	21.73	41.84	5.19	22.71	5.26
TAS14-77_03	20.91	1.83	0.08	****	0.06	2.57	0.52	0.12	208.82	21.11	41.58	5.20	22.31	5.18
TAS14-78_01	16.54	1.76	0.08	****	0.06	3.04	0.56	0.88	139.22	13.75	28.22	3.59	16.31	4.06
TAS14-78_02	15.88	1.99	0.09	0.05	0.11	1.59	0.44	0.90	136.28	13.18	27.16	3.57	16.96	4.21
TAS14-78_03	16.44	1.87	*****	0.42	0.72	12.09	0.59	0.95	142.00	13.85	27.96	3.67	16.13	4.19
TAS14-79_01	4.90	0.83	0.14	0.51	0.06	11.42	0.55	1.58	185.35	12.06	24.12	3.07	13.20	3.17
TAS14-79_02	4.80	0.81	0.10	0.27	0.11	10.15	0.67	1.60	182.81	11.55	23.71	3.08	12.54	3.04
TAS14-79_03	4.61	0.73	0.06	0.40	0.07	4.36	0.62	1.75	184.87	11.71	24.63	3.04	12.95	3.01
TAS14-80_01	22.02	1.72	0.03	****	0.20	2.31	0.61	< ****	172.70	21.09	41.30	5.32	23.18	4.92
TAS14-80_02	20.80	1.75	0.07	0.07	0.15	5.84	0.63	0.22	162.20	19.73	39.37	4.99	21.25	5.08
TAS14-80_03	23.19	1.77	0.12	0.36	0.10	6.24	0.64	0.26	179.97	21.87	43.09	5.56	24.01	5.64

Sample	Eu	Gd	Tb	Dy	Ho	Er	Tm	Yb	Lu	Hf	Ta	W	Re	Tl	Pb206	Pb208	Bi	Th	U
TAS14-01_01	1.70	5.23	0.66	3.71	0.67	1.81	0.20	1.45	0.21	3.18	1.72	0.15	0.00	0.05	2.62	2.42	< 0.02	3.96	1.16
TAS14-01_02	1.75	5.41	0.74	4.00	0.68	1.79	0.24	1.42	0.20	3.31	1.80	0.16	< 0.03	0.05	2.91	2.63	< 0.02	4.20	1.13
TAS14-01_03	1.54	4.83	0.60	3.76	0.64	1.66	0.21	1.37	0.20	3.16	1.67	0.18	< 0.02	0.05	2.68	2.44	< 0.02	3.96	1.14
TAS14-02_01	1.82	5.78	0.70	4.29	0.74	1.83	0.27	1.53	0.20	3.44	1.83	4.75	0.01	< 0.02	2.28	2.31	0.01	2.98	0.70
TAS14-02_02	1.80	5.46	0.75	3.97	0.73	1.67	0.21	1.38	0.21	3.35	1.71	4.55	0.01	< 0.02	2.39	2.26	< 0.01	2.81	0.73
TAS14-02_03	1.78	5.31	0.67	3.88	0.75	1.77	0.24	1.64	0.20	3.22	1.71	4.56	< 0.03	0.01	2.19	2.19	0.01	2.73	1.00
TAS14-03_01	1.66	5.50	0.68	3.68	0.70	1.73	0.22	1.48	0.22	3.33	1.59	0.17	< 0.02	0.03	2.43	2.25	< 0.02	3.33	0.89
TAS14-03_02	1.74	5.43	0.69	3.85	0.64	1.77	0.24	1.55	0.21	3.20	1.59	0.23	< 0.03	0.01	2.56	2.43	< 0.01	3.30	0.81
TAS14-03_03	1.74	5.03	0.69	3.54	0.70	1.72	0.23	1.52	0.21	3.12	1.66	0.20	< 0.02	0.03	2.66	2.39	0.01	3.49	2.65
TAS14-04_01	1.24	4.15	0.60	3.66	0.67	1.72	0.24	1.46	0.21	2.36	0.77	0.29	< 0.02	0.03	1.91	1.75	0.01	2.32	0.57
TAS14-04_02	1.37	4.80	0.67	3.66	0.73	1.95	0.26	1.58	0.24	2.89	0.83	0.38	< 0.02	0.05	2.10	1.88	< 0.01	2.54	0.65
TAS14-04_03	1.29	4.43	0.62	3.75	0.73	1.89	0.23	1.48	0.21	2.79	0.82	0.42	0.01	0.06	1.95	1.91	< 0.02	2.33	0.67
TAS14-05_01	2.34	8.89	1.34	7.97	1.63	4.43	0.55	3.48	0.49	2.95	0.88	0.44	< 0.02	0.04	2.01	2.01	< 0.02	2.73	0.72
TAS14-05_02	2.16	8.37	1.26	8.08	1.57	4.26	0.52	3.25	0.47	2.95	0.85	0.37	0.02	0.02	2.13	2.07	< 0.02	2.63	0.69

(*continued on next page*)

Table 4 (*continued*)

Sample	Eu	Gd	Tb	Dy	Ho	Er	Tm	Yb	Lu	Hf	Ta	W	Re	Tl	Pb206	Pb208	Bi	Th	U
TAS14-05_03	2.21	8.50	1.30	7.76	1.63	4.26	0.55	3.37	0.48	2.83	0.86	0.43	< 0.03	0.02	2.21	2.04	< 0.02	2.58	0.72
TAS14-06_01	1.50	5.14	0.79	4.21	0.80	2.02	0.26	1.75	0.24	2.81	0.91	0.54	0.01	0.04	2.00	2.03	0.02	2.45	0.89
TAS14-06_02	1.52	4.97	0.76	4.37	0.80	1.92	0.27	1.75	0.23	2.99	0.95	0.44	< 0.02	0.05	2.27	1.94	0.06	2.47	0.83
TAS14-06_03	1.58	5.08	0.77	4.30	0.82	2.04	0.26	1.66	0.23	2.82	0.92	0.54	0.01	0.04	2.11	2.05	< 0.01	2.60	0.90
TAS14-07_01	1.57	5.07	0.75	4.19	0.79	1.95	0.26	1.55	0.24	2.85	0.84	0.54	< 0.03	0.04	2.07	1.85	< 0.02	2.46	0.87
TAS14-07_02	1.55	4.65	0.74	4.03	0.76	1.97	0.25	1.54	0.21	2.83	0.89	< 0.47	< 0.02	0.05	1.93	1.87	< 0.02	2.41	0.81
TAS14-07_03	1.58	5.04	0.80	4.51	0.84	2.09	0.27	1.72	0.25	3.05	0.94	0.53	0.01	0.03	2.17	1.97	0.02	2.60	0.85
TAS14-08_01	1.35	4.22	0.63	3.80	0.71	1.68	0.25	1.48	0.21	2.58	0.70	0.42	0.02	0.03	1.99	1.72	0.02	1.97	0.74
TAS14-08_02	1.25	4.18	0.63	3.60	0.72	1.79	0.21	1.47	0.20	2.55	0.75	0.31	0.01	0.04	1.95	1.73	< 0.01	1.88	0.67
TAS14-08_03	1.32	4.21	0.59	3.59	0.72	1.76	0.22	1.45	0.19	2.62	0.74	0.58	< 0.03	0.03	1.85	1.74	< 0.02	1.89	0.74
TAS14-09_01	1.35	4.62	0.62	3.56	0.73	1.83	0.23	1.40	0.19	2.73	0.75	0.38	< 0.03	< 0.03	1.76	1.63	0.03	1.98	0.68
TAS14-09_02	1.33	4.04	0.69	3.66	0.73	1.94	0.23	1.57	0.19	2.49	0.76	0.33	0.02	0.05	2.03	1.70	< 0.02	1.97	0.71
TAS14-09_03	1.30	4.34	0.69	4.13	0.72	1.89	0.21	1.81	0.22	2.72	0.75	0.44	< 0.02	< 0.03	1.85	2.17	0.02	2.04	0.80
TAS14-10_01	5.60	15.02	1.86	8.67	1.50	3.26	0.40	1.98	0.25	11.17	6.02	1.77	< 0.04	< 0.03	5.33	4.86	0.02	11.40	3.39
TAS14-10_02	5.28	15.27	1.85	8.66	1.43	3.30	0.40	2.00	0.24	11.41	6.11	1.99	< 0.04	< 0.02	5.63	5.02	< 0.03	11.51	3.24
TAS14-10_03	5.39	15.62	1.84	8.66	1.49	3.21	0.37	1.90	0.24	11.30	6.32	1.94	< 0.02	< 0.02	5.54	5.12	0.02	11.67	3.38
TAS14-11_01	1.73	5.50	0.68	3.81	0.71	1.83	0.25	1.55	0.21	3.69	1.64	0.28	< 0.04	0.03	2.12	2.05	< 0.02	3.13	0.95
TAS14-11_02	1.72	5.18	0.67	3.69	0.70	1.78	0.23	1.41	0.21	3.50	1.60	0.22	< 0.04	< 0.02	2.41	2.08	< 0.02	3.10	0.90
TAS14-11_03	1.70	5.04	0.66	3.85	0.73	1.79	0.22	1.51	0.26	3.58	1.61	0.26	< 0.03	0.02	2.26	2.15	< 0.02	3.22	0.93
TAS14-12_01	2.15	6.78	0.98	4.97	0.97	2.59	0.32	2.22	0.31	4.69	3.54	0.48	< 0.04	< 0.04	2.19	2.05	< 0.02	4.80	1.18
TAS14-12_02	2.45	7.66	1.00	5.75	1.07	2.86	0.41	2.60	0.40	4.90	3.93	1.18	0.01	< 0.04	2.50	2.29	< 0.02	5.34	1.32
TAS14-12_03	2.61	7.34	0.96	5.53	1.04	2.88	0.38	2.62	0.36	5.64	3.97	0.50	< 0.03	< 0.04	2.47	2.53	< 0.03	5.46	1.38
TAS14-13_01	2.22	6.31	0.91	5.49	1.03	2.81	0.41	2.45	0.36	5.53	4.21	45.59	0.01	0.00	2.88	2.58	0.02	6.42	1.53
TAS14-13_02	2.29	6.58	0.97	5.58	1.12	2.98	0.43	2.63	0.35	5.85	4.20	46.40	0.02	*****	2.89	2.73	*****	6.65	1.57
TAS14-13_03	2.13	6.12	0.87	5.11	1.00	2.62	0.37	2.28	0.35	5.43	4.02	45.77	0.01	0.02	2.91	2.74	0.01	6.35	1.54
TAS14-14_01	2.25	6.19	0.87	5.19	0.99	2.68	0.35	2.15	0.33	5.38	3.93	75.79	*****	0.00	2.43	2.36	0.01	6.11	1.53
TAS14-14_02	2.15	6.33	0.85	4.78	0.97	2.55	0.36	2.23	0.31	5.28	4.07	77.51	0.01	*****	2.61	2.46	0.02	6.14	1.55
TAS14-14_03	2.22	6.04	0.88	5.12	0.94	2.47	0.36	2.28	0.34	5.37	4.05	80.21	0.02	*****	2.76	2.57	0.00	6.19	1.57
TAS14-15_01	1.92	5.61	0.81	4.65	0.88	2.35	0.31	2.11	0.30	4.56	3.23	30.23	*****	*****	2.02	2.02	0.15	4.59	1.22
TAS14-15_02	2.09	5.85	0.85	4.92	0.94	2.72	0.33	2.25	0.32	4.74	3.31	30.21	0.02	0.00	2.44	2.25	0.01	4.76	1.19
TAS14-15_03	2.07	5.76	0.84	4.90	0.92	2.59	0.33	2.09	0.35	5.06	3.49	30.42	*****	0.62	2.52	2.47	0.01	4.93	1.19
TAS14-16_01	2.12	5.93	0.85	4.74	0.93	2.63	0.33	2.36	0.30	4.94	3.63	47.05	0.02	0.02	2.30	2.17	0.01	5.47	1.41
TAS14-16_02	2.17	6.11	0.87	4.97	0.97	2.50	0.36	2.40	0.33	5.03	3.79	49.50	0.03	0.01	2.67	2.43	*****	5.61	1.41
TAS14-16_03	2.22	5.90	0.82	4.86	0.93	2.53	0.33	2.22	0.31	5.47	3.81	50.20	*****	*****	2.69	2.48	*****	5.73	1.43
TAS14-17_01	3.44	9.13	1.25	6.49	1.09	2.48	0.30	1.50	0.21	6.15	5.18	21.78	0.02	*****	3.20	2.89	0.02	6.58	2.40
TAS14-17_02	3.24	8.63	1.17	6.09	1.00	2.25	0.26	1.55	0.18	5.70	4.98	21.59	*****	*****	2.87	2.82	0.01	6.32	2.35
TAS14-17_03	3.36	9.10	1.24	6.42	1.04	2.35	0.26	1.46	0.20	6.22	5.29	22.20	*****	*****	3.12	2.97	*****	6.63	2.44
TAS14-18_01	2.94	8.00	1.04	5.85	1.00	2.40	0.27	1.71	0.21	5.57	4.52	1.60	*****	*****	2.55	2.36	0.01	5.43	2.02
TAS14-18_02	2.86	7.76	1.05	5.48	0.93	2.28	0.30	1.70	0.21	5.25	4.47	1.73	0.02	0.02	2.68	2.31	0.01	5.29	2.04
TAS14-18_03	3.06	8.88	1.15	6.00	1.05	2.45	0.28	1.71	0.22	5.97	4.79	1.64	0.01	*****	2.59	2.58	0.01	5.65	2.12
TAS14-19_01	3.05	8.34	1.08	5.97	1.02	2.43	0.28	1.64	0.20	5.60	4.72	54.06	*****	0.00	3.45	2.98	0.01	5.96	2.11
TAS14-19_02	2.89	7.95	1.17	5.88	1.06	2.49	0.28	1.69	0.23	6.04	4.74	54.46	*****	*****	3.63	3.21	0.00	6.00	2.09
TAS14-19_03	2.93	8.12	1.06	5.61	0.99	2.34	0.28	1.61	0.20	5.66	4.58	54.75	*****	0.00	3.26	3.04	0.00	5.91	2.11
TAS14-20_01	2.81	7.70	1.12	5.65	0.96	2.33	0.28	1.62	0.20	5.77	4.65	1.53	*****	0.02	2.91	2.97	0.02	5.87	2.14
TAS14-20_02	2.97	8.50	1.18	5.80	1.07	2.46	0.29	1.77	0.22	6.00	4.71	0.75	*****	*****	3.47	3.16	0.00	6.43	2.10
TAS14-20_03	2.97	8.26	1.17	5.92	1.00	2.43	0.30	1.63	0.23	5.64	4.92	1.05	*****	1.82	3.54	3.13	0.02	6.14	2.22
TAS14-21_01	4.15	11.63	1.44	7.04	1.21	2.48	0.30	1.59	0.19	7.70	6.67	0.34	0.03	0.00	3.36	3.20	0.01	8.27	3.21
TAS14-21_02	4.19	11.91	1.51	7.41	1.28	2.60	0.33	1.68	0.19	7.90	6.85	0.36	*****	*****	3.56	3.29	0.03	8.45	3.14
TAS14-21_03	4.12	11.79	1.58	7.44	1.16	2.71	0.29	1.61	0.21	7.79	6.99	0.36	*****	0.01	3.67	3.20	*****	8.54	3.37
TAS14-22_01	4.03	10.45	1.37	6.97	1.13	2.50	0.25	1.53	0.18	7.49	6.57	0.20	*****	*****	3.48	3.13	0.02	8.12	3.13
TAS14-22_02	4.08	11.51	1.43	7.46	1.23	2.62	0.31	1.68	0.22	7.51	6.82	0.23	*****	0.01	4.14	3.61	0.02	8.48	3.25
TAS14-22_03	3.93	11.17	1.45	7.60	1.13	2.67	0.29	1.56	0.20	7.54	6.68	0.27	0.02	0.00	3.92	3.54	0.07	8.51	3.20
TAS14-23_01	4.20	10.92	1.89	7.16	1.27	2.90	0.75	1.75	0.39	7.85	6.60	39.49	0.01	0.04	4.79	3.46	0.08	8.06	3.16

(*continued on next page*)

Table 4 (*continued*)

Sample	Eu	Gd	Tb	Dy	Ho	Er	Tm	Yb	Lu	Hf	Ta	W	Re	Tl	Pb206	Pb208	Bi	Th	U
TAS14-23_02	3.96	11.10	1.47	7.34	1.22	2.71	0.34	1.75	0.22	7.71	6.73	40.08	*****	0.02	3.97	3.96	0.05	8.77	3.30
TAS14-23_03	4.27	11.48	1.50	7.73	1.31	2.78	0.39	1.71	0.21	8.20	6.80	40.36	0.01	0.01	3.86	4.38	0.08	8.32	3.36
TAS14-24_01	2.48	6.21	0.95	4.99	0.87	2.11	0.31	1.45	0.21	4.14	3.05	53.12	*****	0.01	2.52	2.40	0.05	4.46	1.52
TAS14-24_02	2.31	6.69	0.93	4.98	0.84	2.05	0.29	1.60	0.23	4.38	2.98	54.77	0.05	0.02	2.69	2.50	0.04	4.43	1.57
TAS14-24_03	2.40	6.77	0.98	4.96	0.89	2.12	0.27	1.65	0.19	4.35	3.10	53.26	*****	0.10	2.97	2.56	*****	4.35	1.61
TAS14-25_01	1.53	5.07	0.78	4.39	0.88	2.26	0.31	1.81	0.26	3.28	0.72	3.11	*****	0.00	1.65	1.37	0.05	1.42	0.54
TAS14-25_02	1.53	4.80	0.79	4.53	0.88	2.23	0.33	1.87	0.29	3.53	0.66	3.09	0.01	*****	1.67	1.34	0.08	1.42	0.46
TAS14-25_03	1.62	4.93	0.83	4.67	0.95	2.31	0.33	2.25	0.29	3.08	0.74	3.11	*****	0.01	1.72	1.69	0.11	1.44	0.51
TAS14-26_01	1.80	5.64	0.82	4.86	0.89	2.18	0.31	1.84	0.25	3.78	1.13	1.65	0.02	*****	1.64	1.65	*****	2.03	0.57
TAS14-26_02	1.82	5.54	0.87	4.96	0.95	2.41	0.30	1.84	0.26	4.09	1.15	1.59	*****	0.02	1.83	1.71	0.03	2.12	0.59
TAS14-26_03	1.79	5.83	0.91	5.13	0.95	2.50	0.32	1.66	0.25	3.96	1.20	1.65	0.02	0.01	1.98	1.96	0.05	2.18	0.59
TAS14-27_01	1.33	4.07	0.66	3.92	0.74	1.94	0.26	1.46	0.22	2.64	0.48	0.22	0.00	0.03	1.14	1.04	0.03	1.09	0.37
TAS14-27_02	1.31	4.14	0.72	3.92	0.76	2.09	0.26	1.76	0.23	2.66	0.55	0.09	0.19	*****	1.40	1.36	0.02	1.09	0.29
TAS14-27_03	1.25	4.05	0.68	3.92	0.75	1.98	0.25	1.58	0.23	2.63	0.49	0.14	0.00	0.02	1.17	1.31	0.01	1.14	0.33
TAS14-28_01	2.02	5.92	0.86	4.89	0.87	2.18	0.28	1.55	0.24	4.26	1.51	0.25	0.00	0.03	1.59	1.64	0.09	2.30	0.68
TAS14-28_02	2.04	5.90	0.92	4.87	0.87	2.18	0.28	1.63	0.23	4.45	1.62	0.18	0.02	0.03	1.60	1.59	0.66	2.26	0.62
TAS14-28_03	2.11	6.01	0.88	4.62	0.85	2.11	0.26	1.78	0.20	4.35	1.57	0.11	0.02	0.03	1.73	1.62	1.64	2.32	0.66
TAS14-29_01	1.40	5.00	0.82	4.32	1.03	2.12	0.32	1.90	0.24	3.50	0.98	0.16	0.00	0.05	1.95	1.67	0.03	2.28	0.61
TAS14-29_02	1.58	4.89	0.77	4.52	1.35	2.16	0.29	1.82	0.27	3.24	1.05	0.29	0.00	0.01	1.79	1.83	0.00	2.29	0.60
TAS14-29_03	1.58	4.96	0.75	4.45	0.88	2.31	0.31	1.69	0.27	3.50	1.03	0.29	*****	0.01	1.93	1.77	0.50	2.26	0.65
TAS14-30_01	2.02	5.61	0.80	4.66	0.84	2.19	0.30	1.65	0.23	4.31	2.60	0.23	0.00	0.02	2.21	1.96	5.61	4.01	1.09
TAS14-30_02	2.00	5.41	0.82	4.28	0.77	2.19	0.25	1.70	0.23	3.99	2.57	0.25	0.03	0.02	2.16	2.00	0.03	3.94	1.07
TAS14-30_03	1.90	5.30	0.85	4.64	0.85	2.15	0.27	1.80	0.25	4.50	2.63	0.29	*****	0.01	2.19	2.17	0.02	4.07	1.13
TAS14-31_01	2.33	6.28	0.85	4.57	0.72	1.92	0.25	1.43	0.17	5.41	3.35	42.26	*****	0.01	2.23	2.25	0.03	4.21	1.45
TAS14-31_02	2.43	6.71	0.98	4.66	0.86	2.05	0.24	1.46	0.19	5.73	3.67	43.79	*****	*****	2.48	2.49	*****	4.68	1.33
TAS14-31_03	2.34	6.22	0.90	4.49	0.72	1.80	0.22	1.38	0.19	5.28	3.31	43.71	*****	*****	2.43	2.45	*****	4.27	1.37
TAS14-32_01	2.30	6.32	0.87	4.54	0.78	1.92	0.23	1.25	0.17	5.57	3.46	33.30	0.01	0.02	2.56	2.49	*****	4.43	1.34
TAS14-32_02	2.49	6.84	0.91	4.63	0.82	1.87	0.25	1.39	0.19	5.73	3.53	33.79	*****	0.06	2.61	2.51	*****	4.53	1.45
TAS14-32_03	2.34	6.86	0.95	4.78	0.86	2.09	0.26	1.47	0.20	5.71	3.64	37.25	0.03	0.02	2.78	2.66	0.02	4.67	1.35
TAS14-33_01	2.19	6.53	0.85	4.65	0.77	1.79	0.23	1.26	0.21	5.13	3.31	60.29	*****	*****	2.57	2.41	*****	4.21	1.29
TAS14-33_02	2.27	6.36	0.87	4.65	0.77	1.95	0.21	1.40	0.18	5.50	3.31	60.23	*****	*****	2.65	2.57	0.00	4.28	1.29
TAS14-33_03	2.37	6.16	0.84	4.54	0.77	1.79	0.24	1.30	0.17	5.08	3.45	63.72	0.02	0.01	2.72	2.61	*****	4.21	1.38
TAS14-34_01	2.16	5.83	0.78	4.19	0.72	1.77	0.21	1.27	0.17	4.43	2.36	1.12	*****	0.01	2.08	2.13	0.01	2.92	2.03
TAS14-34_02	2.18	6.27	0.84	4.34	0.73	1.76	0.24	1.44	0.18	4.47	2.55	0.48	*****	0.00	2.25	2.29	0.02	3.10	1.19
TAS14-34_03	2.17	5.78	0.79	4.29	0.75	1.77	0.22	1.29	0.20	4.41	2.54	0.53	0.01	*****	2.17	2.18	0.00	2.96	1.25
TAS14-34B_01	2.06	5.83	0.80	4.40	0.74	1.86	0.23	1.53	0.17	4.64	2.52	4.47	*****	0.02	2.09	1.99	0.02	3.04	1.15
TAS14-34B_02	2.07	5.77	0.78	4.20	0.70	1.76	0.23	1.44	0.16	4.56	2.45	4.39	*****	*****	2.16	2.23	0.03	3.15	1.21
TAS14-34B_03	2.11	5.47	0.76	4.27	0.74	1.79	0.22	1.31	0.16	4.43	2.50	4.66	0.04	0.02	2.29	2.32	0.02	3.01	1.30
TAS14-35_01	2.11	6.34	0.83	4.38	0.77	1.76	0.23	1.41	0.20	4.52	2.62	0.24	*****	*****	2.16	2.12	0.03	2.97	1.23
TAS14-35_02	2.10	5.68	0.78	4.10	0.75	1.73	0.22	1.28	0.17	4.44	2.51	0.30	*****	0.02	2.31	2.07	*****	3.01	1.24
TAS14-35_03	2.25	5.78	0.80	4.11	0.68	1.77	0.20	1.31	0.18	4.49	2.62	0.29	*****	0.02	2.42	2.02	0.04	3.06	1.39
TAS14-36_01	1.69	5.20	0.71	4.43	0.87	2.27	0.31	1.94	0.27	4.11	1.65	0.68	0.00	0.02	1.80	1.82	0.03	2.47	0.76
TAS14-36_02	1.66	4.88	0.78	4.54	0.80	2.16	0.28	2.11	0.25	3.75	1.64	0.67	0.01	0.02	2.05	1.90	0.01	2.39	0.76
TAS14-36_03	1.70	5.12	0.70	4.28	0.78	2.18	0.27	1.70	0.25	3.83	1.52	0.67	*****	0.04	1.99	1.91	0.04	2.41	0.77
TAS14-37_01	1.83	5.57	0.76	4.46	0.86	2.08	0.26	1.87	0.23	4.28	2.43	0.23	*****	*****	1.99	1.94	0.01	3.20	0.99
TAS14-37_02	1.92	5.07	0.79	4.53	0.81	2.02	0.27	1.54	0.23	3.77	2.36	0.46	*****	0.02	2.08	2.00	0.02	3.12	0.99
TAS14-37_03	1.88	5.30	0.77	4.55	0.80	2.04	0.25	1.70	0.21	4.21	2.51	0.37	0.00	0.03	2.16	2.13	0.01	3.24	0.97
TAS14-38_01	1.36	4.34	0.66	3.96	0.81	2.15	0.28	1.83	0.24	3.14	1.17	0.27	*****	0.02	1.92	2.48	0.01	2.36	0.51
TAS14-38_02	1.38	4.23	0.71	3.92	0.78	2.01	0.29	1.55	0.24	2.90	1.14	0.24	0.02	0.05	1.82	1.81	*****	2.23	0.51
TAS14-38_03	1.39	4.51	0.67	4.24	0.79	2.09	0.28	1.83	0.23	3.02	1.21	0.21	0.01	0.05	1.97	1.92	0.01	2.35	0.53
TAS14-39_01	1.35	4.04	0.64	4.09	0.74	1.92	0.24	1.65	0.21	3.00	0.81	0.25	*****	0.08	1.37	1.25	*****	1.87	0.50
TAS14-39_02	1.28	4.01	0.61	3.49	0.69	1.86	0.24	1.61	0.21	2.96	0.77	0.27	*****	0.04	1.50	1.25	0.01	1.74	0.51
TAS14-39_03	1.26	3.66	0.58	3.33	0.68	1.73	0.23	1.49	0.22	2.97	0.77	0.26	0.01	*****	1.43	4.16	0.00	1.76	0.53

(*continued on next page*)

Table 4 *(continued)*

Sample	Eu	Gd	Tb	Dy	Ho	Er	Tm	Yb	Lu	Hf	Ta	W	Re	Tl	Pb206	Pb208	Bi	Th	U
TAS14-40_01	1.50	5.12	0.73	4.35	0.86	2.30	0.30	1.79	0.28	4.08	1.12	0.48	0.02	*****	2.08	1.95	0.05	3.22	0.73
TAS14-40_02	1.49	4.45	0.73	4.42	0.75	2.15	0.33	1.74	0.26	3.70	1.12	0.32	0.01	0.07	2.22	1.93	0.02	3.02	0.81
TAS14-40_03	1.46	4.46	0.71	4.27	0.79	1.98	0.27	1.79	0.27	3.73	1.12	0.45	0.09	0.02	2.13	1.97	0.02	3.03	0.82
TAS14-41_01	1.53	5.29	0.78	4.42	0.89	2.32	0.30	1.98	0.27	4.40	1.22	0.48	*****	0.02	2.74	2.55	0.23	3.18	0.91
TAS14-41_02	1.53	5.01	0.77	4.53	0.84	2.09	0.30	1.76	0.26	4.08	1.22	0.49	0.01	0.07	2.81	4.67	0.26	3.28	0.87
TAS14-41_03	1.58	4.80	0.78	4.37	0.81	2.26	0.28	1.86	0.27	4.25	1.12	0.51	*****	0.05	2.67	2.59	0.24	3.26	0.89
TAS14-42A_01	1.49	4.83	0.71	4.00	0.78	2.04	0.28	1.63	0.23	3.18	0.89	7.68	*****	0.03	2.74	2.22	0.03	2.43	0.58
TAS14-42A_02	1.45	4.10	0.69	3.93	0.76	2.05	0.27	1.57	0.24	3.30	0.94	7.90	0.02	0.06	2.21	2.25	0.03	2.33	0.62
TAS14-42A_03	1.49	4.56	0.68	4.19	0.80	2.04	0.26	1.62	0.22	3.19	0.92	7.99	*****	0.05	2.35	2.39	0.02	2.40	0.64
TAS14-42B_01	1.53	4.99	0.77	4.23	0.87	2.06	0.31	1.73	0.25	3.64	0.96	6.96	0.03	0.00	2.23	2.23	0.04	2.45	0.60
TAS14-42B_02	1.50	4.37	0.67	4.04	0.74	1.99	0.26	1.78	0.24	3.16	0.94	6.97	0.01	0.03	2.25	2.19	0.02	2.40	0.62
TAS14-42B_03	1.58	4.68	0.71	4.14	0.79	2.06	0.25	1.63	0.22	3.32	0.95	6.87	*****	0.03	2.55	2.29	0.02	2.52	0.98
TAS14-43_01	2.48	6.61	0.97	5.02	0.95	2.21	0.28	1.64	0.24	5.33	2.52	30.67	*****	0.00	12.33	2.49	0.03	3.63	1.17
TAS14-43_02	2.47	7.10	0.99	5.18	0.89	2.23	0.23	1.59	0.24	5.14	2.54	33.03	0.48	*****	2.56	2.67	0.01	3.70	1.11
TAS14-43_03	2.41	6.95	0.97	5.45	0.89	2.28	0.24	1.58	0.25	5.30	2.54	32.15	0.03	0.03	2.59	2.47	0.01	3.68	1.15
TAS14-44_01	1.74	5.11	0.74	4.27	0.82	1.94	0.29	1.86	0.24	3.58	1.76	0.38	*****	0.03	2.72	2.59	0.02	3.12	0.89
TAS14-44_02	1.77	5.09	0.79	4.41	0.82	2.20	0.30	1.96	0.26	3.73	1.78	0.33	0.00	0.01	2.72	2.73	0.03	3.14	0.91
TAS14-44_03	1.75	4.89	0.76	4.36	0.82	2.09	0.28	1.68	0.28	3.71	1.81	0.26	0.03	*****	3.04	2.83	0.00	3.14	0.90
TAS14-45_01	1.77	5.35	0.76	4.20	0.74	1.70	0.22	1.30	0.19	4.54	2.19	0.18	*****	0.02	1.67	1.60	0.01	2.71	1.11
TAS14-45_02	1.87	5.22	0.73	3.98	0.71	1.79	0.24	1.33	0.18	4.43	2.25	0.23	*****	0.01	1.82	1.63	0.00	2.77	1.06
TAS14-45_03	1.93	5.10	0.72	4.00	0.70	1.87	0.21	1.25	0.19	4.38	2.13	0.23	0.03	0.03	1.73	1.65	0.00	2.85	1.05
TAS14-46_01	1.93	5.66	0.82	4.41	0.81	2.02	0.27	1.35	0.20	4.81	2.61	0.27	0.04	0.01	1.95	1.89	*****	3.31	1.20
TAS14-46_02	2.09	5.81	0.83	4.29	0.79	2.04	0.25	1.57	0.20	4.88	2.66	0.18	*****	*****	2.19	1.93	0.01	3.28	1.26
TAS14-46_03	1.96	5.83	0.81	4.44	0.76	1.89	0.22	1.55	0.19	4.80	2.62	0.22	*****	0.02	2.20	2.00	0.01	3.26	1.29
TAS14-47_01	2.20	6.38	2.62	5.44	0.91	2.43	0.24	1.66	0.21	4.85	1.80	0.33	0.03	0.03	1.78	1.69	*****	2.53	0.80
TAS14-47_02	2.13	6.26	0.93	5.26	0.90	2.08	0.26	1.62	0.21	5.02	1.79	0.10	0.00	0.66	1.74	1.59	0.12	2.38	0.69
TAS14-47_03	1.93	5.49	0.80	4.39	0.82	1.89	0.23	1.43	0.20	3.98	1.52	0.16	0.03	0.01	1.60	1.40	*****	2.18	0.59
TAS14-48_01	1.51	4.86	0.73	4.09	0.83	2.00	0.29	1.74	0.30	3.54	1.50	4.58	0.01	*****	1.59	1.52	0.02	2.51	0.60
TAS14-48_02	1.66	4.46	0.72	4.27	0.85	2.07	0.29	1.84	0.24	3.33	1.56	5.57	0.03	0.00	1.69	1.70	*****	2.46	0.67
TAS14-48_03	1.56	4.92	0.73	4.21	0.86	2.12	0.26	2.05	0.25	3.24	1.50	5.50	*****	0.01	1.77	1.67	*****	2.58	0.63
TAS14-49_01	1.38	4.10	0.68	3.92	0.80	2.10	0.28	1.70	0.26	3.02	0.71	0.16	0.02	0.02	1.95	1.76	0.02	2.03	0.42
TAS14-49_02	1.51	4.45	0.78	4.52	0.87	2.26	0.28	1.98	0.26	3.13	0.81	0.21	0.04	0.01	2.14	2.05	0.04	2.23	0.42
TAS14-49_03	1.49	4.64	0.74	4.54	0.80	2.10	0.33	1.69	0.25	3.12	0.76	0.20	0.27	0.00	2.20	2.00	0.01	2.15	0.43
TAS14-50_01	2.06	5.82	0.85	4.88	0.89	2.30	0.28	1.74	0.20	4.33	1.75	9.69	0.01	0.01	2.13	2.19	0.00	3.07	0.80
TAS14-50_02	1.94	5.93	0.92	4.97	0.91	2.34	0.26	1.77	0.26	4.37	1.83	9.92	0.02	*****	2.34	2.03	0.02	3.14	0.86
TAS14-50_03	2.02	6.13	1.00	4.86	0.88	2.33	0.28	1.62	0.21	4.62	1.90	10.43	*****	*****	3.03	2.49	0.03	3.17	0.82
TAS14-51_01	1.89	6.07	0.85	4.76	0.89	2.25	0.25	1.77	0.23	4.41	1.88	0.35	*****	0.00	2.40	2.15	0.01	3.27	0.84
TAS14-51_02	2.02	5.67	0.87	4.89	0.85	2.31	0.26	1.71	0.23	4.49	1.83	0.41	*****	0.03	2.15	2.17	0.01	3.17	0.82
TAS14-51_03	1.90	5.75	0.84	4.77	0.88	2.16	0.29	1.71	0.23	4.43	1.75	0.30	0.02	0.05	2.84	2.21	0.02	3.21	0.88
TAS14-52_01	2.00	5.59	0.99	4.64	0.82	2.12	0.27	1.57	0.21	4.42	1.74	0.18	0.03	*****	2.39	2.30	0.01	3.09	0.76
TAS14-52_02	2.17	5.75	0.82	4.76	0.80	2.12	0.29	1.50	0.23	4.33	1.79	0.28	0.03	0.03	2.44	2.30	0.15	3.11	0.84
TAS14-52_03	1.92	5.83	0.85	4.51	0.88	2.06	0.28	1.74	0.21	4.50	1.83	0.16	*****	0.01	2.55	2.47	*****	3.19	0.81
TAS14-53_01	1.54	4.33	0.70	4.12	0.82	2.07	0.29	1.63	0.23	3.00	0.78	0.26	*****	0.03	2.65	2.53	0.02	1.98	0.61
TAS14-53_02	1.33	4.18	0.65	4.14	0.85	2.09	0.29	1.76	0.25	2.86	0.76	0.25	0.02	0.02	2.67	2.47	0.01	1.83	0.53
TAS14-53_03	1.44	4.30	0.72	4.18	0.82	2.04	0.31	1.75	0.25	2.89	0.78	0.33	0.03	0.04	2.83	2.68	0.04	1.98	0.58
TAS14-54_01	1.49	4.82	0.81	4.79	0.89	2.56	0.33	2.22	0.29	3.29	0.69	0.26	0.02	0.04	2.22	1.93	0.02	1.95	0.53
TAS14-54_02	1.59	5.34	0.82	4.89	1.00	2.55	0.33	2.25	0.26	3.49	0.72	0.25	*****	0.03	2.21	2.11	0.04	2.18	0.54
TAS14-54_03	1.53	4.90	0.80	4.74	0.89	2.59	0.30	2.18	0.26	3.18	0.70	0.25	0.02	0.04	2.35	2.29	0.03	2.04	0.56
TAS14-55_01	1.52	5.24	0.78	5.01	0.93	2.60	0.33	2.20	0.29	3.38	0.75	0.03	0.00	0.03	1.95	1.94	*****	2.15	0.56
TAS14-55_02	1.49	5.17	0.82	4.71	0.96	2.47	0.36	2.11	0.29	3.30	0.72	0.31	*****	0.03	2.19	2.03	0.03	2.16	0.54
TAS14-55_03	1.57	5.24	0.87	5.01	0.98	2.54	0.33	2.23	0.31	3.53	0.75	0.30	0.03	0.05	2.41	2.24	0.01	2.19	0.59
TAS14-56A_01	1.71	4.79	0.70	4.32	0.78	2.09	0.27	1.86	0.25	3.32	1.04	0.37	*****	0.03	3.41	3.27	0.00	2.69	0.74
TAS14-56A_02	1.49	4.82	0.73	4.49	0.83	2.16	0.28	1.72	0.26	3.52	1.11	0.38	*****	*****	3.53	3.43	0.02	2.74	0.78

(continued on next page)

Table 4 (*continued*)

Sample	Eu	Gd	Tb	Dy	Ho	Er	Tm	Yb	Lu	Hf	Ta	W	Re	Tl	Pb206	Pb208	Bi	Th	U
TAS14-56A_03	1.55	4.76	0.71	4.29	0.86	2.21	0.28	1.77	0.25	3.59	1.12	0.41	0.00	0.02	3.83	3.52	0.02	2.78	0.78
TAS14-56B_01	1.47	4.76	0.74	4.12	1.75	2.17	0.28	1.77	0.24	3.50	1.11	7.12	*****	0.00	3.72	< ****	0.03	2.72	0.77
TAS14-56B_02	1.50	4.66	0.74	4.32	0.80	2.04	0.31	1.88	0.24	3.46	1.07	2.83	0.04	0.04	3.52	3.33	0.05	2.74	0.79
TAS14-56B_03	1.50	4.87	0.76	4.49	0.83	2.28	0.28	1.97	0.23	3.42	1.09	3.02	*****	0.03	3.76	3.63	*****	2.75	0.79
TAS14-57_01	1.51	4.94	0.76	4.49	0.84	2.23	0.29	1.83	0.26	3.51	1.04	0.41	*****	0.05	3.35	3.57	0.10	2.76	0.75
TAS14-57_02	1.54	5.08	0.78	4.33	0.95	2.51	0.31	1.93	0.29	3.60	1.06	0.39	0.05	0.05	4.00	3.67	0.02	2.81	0.82
TAS14-57_03	1.51	4.78	0.78	4.29	0.79	2.25	0.28	1.84	0.28	3.23	1.02	0.35	*****	0.03	3.64	3.51	0.04	2.76	0.78
TAS14-58_01	1.64	5.34	0.83	4.97	0.94	2.49	0.34	2.66	0.29	3.32	0.78	0.54	*****	*****	2.42	2.17	0.02	2.55	0.68
TAS14-58_02	1.75	5.17	0.86	4.90	1.01	2.53	0.34	2.12	0.29	3.36	0.80	8.51	0.00	0.00	2.39	2.23	0.02	2.48	0.69
TAS14-58_03	1.57	5.29	0.83	4.76	0.93	2.52	0.32	2.08	0.30	3.25	0.79	0.46	*****	0.04	2.45	2.33	0.02	2.41	0.69
TAS14-59_01	2.33	6.68	0.94	5.24	0.89	2.34	0.27	1.52	0.20	5.25	2.40	0.19	0.00	0.03	2.09	1.91	0.01	3.34	0.99
TAS14-59_02	2.32	6.73	0.92	5.25	0.87	2.23	0.26	1.51	0.20	5.01	2.35	0.21	0.00	0.06	2.23	1.95	0.01	3.25	1.02
TAS14-59_03	2.46	7.09	0.94	5.40	0.84	2.23	0.25	1.65	0.21	5.21	2.48	0.20	*****	0.02	2.32	2.22	0.01	3.49	0.99
TAS14-60_01	3.74	10.16	1.04	6.93	1.14	2.48	0.35	1.87	0.25	5.91	6.44	6.59	0.06	*****	3.84	3.51	1.26	10.93	3.09
TAS14-60_02	3.81	9.96	1.29	6.55	1.11	2.60	0.30	1.85	0.24	5.72	6.15	5.50	*****	0.02	3.89	3.49	0.01	11.11	3.06
TAS14-60_03	3.58	9.97	1.22	6.60	1.07	2.63	0.32	1.80	0.22	5.48	6.04	5.50	*****	0.01	3.94	3.61	0.01	10.99	3.17
TAS14-61_01	3.68	9.66	1.25	6.47	1.07	2.68	0.30	1.78	0.23	5.83	5.95	0.15	*****	0.01	3.46	3.40	0.01	10.78	3.13
TAS14-61_02	3.81	10.07	1.27	6.60	1.15	2.71	0.28	1.69	0.25	5.68	6.09	0.13	0.01	0.01	3.83	3.74	*****	10.79	3.20
TAS14-61_03	3.68	9.81	1.31	6.48	1.09	2.64	0.28	1.72	0.23	5.69	6.20	0.09	0.02	*****	3.83	3.67	0.01	11.01	3.30
TAS14-62_01	3.77	10.47	1.33	6.59	1.19	2.75	0.35	1.89	0.26	5.96	6.28	0.04	*****	0.01	3.81	3.67	*****	11.22	3.07
TAS14-62_02	3.87	10.71	1.33	7.02	1.15	2.65	0.33	1.88	0.26	6.03	6.18	0.09	0.00	0.04	4.12	3.70	0.01	11.06	3.08
TAS14-62_03	3.82	10.36	1.37	6.86	1.15	2.84	0.34	1.96	0.23	6.22	6.42	0.06	0.02	*****	4.23	3.93	0.02	11.60	3.28
TAS14-63_01	3.54	9.90	1.27	6.47	1.10	2.65	0.30	1.81	0.22	5.55	5.79	6.53	0.02	0.01	3.45	3.34	0.01	10.58	2.96
TAS14-63_02	3.82	10.59	1.35	6.80	1.11	2.77	0.32	1.83	0.24	5.93	6.29	6.91	0.01	0.02	4.23	3.80	0.03	11.19	3.11
TAS14-63_03	3.66	10.13	1.27	6.50	1.12	2.64	0.30	1.85	0.21	5.62	6.23	7.44	0.02	0.03	3.96	3.58	0.02	11.40	3.04
TAS14-64_01	1.02	4.10	0.66	4.34	0.95	2.87	0.38	3.05	0.45	3.41	0.37	3.10	*****	0.28	6.32	5.90	0.01	4.21	1.11
TAS14-64_02	0.96	3.93	0.67	4.47	0.94	2.86	0.38	2.91	0.43	3.26	0.40	3.03	*****	0.15	6.13	5.83	0.03	4.29	1.09
TAS14-64_03	0.99	3.74	0.67	4.30	0.91	2.73	0.38	2.83	0.45	3.13	0.41	3.02	0.02	0.18	6.61	6.10	0.01	4.19	1.14
TAS14-65_01	1.40	4.64	0.70	4.42	0.81	2.20	0.31	2.08	0.29	3.05	0.80	0.26	0.02	0.04	2.58	2.27	0.02	2.05	0.58
TAS14-65_02	1.39	4.71	0.73	4.42	0.87	2.22	0.32	1.89	0.27	3.08	0.85	0.22	0.02	0.02	2.52	2.34	0.04	2.17	0.63
TAS14-65_03	1.40	4.21	0.72	4.21	0.82	2.23	0.27	1.74	0.23	2.95	0.79	0.24	0.02	0.04	2.47	2.33	0.01	2.07	0.58
TAS14-66_01	2.21	6.38	0.93	4.90	0.93	2.29	0.28	1.54	0.23	4.62	2.26	0.40	*****	0.03	3.15	3.03	0.02	4.15	1.23
TAS14-66_02	2.24	6.76	0.99	5.21	0.93	2.25	0.30	1.68	0.24	4.67	2.33	0.36	*****	0.05	3.63	3.20	0.04	4.25	1.24
TAS14-66_03	2.18	6.88	0.93	5.13	0.93	2.21	0.34	1.74	0.23	4.83	2.45	0.37	0.00	0.02	3.73	3.46	0.03	4.46	1.16
TAS14-67_01	1.52	4.25	0.75	4.13	0.86	2.24	0.31	1.44	0.27	2.91	0.75	0.20	0.03	0.01	1.29	1.18	0.02	1.37	1.00
TAS14-67_02	1.54	4.68	0.75	4.46	0.83	2.23	0.28	1.80	0.26	2.93	0.69	0.24	*****	0.00	1.27	1.16	0.00	1.42	0.95
TAS14-67_03	1.39	4.28	0.64	4.08	0.75	2.02	0.26	1.71	0.24	2.80	0.68	0.22	*****	0.01	1.26	1.17	0.03	1.31	0.93
TAS14-68_01	1.36	4.67	0.72	4.19	0.92	2.37	0.31	2.07	0.31	2.63	0.73	0.30	0.00	*****	1.57	1.53	0.03	1.88	0.44
TAS14-68_02	1.36	4.74	0.73	4.48	0.85	2.26	0.29	1.81	0.27	2.53	0.68	0.30	*****	0.04	1.72	1.64	0.01	1.84	0.42
TAS14-68_03	1.32	4.48	0.67	4.10	0.84	2.24	0.26	1.82	0.89	2.29	0.70	0.25	*****	0.02	1.72	1.57	0.05	1.88	0.43
TAS14-69_01	1.59	5.17	0.80	4.56	0.91	2.30	0.30	1.95	0.27	3.12	0.86	0.30	*****	0.03	1.62	1.43	*****	2.01	1.08
TAS14-69_02	1.70	5.46	0.85	4.70	0.89	2.38	0.31	1.91	0.24	3.17	0.95	0.42	0.01	0.04	1.82	1.58	0.00	2.08	0.51
TAS14-69_03	1.69	5.31	0.77	4.82	0.92	2.43	0.30	1.91	0.28	3.31	0.93	0.38	0.01	*****	1.66	3.32	0.02	2.20	0.64
TAS14-70_01	0.62	2.68	0.44	2.78	0.61	1.80	0.26	1.90	0.27	1.95	0.24	0.29	0.01	0.08	3.56	3.26	0.02	2.68	0.67
TAS14-70_02	0.65	2.61	0.39	2.80	0.65	1.84	0.25	1.78	0.27	1.83	0.25	0.31	0.02	0.09	3.74	3.55	0.01	2.56	0.66
TAS14-70_03	0.61	2.42	0.40	2.85	0.62	1.82	0.27	1.79	0.28	1.89	0.26	0.28	0.03	2.08	3.93	3.63	******	2.64	0.66
TAS14-71_01	0.78	3.18	0.56	3.67	0.80	2.20	0.35	2.37	0.36	2.59	0.32	6.56	0.02	0.10	4.64	4.38	0.04	3.29	0.84
TAS14-71_02	0.85	3.17	0.55	3.50	0.79	2.33	0.35	2.31	0.35	2.54	0.36	7.24	0.02	0.07	4.90	4.43	0.07	3.46	0.87
TAS14-71_03	0.73	3.32	0.53	3.51	0.72	2.32	0.34	2.31	0.34	2.49	0.30	7.28	0.01	0.13	5.04	4.72	0.08	3.33	0.81
TAS14-72_01	1.11	3.80	0.62	3.90	0.76	2.24	0.33	2.01	0.31	2.29	0.69	0.58	*****	0.04	1.95	1.82	0.02	2.08	0.51
TAS14-72_02	1.12	3.79	0.59	3.78	0.83	2.23	0.31	1.97	0.28	2.02	0.66	0.27	*****	0.00	1.57	1.52	0.01	1.98	0.50
TAS14-72_03	1.18	3.81	0.61	3.82	0.76	2.19	0.32	1.97	0.32	2.19	0.73	0.31	0.01	0.01	1.74	1.77	0.00	2.02	0.49
TAS14-73_01	3.39	9.00	1.15	5.93	1.00	2.18	0.25	1.53	0.19	7.58	3.50	0.56	0.04	*****	2.73	2.78	0.04	5.37	1.38
TAS14-73_02	3.47	9.41	1.25	6.10	1.02	2.30	0.26	1.52	0.19	7.96	3.74	0.67	*****	*****	2.88	2.54	0.01	5.52	0.55
TAS14-73_03	3.40	9.32	1.20	6.19	1.00	2.26	0.25	1.51	0.19	7.85	3.66	0.70	*****	*****	3.00	2.80	0.02	5.43	1.56

(*continued on next page*)

Table 4 (*continued*)

Sample	Eu	Gd	Tb	Dy	Ho	Er	Tm	Yb	Lu	Hf	Ta	W	Re	Tl	Pb206	Pb208	Bi	Th	U
TAS14-74_01	4.05	10.95	1.43	7.54	1.27	3.28	0.40	2.21	0.29	8.47	6.10	32.63	*****	0.02	3.84	3.76	0.01	9.56	3.45
TAS14-74_02	4.03	11.11	1.47	7.46	1.34	3.11	0.38	2.31	0.33	8.64	6.20	34.25	*****	*****	4.04	3.84	48.51	9.98	3.58
TAS14-74_03	4.04	10.88	1.48	7.55	1.32	3.02	0.35	2.06	0.26	8.31	6.29	34.29	0.03	*****	4.23	3.78	0.03	9.73	3.62
TAS14-75_01	1.34	4.49	0.71	3.93	0.74	1.94	0.24	1.57	0.21	3.22	1.07	1.18	*****	0.04	2.92	2.56	0.04	2.45	1.23
TAS14-75_02	1.39	4.44	0.69	3.94	0.74	1.88	0.27	1.76	0.22	3.19	1.03	0.53	*****	0.02	3.18	3.02	0.02	2.48	1.26
TAS14-75_03	1.40	4.47	0.69	4.09	0.74	1.91	0.24	1.65	0.22	3.06	1.03	0.52	*****	0.03	3.23	2.92	0.06	2.46	1.23
TAS14-76_01	1.43	4.41	0.67	3.86	0.78	1.92	0.26	1.56	0.23	2.97	0.82	34.54	*****	0.01	2.59	2.31	0.02	2.03	0.92
TAS14-76_02	1.31	4.42	0.69	3.75	0.73	1.95	0.25	1.61	0.24	2.99	0.83	36.29	0.01	0.02	2.57	2.45	0.02	1.94	0.96
TAS14-76_03	1.39	4.40	0.65	3.67	0.72	2.02	0.25	1.65	0.22	2.77	0.84	35.78	0.02	0.01	2.76	2.53	0.03	1.97	0.88
TAS14-77_01	1.80	5.12	0.72	4.21	0.79	2.01	0.24	1.58	0.22	3.06	1.12	21.27	*****	0.01	2.09	1.98	*****	2.60	0.68
TAS14-77_02	1.79	5.41	0.79	4.47	0.78	2.00	0.25	1.58	0.24	3.25	1.20	21.73	0.09	0.01	2.30	1.94	*****	2.82	0.71
TAS14-77_03	1.82	5.01	0.73	4.18	0.73	1.78	0.23	1.60	0.22	3.01	1.17	22.40	0.01	0.01	2.11	6.78	0.04	2.65	0.70
TAS14-78_01	1.36	4.43	0.70	3.97	0.80	2.02	0.27	1.70	0.22	3.16	1.01	1.25	*****	0.03	3.29	2.77	0.04	2.41	1.19
TAS14-78_02	1.44	4.30	0.68	3.72	0.72	1.98	0.26	1.61	0.25	3.13	1.03	0.61	0.01	0.03	3.21	2.81	0.07	2.44	1.15
TAS14-78_03	1.49	4.67	0.68	4.43	0.80	2.12	0.24	1.70	0.24	3.37	1.07	0.39	*****	0.04	3.60	3.03	0.02	2.43	1.22
TAS14-79_01	0.80	3.62	0.58	3.97	0.78	2.54	0.36	2.51	0.39	2.58	0.34	0.91	0.00	0.12	5.14	5.05	0.01	3.53	0.86
TAS14-79_02	0.79	3.38	0.58	3.86	0.82	2.29	0.35	2.29	0.34	2.75	0.31	0.96	0.00	0.18	4.94	4.75	0.03	3.44	0.81
TAS14-79_03	0.83	3.21	0.53	3.79	0.84	2.38	0.34	2.41	0.37	2.68	0.32	0.95	0.04	0.16	5.47	5.16	0.02	3.44	0.86
TAS14-80_01	1.74	5.46	0.85	4.42	0.85	2.18	0.27	1.64	0.23	3.36	1.24	43.63	*****	*****	2.20	1.94	0.01	2.52	0.73
TAS14-80_02	1.75	4.90	0.70	4.12	0.72	1.92	0.23	1.45	0.20	3.10	1.12	40.82	0.02	0.01	1.88	1.67	0.01	2.24	1.45
TAS14-80_03	1.86	5.54	0.82	4.44	0.83	2.27	0.27	1.71	0.24	3.37	1.35	45.07	0.03	*****	2.18	1.89	*****	2.63	0.64

McLennan, 1985) and in contrast to the silica-undersaturated Cenozoic suite, this upper continental crust signature is shown in positive K and Pb anomalies and negative Nb and Ta.

4.2. Sr, Nd and Pb isotopes

Isotopic compositions for Sr, Nd and Pb in a subgroup of 13 Cenozoic samples are shown in Table 5. This subgroup was selected to cover a wide spread of MgO content, ages and to fill any geographical gaps in the literature data. $^{87}Sr/^{86}Sr$ isotope ratios range from 0.702681 to 0.705544, $^{143}Nd/^{144}Nd$ ratios range between 0.512635 and 0.513013, $^{206}Pb/^{204}Pb$ ratios range from 19.04 to 19.58, $^{207}Pb/^{204}Pb$ ratios range from 15.41 to 15.64 and $^{208}Pb/^{204}Pb$ ratios range between 38.33 and 39.69 (Table 5). Isotope ratios were corrected to initial values using published radiometric ages in their vicinity (Vasconcelos et al. (2008) and references therein, Table 5). Of these used ages, sample TAS14-67, a vesicular lava flow from the Lyell Highway (Big Snake Hill) was presumed the oldest with an age of ~40 Ma and TAS14-36, a lava flow from Mt. Hicks road north of Yolla, the youngest with a presumed age of ~12 Ma. Initial Sr isotope compositions are indistinguishable from measured values with differences ranging from 8.6 E−10% to 8.3 E−9% from the measured isotope composition. Nd initial isotope compositions vary 0.002% to 0.008% from measured isotope compositions. Initial εNd values are all positive and range from 0.57 to 7.69 (Table 5).

Isotope data measured for this study fall well within previously published data for Cenozoic volcanism in Tasmania (Corbett et al., 2014 and references therein). On a $^{143}Nd/^{144}Nd$ versus $^{87}Sr/^{86}Sr$ plot the data shows a spread along the 'mantle array', spanning from depleted mantle towards enriched mantle (Fig. 8). Three samples from previously published studies and one from this study plot towards the right of the mantle array and have higher $^{87}Sr/^{86}Sr$ value for similar $^{143}Nd/^{144}Nd$ values. This could be due to alteration as Sr is more mobile during weathering and there is no clear spatial relationship between those samples that suggests a different origin. Compared with mainland Australia, the majority of Tasmanian Cenozoic samples overlap the Older and Newer Volcanic Province fields in Victoria across the Bass Strait, and extend towards higher $^{87}Sr/^{86}Sr$ and lower $^{143}Nd/^{144}Nd$ (Fig. 8). Pb isotopes of the Cenozoic Tasmanian samples (Fig. 9) mainly plot along and above the Northern Hemisphere Reference Line (NHRL, Hart (1984)). Compared to the rest of the Eastern Australian Cenozoic Magmatic Province, the Tasmanian Cenozoic samples tend towards a HIMU-like mantle endmember (Fig. 10).

4.3. $^{39}Ar/^{40}Ar$ analyses

A total of six samples were analysed for $^{39}Ar/^{40}Ar$ (Table 6). Of these six samples, only two show the formation age. Sample TAS14-42 shows a plateau age of 26.5 ± 1.12 Ma and sample TAS14-69 shows a plateau age of 179.6 ± 0.71 Ma. Additionally, sample TAS14-68 shows two steps in the age spectrum, one at 43.6 ± 2.69 Ma and one at 191.6 ± 5.42 Ma (Fig. 11). Other samples analysed show either excess Ar or plagioclase crystals were too contaminated for analysis.

The age obtained for sample TAS14-42 falls within the previously determined age range of the Cenozoic basalts in this area. Several ages are available for an area 69 km NNW of the location of TAS14-42 with an olivine nephelinite dated at 26.4 ± 0.2 Ma (1σ) (Sutherland et al., 1996) and a melilite nephelinite dated at 26.3 ± 0.3 Ma (1σ) (Sutherland and Wellman, 1986). A drill hole sample 33 km NNE of TAS14-42 was dated at 26.7 ± 0.3 Ma (1σ) (MacPhail and Hill, 1994). Additional work is necessary to interpret the two steps in the age spectrum for sample TAS14-68.

The Jurassic age for sample TAS14-69 overlaps within error of published ages of the Jurassic dolerites in Tasmania. K–Ar ages of 175 ± 8 Ma (Schmidt and McDougall (1977), recalculated according to the decay constants of Steiger and Jager (1977)), Re–Os ages of

Table 5
Sr-Nd-Pb isotopes for Cenozoic mafic rocks in Tasmania and standards. * denotes standard reference values by (i) Elburg et al. (2005) (ii) Raczek et al. (2003) (iii) IsotopX Phoenix.

Sample	presumed age (Ma)	Sr (ppm)	Nd (ppm)	Sm (ppm)	Pb (ppm)	$^{87}Sr/^{86}Sr$	2σ	$^{143}Nd/^{144}Nd$	2σ	$^{206}Pb/^{204}Pb$	$^{207}Pb/^{204}Pb$	$^{208}Pb/^{204}Pb$
TAS14-01	30	572	26.40	5.60	5	0.704075	2.3E−05	0.512790	1.9E−05			
TAS14-21	15	1220	67.66	13.26	4	0.702681	3.3E−05	0.513025	2.3E−05	19.189	15.555	38.619
TAS14-31	13	762	34.96	7.09	3	0.703132	2.6E−05	0.512936	1.6E−05	19.198	15.580	38.889
TAS14-31										19.061	15.414	38.334
TAS14-36	12	472	21.89	4.97	2	0.703660	4.6E−05	0.512854	1.9E−05	19.265	15.630	39.136
TAS14-36	12	472	21.89	4.97	2	0.703669	3.6E−05	0.512854				
TAS14-41	25	346	20.07	4.74	3	0.705544	2.5E−05	0.512659	1.5E−05	19.263	15.641	39.152
TAS14-42	27	298	17.15	4.32	2	0.703836	3.3E−05	0.512798	1.9E−05	19.580	15.640	39.689
TAS14-42	27	298	17.15	4.32	2	0.703845	2.8E−05	0.512798				
TAS14-46	26	613	30.09	6.51	2	0.703352	3.0E−05	0.512917	1.8E−05	19.386	15.606	39.067
TAS14-47	24	424	25.70	6.24	2	0.703231	3.6E−05	0.512935	1.9E−05	19.170	15.586	38.894
TAS14-48	23	402	19.43	4.49	2	0.704125	4.1E−05	0.512806	2.3E−05	19.309	15.626	39.300
TAS14-50	23	440	24.61	5.79	2	0.704051	3.0E−05	0.512875	2.0E−05	19.036	15.603	39.005
TAS14-61	30	1440	64.05	11.31	4	0.703508	3.4E−05	0.512957	1.7E−05	19.523	15.587	39.141
TAS14-61	30	1440	64.05	11.31	4	0.703518	4.7E−05	0.512957	0.0E+00	19.516	15.580	39.125
TAS14-61										19.501	15.584	39.170
TAS14-67	40	246	15.10	3.93	2	0.704402	2.7E−05	0.512812	1.7E−05	19.316	15.644	39.290
TAS14-80	24	397	22.76	5.15	2	0.703588	2.7E−05	0.512910	2.6E−05	19.244	15.623	39.043
SRM 987						0.710224	3.1E−05					
SRM 987						0.710232	3.4E−05					
SRM 987						0.710231	3.6E−05					
*SRM 987**						*0.710244* (i)						
BCR-2						0.704996	2.9E−05	0.512628	1.8E−05	18.778	15.630	38.740
BCR-2						0.704989	2.9E−05	0.512629	1.7E−05	18.781	15.631	38.741
BCR-2										18.736	15.625	38.689
*BCR-2**						*0.705003* (i)		*0.512633* (ii)		*18.758* (i)	*15.628* (i)	*38.738* (i)
BHVO-2 68						0.703473	3.4E−05	0.512978	3.2E−05			
BHVO-2 68						0.703474	3.3E−05	0.512972	1.9E−05			
*BHVO-2**						*0.703469* (i)		*0.512957* (ii)				
JNdi 150617a								0.512139	1.4E−04			
JNdi 150617a								0.512114	2.2E−05			
JNdi 150617b								0.512105	2.6E−05			
*Jndi**								*0.512108* (iii)				

175.1 ± 5.4 Ma (2σ) (Brauns et al., 2000) and 177.3 ± 3.5 Ma (Hergt and Brauns, 2001) and ID-TIMS single crystal U−Pb zircon and baddeleyite ages of 182.90 ± 0.21 Ma (Ivanov et al., 2017), have been reported for the Tasmanian Jurassic dolerites.

5. Discussion

5.1. Earlier proposed mantle sources and petrogenesis

The origin of Cenozoic magmatic activity in eastern Australia, and Tasmania in particular, has been a longstanding topic of debate with competing theories about the relative roles of asthenospheric and lithospheric sources (e.g. Adam and Green, 2011; Sun et al., 1989). Early attempts at major and trace element modelling explained the compositional diversity by suggesting that the olivine melilitites and nephelinites were extracted from an enriched mantle source by very low degrees of melting (0.5–4%), whereas a higher degree of melting (> 20%) was suggested for the primitive tholeiites (Frey et al., 1978). Subsequent models which included consideration of the large range of Nd and Sr isotopic signatures, suggested a mixing model between a plume and a MORB-type mantle at the sub-continental lithospheric mantle (SCLM) explaining variations in both the Newer Volcanic Province of Victoria and the primitive Tasmanian alkaline basalts (McDonough et al., 1985). Based on Pb isotopes, this MORB-type source is believed to be of Pacific-MORB type asthenosphere, as suggested by samples from eastern Australia (Zhang et al., 1999) and seafloor samples to the west of Tasmania (Lanyon et al., 1995; Pyle et al., 1995). However, previous discussions (e.g. Adam, 1990; Adam and Green, 2011) demonstrate that the origin of the extremely undersaturated melts provides a conundrum as it is impossible to obtain the trace element pattern observed here by even the smallest percentage of melting of a MORB-like source. The presence of residual phlogopite in the SCLM source together with low-degree partial melting was suggested to explain the observed incompatible element signatures of these basalts (Sun et al., 1989). A local study of the highly undersaturated Oatland Volcanics (Adam and Green, 2011) suggests that the basalts are the result of near-solidus open-system melting in the asthenosphere, enriching both residual melts and host rock in incompatible elements during ascent and resulting in decompression melting of incompatible-element-enriched peridotite at shallower depths.

Geodynamically, the region is still not fully understood. Thermal anomalies that drove the Cenozoic magmatism in Tasmania have been linked into the larger melting processes in eastern Australia. It has been suggested that the passage over the Balleny plume (Crawford et al., 1997; Sun et al., 1989), asthenospheric upwellings associated with the Tasman Sea rifting (Sutherland, 1991), or upwelling related to the failed spreading in the Bass Basin (Sutherland et al., 2002) could have triggered the magmatism in Tasmania.

Table 6
Ar^{39}/Ar^{40} analyses for selected samples.

Foil B1 Sample TAS14-36, Plagioclase

Temp (°C)	Ar^{36} (mol)	err (%)	Ar^{37} (mol)	err (%)	Ar^{38} (mol)	err (%)	Ar^{39} (mol)	err (%)	Ar^{40} (mol)	err (%)	% Ar^{40*}	Ar^{40*}/Ar^{39}(K)	Cumulative Ar^{39}(%)	Calculated Age (Ma ± 1 s.d.)	Ca/K	Cl/K
450	2.70E-16	2.83	9.27E-17	5.95	4.88E-17	3.57	1.96E-16	2.76	7.30E-14	2.78	-9.3	0	0.19	0 ± 43.49	9.02E-01	-2.71E-01
500	1.08E-15	1.14	1.70E-15	1.42	2.53E-16	1.29	1.62E-15	0.95	3.54E-13	1.01	10.1	21.99	1.77	60.47 ± 8.49	1.99E+00	2.37E-01
540	3.11E-15	0.67	8.35E-15	1.29	7.20E-16	0.69	7.30E-15	0.32	1.87E-12	0.46	50.9	130.83	8.86	333.16 ± 3.36	2.18E+00	8.07E-02
540	1.62E-15	0.9	4.90E-15	0.75	3.90E-16	3.73	4.32E-15	0.14	5.13E-13	0.41	6.6	7.88	13.05	21.9 ± 3.08	2.16E+00	9.64E-02
570	1.06E-15	1.33	4.03E-15	1.32	2.96E-16	4.24	3.86E-15	0.93	5.60E-13	0.95	44.2	64.27	16.79	171.35 ± 4.45	1.99E+00	1.64E-01
570	9.25E-16	0.89	4.62E-15	0.78	2.67E-16	2.09	3.80E-15	0.29	3.53E-13	0.38	22.5	20.95	20.48	57.67 ± 1.98	2.31E+00	1.54E-01
600	6.92E-16	0.91	4.28E-15	0.86	1.91E-16	2.31	3.34E-15	0.38	6.09E-13	0.45	66.4	121.28	23.72	310.82 ± 2.34	2.44E+00	7.91E-02
600	6.36E-16	0.93	5.56E-15	1.01	1.70E-16	2.77	3.63E-15	0.5	3.06E-13	0.64	38.6	32.54	27.24	88.78 ± 1.93	2.91E+00	2.38E-02
630	7.20E-16	1.17	7.34E-15	1.43	2.04E-16	8.54	4.22E-15	0.59	8.25E-13	0.65	74.2	145.37	31.33	366.64 ± 3.2	3.31E+00	5.40E-02
630	4.94E-16	0.63	7.63E-15	0.49	1.81E-16	1.85	4.08E-15	0.25	3.12E-13	0.49	53.2	40.73	35.29	110.46 ± 1.15	3.56E+00	1.20E-01
660	5.95E-16	1.84	9.54E-15	1.66	1.76E-16	9.44	5.09E-15	1.14	6.87E-13	1.18	74.4	100.65	40.23	261.59 ± 4.14	3.57E+00	9.64E-03
660	4.04E-16	0.76	8.73E-15	0.64	1.29E-16	1.04	4.32E-15	0.42	3.15E-13	0.54	62.2	45.56	44.42	123.13 ± 1.17	3.85E+00	5.68E-03
690	3.68E-16	0.73	1.10E-14	1.43	1.40E-16	5.93	4.95E-15	0.39	4.20E-13	0.5	74.2	63.2	49.21	168.63 ± 1.16	4.22E+00	2.95E-02
690	3.04E-16	1.15	1.19E-14	0.62	1.23E-16	0.67	4.43E-15	0.3	3.15E-13	0.5	71.5	50.96	53.51	137.18 ± 1.1	5.13E+00	3.66E-02
720	2.81E-16	0.67	1.13E-14	1.15	1.15E-16	0.78	3.90E-15	0.3	3.07E-13	0.51	73.1	57.76	57.28	154.71 ± 1.09	5.52E+00	4.99E-02
720	2.24E-16	0.87	9.88E-15	0.92	9.02E-17	1.37	3.57E-15	0.43	2.89E-13	0.47	77.1	62.48	60.74	166.78 ± 1.06	5.27E+00	1.97E-02
750	1.95E-16	1.02	8.27E-15	0.94	7.76E-17	1.02	3.12E-15	0.42	2.76E-13	0.52	79.2	70.09	63.77	186.09 ± 1.25	5.04E+00	1.53E-02
750	1.69E-16	1.51	6.07E-15	1.2	7.14E-17	3.83	2.87E-15	0.34	2.54E-13	0.46	80.4	71.42	66.55	189.44 ± 1.22	4.03E+00	2.34E-02
780	1.54E-16	0.98	5.34E-15	1.05	5.97E-17	5.01	2.43E-15	0.44	2.62E-13	0.56	82.7	89.29	68.91	233.89 ± 1.54	4.18E+00	9.28E-03
780	1.07E-16	1.12	4.15E-15	0.65	4.85E-17	2.66	2.13E-15	0.49	2.03E-13	0.6	84.5	80.74	70.98	212.76 ± 1.48	3.72E+00	1.84E-02
820	1.29E-16	1.29	4.51E-15	1.32	5.36E-17	2.04	2.39E-15	0.74	2.85E-13	0.83	86.7	103.51	73.29	268.48 ± 2.43	3.59E+00	5.57E-03
820	7.36E-17	2.25	3.02E-15	0.82	3.68E-17	5.76	1.76E-15	0.54	1.74E-13	0.64	87.5	86.52	75	227.07 ± 1.69	3.27E+00	1.46E-02
860	9.02E-17	1.56	3.01E-15	1.75	4.57E-17	1.31	1.87E-15	0.32	2.11E-13	0.42	87.4	98.65	76.81	256.73 ± 1.27	3.06E+00	4.28E-02
860	5.23E-17	5.05	2.10E-15	4.1	3.97E-17	5.47	2.13E-15	1.58	2.19E-13	2.5	92.9	95.69	78.88	249.54 ± 6.32	1.87E+00	2.59E-02
900	4.61E-16	1.02	2.29E-15	1.59	1.11E-16	1.49	1.63E-15	0.67	2.90E-13	0.73	52.9	93.96	80.47	245.33 ± 3.78	2.67E+00	3.71E-02
950	8.39E-16	0.63	4.51E-15	1.27	2.06E-16	1.23	3.54E-15	0.25	6.27E-13	0.32	60.5	107.11	83.9	277.13 ± 1.73	2.42E+00	2.28E-02
1000	2.48E-16	0.84	5.85E-15	0.64	1.07E-16	1.62	4.24E-15	0.17	9.48E-13	0.31	92.3	206.55	88.02	501.16 ± 1.52	2.62E+00	2.86E-02
1040	5.05E-16	1.61	6.77E-15	0.87	1.78E-16	2.88	3.95E-15	0.52	2.53E-12	0.6	94.1	604.49	91.85	1192.86 ± 5.67	3.26E+00	1.11E-01
1080	7.07E-16	1.09	7.69E-15	1.66	2.43E-16	5.57	4.66E-15	0.93	4.10E-12	1.01	94.9	835.9	96.37	1499.39 ± 10.85	3.14E+00	1.45E-01
1110	2.62E-16	2.65	6.13E-15	2.46	8.47E-17	7.32	1.96E-15	1.52	1.50E-12	1.58	94.9	729.52	98.26	1364.9 ± 16.01	5.96E+00	7.71E-02
1150	9.02E-17	4.35	4.80E-15	3.1	2.94E-17	18.85	4.61E-16	2.32	2.73E-13	2.38	90.3	539.36	98.71	1096.29 ± 21.76	2.00E+01	1.88E-01
1200	1.39E-16	1.8	9.74E-15	1.06	3.81E-17	2.37	4.89E-16	0.7	3.16E-13	0.81	87.1	573.49	99.17	1147.53 ± 8.09	3.86E+01	1.59E-01
1300	2.66E-16	1.68	1.66E-14	0.8	8.87E-17	2.1	8.39E-16	0.67	8.15E-13	0.71	90.4	896.1	99.97	1571.27 ± 8.3	3.82E+01	4.23E-01
1450	6.90E-17	4.48	4.75E-17	19.04	1.48E-17	9.57	2.91E-17	4.04	1.54E-13	4.07	86.8	4586.4	100	3776.14 ± 74.9	3.10E+00	6.26E-01
Total	1.73E-14		2.12E-13		5.03E-15		1.03E-13		2.15E-11			159.692		399.05 ± 3.37		

Lambda K40 = 5.5430E-10 J = 1.5503E-3; %error J = 0.3525

Foil B2 Sample TAS14-42, Plagioclase

Temp (°C)	Ar^{36} (mol)	err (%)	Ar^{37} (mol)	err (%)	Ar^{38} (mol)	err (%)	Ar^{39} (mol)	err (%)	Ar^{40} (mol)	err (%)	% Ar^{40*}	Ar^{40*}/Ar^{39}(K)	Cumulative Ar^{39}(%)	Calculated Age (Ma ± 1 s.d.)	Ca/K	Cl/K
500	5.66E-17	2.28	9.09E-16	2.99	1.29E-17	6.27	5.38E-17	1.94	1.77E-14	1.97	5.5	18.41	0.16	51.01 ± 26.2	3.27E+01	3.83E-01
500	9.63E-17	1.36	1.91E-15	1.42	2.12E-17	5.3	1.39E-16	0.93	3.08E-14	1.07	7.6	17.13	0.59	47.5 ± 10.02	2.65E+01	1.34E-01
550	1.38E-16	1.27	5.31E-15	1.25	3.50E-17	3.21	3.78E-16	1.12	4.28E-14	1.14	5.3	6.11	1.74	17.09 ± 5.23	2.70E+01	1.52E-01
550	8.98E-17	1.59	3.20E-15	1.97	2.27E-17	5.96	2.40E-16	1.4	3.14E-14	1.45	15.9	21.04	2.47	58.18 ± 7.05	2.57E+01	1.55E-01
600	1.12E-16	1.83	9.03E-15	1.02	3.11E-17	6.28	6.44E-16	0.28	4.00E-14	0.61	17.8	11.24	4.43	31.3 ± 2.81	2.70E+01	4.75E-02
600	1.15E-16	0.79	8.86E-15	0.74	3.16E-17	1.35	6.07E-16	0.48	4.12E-14	0.61	18.1	12.45	6.28	34.65 ± 1.68	2.82E+01	5.93E-02
650	1.30E-16	2.39	2.70E-14	0.9	5.96E-17	1.96	1.66E-15	0.57	5.44E-14	0.65	30.7	10.27	11.31	28.62 ± 1.65	3.15E+01	1.18E-01
650	1.09E-16	1.06	2.53E-14	0.44	5.82E-17	3.24	1.41E-15	0.19	4.47E-14	0.49	30	9.71	15.57	27.08 ± 0.8	3.49E+01	1.88E-01
700	1.13E-16	1.39	6.22E-14	0.76	9.60E-17	1.52	3.26E-15	0.68	6.19E-14	0.72	49.3	9.53	25.47	26.59 ± 0.55	3.69E+01	1.39E-01

(*continued on next page*)

Table 6 (*continued*)

Foil B2 Sample TAS14-42, Plagioclase

Temp (°C)	Ar^{36} (mol)	err (%)	Ar^{37} (mol)	err (%)	Ar^{38} (mol)	err (%)	Ar^{39} (mol)	err (%)	Ar^{40} (mol)	err (%)	% Ar^{40_R}	Ar^{40_R}/Ar^{39}(K)	Cumulative Ar^{39}(%)	Calculated Age (Ma ± 1 s.d.)	Ca/K	Cl/K
700	8.02E-17	1.11	4.36E-14	0.48	6.25E-17	2.75	2.27E-15	0.13	4.29E-14	0.28	48.2	9.3	32.34	25.95 ± 0.35	3.73E+01	1.15E-01
750	9.76E-17	0.8	9.41E-14	0.64	8.19E-17	2.92	4.96E-15	0.5	7.09E-14	0.58	63.7	9.27	47.38	25.86 ± 0.26	3.67E+01	1.61E-02
750	5.93E-17	1.94	4.40E-14	1.29	3.87E-17	3.2	2.24E-15	0.74	3.68E-14	0.91	56.4	9.42	54.18	26.27 ± 0.59	3.79E+01	9.82E-03
800	6.69E-17	2.54	5.05E-14	0.85	4.57E-17	2.38	2.77E-15	0.57	4.39E-14	0.6	58.8	9.48	62.59	26.45 ± 0.57	3.52E+01	5.54E-03
800	3.58E-17	3.79	1.65E-14	0.76	1.97E-17	1.67	1.02E-15	0.58	1.94E-14	0.61	48.3	9.38	65.68	26.17 ± 1.14	3.14E+01	1.54E-02
850	3.96E-17	0.9	2.05E-14	0.63	2.61E-17	3.11	1.39E-15	0.46	2.41E-14	0.56	54.1	9.51	69.91	26.52 ± 0.34	2.84E+01	2.22E-02
850	2.25E-17	2.62	8.55E-15	1.24	1.36E-17	10.29	6.14E-16	0.73	1.21E-14	0.87	47.5	9.53	71.78	26.57 ± 0.92	2.68E+01	4.39E-02
900	3.10E-17	3.06	1.86E-14	0.93	2.33E-17	3.35	1.27E-15	0.12	2.07E-14	0.32	58.7	9.69	75.66	27.02 ± 0.63	2.81E+01	2.59E-02
900	1.78E-17	3.08	6.68E-15	1.24	1.11E-17	11.94	4.81E-16	0.9	9.40E-15	1.07	46.3	9.16	77.12	25.55 ± 1.1	2.68E+01	5.58E-02
950	2.68F-17	3.23	9.83F-15	0.82	1.70F-17	4.18	8.83F-16	0.33	1.58E-14	0.48	52	9.43	79.82	26.31 ± 0.84	2.14F+01	2.37F-02
950	1.13E-17	7.86	3.65E-15	1.4	6.39E-18	13.93	3.64E-16	0.91	6.63E-15	0.96	51.6	9.49	80.93	26.47 ± 2.05	1.93E+01	8.08E-04
1000	2.15E-17	2.63	9.26E-15	0.99	1.24E-17	10.24	7.03E-16	0.59	1.27E-14	0.67	52.3	9.59	83.08	26.76 ± 0.74	2.54E+01	2.49E-03
1000	1.26E-17	4.8	4.47E-15	0.98	6.22E-18	18.07	2.56E-16	0.6	5.96E-15	0.65	40.1	9.5	83.85	26.49 ± 1.98	3.38E+01	4.35E-02
1050	2.45E-17	3.73	1.64E-14	0.9	1.58E-17	7.69	7.85E-16	0.63	1.43E-14	0.71	53.1	9.89	86.23	27.57 ± 1.02	4.05E+01	3.42E-02
1050	1.32E-17	15.27	8.23E-15	1.42	7.13E-18	19.17	3.69E-16	1.21	7.11E-15	1.26	49	9.66	87.34	26.94 ± 4.52	4.33E+01	1.45E-02
1100	2.98E-17	2.81	1.78E-14	1.12	1.80E-17	7.55	7.06E-16	0.73	1.48E-14	0.86	44.4	9.52	89.47	26.56 ± 1.09	4.90E+01	7.55E-02
1100	1.16E-17	2.21	8.03E-15	1.51	9.30E-18	16.95	3.38E-16	0.59	7.17E-15	0.7	56.1	12.19	90.49	33.94 ± 0.74	4.62E+01	1.19E-01
1150	2.89F-17	3.74	1.72F-14	0.92	1.45F-17	7.28	6.78F-16	0.62	1.44F-14	0.7	44.4	9.64	92.53	26.89 ± 1.37	4.93F+01	2.54F-02
1200	3.79E-17	3.42	2.10E-14	0.78	1.90E-17	2.6	8.65E-16	0.15	1.89E-14	0.48	44.5	9.96	95.14	27.78 ± 1.26	4.72E+01	2.92E-02
1300	6.29E-17	1.26	3.14E-14	0.82	2.75E-17	7.48	1.25E-15	0.39	3.12E-14	0.45	43.7	11.14	98.92	31.04 ± 0.6	4.88E+01	1.43E-02
1450	4.67E-17	1.29	9.18E-15	0.93	1.53E-17	10.8	3.59E-16	0.7	2.21E-14	0.77	39	24.69	100	68.07 ± 1.85	4.98E+01	8.49E-02
Total	1.74E-15		6.03E-13		8.59E-16		3.30E-14		8.16E-13		9.955			27.76 ± 1		
Lambda K40 = 5.5430E-10 J = 1.558E-3; %error J = 0.3509																
		0.001558	5.47E-06													

Foil B3 Sample TAS14-68, Plagioclase

Temp (°C)	Ar^{36} (mol)	err (%)	Ar^{37} (mol)	err (%)	Ar^{38} (mol)	err (%)	Ar^{39} (mol)	err (%)	Ar^{40} (mol)	err (%)	% Ar^{40_R}	Ar^{40_R}/Ar^{39}(K)	Cumulative Ar^{39}(%)	Calculated Age (Ma ± 1 s.d.)	Ca/K	Cl/K
450	3.78E-17	5.6	2.39E-17	57.31	1.01E-17	15.55	2.27E-17	4.85	1.16E-14	4.86	3.6	18.56	0.18	51.6 ± 101.82	2.01E+00	1.48E+00
450	6.12E-17	3.74	2.35E-17	21.45	1.45E-17	3.18	4.35E-17	2.74	1.83E-14	2.76	1.1	4.79	0.54	13.47 ± 54.37	1.03E+00	6.93E-01
500	8.45E-17	2.71	1.54E-16	9.01	2.07E-17	5.19	1.15E-16	2.63	3.33E-14	2.64	25	72.23	1.47	193.05 ± 24.38	2.55E+00	3.68E-01
500	1.45E-16	1.1	1.28E-16	10.58	3.66E-17	2.28	2.24E-16	0.78	4.65E-14	0.97	8	16.56	3.29	46.13 ± 8.02	1.09E+00	3.65E-01
550	2.05E-16	0.95	6.40E-16	2.36	6.65E-17	3.95	5.79E-16	0.45	9.10E-14	0.49	33.5	52.66	7.98	142.75 ± 3.29	2.10E+00	4.47E-01
550	2.07E-16	1.27	5.90E-16	3.53	5.48E-17	2.57	6.67E-16	0.65	7.15E-14	0.73	14.3	15.37	13.39	42.85 ± 3.88	1.68E+00	1.45E-01
600	2.71E-16	1.05	1.30E-15	1.15	8.62E-17	2.38	1.74E-15	0.59	1.17E-13	0.64	31.7	21.41	27.49	59.4 ± 1.77	1.42E+00	1.03E-01
600	2.69E-16	1.18	1.65E-15	1.7	7.01E-17	2.03	6.88E-16	0.63	9.52E-14	0.68	16.4	22.81	33.06	63.23 ± 4.52	4.58E+00	2.01E-01
650	3.98E-16	1.04	4.06E-15	0.87	1.07E-16	1.89	9.23E-16	0.28	1.70E-13	0.46	30.6	56.56	40.52	152.89 ± 4.06	8.40E+00	2.80E-01
650	2.24E-16	1.18	4.07E-15	1.08	6.10E-17	1.01	5.53E-16	0.33	1.02E-13	0.45	35.3	65.57	44.98	176.1 ± 4.19	1.41E+01	2.73E-01
700	2.64E-16	0.77	7.93E-15	0.59	6.64E-17	0.63	7.10E-16	0.17	1.28E-13	0.26	39.4	71.86	50.68	192.13 ± 2.45	2.15E+01	1.48E-01
700	1.76E-16	0.91	6.92E-15	0.95	4.44E-17	2.4	4.91E-16	0.71	8.59E-14	0.77	39.7	70.31	54.62	188.18 ± 4.22	2.71E+01	1.39E-01
750	1.74E-16	0.94	1.06E-14	0.65	4.30E-17	2.48	6.23E-16	0.46	9.51E-14	0.52	46.4	71.96	59.59	192.39 ± 2.81	3.28E+01	6.22E-02
750	1.12E-16	1.19	8.79E-15	0.92	3.03E-17	4.03	4.65E-16	0.64	6.56E-14	0.71	50.2	72.17	63.3	192.89 ± 3.32	3.66E+01	1.04E-01
800	1.20E-16	1.57	1.10E-14	0.79	3.01E-17	6.6	5.81E-16	0.69	7.75E-14	0.8	54.5	74.09	67.93	197.77 ± 3.63	3.67E+01	1.74E-02
800	9.11E-17	1.8	8.46E-15	1	2.23E-17	2.53	3.61E-16	0.66	5.23E-14	0.7	49.1	72.8	70.79	194.49 ± 4.26	4.56E+01	3.58E-02
850	8.75E-17	1.36	8.65E-15	0.47	2.10E-17	4.79	3.85E-16	0.25	6.23E-14	0.36	59	97.68	73.85	256.45 ± 2.64	4.37E+01	4.46E-03

(*continued on next page*)

Table 6 (*continued*)

Foil B3 Sample TAS14-68, Plagioclase

Temp (°C)	Ar^{36} (mol)	err (%)	Ar^{37} (mol)	err (%)	Ar^{38} (mol)	err (%)	Ar^{39} (mol)	err (%)	Ar^{40} (mol)	err (%)	% Ar^{40*}	$Ar^{40*}/Ar^{39}(K)$	Cumulative Ar^{39}(%)	Calculated Age (Ma ± 1 s.d.)	Ca/K	Cl/K
850	4.88E-17	2.77	5.32E-15	1.22	1.19E-17	6.41	2.35E-16	0.77	4.01E-14	0.85	64.5	112.35	75.71	292 ± 5.34	4.39E+01	4.24E-03
900	5.92E-17	1.85	4.65E-15	1.44	1.51E-17	10.9	2.40E-16	0.97	5.16E-14	1.03	66.4	145.28	77.63	369.33 ± 5.96	3.75E+01	6.13E-02
900	4.77E-17	2.78	2.75E-15	1.41	1.24E-17	1.04	1.58E-16	0.18	3.83E-14	0.38	63.5	157.04	78.88	396.16 ± 6.02	3.38E+01	1.25E-01
950	3.91E-17	3.33	3.13E-15	2.84	1.20E-17	3.46	2.49E-16	2.47	6.45E-14	2.49	82.2	215.7	80.88	524.35 ± 14.02	2.42E+01	8.56E-02
950	3.17E-17	2.98	2.04E-15	1.86	7.72E-18	13.15	1.50E-16	0.58	4.71E-14	0.64	80.3	255.38	82.08	606.18 ± 5.52	2.62E+01	2.27E-03
1000	3.10E-17	4.12	3.71E-15	1.22	1.18E-17	9.67	3.20E-16	1.05	1.12E-13	1.09	92	326.65	84.65	744.43 ± 7.51	2.23E+01	8.72E-02
1000	2.28E-17	1.86	1.63E-15	1.87	7.32E-18	7.08	1.80E-16	1.48	8.39E-14	1.51	92	432.73	86.1	932.38 ± 11.88	1.73E+01	6.36E-02
1050	3.53E-17	3.9	3.43E-15	1.53	1.50E-17	9.15	4.78E-16	1.17	2.24E-13	1.2	95.4	451.21	89.95	963.2 ± 9.4	1.37E+01	7.08E-02
1050	1.56E-17	1.5	1.52E-15	1.07	6.88E-18	8.31	2.18E-16	0.72	1.06E-13	0.84	95.7	465.83	91.71	987.22 ± 6.66	1.33E+01	7.72E-02
1100	3.30E-17	5.1	5.21E-15	1.8	1.16E-17	9.31	3.45E-16	1.73	1.69E-13	1.8	94.3	468.91	94.47	992.24 ± 14.57	2.91E+01	4.79E-02
1200	4.79E-17	1.94	7.85E-15	0.82	1.64E-17	6.05	3.32E-16	0.39	8.81E-14	0.51	84.2	229.16	97.09	552.53 ± 3.29	4.60E+01	1.33E-01
1300	8.13E-17	2.35	1.02E-14	1.44	2.02E-17	7.86	3.35E-16	0.98	7.76E-14	1.06	69.5	165.77	99.74	415.84 ± 6.66	5.96E+01	4.07E-02
1450	5.31E-17	5.93	4.88E-16	5.32	1.09E-17	6	3.30E-17	4.51	5.01E-14	4.57	68.7	1058.66	100	1761.9 ± 79.6	2.85E+01	1.83E-01
Total	4.20E-15		6.62E-14		7.52E-14		5.56E-12		1.43E-10			25.43		366.4 ± 1.86		

Lambda K40 = 5.5430E-10 J = 1.564E-3; %error J = 0.3495

Foil B4 Sample TAS14-69, Plagioclase

Temp (°C)	Ar^{36} (mol)	err (%)	Ar^{37} (mol)	err (%)	Ar^{38} (mol)	err (%)	Ar^{39} (mol)	err (%)	Ar^{40} (mol)	err (%)	% Ar^{40*}	$Ar^{40*}/Ar^{39}(K)$	Cumulative Ar^{39}(%)	Calculated Age (Ma ± 1 s.d.)	Ca/K	Cl/K
500	1.45E-16	2.02	4.58E-16	3.77	3.14E-17	2.51	1.57E-16	1.8	5.23E-14	1.84	17.9	59.8	0.06	161.63 ± 21.28	5.55E+00	1.68E-01
500	1.09E-16	1.5	7.08E-16	1.19	2.60E-17	4.86	2.12E-16	0.59	4.54E-14	0.64	29.1	62.58	0.14	168.81 ± 6.85	6.37E+00	1.74E-01
550	4.43E-16	1.03	2.33E-15	1.23	9.50E-17	2.22	7.53E-16	0.72	1.73E-13	0.8	24.5	56.5	0.44	153.08 ± 6.66	5.88E+00	4.68E-02
550	1.64E-16	1.37	2.80E-15	1.09	5.00E-17	2.28	8.48E-16	0.72	1.01E-13	0.83	51.9	61.72	0.77	166.6 ± 3.24	6.29E+00	1.32E-01
600	6.56E-16	0.72	6.99E-15	0.96	1.64E-16	0.92	2.36E-15	0.25	3.40E-13	0.36	43.1	62.09	1.69	167.55 ± 2.01	5.64E+00	6.72E-02
600	2.45E-16	0.74	6.66E-15	1.49	7.18E-17	1.4	2.10E-15	0.36	2.03E-13	0.41	64.5	62.8	2.51	169.37 ± 1.21	6.05E+00	5.83E-03
650	1.08E-15	0.71	1.69E-14	0.58	2.74E-16	1.35	5.84E-15	0.31	6.87E-13	0.45	53.7	63.4	4.78	170.91 ± 1.69	5.52E+00	4.25E-03
650	2.49E-16	0.91	1.18E-14	0.89	9.91E-17	1.09	4.11E-15	0.23	3.46E-13	0.4	78.8	66.59	6.38	179.11 ± 0.95	5.45E+00	1.06E-02
700	6.84E-16	0.85	2.44E-14	0.64	2.50E-16	1.03	9.49E-15	0.25	8.34E-13	0.37	75.8	66.77	10.08	179.56 ± 0.96	4.89E+00	1.18E-02
700	1.78E-16	1.19	1.95E-14	0.53	1.34E-16	0.89	7.59E-15	0.39	5.56E-13	0.49	90.6	66.54	13.04	178.98 ± 0.94	4.89E+00	1.72E-02
750	4.78E-16	0.8	4.42E-14	0.47	2.62E-16	1.37	1.43E-14	0.21	1.09E-12	0.48	87.1	66.72	18.6	179.44 ± 0.96	5.91E+00	2.55E-03
750	1.14E-16	0.62	3.06E-14	0.81	1.53E-16	1.26	1.09E-14	0.25	7.61E-13	0.37	95.7	66.84	22.86	179.74 ± 0.67	5.34E+00	2.05E-03
800	1.97E-16	1.27	5.57E-14	0.79	2.73E-16	1.68	1.92E-14	0.13	1.34E-12	0.31	95.8	67.11	30.34	180.45 ± 0.56	5.53E+00	5.70E-03
800	7.35E-17	1.98	3.41E-14	0.89	1.81E-16	2.05	1.38E-14	0.56	9.40E-13	0.68	97.8	66.82	35.72	179.7 ± 1.18	4.71E+00	2.94E-03
850	4.74E-17	1.29	4.53E-14	0.99	2.53E-16	2.91	1.94E-14	0.35	1.31E-12	0.49	99	66.77	43.28	179.56 ± 0.85	4.45E+00	8.88E-03
850	1.26E-16	2.7	2.38E-14	0.97	1.74E-16	1.66	1.22E-14	0.26	8.50E-13	0.55	95.7	66.92	48.03	179.94 ± 1	3.72E+00	6.26E-03
900	2.19E-16	1.93	3.01E-14	1.16	2.57E-16	2.75	1.72E-14	0.69	1.21E-12	0.88	94.7	66.71	54.74	179.42 ± 1.6	3.33E+00	8.17E-03
900	1.21E-16	1.52	1.51E-14	0.49	1.68E-16	3.84	1.10E-14	0.25	7.74E-13	0.33	95.4	67.07	59.04	180.34 ± 0.61	2.60E+00	1.59E-02
950	2.31E-16	1.48	2.46E-14	1.16	2.46E-16	0.89	1.61E-14	0.5	1.14E-12	0.56	94.1	66.74	65.33	179.49 ± 1.02	2.90E+00	8.85E-03
950	1.29E-16	2.24	1.30E-14	1.5	1.44E-16	2.79	9.80E-15	0.48	6.90E-13	0.76	94.5	66.68	69.16	179.34 ± 1.39	2.53E+00	4.43E-03
1000	3.91E-16	1.18	2.84E-14	0.72	2.71E-16	1.62	1.56E-14	0.3	1.15E-12	0.48	90	66.57	75.24	179.05 ± 0.93	3.47E+00	9.68E-03
1000	1.41E-16	0.9	1.46E-14	1.13	1.42E-16	1.72	8.93E-15	0.58	6.37E-13	0.69	93.5	66.83	78.73	179.71 ± 1.26	3.11E+00	1.24E-02
1050	2.25E-16	1.44	2.97E-14	0.58	3.78E-16	0.85	2.63E-14	0.21	1.82E-12	0.34	96.4	66.68	88.99	179.33 ± 0.6	2.15E+00	1.09E-02

(*continued on next page*)

Table 6 (*continued*)

Foil B4 Sample TAS14-69, Plagioclase

Temp (°C)	Ar^{36} (mol)	err (%)	Ar^{37} (mol)	err (%)	Ar^{38} (mol)	err (%)	Ar^{39} (mol)	err (%)	Ar^{40} (mol)	err (%)	% Ar^{40*}	Ar^{40*}/Ar^{39}(K)	Cumulative Ar^{39}(%)	Calculated Age (Ma ± 1 s.d.)	Ca/K	Cl/K
1050	7.69E-17	0.89	1.06E-14	0.68	1.24E-16	0.87	8.94E-15	0.2	6.18E-13	0.31	96.3	66.75	92.48	179.52 ± 0.55	2.25E+00	4.53E-03
1100	5.62E-17	1.89	1.56E-14	0.9	1.75E-16	3.81	1.26E-14	0.28	8.56E-13	0.34	98.1	66.76	97.4	179.55 ± 0.6	2.36E+00	1.43E-02
1100	9.60E-17	2.19	1.91E-14	1.26	5.41E-17	10.35	2.41E-15	0.55	1.87E-13	0.73	85.2	66.66	98.33	179.29 ± 1.59	1.51E+01	3.96E-02
1150	3.43E-17	0.99	7.78E-15	1.03	1.77E-17	5.88	6.52E-16	0.36	5.30E-14	0.47	81.3	66.86	98.58	179.8 ± 1.05	2.29E+01	6.93E-02
1200	5.26E-17	1.59	1.04E-14	0.66	2.50E-17	3.87	7.21E-16	0.34	6.26E-14	0.53	75.7	66.74	98.86	179.49 ± 1.46	2.79E+01	1.15E-01
1300	2.23E-16	1.26	5.01E-14	0.71	7.14E-17	2.03	2.43E-15	0.31	2.30E-13	0.59	72	69.66	99.79	186.94 ± 1.68	4.00E+01	8.08E-03
1450	9.06E-17	1.12	1.38E-14	1.18	2.64E-17	3.47	5.46E-16	0.69	6.49E-14	0.78	59.4	72.39	100	193.89 ± 2.73	4.93E+01	7.21E-02
Total	7.07E-15		6.09E-13		4.59E-15		2.56E-13		1.91E-11			66.61		179.16 ± 1		

Lambda K40 = 5.5430E-10 J = 1.567E-3; %error J = 0.3488

Foil B5 Sample TAS14-72, Plagioclase

Temp (°C)	Ar^{36} (mol)	err (%)	Ar^{37} (mol)	err (%)	Ar^{38} (mol)	err (%)	Ar^{39} (mol)	err (%)	Ar^{40} (mol)	err (%)	% Ar^{40*}	Ar^{40*}/Ar^{39}(K)	Cumulative Ar^{39}(%)	Calculated Age (Ma ± 1 s.d.)	Ca/K	Cl/K
500	4.81E-17	2.51	1.28E-15	3.41	1.14E-17	7.46	1.42E-16	1.65	6.53E-14	1.66	78.3	363.57	0.32	815.68 ± 14.52	1.73E+01	5.68E-02
500	4.94E-17	3.41	1.67E-15	1.99	1.74E-17	7.53	1.74E-16	1.68	3.37E-14	1.7	56.8	111.36	0.71	291.09 ± 10.54	1.84E+01	4.29E-01
550	8.18E-17	3.67	4.72E-15	1.81	2.54E-17	9.65	4.33E-16	0.32	2.13E-13	0.51	88.7	440.88	1.68	950.07 ± 5.43	2.10E+01	1.42E-01
550	5.38E-17	2.49	4.59E-15	1.65	2.14E-17	7.76	5.18E-16	1.25	6.57E-14	1.26	76	97.23	2.85	256.66 ± 4.36	1.70E+01	1.23E-01
600	8.11E-17	1.46	1.28E-14	0.81	4.66E-17	3.47	1.42E-15	0.36	3.54E-13	0.4	93.4	235.94	6.04	569.22 ± 2.16	1.73E+01	1.28E-01
600	4.87E-17	0.73	1.34E-14	0.75	2.73E-17	6.78	1.37E-15	0.39	1.35E-13	0.58	89.7	89.43	9.12	237.36 ± 1.44	1.89E+01	1.95E-02
650	9.47E-17	1.4	3.80E-14	0.91	6.24E-17	5.22	3.24E-15	0.19	5.08E-13	0.36	94.7	150.14	16.41	382.34 ± 1.32	2.25E+01	2.57E-02
650	4.69E-17	1.99	3.21E-14	0.78	4.20E-17	4.74	2.47E-15	0.19	2.08E-13	0.32	93.9	80.27	21.96	214.42 ± 0.74	2.50E+01	2.24E-02
700	7.62E-17	1.27	6.57E-14	0.55	6.39E-17	3.71	4.20E-15	0.27	4.85E-13	0.41	95.8	112.35	31.36	293.47 ± 1.15	3.02E+01	3.20E-03
700	4.15E-17	2.77	4.17E-14	0.74	4.16E-17	1.87	2.44E-15	0.28	1.99E-13	0.44	94.5	78.15	36.82	209.08 ± 0.97	3.30E+01	2.83E-02
750	6.46E-17	1.3	7.96E-14	0.68	7.60E-17	2.95	4.51E-15	0.52	4.66E-13	0.67	96.5	101.56	46.9	267.28 ± 1.7	3.42E+01	3.24E-02
750	3.18E-17	2.62	2.94E-14	0.77	2.77E-17	3.5	1.80E-15	0.1	1.57E-13	0.2	94.6	84.04	50.93	223.89 ± 0.56	3.15E+01	6.35E-03
800	5.68E-17	3.08	4.87E-14	1.12	5.68E-17	8.8	3.05E-15	0.54	4.12E-13	0.73	96.3	132.12	57.76	340.51 ± 2.36	3.08E+01	4.39E-02
800	2.24E-17	1.78	1.58E-14	0.94	2.00E-17	7.96	1.25E-15	0.6	1.58E-13	0.67	96.1	123.14	60.56	319.31 ± 2.02	2.43E+01	1.22E-02
850	4.58E-17	2.4	1.83E-14	1.06	3.01E-17	2.68	1.77E-15	0.7	3.74E-13	0.74	96.5	205.96	64.56	506.11 ± 3.37	1.98E+01	5.81E-03
850	1.99E-17	1.7	7.31E-15	1.16	1.60E-17	5.09	1.02E-15	0.51	2.26E-13	0.55	97.5	217.78	66.86	531.26 ± 2.59	1.37E+01	4.19E-03
900	2.69E-17	1.12	8.58E-15	1.36	2.33E-17	3.19	1.50E-15	0.33	5.10E-13	0.45	98.5	337.06	70.25	767.19 ± 2.85	1.09E+01	5.07E-03
900	1.59E-17	6.32	4.47E-15	1.79	1.50E-17	4.52	9.58E-16	0.44	2.93E-13	0.65	98.4	302.39	72.42	701.72 ± 3.89	8.91E+00	8.59E-03
950	2.45E-17	5.85	7.25E-15	1.15	2.66E-17	5.52	1.56E-15	0.67	5.64E-13	0.72	98.8	359.44	75.94	808.21 ± 4.78	8.89E+00	2.87E-02
950	1.51E-17	7.75	3.48E-15	1.11	1.68E-17	8.9	1.04E-15	0.37	3.15E-13	0.45	98.6	300.25	78.3	697.6 ± 2.73	6.39E+00	1.95E-02
1000	3.30E-17	3.1	1.62E-14	0.88	3.99E-17	6.3	2.36E-15	0.16	6.93E-13	0.25	98.7	291.16	83.64	680.01 ± 1.47	1.31E+01	3.08E-02
1000	1.95E-17	7	6.41E-15	1.31	2.48E-17	10.73	1.42E-15	0.29	3.68E-13	0.64	98.5	256.28	86.85	610.84 ± 3.4	8.63E+00	3.82E-02
1050	3.34E-17	3.17	2.04E-14	0.58	4.78E-17	2.94	2.86E-15	0.24	7.17E-13	0.3	98.7	249.18	93.32	596.41 ± 1.57	1.37E+01	3.40E-02
1050	1.59E-17	7.46	8.65E-15	1.35	1.30E-17	9.06	8.14E-16	0.5	1.99E-13	0.53	97.8	241.73	95.15	581.16 ± 2.81	2.04E+01	7.51E-03
1100	2.93E-17	2.45	1.86E-14	1.06	1.40E-17	4.98	6.95E-16	0.45	2.12E-13	0.49	96.2	301.3	96.7	699.63 ± 2.96	5.21E+01	1.02E-02
1100	1.65E-17	5.25	7.30E-15	1.7	5.90E-18	4.31	2.10E-16	1.53	4.81E-14	1.55	90.4	214.19	97.16	523.66 ± 7.98	6.83E+01	2.68E-02
1150	2.98E-17	3.74	1.25E-14	0.96	1.15E-17	10.56	3.56E-16	0.72	1.09E-13	0.75	92.3	291.75	97.94	681.16 ± 4.83	6.94E+01	6.65E-02
1200	4.15E-17	3	1.66E-14	1.44	1.41E-17	9.99	4.59E-16	1.29	2.72E-13	1.32	95.7	588.45	98.95	1181.77 ± 11.61	7.10E+01	3.20E-02
1300	5.02E-17	1.96	1.80E-14	1.14	1.97E-17	4.88	4.35E-16	0.36	5.00E-13	0.59	97.2	1163.75	99.9	1876.61 ± 6.86	8.17E+01	1.54E-01

(*continued on next page*)

Table 6 (*continued*)

Foil B5 Sample TAS14-72, Plagioclase

Temp (°C)	Ar^{36} (mol)	err (%)	Ar^{37} (mol)	err (%)	Ar^{38} (mol)	err (%)	Ar^{39} (mol)	err (%)	Ar^{40} (mol)	err (%)	% Ar^{40*}	$Ar^{40*}/Ar^{39}(K)$	Cumulative Ar^{39}(%)	Calculated Age (Ma ± 1 s.d.)	Ca/K	Cl/K
1450	4.82E-17	11.46	1.93E-15	11.35	1.43E-17	14.39	4.71E-17	11.06	5.11E-13	11.07	97.2	10983.93	100	5241.35 ± 186.56	8.11E+01	1.24E+00
Total	1.26E-15		5.65E-13		8.73E-16		4.45E-14		9.37E-12			205.15		504.37 ± 2.46		

Lambda K40 = 5.5430F-10 J = 1.5723F-3; %error J = 0.3476

Foil B6 Sample TAS14-75, Plagioclase

Temp (°C)	Ar^{36} (mol)	err (%)	Ar^{37} (mol)	err (%)	Ar^{38} (mol)	err (%)	Ar^{39} (mol)	err (%)	Ar^{40} (mol)	err (%)	% Ar^{40*}	$Ar^{40*}/Ar^{39}(K)$	Cumulative Ar^{39}(%)	Calculated Age (Ma ± 1 s.d.)	Ca/K	Cl/K
500	5.45E-17	2.66	7.41E-16	3	2.10E-17	6.23	5.40E-16	0.78	7.07E-14	0.81	77.2	101.38	0.48	268 ± 3.26	2.61E+00	9.73E-02
500	5.55E-17	1.03	8.44E-16	2.36	2.30E-17	5.67	7.49E-16	0.33	4.85E-14	0.4	66.2	42.91	1.16	118.32 ± 0.92	2.14E+00	5.99E-02
550	7.43E-17	2.5	2.60E-15	1.06	3.85E-17	5.11	1.40E-15	0.46	3.34E-13	0.52	93.4	222.76	2.41	543.92 ± 2.72	3.52E+00	6.85E-02
550	6.49E-17	2.42	3.45E-15	1.34	4.44E-17	4.25	1.79E-15	0.33	1.15E-13	0.39	83.4	53.88	4.02	147.37 ± 0.95	3.67E+00	7.48E-02
600	7.32E-17	2.16	8.39E-15	1.19	6.45E-17	3.03	3.08E-15	0.75	4.89E-13	0.84	95.6	152.03	6.78	388.3 ± 3.07	5.19E+00	5.67E-02
600	6.88E-17	2.32	1.34E-14	0.85	8.46E-17	2.05	4.48E-15	0.33	3.19E-13	0.5	93.7	67.05	10.79	181.63 ± 0.96	5.69E+00	5.10E-02
650	6.91E-17	0.99	2.17E-14	0.93	9.69E-17	2.25	5.39E-15	0.34	8.14E-13	0.38	97.6	147.99	15.61	379.01 ± 1.33	7.67E+00	4.60E-02
650	3.33E-17	2.04	1.96E-14	0.77	6.41E-17	3.29	4.01E-15	0.6	3.36E-13	0.63	97.2	81.78	19.19	219.19 ± 1.33	9.33E+00	3.23E-02
700	6.85E-17	4.87	4.80E-14	0.64	1.20E-16	2.45	7.53E-15	0.53	1.05E-12	0.64	98.2	138.1	25.91	356.02 ± 2.1	1.22E+01	3.02E-02
700	3.06E-17	2.77	3.36E-14	0.53	5.54E-17	3.24	3.88E-15	0.28	3.23E-13	0.36	97.5	81.84	29.36	219.35 ± 0.78	1.66E+01	1.31E-02
750	6.75E-17	1.16	6.89E-14	0.84	1.06E-16	0.79	6.51E-15	0.17	8.65E-13	0.35	97.9	131.45	35.15	340.39 ± 1.11	2.03E+01	3.31E-02
750	3.04E-17	3.48	4.31E-14	0.63	4.76E-17	1.3	2.98E-15	0.42	2.48E-13	0.62	96.9	81.83	37.78	219.3 ± 1.34	2.79E+01	3.07E-02
800	5.97E-17	5.1	1.05E-13	1.47	1.22E-16	9.5	8.34E-15	0.6	9.72E-13	1.06	98.5	116.2	45.18	304.04 ± 2.99	2.42E+01	2.07E-02
800	4.79E-17	2.34	5.92E-14	0.66	7.02E-17	1.27	4.79E-15	0.34	4.35E-13	0.44	97.2	89.43	49.43	238.4 ± 1.01	2.38E+01	1.40E-02
850	6.67E-17	1.04	6.54E-14	0.46	9.35E-17	1.94	6.22E-15	0.28	1.05E-12	0.38	98.3	167.88	54.96	424.38 ± 1.45	2.02E+01	1.64E-02
850	4.12E-17	1.85	3.22E-14	0.59	5.44E-17	3.29	3.88E-15	0.21	6.99E-13	0.47	98.4	178.55	58.42	448.24 ± 1.87	1.59E+01	3.54E-03
900	5.90E-17	3.88	3.21E-14	0.65	1.01E-16	8.08	6.12E-15	0.37	1.92E-12	0.44	99.1	312.05	63.89	722.98 ± 2.65	1.00E+01	3.50E-02
900	2.97E-17	2.39	8.84E-15	1.42	4.25E-17	9.79	2.56E-15	0.7	8.06E-13	0.73	98.9	312.29	66.18	723.43 ± 4.39	6.57E+00	3.13E-02
950	3.86E-17	10.46	1.07E-14	0.91	7.24E-17	10.72	5.00E-15	0.44	1.64E-12	0.54	99.3	326.4	70.66	750.17 ± 3.34	4.07E+00	1.44E-02
950	1.70E-17	7.82	4.76E-15	2.05	3.88E-17	5.87	2.64E-15	0.67	9.14E-13	0.7	99.5	344.64	73.03	784.15 ± 4.47	3.43E+00	1.97E-02
1000	1.32E-16	9.07	1.08E-14	1.23	1.00E-16	3.81	5.57E-15	0.5	1.96E-12	0.53	98	345.93	78.02	786.52 ± 3.65	3.70E+00	2.10E-02
1000	3.04E-17	5.52	3.92E-15	2.31	5.07E-17	7.94	2.98E-15	0.29	1.03E-12	0.44	99.1	341.64	80.69	778.6 ± 2.84	2.51E+00	3.95E-02
1050	6.54E-17	3.11	1.19E-14	1.64	1.16E-16	5.81	6.50E-15	0.43	2.16E-12	0.55	99.1	330.42	86.51	757.71 ± 3.41	3.49E+00	5.05E-02
1050	3.44E-17	4.71	5.45E-15	1.38	8.18E-17	2.79	5.01E-15	0.33	1.29E-12	0.41	99.2	255.67	91.01	612.02 ± 2.13	2.07E+00	3.83E-02
1100	3.14E-17	7.11	9.84E-15	1.63	1.10E-16	3.28	7.24E-15	0.6	1.75E-12	0.66	99.5	240.04	97.5	579.99 ± 3.31	2.59E+00	3.12E-02
1100	1.86E-17	5.81	3.38E-15	1.33	1.60E-17	11.59	1.02E-15	0.64	2.14E-13	0.69	97.5	205.38	98.42	506.91 ± 3.19	6.32E+00	5.01E-03
1150	3.31E-17	5.32	4.14E-15	1.78	1.94E-17	2.35	7.31E-16	0.73	1.99E-13	0.82	95.2	260.79	99.07	622.36 ± 4.75	1.08E+01	7.63E-02
1200	3.08E-17	2.25	5.46E-15	1.3	1.48E-17	4.07	6.09E-16	1.09	1.55E-13	1.11	94.2	241.17	99.61	582.34 ± 5.83	1.72E+01	3.69E-02
1300	9.07E-17	1.57	1.00E-14	1.36	2.21E-17	3.91	4.15E-16	0.99	2.03E-13	1.05	87	435.68	99.98	944.77 ± 8.82	4.71E+01	9.08E-03
1450	4.40E-17	7.09	4.89E-16	6.62	1.22E-17	6.37	2.79E-17	5.69	1.45E-13	5.69	91	4802.93	100	3879.24 ± 98.56	3.39E+01	1.59E+00
Total	1.56E-15		6.48E-13		1.91E-15		1.12E-13		2.25E-11			198.488		492.03 ± 2.4		

Lambda K40 = 5.5430E-10 J = 1.580E-3; %error J = 0.3460

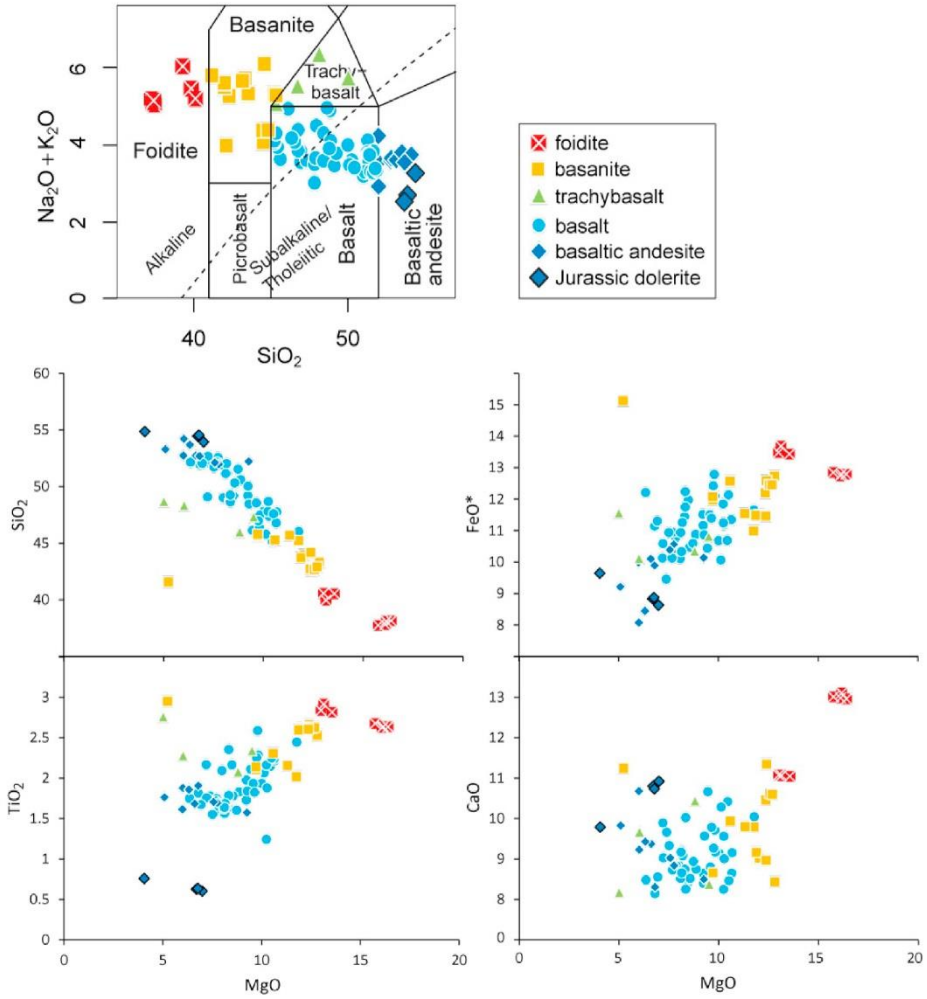

Fig. 4. Total Alkali-Silica diagram (Le Bas et al., 1986). Major elements vs. MgO. Rock types are indicated by symbols and colours.

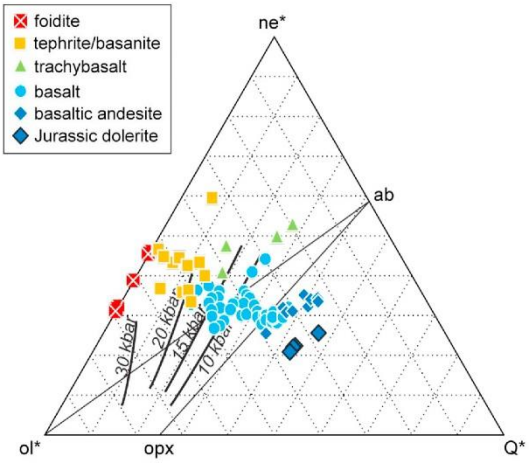

Fig. 5. Olivine – nepheline – quartz plot with indicated melting pressures following Hirose and Kushiro (1993). Projection scheme after Irvine and Baragar (1971) (ne* = ne + 0.6 ab; Q* = Q + 0.4 ab + 0.25 opx; ol* = ol + 0.75 opx). Rock types are indicated by colours and symbols.

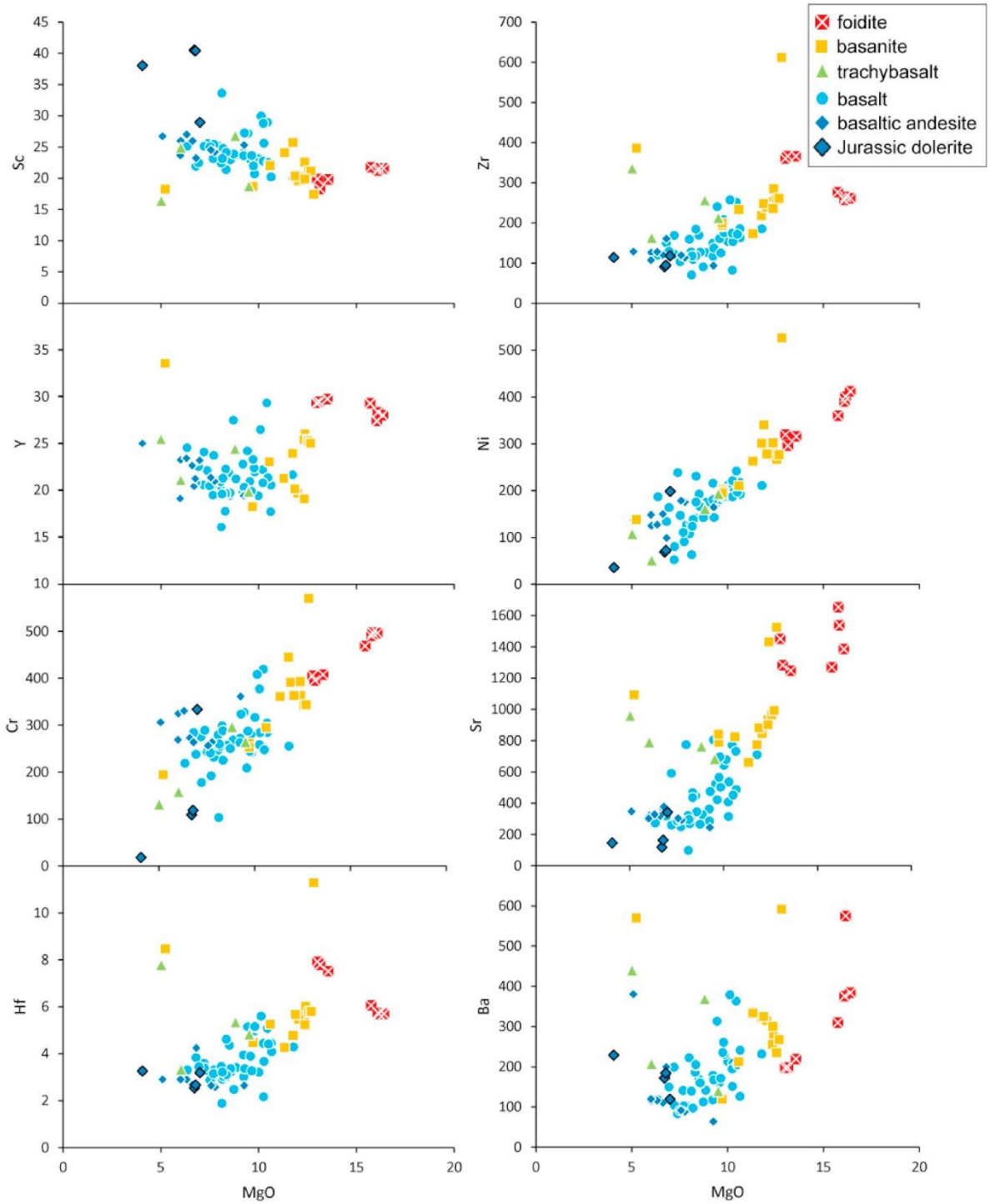

Fig. 6. Selected trace elements versus MgO. Rock types are indicated by symbols and colours.

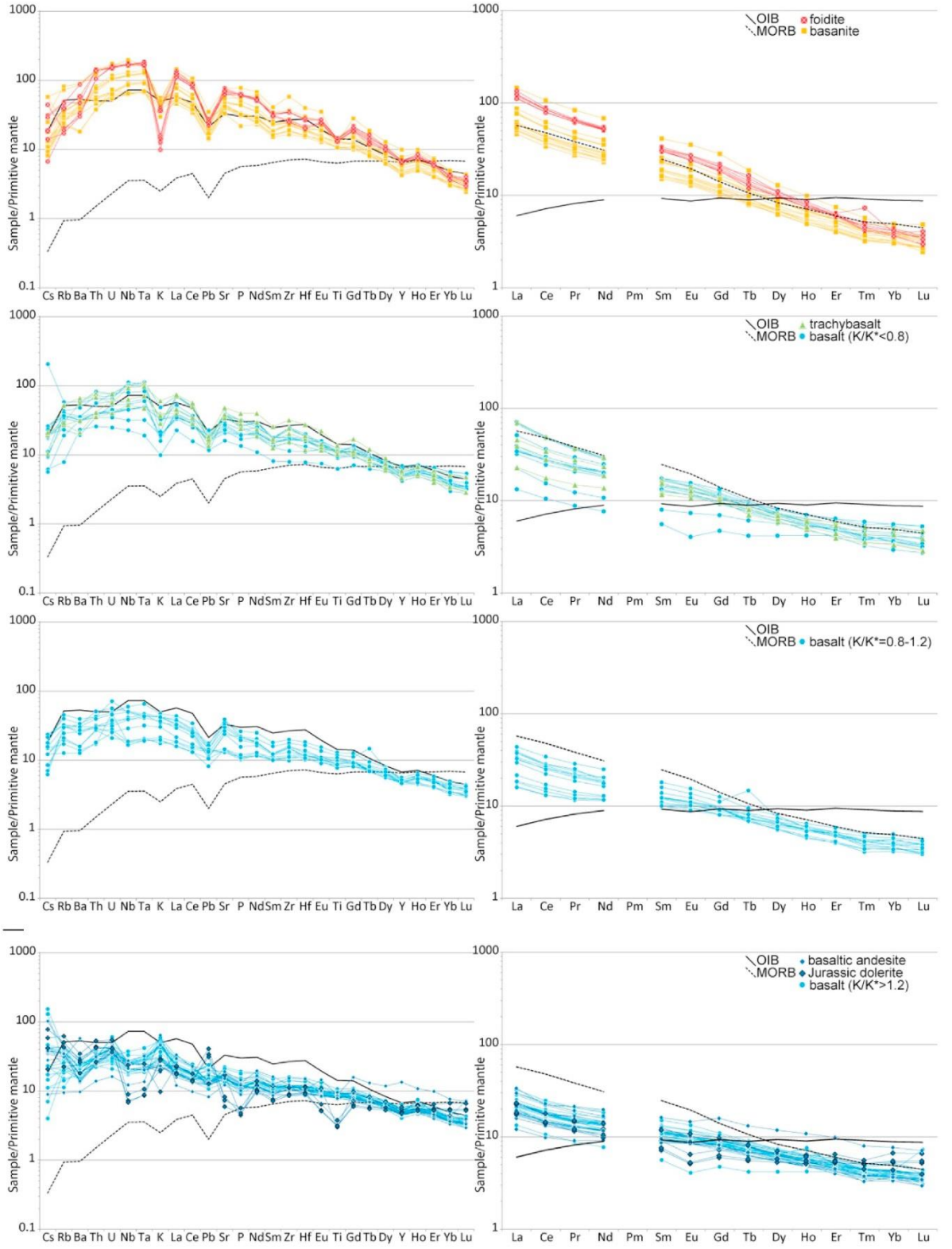

(caption on next page)

Fig. 7. Primitive mantle normalized incompatible element diagram (left) and primitive mantle normalized rare earth element diagram (right) showing the analysed Cenozoic samples (McDonough and Sun, 1995), colour- and symbol-coded according to rock type. Black continuous line represents OIB values and black dotted line represents MORB values (Sun and McDonough, 1989).

5.2. Evidence for polybaric mixing and multisource origin

5.2.1. Polybaric mixing and lithospheric architecture

The samples taken for this study span a range of compositions, from Q- and olivine tholeiites to highly SiO_2-undersaturated nephelinites and melilitites. The more SiO_2-undersaturated examples are richer in MgO, TiO_2, CaO, P_2O_5, Ni, Cr, Hf, Ho, La, Nb, Nd, Pb, Sm, Sr, Ta, Th, and U. Mantle normalized incompatible element diagrams (Fig. 7) and Dy/Dy^* versus Dy_N/Yb_N plots (Davidson et al., 2013) indicate that most of the original magmas would have in equilibrated with residual garnet during melting, indicating reasonable pressures (> 25 kbar). The most undersaturated samples lie towards the higher end of Dy_N/Yb_N (2.3–3.0), indicating higher pressures of origin. Geothermobarometry calculations using the Lee et al. (2009) calculations confirm this trend, even though absolute values of pressures and temperatures are most likely too high due to additional phases fractionating next to olivine. Although calibrated for different source material, this is also confirmed by variations in ne*-ol*-Q* projection (Fig. 5) (Hirose and Kushiro, 1993), which indicates that unfractionated, undersaturated olivine melilitites and nephelinites have been extracted at higher pressures (> 20 kbar) and temperatures than the olivine basalts and Q-tholeiites.

5.2.2. Lithospheric architecture

The older Proterozoic and Palaeozoic terranes of western Tasmania are separated from the Palaeozoic basement of eastern Tasmania by the Tamar Graben. This continues southwards as the Tamar Lineament (Seymour et al., 2013). This structure is defined by seismic tomography, showing a transition from slow velocity crust in the west towards high velocity crust in the east (Appendix Fig. A2: Rawlinson et al., 2010). Geothermobarometric calculations using the Lee et al. (2009) calculations show a similar separation between eastern and western Tasmania along the Tamar Lineament (Fig. 12). These calculations show that a cluster of higher melting temperatures and pressures is present east of the Tamar Lineament, compared to west of the Lineament. This coincides well with rare high pressure xenoliths found in tholeiitic basalts near Andover (Sutherland, 1974). The Lee et al. (2009) calculations are not calibrated for very undersaturated rocks such as the anomalously high pressure melilitites found at Laughing Jack Marsh. These anomalously high pressure melts fall outside of the eastern terrane and their high pressure cannot be easily explained by lithospheric architecture as it is less well known in this area. Thickness of the Tasmanian lithosphere is estimated to be ~80–90 km (Fishwick et al., 2008; Fishwick and Rawlinson, 2012), with thinner lithosphere in the eastern terrane and the Rocky Cape Block in the northwest (Rawlinson et al., 2010). This, together with the evidence for residual garnet during melting, suggests that most SiO_2-undersaturated melts have been formed at asthenospheric depths.

5.2.3. Multisource origin

Tasmania has witnessed several magmatic events before the Cenozoic. The biggest, most widespread and distinct event occurred during the Jurassic, and forms part of the Ferrar Large Igneous Province which preceded Gondwana break-up (Ivanov et al., 2017). In Tasmania, this large event is preceded by a small event during the Triassic and

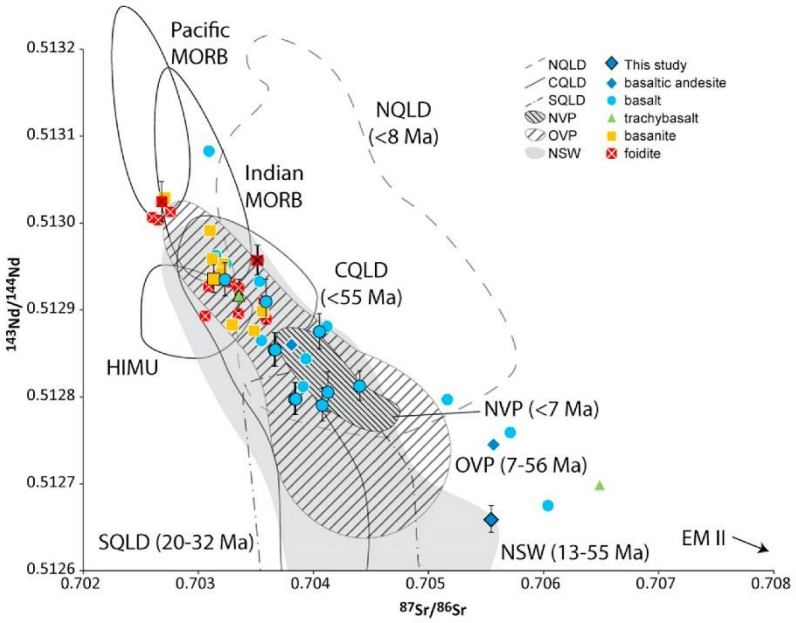

Fig. 8. $^{143}Nd/^{144}Nd$ versus $^{87}Sr/^{86}Sr$ isotope plot for Tasmanian Cenozoic samples analysed for this study (black outlines) with indicated error bars (2σ, horizontal error bars are smaller than symbols) and published data (Adam and Green, 2011; Everard et al., 1997; Ewart et al., 1988; Matthews et al., 1996; McDonough et al., 1985; Nasir et al., 2010; Sutherland, 2003; Zhang and Everard, 2014) with colour- and symbol-coded rock types and indication of mantle endmembers (Zindler and Hart, 1986) and for the different magmatic provinces within the Eastern Australian Cenozoic Magmatic Province. Australian fields compiled from: North Queensland: (Ewart et al., 1980; O'Reilly and Zhang, 1995; Zhang et al., 2001), Central Queensland: (Ewart, 1982; Ewart et al., 1980; Sutherland, 2003), South Queensland: (Ewart, 1982; Ewart et al., 1980), New South Wales: (Menzies and Wass, 1983; Nelson et al., 1986; O'Reilly and Griffin, 1984; O'Reilly and Zhang, 1995; Sutherland et al., 2007; Zhang et al., 2001), Older Volcanic Province: (Paul et al., 2007; Price et al., 2014), Newer Volcanic Province: (Ewart et al., 1980; Oostingh et al., 2016).

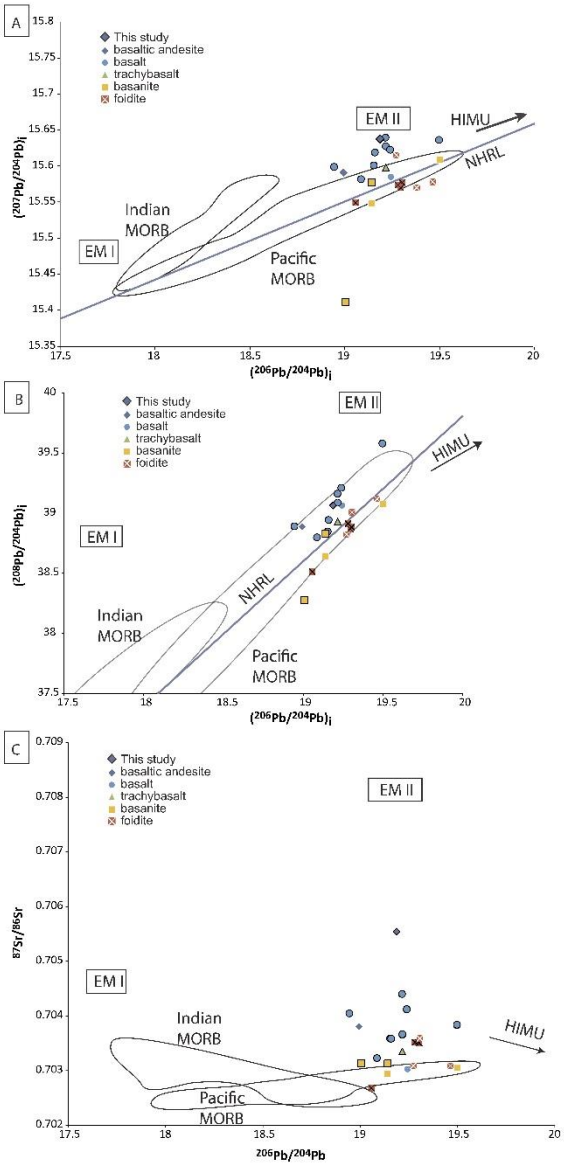

Fig. 9. Initial $^{207}Pb/^{204}Pb$ versus initial $^{206}Pb/^{204}Pb$ (a), initial $^{208}Pb/^{204}Pb$ versus initial $^{206}Pb/^{204}Pb$ (b) and $^{87}Sr/^{86}Sr$ versus $^{206}Pb/^{204}Pb$ (c) plot for samples of this study (black outlines) and published data (Ewart et al., 1988; Nasir et al., 2010) with colour- and symbol-coded rock types and indication of mantle endmembers (EMI and EMII: (Jackson and Dasgupta, 2008; Workman et al., 2004) Indian MORB: (Klein et al., 1991), Pacific MORB: (White et al., 1987)). NHRL: Northern Hemisphere Reference Line (Hart, 1984).

followed by a small event during the Cretaceous and eventually the larger Cenozoic event. $^{143}Nd/^{144}Nd$ values (Fig. 13) are observed to progressively increase as the events get younger (~0.5124 for Jurassic dolerites over ~0.5126 for the Cretaceous lavas to 0.5128–0.5130 for the Cenozoic lavas). $^{87}Sr/^{86}Sr$ does not show a similar trend, however, the Jurassic dolerites are very distinct in that their Sr isotopes are significantly higher (0.71088–0.7143) and Nd isotopes significantly lower (0.512236–0.512344). Within the Cenozoic samples, the most silica-undersaturated samples show the highest $^{143}Nd/^{144}Nd$ and lowest $^{87}Sr/^{86}Sr$ values. The array of isotope values and a plot of $(^{87}Sr/^{86}Sr)_i$ versus Sr (ppm), seems to suggest a mixing line with a high $^{87}Sr/^{86}Sr$ endmember.

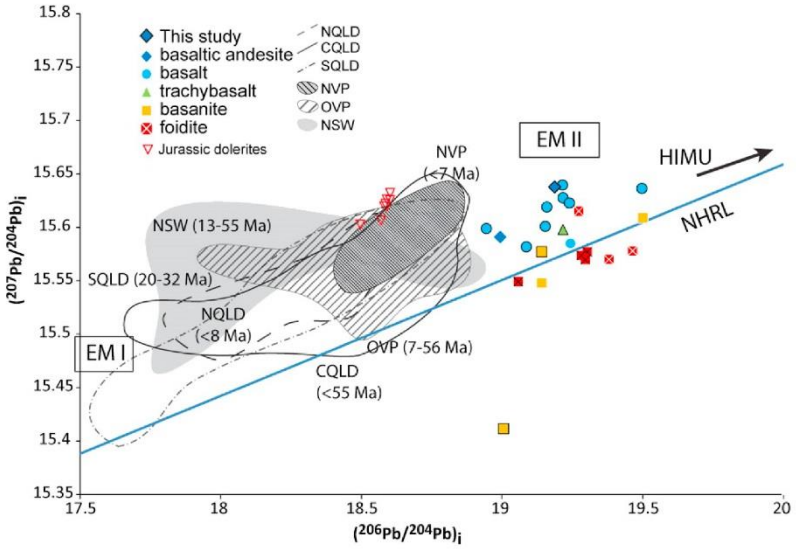

Fig. 10. ($^{207}Pb/^{204}Pb$)i versus ($^{206}Pb/^{204}Pb$)i plot for the different magmatic provinces within the Eastern Australian Cenozoic Magmatic Province. Data compiled from: North Queensland: (Ewart et al., 1980; O'Reilly and Zhang, 1995; Zhang et al., 2001), Central Queensland: (Ewart, 1982; Ewart et al., 1980; Sutherland, 2003), South Queensland: (Ewart, 1982; Ewart et al., 1980), New South Wales: (Ewart et al., 1980; Nelson et al., 1986; Sutherland et al., 2007), Older Volcanic Province: (Nelson et al., 1986; Paul et al., 2007; Price et al., 2014), Newer Volcanic Province: (Ewart et al., 1980; Oostingh et al., 2016), Tasmanian Jurassic dolerites: (Hergt et al., 1989; Sossi, 2010).

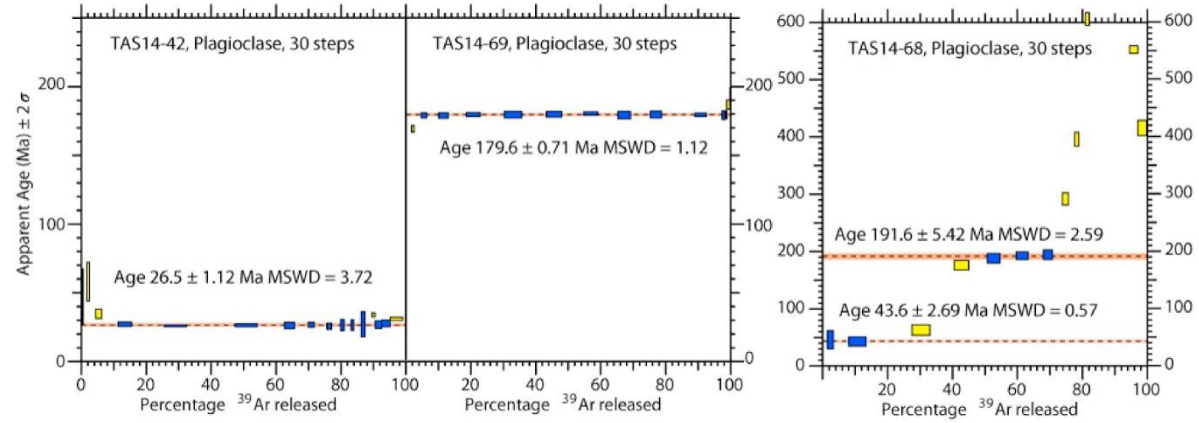

Fig. 11. Apparent age plots for selected samples: TAS14-42, TAS14-69 and TAS14-68, using *e-Argon* software (written by Prof. G. Lister, ANU). Blue and yellow steps indicate accepted and rejected heating steps respectively. Box heights indicate the 2σ error. (For interpretation of the references to colour in this figure legend, the reader is referred to the web version of this article.)

Calculated mixing lines between the Cenozoic sample with the most MORB-like isotopes, TAS14-21, with a sample of the Jurassic dolerites seems to suggest that mixing between these two endmembers could be the cause of the wide range of values present in the Cenozoic samples (Fig. 13). If the assumption is true that the Cenozoic samples in Tasmania do indeed show a mixing component with the source responsible for the Jurassic endmember, then this would also show up in the trace elements, as these are quite distinct from each other. Fig. 14 shows mixing between sample SRN (Cenozoic) and PS65 (Jurassic: quenched sill margin sample from Sossi (2010)). Of the elements plotted, K_N changes from a negative peak for Cenozoic samples, to a positive peak for Jurassic samples, and is here used as a proxy of the proportion of mixing or contamination. This K anomaly is believed to be caused by a residual K-bearing phase such as phlogopite (Adam and Green, 2011). Apart from a possible influence by mixing, the variation of K is also influenced by fractionation and/or partial melting. The K/K* value shows systematic positive co-variation with the $^{87}Sr/^{86}Sr$ ratio and a negative co-variation with $^{143}Nd/^{144}Nd$ (Fig. 15). This implies that the variation in K/K* is generated by mixing between the Jurassic source and melts from the asthenosphere.

The Cretaceous samples are quite fractionated and on the K/K* versus $^{87}Sr/^{86}Sr$ or versus $^{143}Nd/^{144}Nd$ diagrams (Fig. 15), they

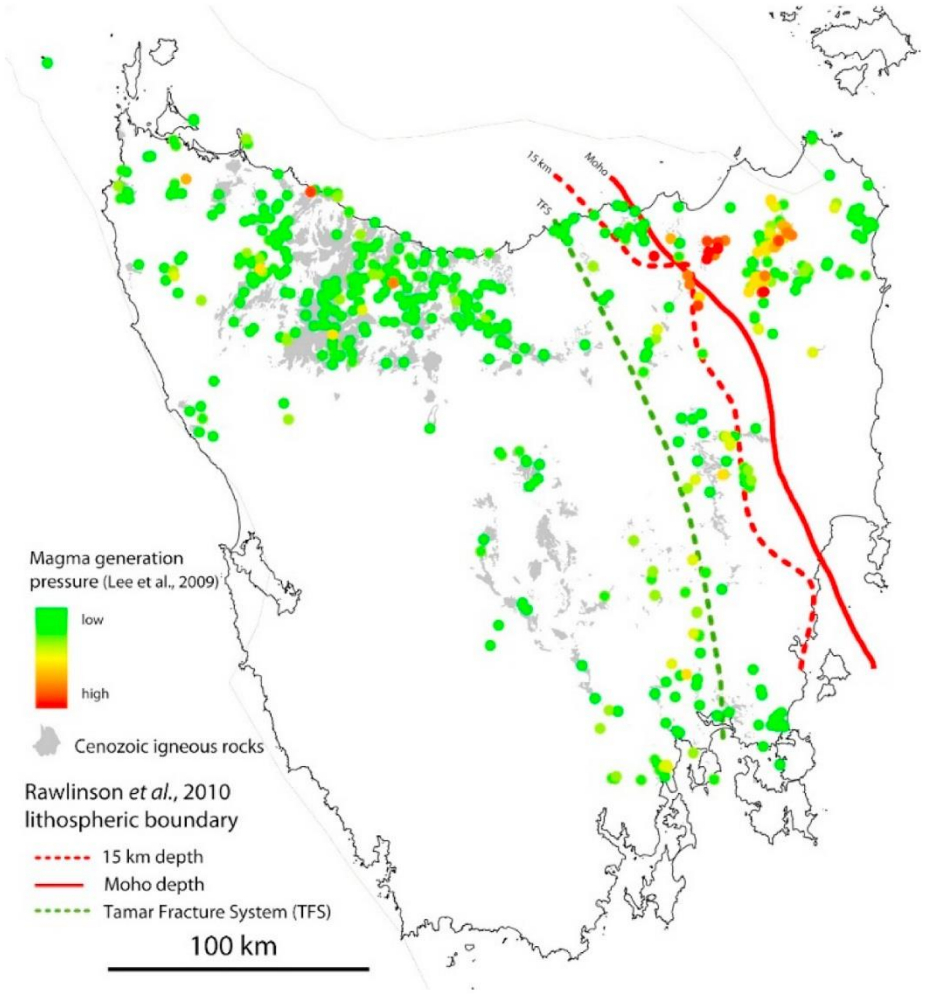

Fig. 12. Calculated temperatures and pressures of magma generation of Cenozoic basalts as per the method of Lee et al. (2009). Note that absolute values are overestimated due to very alkaline compositions and very undersaturated samples such as melilitites from Laughing Jack Marsh are not depicted on this map. Tamar Fracture System (TFS) as by Reed (2001).

approach the apparent mixing trend between the Cenozoic and Jurassic samples. The same mixing trend exists for K/K* versus $^{206}Pb/^{204}Pb$, $^{207}Pb/^{204}Pb$ and to some extent $^{208}Pb/^{204}Pb$. The trace element compositions of the Cretaceous suites are also more like those of the Jurassic than the Cenozoic examples but plot between the two (Fig. 16). It is estimated that the Jurassic low Ti tholeiites were generated by very shallow partial melting in the SCLM but that their source was a refractory harzburgite contaminated by crustal material (Sossi, 2010).

The mixing relation suggested in the data presented here imply that the availability of this Jurassic source declined between the Jurassic and the Cenozoic due to periodic melt extraction. The K/K* variation appears to have significant geographic control (Fig. 17). The Cenozoic samples with K/K* values above 0.9 mostly occur in the northwest and scatter southwards to the Tasmanian Midlands. The suites where K/K* is lower than 0.9 occur in the east and northeast. A separation between the two suites seems to be partially defined by the Tamar Lineament. This could be due to the differences in lithospheric architecture and/or absence of a Jurassic source in the central part of the eastern Terrane, as no Jurassic dolerites have been mapped in this area. Secondly, the geographic control may also be influenced by the presence of Jurassic dolerite, implying that Jurassic sources might already be depleted in these areas, generating a lower K/K*. Geochemically, K/K* are lowest in the most SiO_2-undersaturated and trace element enriched samples, as they are more resistant to any influences of the Jurassic source.

5.3. Comparison with the Eastern Australian Cenozoic Magmatic Province

Tasmania is situated at the southern end of the Eastern Australian

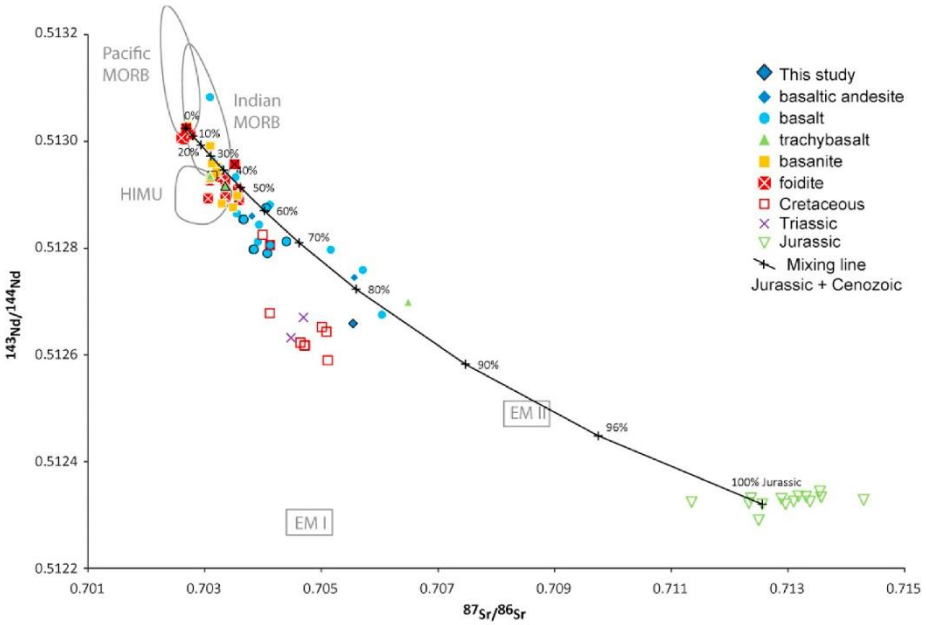

Fig. 13. $^{143}Nd/^{144}Nd$ versus $^{87}Sr/^{86}Sr$ isotope plot for samples of this study (black outlines), published Cenozoic data (Adam and Green, 2011; Everard et al., 1997; Ewart et al., 1988; Matthews et al., 1996; McDonough et al., 1985; Nasir et al., 2010; Sutherland, 2003; Zhang and Everard, 2014) with colour- and symbol-coded rock types, published Cretaceous data: (Bottrill, 2004; Everard, 2014; Taheri and Bottrill, 1999), Triassic: (Turner and Calver, 1987) and Jurassic dolerites: (Hergt et al., 1989; Sossi, 2010) and indication of mantle endmembers (Zindler and Hart, 1986).

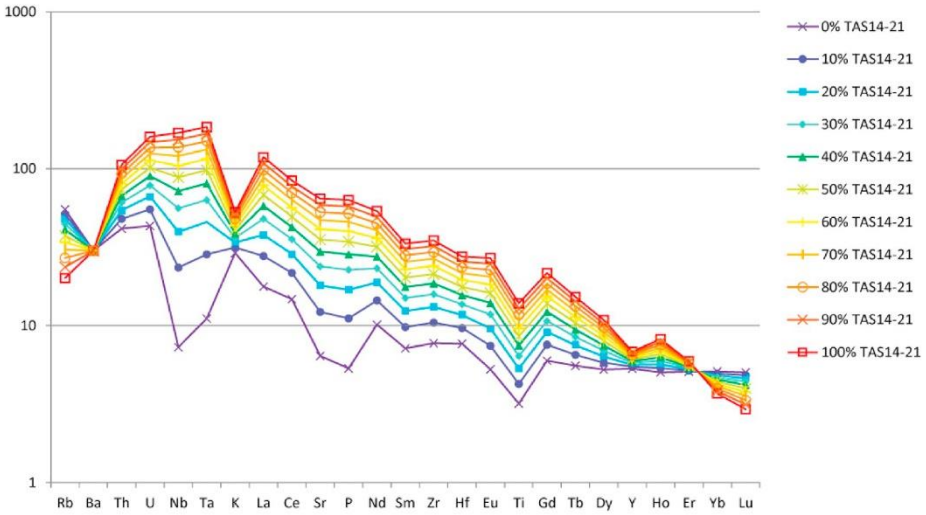

Fig. 14. Primitive mantle normalized incompatible element diagram showing calculated mixing compositions of one Cenozoic sample (TAS14-21) and a Jurassic sample PS65 (Sossi, 2010).

Cenozoic Magmatic Province (EACMP), which extends from northern Queensland, over New South Wales and Victoria into Tasmania. Although it forms part of the province, the Tasmanian Cenozoic volcanism Pb isotopes are quite distinct from the magmatism occurring in the rest of the province, mainland Australia. Typical for the central volcanoes in EACMP is the southward age progression from ~34 Ma in northern Queensland to ~3 Ma in southern Victoria (e.g. Vasconcelos et al., 2008; Wellman and McDougall, 1974), however, lava fields, including the Tasmanian volcanic rocks, do not show a clear age progression (Fig. 1). Additionally, magmatism ceased at 8 Ma whereas magmatism continued in mainland Australia, with youngest volcanic rocks of ~5000 years old (Smith and Prescott, 1987). Petrologically, the

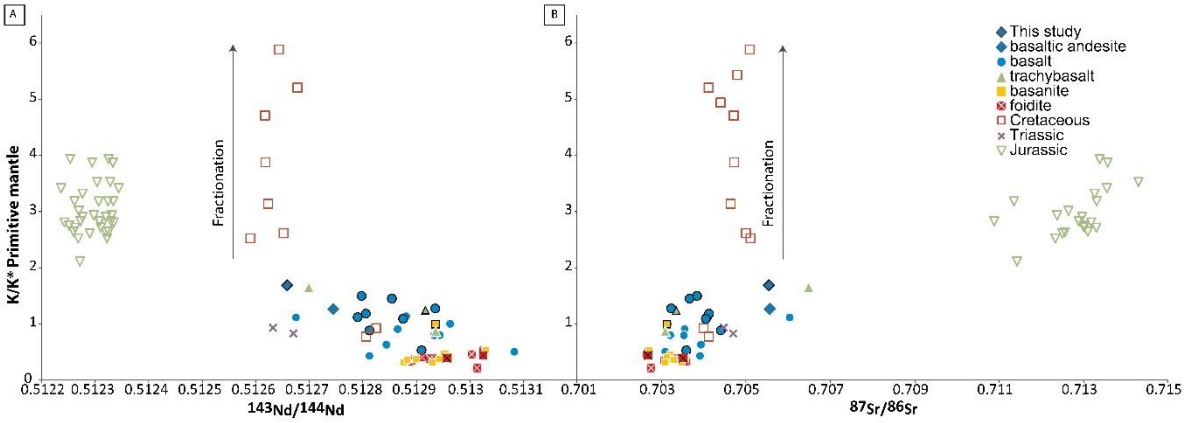

Fig. 15. K/K* normalized to primitive mantle (Sun and McDonough, 1989) where K* is calculated based on values for Nb_N & La_N, versus $^{143}Nd/^{144}Nd$ (a) and $^{87}Sr/^{86}Sr$ (b).

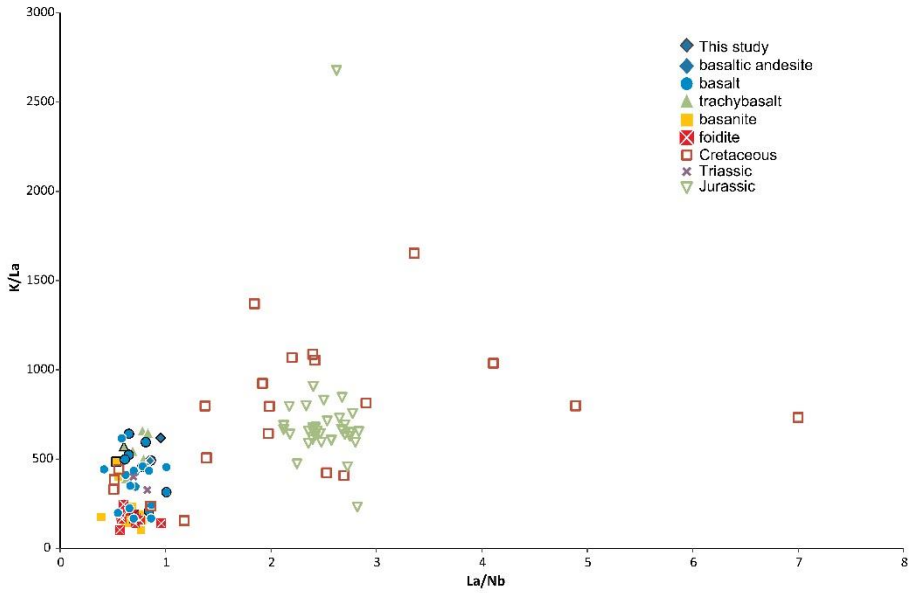

Fig. 16. K/La versus La/Nb for Triassic (Turner and Calver, 1987), Cretaceous (Bottrill, 2004; Everard, 2014; Ford, 1983; Taheri and Bottrill, 1999), Jurassic (Hergt et al., 1989; Matthews et al., 1996; Sossi, 2010) and Cenozoic samples (Adam and Green, 2011; Compston et al., 1968; Everard et al., 1997; Ewart et al., 1988; Matthews et al., 1996; McDonough et al., 1985; Nasir et al., 2010; Sutherland, 2003; Zhang and Everard, 2014), showing an intermediate trace element geochemistry for Cretaceous samples in between Cenozoic samples and Jurassic dolerites. (For interpretation of the references to colour in this figure legend, the reader is referred to the web version of this article.)

lava fields are compositionally distinct from central volcanoes due to the lack of fractionated, felsic rocks.

The most primitive and SiO_2-undersaturated Tasmanian samples have higher $^{143}Nd/^{144}Nd$ and lower $^{87}Sr/^{86}Sr$ values than other mafic volcanics in the EACMP (Fig. 8). These high Nd, low Sr samples seem to overlap the field of Pacific MORB, with lower $^{87}Sr/^{86}Sr$ than Indian Ocean MORB. Trace element data however, show that the samples are more enriched in incompatible elements than MORB (Fig. 7). This could be due to a lower amount of melting of a primitive MORB-source, but this is highly unlikely as the source would have to be strongly enriched in incompatible minor and trace elements to produce similar trace element patterns (Adam and Green, 2011). Based on Pb-isotope data

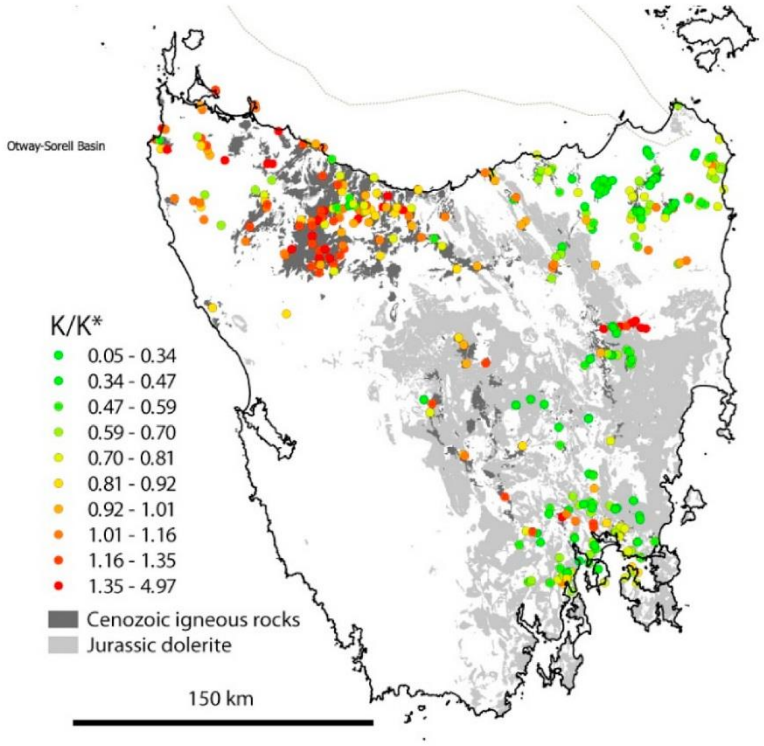

Fig. 17. Location of Cenozoic (dark grey) and Jurassic (light grey) magmatic rocks in Tasmania. Coloured dots show K/K* values for available analyses.

(Fig. 9), these more primitive samples are trending towards a HIMU source instead of a depleted mantle (DM) or MORB source. Alternatively, when taking all of the EACMP samples into account, one could argue that Pb isotopes of EACMP samples indicate a mixing trend between enriched mantle II (EMII), Indian MORB and a HIMU-like source, with Tasmanian samples closest to the HIMU endmember (Fig. 10). This HIMU source has been mentioned before (Ewart et al., 1988; Nasir et al., 2010; Sutherland et al., 2004; Sutherland et al., 1996) and requires an exceptionally high U/Pb and Th/Pb ratio. The HIMU (high $\mu = {}^{238}U/{}^{204}Pb$) signatures recognized in Pb isotope data were previously attributed to a "St. Helena type" SCLM source (Ewart et al., 1988) or a lithospheric mantle signature developed by CO_2-rich, metasomatised melts derived from old sub-lithospheric sources after the Jurassic dolerite event at ~180 Ma (Sun et al., 1989). A similar HIMU signature has also been recognized by Lanyon et al. (1993) in the Balleny plume, who therefore suggested a Balleny plume influence on Tasmanian Tertiary volcanism. Sutherland et al. (2004) argues that observed HIMU values in Tasmania however, are less than true HIMU values, termed lower μ (Panter et al., 2000) and may relate to a series of plumes along the Tasman – Ross Sea – Marie Byrd Land margin (Sutherland, 1994). Additionally, Sutherland et al. (2004) suggests that the lack of a lower μ signature in the oldest alkali basalts (59 Ma) in south-eastern Tasmania (Lanyon, 1994) fits a discrete plume model, as Tasmania was distant from the Balleny plume at that time, while the lower μ signatures in the 47 Ma northern-northeastern basalts correlate with the offshore Balleny plume position for that later time. However, addition of our new Pb-isotope data does not seem to support this theory and tectonic plate reconstruction modelling using the G-plates software (Boyden et al., 2011) indicates that the projected position of the Balleny plume was quite distant from Tasmania at times of volcanic activity during the Cenozoic (Gaina et al., 2000). Other plume theories proposed are a dispersed 'fossil' plume head (Crawford et al., 1997) or mixing with a large weak HIMU plume head that lacked volcanism (Hart et al., 1997). This lower μ signature coincides well with data.

6. Conclusions

Cenozoic volcanism in Tasmania has a complex origin. We have shown that the composition of these basalts resulted from a combination of several factors. The wide range of compositions was controlled by variable degrees of melting during decompression melting of a peridotite source and contamination by a residual source responsible for the Jurassic dolerites. The most SiO_2-undersaturated samples are generated at higher pressures (> 20 kbar) than the SiO_2-oversaturated samples. Thermal upwelling of a HIMU plume through a Pacific MORB-like asthenosphere released small degree melts/fluids which were generated within the garnet-lherzolite stability field. These subsequently interacted with the mantle lithosphere (plate 1, Fig. 18). Further heating of the lithosphere allowed low degree melts to rise rapidly to the surface creating alkaline melts with a garnet signature (pathway A, plate 2, Fig. 18). More extensive heating causes higher degree melting and allowed for mixing with Jurassic source remnants (pathway B, plate 2, Fig. 18). The depth of melting is believed to be at least partially controlled by lithospheric structures in Tasmania, with a

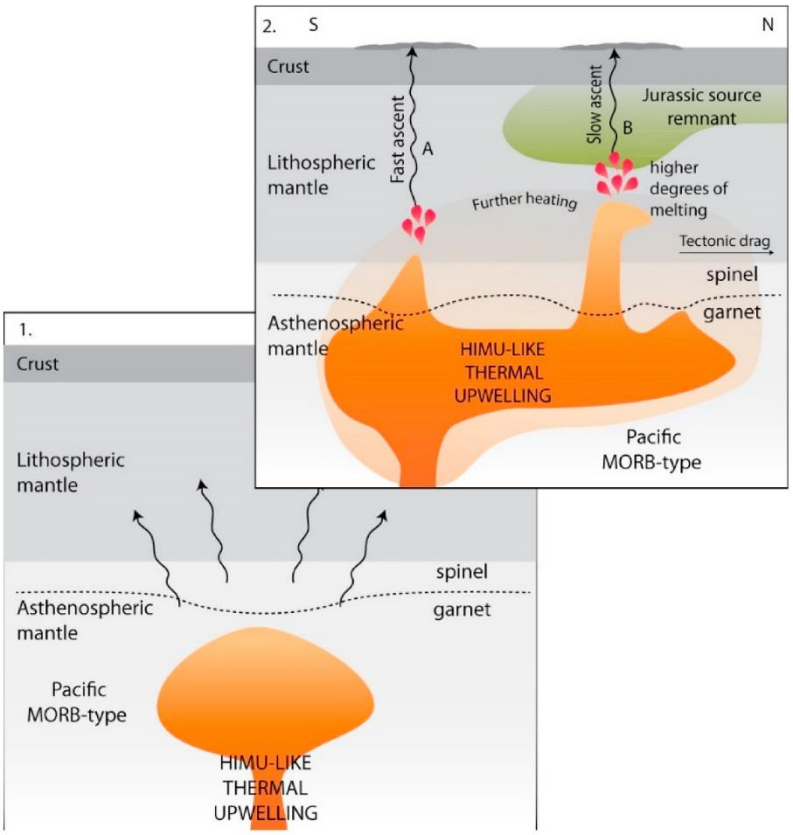

Fig. 18. Schematic overview explaining wide range in compositions and isotope signatures for Cenozoic Tasmanian magmatism.

cluster of deeper melt generation occurring in the eastern terrane of Tasmania.

Acknowledgements

The authors would like to thank L. Sutherland, J. Adams and an anonymous reviewer for their thorough feedback and suggestions. C. Chauvel is thanked for editorial handling and comments. This research forms part of a PhD project supported by the ASEG Research Foundation (RF14P05) for which funding is greatly acknowledged. The authors would also like to thank the University of Adelaide for scholarship funding. We thank Mr. David Bruce for his guidance and assistance in the geochemistry lab.

Appendix A. Supplementary data

Supplementary data to this article can be found online at https://doi.org/10.1016/j.chemgeo.2018.12.025.

References

Adam, J., 1990. The geochemistry and experimental petrology of sodic alkaline basalts from Oatlands, Tasmania. J. Petrol. 31 (6), 1201–1223.
Adam, J., Green, T., 2011. Trace element partitioning between mica- and amphibole-bearing garnet lherzolite and hydrous basanitic melt: 2. Tasmanian Cainozoic basalts and the origins of intraplate basaltic magmas. Contrib. Mineral. Petrol. 161 (6), 883–899.
Anderson, D.L., 1998. The scales of mantle convection. Tectonophysics 284 (1), 1–17.
Bacon, C.A., Everard, J.L., 1981. Pyroclastics in the upper Parmeneer Super-group, near Bicheno, Eastern Tasmania. Pap. Proc. R. Soc. Tasmania 115, 29–36.
Baillie, P.W., 1986a. A Radiometric Age for the Moriarty Basalt, North-Western Tasmania. Tasmania Department of Mines.
Baillie, P.W., 1986b. Radiometric Ages for Circular Head and the Green Hills Basalt, North-western Tasmania. Tasmania Department of Mines.
Birch, G.F., 1987. Igneous Rocks of the Gippsland Basin. Esso Australia Ltd.
Blevin, J.E., Trigg, K.R., Partridge, E.D., Boreham, C.J., Lang, S.C., 2005. Tectonostratigraphy and potential source rocks of the Bass Basin. APPEA J. 45, 601–622.
Bottrill, R.S., 2004. Petrology and Geochemistry of Some Rock Samples Collected for the WTRMP Project, Northwestern Tasmania.
Bottrill, R.S., Everard, J.L., Taheri, J., 2014. Cretaceous igneous rocks. In: Corbett, K.D., Quilty, P.G., Calver, C.R. (Eds.), Geological Evolution of Tasmania. Geological Society of Australia (Tasmania Division), pp. 453–462.
Boyden, J.A., et al., 2011. Next-generation plate-tectonic reconstructions using GPlates. In: Keller, G.R., Baru, C. (Eds.), Geoinformatics: Cyberinfrastructure for the Solid Earth. Cambridge University Press, Cambridge, pp. 95–114.
Brauns, C.M., Hergt, J.M., Woodhead, J.D., Maas, R., 2000. Os isotopes and the origin of the Tasmanian Dolerites. J. Petrol. 41 (7), 905–918.
Clouard, V., Bonneville, A., 2001. How many Pacific hotspots are fed by deep-mantle plumes? Geology 29 (8), 695–698.
Coffin, M.F., Eldholm, O., 1994. Large igneous provinces: crustal structure, dimensions, and external consequences. Rev. Geophys. 32 (1), 1–36.
Compston, W., McDougall, I., Heier, K.S., 1968. Geochemical comparison of the mesozoic basaltic rocks of Antarctica, South Africa, South America and Tasmania. Geochim. Cosmochim. Acta 32 (2), 129–149.
Corbett, K.D., Quilty, P.G., Calver, C.R., 2014. Geological evolution of Tasmania, Geological Society of Australia Special Publication 24. Geological Society of Australia (Tasmania Division).
Courtillot, V., Davaille, A., Besse, J., Stock, J., 2003. Three distinct types of hotspots in the Earth's mantle. Earth Planet. Sci. Lett. 205 (3–4), 295–308.
Crawford, A.J., Lanyon, R., Elmes, M., Eggins, S., 1997. Geochemistry and significance of basaltic rocks dredged from the South Tasman Rise and adjacent seamounts. Aust. J. Earth Sci. 44 (5), 621–632.
Davidson, J., Turner, S., Plank, T., 2013. Dy/Dy*: variations arising from mantle sources and petrogenetic processes. J. Petrol. 54 (3), 525–537.
Davies, D.R., Rawlinson, N., Iaffaldano, G., Campbell, I.H., 2015. Lithospheric controls on magma composition along Earth's longest continental hotspot track. Nature 525 (7570), 511–514.

Eggins, S.M., 2003. Laser ablation ICP-MS analysis of geological materials prepared as lithium borate glasses. Geostand. Newslett. 27 (2), 147–162.

Elburg, M., Vroon, P., van der Wagt, B., Tchalikian, A., 2005. Sr and Pb isotopic composition of five USGS glasses (BHVO-2G, BIR-1G, BCR-2G, TB-1G, NKT-1G). Chem. Geol. 223, 196–207.

Elliot, D.H., Fleming, T.H., 2004. Occurrence and dispersal of magmas in the Jurassic Ferrar large igneous province, Antarctica. Gondwana Res. 7 (1), 223–237.

Encarnación, J., Fleming, T.H., Elliot, D.H., Eales, H.V., 1996. Synchronous emplacement of Ferrar and Karoo dolerites and the early breakup of Gondwana. Geology 24 (6), 535–538.

Everard, J.E., 2014. Geological Evolution of Tasmania/editors. In: Corbett, Keith D., Quilty, Patrick G., Calver, Clive R., Pongratz, June (Eds.), Special Publication (Geological Society of Australia). 24. Geological Society of Australia (Tasmanian Division), Sydney, NSW, pp. 0072–1085.

Everard, J.L., Calver, C.R., Pemberton, J., Taheri, J., Dixon, G., 1997. Geology of the Islands of Southwestern Bass Strait.

Everard, J.L., Sutherland, F.L., Forsyth, S.M., 2007. A Late Oligocene Basalt from Keach Hill, near Campbell Town, and Its Stratigraphic Significance. Tasmanian Geological Survey.

Ewart, A., 1982. Petrogenesis of the tertiary anorogenic volcanic series of Southern Queensland, Australia, in the light of trace element geochemistry and O, Sr and Pb isotopes. J. Petrol. 23 (3), 344–382.

Ewart, A., Baxter, K., Ross, J., 1980. The petrology and petrogenesis of the tertiary anorogenic mafic lavas of southern and central Queensland, Australia - possible implications for crustal thickening. Contrib. Mineral. Petrol. 75 (2), 129–152.

Ewart, A., Chappell, B.W., Menzies, M.A., 1988. An overview of the geochemical and isotopic characteristics of the Eastern Australian Cainozoic Volcanic Provinces. In: Menzies, M.A., Cox, K.G. (Eds.), Oceanic and Continental Lithosphere: Similarities and Differences. Journal of Petrology Special Volumepp. 225–274.

Fishwick, S., Rawlinson, N., 2012. 3-D structure of the Australian lithosphere from evolving seismic datasets. Aust. J. Earth Sci. 59 (6), 809–826.

Fishwick, S., Heintz, M., Kennett, B.L.N., Reading, A.M., Yoshizawa, K., 2008. Steps in lithospheric thickness within eastern Australia, evidence from surface wave tomography. Tectonics 27.

Ford, R.J., 1983. The alkaline rocks of Port Cygnet, Tasmania. In: University of Tasmania.

Forster, M.A., Lister, G.S., 2009. Core-complex-related extension of the Aegean lithosphere initiated at the Eocene-Oligocene transition. J. Geophys. Res. Solid Earth 114 (B2).

Forsyth, S.M., 1984. Geological Survey explanatory report. Geological atlas 1:50,000 series. Sheet 68 (8313S). Oatlands., Tasmania Department of Mines.

Forsyth, S.M., 1989. Geological Survey explanatory report. Geological atlas 1:50,000 series. Sheet 61 (8313N). Interlaken., Tasmania Department of Mines.

Frey, F.A., Green, D.H., Roy, S.D., 1978. Integrated models of basalt petrogenesis: a study of quartz tholeiites to olivine melilitites from south eastern Australia utilizing geochemical and experimental petrological data. J. Petrol. 19 (3), 463–513.

Gaina, C., Dietmar Müller, R., Cande, S.C., 2000. Absolute Plate Motion, Mantle Flow, and Volcanism at the Boundary Between the Pacific and Indian Ocean Mantle Domains Since 90 MA, the History and Dynamics of Global Plate Motions. American Geophysical Union, pp. 189–210.

Gibson, D., 2007. Potassium-Argon ages of Late Mesozoic and Cainozoic igneous rocks of eastern Australia. In: CRC Leme Open File Report 193.

Hart, S.R., 1984. A large-scale isotope anomaly in the Southern Hemisphere mantle. Nature 309 (5971), 753–757.

Hart, S.R., Blusztanjn, J., LeMasurier, W.F., Rex, D.C., 1997. Hobbs Coast Cenozoic volcanism: Implications for the West Antarctic rift system. Chem. Geol. 139, 223–248.

Hergt, J.M., Brauns, C.M., 2001. On the origin of Tasmanian dolerites. Aust. J. Earth Sci. 48 (4), 543–549.

Hergt, J.M., Chappell, B.W., McCulloch, M.T., McDougall, I., Chivas, A.R., 1989. Geochemical and Isotopic Constraints on the Origin of the Jurassic Dolerites of Tasmania. J. Petrol. 30 (4), 841–883.

Hill, P.J., Meixner, A.J., Moore, A.M.G., Exon, N.F., 1997. Structure and development of the west Tasmanian offshore sedimentary basins: results of recent marine and aeromagnetic surveys. Aust. J. Earth Sci. 44 (5), 579–596.

Hirose, K., Kushiro, I., 1993. Partial melting of dry peridotites at high pressures: determination of compositions of melts segregated from peridotite using aggregates of diamond. Earth Planet. Sci. Lett. 114 (4), 477–489.

Holford, S.P., Schofield, N., Macdonald, J.D., Duddy, I.R., Green, P.F., 2012. Seismic analysis of igneous systems in sedimentary basins and their impacts on hydrocarbon prospectivity: examples from the southern Australian margin. APPEA J. 52, 229–252.

Holford, S.P., Schofield, N., Reynolds, P., 2017. Subsurface fluid flow focused by buried volcanoes in sedimentary basins: evidence from 3D seismic data, Bass Basin, offshore southeastern Australia. Interpretation 5 (3), SK39–SK50.

Irvine, T.N., Baragar, W.R.A., 1971. A guide to the chemical classification of the common volcanic rocks. Can. J. Earth Sci. 8 (5), 523–548.

Ishizuka, O., Taylor, R.N., Milton, J.A., Nesbitt, R.W., 2003. Fluid–mantle interaction in an intra-oceanic arc: constraints from high-precision Pb isotopes. Earth Planet. Sci. Lett. 211 (3), 221–236.

Ivanov, A., et al., 2017. Timing and genesis of the Karoo-Ferrar large igneous province: New high precision U-Pb data for Tasmania confirm short duration of the major magmatic pulse. Chem. Geol. 455, 32–43.

Jackson, M.G., Dasgupta, R., 2008. Compositions of HIMU, EM1, and EM2 from global trends between radiogenic isotopes and major elements in ocean island basalts. Earth Planet. Sci. Lett. 276 (1–2), 175–186.

Johnson, C.M., Beard, B.L., 1999. Correction of instrumentally produced mass fractionation during isotopic analysis of fe by thermal ionization mass spectrometry. Int. J. Mass Spectrom. 193 (1), 87–99.

Klein, E.M., Langmuir, C.H., Staudigel, H., 1991. Geochemistry of basalts from the Southeast Indian Ridge, 115°E–138°E. J. Geophys. Res. 96 (B2), 2089–2107.

Kyle, P.R., 1980. Development of heterogeneities in the subcontinental Mantle: evidence from the Ferrar Group, Antarctica. Contrib. Mineral. Petrol. 73 (1), 89–104.

Kyle, P.R., 1981. Mineralogy and geochemistry of a basanite to phonolite sequence at Hut Point Peninsula, Antarctica, based on core from Dry Valley Drilling Project Drillholes 1, 2 and 3. J. Petrol. 22 (4), 451–500.

Lanyon, R., 1994. Mantle Reservoirs and Mafic Magmatism Associated With Break-up of Gondwana - The Balleny Plume and the Australian - Antarctic Discordance. University of Tasmania, Hobart.

Lanyon, R., Varne, R., Crawford, A.J., 1993. Tasmanian Tertiary basalts, the Balleny plume, and opening of the Tasman Sea (southwest Pacific Ocean). Geology 21 (6), 555–558.

Lanyon, R., Crawford, A.J., Eggins, S.M., 1995. Westward migration of Pacific Ocean upper mantle into the Southern Ocean region between Australia and Antarctica. Geology 23 (6), 511–514.

Le Bas, M.J., Le Maitre, R.W., Streckeisen, A., Zanettin, B., Rocks, I.S.o.t.S.o.I., 1986. A chemical classification of volcanic rocks based on the Total Alkali-Silica Diagram. J. Petrol. 27 (3), 745–750.

Lee, C.T.A., Luffi, P., Plank, T., Dalton, H., Leeman, W.P., 2009. Constraints on the depths and temperatures of basaltic magma generation on Earth and other terrestrial planets using new thermobarometers for mafic magmas. Earth Planet. Sci. Lett. 279 (1–2), 20–33.

Lister, G.S., Etheridge, M.A., 1989. Detachment models for uplift and volcanism in the Eastern Highlands, and their application to the origin of passive margin mountains. In: Johnson, R.W. (Ed.), Intraplate Volcanism in Eastern Australia and New Zealand. Cambridge University Press, Cambridge.

Lovera, O.M., Richter, F.M., Harrison, T.M., 1989. 40Ar/39Ar thermochronometry for slowly cooled samples having a distribution of diffusion domain sizes. J. Geophys. Res. 94, 17917–17935.

MacPhail, M.K., Hill, R.S., 1994. K-Ar dated palynofloras in Tasmania 1: Early Oligocene, *Proteacidites tuberculatus* Zone sediments, Wilmot Dam, northwestern Tasmania. Pap. Proc. R. Soc. Tasmania 128, 1–15.

Matthews, W.I., Everard, J.F., Clarke, M.J., 1996. Geological atlas 1:50,000 series. Sheet 54 (8314S). Lake River.

McDonough, W.F., Sun, S.S., 1995. Composition of the Earth. Chem. Geol. 120, 223–253.

McDonough, W.F., McCulloch, M.T., Sun, S.S., 1985. Isotopic and geochemical systematics in tertiary-recent basalts from southeastern Australia and implications for the evolution of the sub-continental lithosphere. Geochim. Cosmochim. Acta 49 (10), 2051–2067.

Mcdougall, I., Brown, F.H., 2006. Precise 40Ar/39Ar geochronology for the upper Koobi Fora Formation, Turkana Basin, northern Kenya. J. Geol. Soc. Lond. 163, 205–220.

Meeuws, F.J.E., Holford, S.P., Foden, J.D., Schofield, N., 2016. Distribution, chronology and causes of Cretaceous – Cenozoic magmatism along the magma-poor rifted southern Australian margin: links between mantle melting and basin formation. Mar. Pet. Geol. 73, 271–298.

Menzies, M.A., Wass, S.Y., 1983. CO2- and LREE-rich mantle below eastern Australia: a REE and isotopic study of alkaline magmas and apatite-rich mantle xenoliths from the Southern Highlands Province, Australia. Earth Planet. Sci. Lett. 65 (2), 287–302.

Morgan, W.J., 1971. Convection Plumes in the Lower Mantle. Nature 230, 42.

Morgan, W.J., 1972. Deep mantle convection plumes and plate motions. AAPG Bull. 56 (2), 203–213.

Mortimer, N., et al., 1995. Ferrar magmatic province rocks discovered in New Zealand: implications for Mesozoic Gondwana geology. Geology 23 (2), 185–188.

Nasir, S.J., Everard, J.L., McClenaghan, M.P., Bombardieri, D., Worthing, M.A., 2010. The petrology of high pressure xenoliths and associated Cenozoic basalts from Northeastern Tasmania. Lithos 118 (1–2), 35–49.

Nelson, D.R., McCulloch, M.T., Sun, S.-S., 1986. The origins of ultrapotassic rocks as inferred from Sr, Nd and Pb isotopes. Geochim. Cosmochim. Acta 50 (2), 231–245.

Oostingh, K., Jourdan, F., Merle, R., Chiaradia, M., 2016. Spatio-temporal geochemical evolution of the SE Australian upper mantle deciphered from Sr, Nd and Pb isotopes of Cainozoic intraplate volcanics. J. Petrol. 57 (8), 1509–1530.

O'Reilly, S.Y., Griffin, W.L., 1984. Sr isotopic heterogeneity in primitive basaltic rocks, southeastern Australia: correlation with mantle metasomatism. Contrib. Mineral. Petrol. 87 (3), 220–230.

O'Reilly, S.Y., Zhang, M., 1995. Geochemical characteristics of lava-field basalts from eastern Australia and inferred sources: connections with the subcontinental lithospheric mantle? Contrib. Mineral. Petrol. 121, 148–170.

Panter, K.S., Hart, S.R., Kyle, P.R., Blusztanjn, J., Wilch, T.I., 2000. Geochemistry of Late Cenozoic basalts from the Crary Mountains: characterization of mantle sources in Marie Byrd Land, Antarctica. Chem. Geol. 165, 215–241.

Paul, B., Hergt, J.M., Woodhead, J.D., 2007. Mantle heterogeneity beneath the Cenozoic volcanic provinces of central Victoria inferred from trace-element and Sr, Nd, Pb and Hf isotope data. Aust. J. Earth Sci. 52 (2), 243–260.

Petke, T., Kodolányi, J., Kamber, B.S., 2018. From ocean to mantle: new evidence for U-cycling with implications for the HIMU source and the secular Pb isotope evolution of Earth's mantle. Lithos 316–317, 66–76.

Price, R.C., Nicholls, I.A., Day, A., 2014. Lithospheric influences on magma compositions of late Mesozoic and Cenozoic intraplate basalts (the Older Volcanics) of Victoria, south-eastern Australia. Lithos 206–207 (0), 179–200.

Pyle, D., Christie, D.M., Mahoney, J., Duncan, R.A., 1995. Geochemistry and geochronology of ancient southeast Indian and southwest Pacific seafloor. J. Geophys. Res. Solid Earth 100 (B11), 22261–22282.

Raczek, I., Jochum, K.P., Hofmann, A.W., 2003. Neodymium and Strontium Isotope Data for USGS Reference Materials BCR-1, BCR-2, BHVO-1, BHVO-2, AGV-1, AGV-2, GSP-1, GSP-2 and Eight MPI-DING Reference Glasses. Geostand. Newslett. 27, 173–179.

Rawlinson, N., Tkalcic, H., Reading, A.M., 2010. Structure of the Tasmanian lithosphere from 3D seismic tomography. Aust. J. Earth Sci. 57 (4), 381–394.
Reed, A.R., 2001. Pre-Tabberabberan deformation in eastern Tasmania: a southern extension of the Benambran Orogeny. Aust. J. Earth Sci. 48 (6), 785–796.
Reynolds, P., Schofield, N., Brown, R.J., Holford, S.P., 2018. The architecture of submarine monogenetic volcanoes – insights from 3D seismic data. Basin Res. 30, 437–451.
Richards, M.A., Duncan, R.A., Courtillot, V.E., 1989. Flood basalts and hot-spot tracks: plume heads and tails. Science 246 (4926), 103–107.
Rudnick, R.L., Gao, S., 2003. 3: The Crust, 3.01 - the composition of the continental crust. In: Holland, H.D., Turekian, K.K. (Eds.), Treatise on Geochemistry. Elsevier-Pergamon, Oxford, pp. 1–64.
Schmidt, P.W., McDougall, I., 1977. Palaeomagnetic and potassium-argon dating studies of the Tasmanian Dolerites. J. Geol. Soc. Aust. 24 (5–6), 321–328.
Schofield, A., Totterdell, J., 2008. Distribution, timing and origin of magmatism in the Bight and Eucla Basins. Geoscience Australia. Theatr. Rec. 2008 (/4), 19.
Seymour, D.B., Green, G.R., Calver, C.R., 2013. The geology and mineral deposits of Tasmania: a summary. Min. Resour. Tasmania Bull. 72.
Smith, B.W., Prescott, J.R., 1987. Thermoluminescence dating of the eruption at Mt Schank, South Australia. Aust. J. Earth Sci. 34, 335–342.
Sossi, P.A., 2010. The Northern Margin of the Ferrar Large Igneous Province: Petrogenesis and Differentiation of the Tasmanian Dolerites and Kangaroo Island Basalts. University of Adelaide, pp. 180.
Spell, T.L., Mcdougall, I., 2003. Characterization and calibration of 40Ar/39Ar dating standards. Chem. Geol. 198, 189–211.
Steiger, R.H., Jager, E., 1977. Subcommission on geochronology: convention on the use of decay constants in geo- and cosmochronology. Earth Planet. Sci. Lett. 36, 359–362.
Sun, S.-s., McDonough, W.F., 1989. Chemical and isotopic systematics of oceanic basalts: implications for mantle composition and processes. Geol. Soc. Lond., Spec. Publ. 42 (1), 313–345.
Sun, S.S., McDonough, W.F., Ewart, A., 1989. Four component dynamic model for East Australian basalts. In: Johnson, R.W. (Ed.), Intraplate Volcanism in Eastern Australia and New Zealand. Cambridge University Press, pp. 333–347.
Sutherland, F.L., 1973. Igneous rocks, Central Plateau. In: Banks, M.R. (Ed.), The Lake Country of Tasmania. The Royal Society of Tasmania, Hobart, pp. 43–54.
Sutherland, F.L., 1974. High-pressure inclusions in tholeiitic basalt and the range of lherzolite-bearing magmas in the Tasmanian volcanic province. Earth Planet. Sci. Lett. 24 (2), 317–324.
Sutherland, F.L., 1981. Migration in relation to possible tectonic and regional controls in eastern Australian volcanism. J. Volcanol. Geotherm. Res. 9 (2–3), 181–213.
Sutherland, F.L., 1991. Cainozoic volcanism, eastern Australia: a predictive model based on migration over multiple 'hotspot' magma sources. In: Williams, M.A.J., de Decker, P., Kershaw, A.P. (Eds.), Cenozoic of the Australian Region; a Reappraisal of the Evidence. Special Publication of the Geological Society of Australia, pp. 15–43.
Sutherland, F.L., 1994. Tasman Sea evolution and hotspot trails. In: Van der Lingen, G.J., Swanson, K.M., Muir, R.J. (Eds.), Evolution of the Tasman Sea Margin. A.A. Balkema, Rotterdam, pp. 33–51.
Sutherland, F.L., 2003. 'Boomerang' migratory intraplate Cenozoic volcanism, eastern Australian rift margins and the Indian-Pacific mantle boundary. Geol. Soc. Am. Spec. Pap. 372, 203–221.
Sutherland, F.L., Hale, G.F.A., 1970. Cainozoic volcanism in and around Great Lake, Central Tasmania. Pap. Proc. R. Soc. Tasmania 104, 17–32.
Sutherland, F.L., Wellman, P., 1986. Potassium-argon ages of Tertiary volcanics rocks, Tasmania. Pap. Proc. R. Soc. Tasmania 120, 77–86.
Sutherland, F.L., Ewart, A., Raynor, L.R., Hollis, J.D., McDonough, W.F., 1989. Tertiary basaltic magmas and the Tasmanian lithosphere. In: Burrett, C.F., Martin, E.L. (Eds.), Geology and Mineral Resources of Tasmania. A Bicentennial Volume. Special Publication of the Geological Society of Australia, pp. 386–398.
Sutherland, F.L., Hendry, D.F., Barron, B.J., Matthews, W.L., Hollis, J.D., 1996. An unusual Tasmanian Tertiary basalt sequence, near boat Harbour, northwest Tasmania. Rec. Aust. Mus. 48 (2), 131–162.
Sutherland, F.L., Forsyth, S.M., Zwingmann, H., 2002. Bassian basalts: dating, Cenozoic biogeohistory and a new model for Tasmanian volcanism. In: Geological Society of Australia Abstracts. 67(251).
Sutherland, F.L., Graham, I.T., Everard, J.L., Forsyth, S.M., Zwingmann, H., 2004. Cenozoic basalts, Tasmania: landscapes, exposures, ages, petrography, geochemistry, entrainments and petrogenesis. In: Field Guide A5: Geological Society of Australia.
Sutherland, F.L., Graham, I.T., Forsyth, S.M., Zwingmann, H., Everard, J.L., 2006. The Tamar Trough revisited: correlations between sedimentary beds, basalts, their ages and valley evolution, north Tasmania. Pap. Proc. R. Soc. Tasmania 140, 49–74.
Sutherland, F.L., Graham, I.T., Zwingmann, H., Pogson, R.E., Barron, B.J., 2007. Belmore Volcanic Province, northeastern New South Wales, and some implications for plume variations along Cenozoic migratory trails. Aust. J. Earth Sci. 52 (6), 897–919.
Taheri, J., Bottrill, R.S., 1999. Porphyry and Sedimentary-hosted Gold Deposits near Cygnet: New Styles of Gold Mineralisation in Tasmania.
Taylor, S.R., McLennan, S.M., 1985. The Continental Crust: Its Composition and Evolution.
Turner, N.J., Calver, C.R., 1987. Geological Survey Explanatory Report, Geological Atlas 1:50 000 series, sheet 49 (8514N) St Marys.
Van Achterbergh, E., Ryan, C.G., Jackson, S.E., Griffin, W.L., 2001. Data reduction software for LA-ICP-MS. In: Sylvester, P.J. (Ed.), Laser-Ablation-ICPMS in the Earth Sciences; Principles and Applications. Mineralogical Association of Canada, Ottowa, pp. 239–243.
Vasconcelos, P., Knesel, K., Cohen, B., Heim, J., 2008. Geochronology of the Australian Cenozoic: a history of tectonic and igneous activity, weathering, erosion, and sedimentation. Aust. J. Earth Sci. 55 (6–7), 865–914.
Vermeesch, P., 2012. On the visualisation of detrital age distributions. Chem. Geol. 312-313, 190–194.
Wellman, P., McDougall, I., 1974. Cainozoic igneous activity in eastern Australia. Tectonophysics 23 (1–2), 49–65.
White, W.M., Hofmann, A.W., Puchelt, H., 1987. Isotope geochemistry of Pacific Mid-Ocean Ridge Basalt. J. Geophys. Res. 92 (B6), 4881–4893.
Willbold, M., Stracke, A., 2006. Trace element composition of mantle end-members: implications for recycling of oceanic and upper and lower continental crust. Geochem. Geophys. Geosyst. 7 (4) (Q04004), 1–30.
Wilson, S.A., 1997a. The collection, preparation, and testing of USGS reference material BCR-2, Columbia River. Basalt: U.S. Geological Survey Open-File Report 98.
Wilson, S.A., 1997b. Data compilation for USGS reference material BHVO-2. U.S. Geological Survey Open-File Report, Hawaiian Basalt.
Workman, R.K., et al., 2004. Recycled metasomatized lithosphere as the origin of the Enriched Mantle II (EM2) end-member: evidence from the Samoan Volcanic Chain. Geochem. Geophys. Geosyst. 5 (4) (n/a–n/a).
Zhang, B., Everard, J.L., 2014. Geological evolution of Tasmania. In: Corbett, Keith D., Quilty, Patrick G., Calver, Clive R., Pongratz, June (Eds.), Special Publication (Geological Society of Australia). 24. 0072-1085 Geological Society of Australia (Tasmanian Division), Sydney, NSW.
Zhang, M., O'Reilly, S.Y., Chen, D., 1999. Location of Pacific and Indian mid-ocean ridge–type mantle in two time slices: evidence from Pb, Sr, and Nd isotopes for Cenozoic Australian basalts. Geology 27 (1), 39–42.
Zhang, M., Stephenson, P.J., O'Reilly, S.Y., McCulloch, M.T., Norman, M., 2001. Petrogenesis and Geodynamic Implications of Late Cenozoic Basalts in North Queensland, Australia: Trace-element and Sr–Nd–Pb isotope evidence. J. Petrol. 42 (4), 685–719.
Zindler, A., Hart, S., 1986. Chemical geodynamics. Annu. Rev. Earth Planet. Sci. 14 (1), 493–571.

Chapter 4

Geochemical and seismic reflection constraints on the nature of Cretaceous magmatic activity in the Gippsland Basin

Statement of Authorship

Title of Paper	Characterising extrusive and intrusive magmatism at the Kipper Field, Gippsland Basin, using 3D seismic data and geochemistry.
Publication Status	☐ Published ☐ Accepted for Publication ☐ Submitted for Publication ☑ Unpublished and Unsubmitted work written in manuscript style
Publication Details	Meeuws, F.J.E., Holford, S.P., Foden, J., Schofield, N. Characterising extrusive and intrusive magmatism at the Kipper Field, Gippsland Basin, using 3D seismic data and geochemistry. Unsubmitted

Principal Author

Name of Principal Author (Candidate)	Fun Julie Ellen Meeuws		
Contribution to the Paper	Performed analyses on the majority of geochemistry samples and all seismic data, interpreted data, wrote manuscript and acted as corresponding author.		
Overall percentage (%)	80		
Certification:	This paper reports on original research I conducted during the period of my Higher Degree by Research candidature and is not subject to any obligations or contractual agreements with a third party that would constrain its inclusion in this thesis. I am the primary author of this paper.		
Signature		Date	2/07/2019

Co-Author Contributions

By signing the Statement of Authorship, each author certifies that:

i. the candidate's stated contribution to the publication is accurate (as detailed above);

ii. permission is granted for the candidate in include the publication in the thesis; and

iii. the sum of all co-author contributions is equal to 100% less the candidate's stated contribution.

Name of Co-Author	Associate Professor Simon Holford		
Contribution to the Paper	Helped in seismic data interpretation, manuscript evaluation and editing.		
Signature		Date	2/07//2019

Name of Co-Author	Emeritus Professor John Foden		
Contribution to the Paper	Helped in geochemistry interpretation and helped with manuscript evaluation.		
Signature		Date	2/07/2019

Name of Co-Author	Dr Nick Schofield		
Contribution to the Paper	Helped in seismic data interpretation and helped with manuscript evaluation.		
Signature		Date	2/07/2019

Please cut and paste additional co-author panels here as required.

ABSTRACT

Although the Gippsland Basin is one of Australia's most important economic hydrocarbon producing basins, a large part of its geology is often overlooked. The Late Cretaceous syn- and post-rift successions of the Gippsland Basin host both intrusive and extrusive igneous rocks emplaced during several magmatic events (Late Cretaceous – Eocene) which have a large influence on several existing hydrocarbon plays. The Kipper Field in particular has benefited from a >100 m thick sequence of Late Cretaceous basalts, top-sealing a 328 m gross gas column and 14 m oil leg, reservoired in the Golden Beach Sub-group of the Latrobe Group sediments. Regional mapping of 3D seismic reflection data reveals an extensive magmatic plumbing system comprising more than 186 intrusions that shallows from the central part of the basin towards the basin–bounding faults at the northern margin, where magmas were extruded onto the paleo-land surface during the Late Cretaceous. Our mapping indicates that magmas can travel significant vertical (3 sec TWT) and horizontal distances (>40 km in this case) before finally extruding. The highest concentration of igneous occurrences are located in the vicinity of broadly ~E-W striking basin-bounding faults, with magmas younging from east (Late Cretaceous – Turonian/Campanian) to west (Eocene) along the northern Rosedale fault system. The major and trace element geochemistry of sampled extrusive and intrusive rocks show strong similarities with Cretaceous and Cenozoic magmas found in onshore Tasmania, with an Upper Continental Crust signature in the Campanian lavas similar to Jurassic and Cretaceous intrusions and lavas onshore Tasmania and an Oceanic Island Basalt signature in younger Eocene lavas and intrusive sills similar to the Cenozoic basalts onshore Tasmania.

1. INTRODUCTION

The Gippsland Basin is one of Australia's most prolific hydrocarbon provinces and forms part of the Australian southern rifted margin, which formed during Early Cretaceous due to the separation of Australia and Antarctica (Blevin and Cathro, 2008). The basin has been proven to be a world-class hydrocarbon province and the geology and its giant oil and gas fields are well-studied (Featherstone et al., 1991; O'Brien et al., 2008; Rahmanian et al., 1990; Sloan et al., 1992). The Gippsland Basin contains a rich-record of magmatic activity which occurred during rifting and subsequent post-rift thermal subsidence. However, even though

46 of the 318 (~14.5%) petroleum exploration wells drilled in the basin have encountered igneous rocks, the nature and origin of this magmatism remains largely undescribed. The presence of volcanic rocks can impact hydrocarbon systems both positively and negatively (e.g. Holford et al., 2013; Holford et al., 2012; Holford et al., 2017; Meeuws et al., 2016b; Schutter, 2003). For example, impermeable networks of intrusive bodies may compartmentalize source and reservoir sequences thereby reducing migration efficiencies, whilst focussed fluid flow associated with sills and dykes may reduce reservoir quality and puncture sealing horizons. On the other hand, intrusion into shallow source rocks may increase levels of maturity, and saucer-shaped sills emplaced within reservoirs can create attractive traps with four-way closures through forced folding (Holford et al., 2012). Knowledge of magmatic plumbing systems in hydrocarbon-rich basins, such as the Gippsland Basin, is therefore of paramount importance to reduce exploration risk.

The advanced understanding of igneous rocks imaged in 3D seismic reflection surveys provide the opportunity to have a better understanding of igneous plumbing systems within sedimentary rift basins and facilitate a better understanding of their impact on possible hydrocarbon systems. The Kipper Field in the Gippsland Basin is a prime example of a hydrocarbon accumulation that has been positively impacted by igneous activity in a petroliferous basin. With the exception of a focussed study on the Kipper Field by O'Halloran and Johnstone (2001), there has been little work on magmatism in the Gippsland Basin and our understanding of igneous processes in general and in neighbouring basins (e.g. magmatic studies of the Bight Basin (Jackson et al., 2013; Magee et al., 2013; Reynolds et al., 2017b; Reynolds et al., 2018a; Schofield and Totterdell, 2008) and Bass Basin (Holford et al., 2017; Reynolds et al., 2018b)) has much evolved since then. The availability of geochemical (e.g major and trace element geochemistry) and petrophysical (e.g wire-line well logs) datasets acquired through drilling of igneous rocks in the Gippsland Basin allows for characterisation of the magmas, while the wide coverage of seismic reflection data provides insight into the nature of the magmatic plumbing system. This unique combination of datasets make the Gippsland Basin an ideal laboratory to investigate magmatic processes in petroliferous sedimentary basins. Here we identify two different styles of magmatic plumbing systems, emplaced at different times, within the Gippsland Basin. Combined with the geochemical signature of the igneous rocks, this provides with a better understanding of magmatism in the

Gippsland Basin and sedimentary rift basins in general and the link with Meso-Cenozoic magmatism in the Bass Strait and in onshore Tasmania.

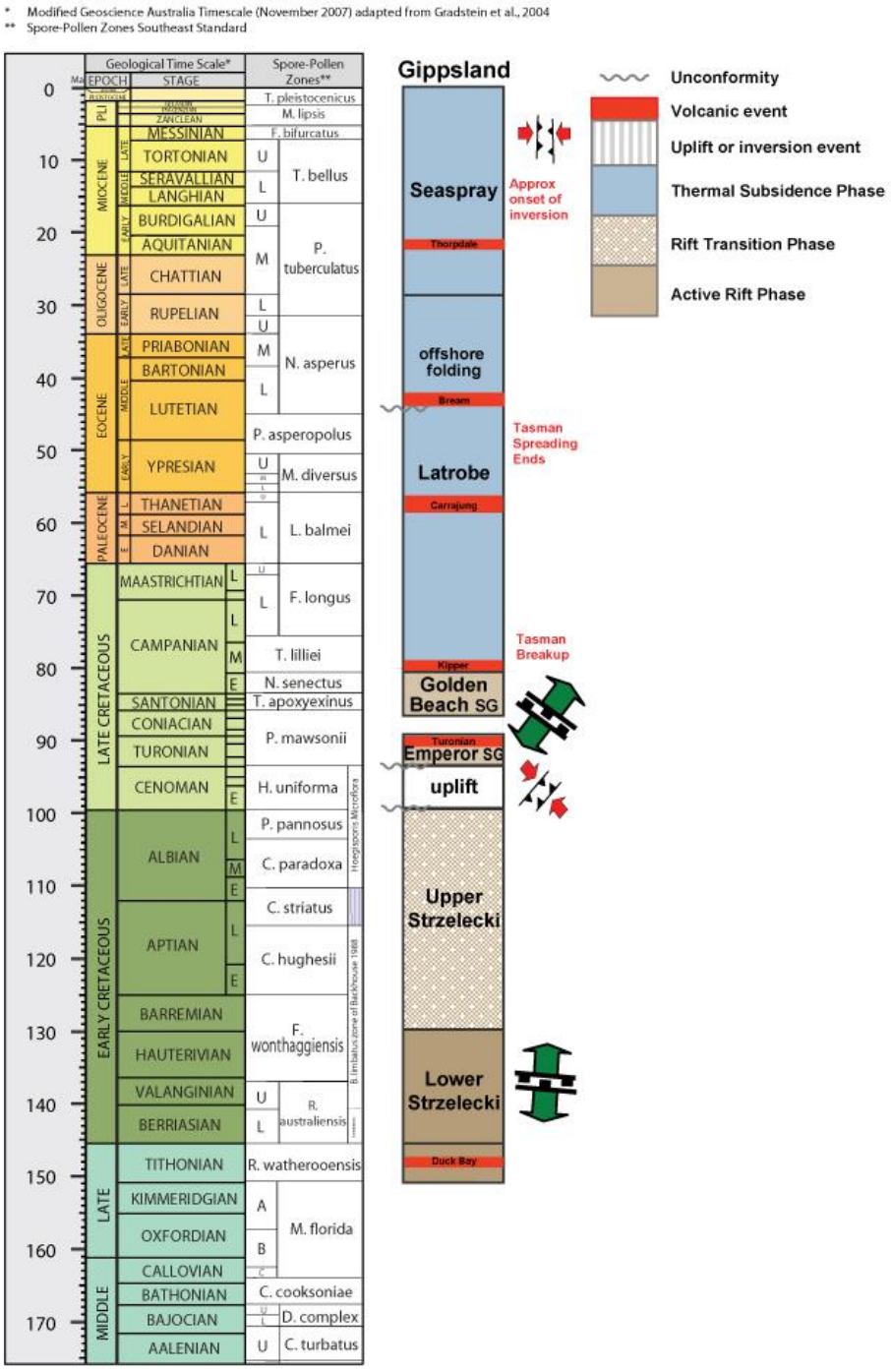

Figure 1: Tectonostratigraphic column of the Gippsland Basin with magmatic and basin events indicated (modified from Meeuws et al. (2016))

2. GIPPSLAND BASIN

As one of the most hydrocarbon-rich basins in Australia, the Gippsland Basin forms the easternmost end of the Australia's rifted southern continental margin. The Gippsland Basin finds its origin during Jurassic to Early Cretaceous rifting and subsidence during the separation of Australia and Antarctica, and a renewed period of Late Cretaceous incomplete rifting of a branch of the Tasman Sea (Norvick and Smith, 2001; Rahmanian et al., 1990). Initially, its architecture consisted of an east-west trending rift valley during the Early Cretaceous, which later evolved due to continued rifting during the Turonian to Campanian, into a broad Central Deep, flanked by fault-bounded platforms and terraces to the north and south (Norvick and Smith, 2001). Post-rift subsidence and a subsequent compressional events during the late Eocene-middle Miocene, gave rise to a series of northeast to east-northeast trending anticlines, resulting in partial basin inversion (Power et al., 2001). An overview of the tectonostratigraphy of the Gippsland Basin is provided in Figure 1.

Spreading of the Tasman Sea is believed to be responsible for a phase of intrusive and extrusive igneous activity around 80 Ma (O'Halloran and Johnstone, 2001). Remnants of this igneous activity are still present within the syn-rift sediments of the Golden Beach and Emperor Subgroups of the Latrobe Group (O'Halloran and Johnstone, 2001), primarily occurring along the northern and southern basin-bounding fault systems, with minor occurrences near the Bream Field, Remora-Sunfish, Whiting-Wirrah and Tuna regions (Birch, 1987) (Figure 2). Mafic magmatic bodies located along the eastern end of the northern basin-bounding faults are most extensive and mainly consist of multi-layered, anastomosing aggregated basalt flows, whilst a feature interpreted to be a single volcanic cone (~100 m high) has been described in the Bream area (Birch, 1987). Based on seismic velocities and petrography of recovered rocks, both intrusive and extrusive features have been recognized and are of olivine basalt or dolerite composition (Birch, 1987; McPhail, 2000). As samples are too altered, no recovered igneous rocks have been dated using absolute dating techniques (Birch, 1987; McPhail, 2000). Biostratigraphic dating of sediments overlying igneous rocks however, indicate ages of 87 to 49 Ma, with the majority of sequences of Late Cretaceous (Campanian) age (Birch, 1987; McPhail, 2000).

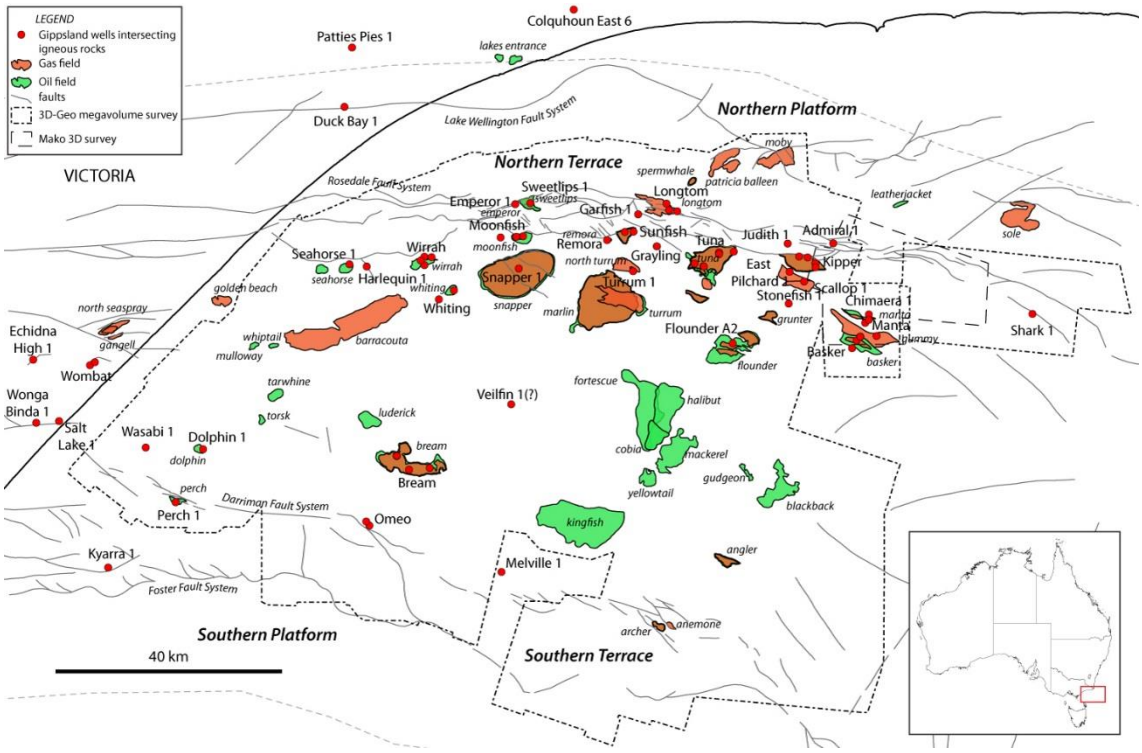

Figure 2: Location map of wells that have been reported to intersect igneous rocks (red dots), oil and gas fields (italic) and main basin bounding faults in the Gippsland Basin, offshore Victoria.

2.1 Kipper Field

The Gippsland Basin hosts several giant oil and gas fields, with the majority of the discoveries reservoired within the siliciclastics of the Late Cretaceous Golden Beach Subgroup of the Latrobe Group (Bernecker and Partridge, 2001; Sloan et al., 1992). The Golden Beach Subgroup sediments consist of braided-stream and alluvial-fan sandstones and conglomerates at the margin of the basin and fluvial, finer grained deposits deeper in the basin, followed by a thick lacustrine unit (Bernecker and Partridge, 2001; Sloan et al., 1992).

The Kipper Field is located ~40 km offshore, on the northern flank of the Gippsland Basin, and forms one of the largest gas fields in the Gippsland Basin (Figure 2). The Field was discovered with the drilling of well Kipper-1 (1986) and constrained by a second well, Kipper-2 (1987). It holds a 328 m gross gas column and a 14 m gross oil leg, trapped by a fault within the Golden Beach reservoir, and top sealed by several volcanic lava flows with a total thickness exceeding 100 m (O'Halloran and Johnstone, 2001).

3. DATA AND METHODOLOGY

3.1 Seismic data and resolution

This study uses a subset of two time-migrated 3D seismic reflection surveys (Mako 3D (2007) and the 3D-Geo seismic megavolume merge of 3D surveys). The 3D-Geo seismic megavolume covers ~11,000 km² and images down to 6 s TWT with a bin spacing of 50 x 50 m. Mako 3D survey has a bin spacing of 25 x 12.5 m, covers ~505 km² and images down to 6 s TWT. Downwards increases of acoustic impedance (e.g. transition from a sedimentary rock into a high density igneous rock) are visualised by a blue reflector. Downwards acoustic impedance decreases (e.g. transition from a high density volcanic rock into a sedimentary rock) are visualised as a red reflector.

Seismic resolution of the data changes greatly within the merged 3D survey. The dominant frequency of the seismic data between 1.6 – 2.2 seconds TWT (below the interpreted extrusive sequences, within the Golden Beach and Emperor Subgroups) is 22 Hz near the Kipper Field and decreases to 13 Hz in the Central Deep of the basin between 4.1 – 4.8 seconds TWT in the Strzelecki Group (where the deepest interpreted intrusions occur). Wireline logs for one of the Kipper wells indicates that seismic velocity beneath the igneous rocks is approximately 3450 m/s, which gives a vertical resolution of approximately 40 m and a detectability of *ca.* 20 m. As there are no wells that penetrate the strata in which the deeper intrusions in the Central Deep occur, the velocity of these sequences is unconstrained. Assuming a seismic velocity of 3500 - 4000 m/s results in a vertical resolution of 68 - 77 m and detectability of *ca.* 34 - 39 m.

3.2 Seismic interpretation strategy

3.2.1. Intrusions

Intrusive features have mainly been identified using their tendency to cross-cut stratigraphy, their laterally discontinuous nature and high seismic amplitudes (Smallwood and Maresh, 2002). From wireline logs it was determined that sills in the Gippsland Basin show lower densities than expected for mafic igneous rocks, which results in a smaller acoustic impedance difference with surrounding sediments and therefore a weaker reflection in the

seismic data. For example, a dolerite intrusion encountered in the Tuna-4 well has a density of ~2500 kg/m³ while dolerites generally have a density of 2900 kg/m³. This difference could be caused by weathering and/or alteration. Calculation of a pseudo relief attribute (quadrature of absolute amplitude values) in GeoTeric© helped visualize the less obvious intrusions in these cases.

3.2.2. Extrusive units

Extrusive igneous sequences were picked as horizons, following identification based on the seismic volcanostratigraphy and seismic geomorphology techniques of Planke et al. (2000) and Planke et al. (2017) respectively. The top of the extrusive sequences surrounding the Kipper Field was picked, interpolated and smoothed. Conventional seismic attributes, such as amplitude, time and envelope, were used to delineate the extent of the Kipper extrusive sequences. A spectral decomposition frequency blend was created for the smoothed horizon of the extrusive sequences. The use of an RGB blend on frequency decomposition analyses allowed for a clearer visualisation of lava flow morphology and allowed for a more precise delineation of its extent. In this dataset, an RGB blend (R: 10 Hz, G: 24 Hz, B: 52 Hz) was used to image the extrusive sequences. A High Definition Frequency Decomposition (HDFD) RGB blend (R: 20 Hz, G: 30 Hz, B: 40 Hz) volume was created of the Bream Field (west) to identify intrusions below the extrusive complex which are otherwise masked by high amplitude coal layers. The top of the Latrobe Group (Top Latrobe horizon) has been identified in seismic data, correlated using well data and is used as a reference horizon in order to account for sediment thickness while comparing depth of the intrusions. This horizon was chosen due to its lateral continuity and the fact that it is easily recognizable on seismic data.

3.3 Geochemical data

Eighteen drill core samples, and where core was not available, six cutting samples were taken from exploration wells intersecting igneous rocks in the Gippsland Basin in order to assess their composition and genesis. Drill core samples were washed in ultrasonic baths and were crushed and powdered using a tungsten-carbide jaw crusher and mill. These powders have been analysed for major elements using X-ray fluorescence (XRF) at the Commonwealth Scientific and Industrial Research Organisation (CSIRO), Adelaide (Appendix C - Table 1). Major elements have been analysed on XRF fused discs using a lithium tetra-borate flux. Trace

elements have been analysed LA-ICP-MS on XRF fused discs as described in (Meeuws et al., under review). Drill cutting samples have been washed in an ultrasonic bath and igneous lithologies have been separated and powdered using a mortar and pestle. These powders have then been analysed using ICP on mixed acid digest using a lithium borate fusion at Bureau Veritas Adelaide (Appendix C - Table 1).

4. OBSERVATIONS AND RESULTS

4.1 Seismic interpretation

4.1.1 Intrusions

A total of 186 features interpreted to be igneous intrusions have been identified on seismic reflection data, though based on well log interpretation and cuttings descriptions, this is likely an underestimate of the number of intrusions present in the area. For example, in the Faroe Shetland Basin, 88% of intrusions intersected by petroleum wells have been shown to be thinner than the vertical resolution of the seismic reflection data at depths at which the majority of intrusions occur (Schofield et al., 2015). Vertical seismic resolution of the rock sequences that contain intrusions ranges between 40 m and >77 m, with detectability between 20 m and 39 m. This is similar to the Faroe Shetland Basin, where vertical seismic resolution is estimated to reduce from 40 m (20 m detectability) at the top of the Cretaceous to 81 m (40 m detectability) at the base of the Cretaceous (Schofield et al., 2015). We infer that that quite a large number of intrusions will be difficult to identify in the Gippsland Basin and even thick intrusions (>40 m) will be missed in the deeper parts of the basin.

The area of mapped intrusions ranges between 0.1 – 80 km², with 121 intrusions smaller than 10 km² in area. Intrusions are generally saucer-shaped and large groups of interconnected sills can be identified. Due to insufficient seismic data quality in the 3D Geo megasurvey, kinematic indicators of flow direction were only visible in intrusions present in the Mako3D survey (e.g. intrusion 34 – Figure 3). When mapped relative to depth below the Top Latrobe horizon, it is clear that the intrusions occur at relatively deeper depths (± 3 sec TWT below Top Latrobe) in the Central Deep of the basin and shallower depths (0.5 – 0 sec TWT below Top Latrobe) near the basin bounding faults (Figure 4). This suggests that intrusions were fed by magmas that originated from beneath the Central Deep and migrated

both laterally and vertically towards the basin-bounding faults in the north and south (Figure 4). Depth conversion in the Gippsland Basin, and especially the Central Deep, is problematic due to the presence of Miocene channels filled with high velocity sediments (Birmingham et al., 1985) and the lack of deep well penetration at the level of the deepest intrusions therefore only allows for a very rough depth estimate of the deepest intrusions of ± 3 km below the Top Latrobe horizon. The lateral distance traversed by the intrusions exceeds 40 km.

Because of their intrusive nature, constraining the timing of emplacement is problematic. Sediments overlying the igneous intrusions will often be folded to accommodate their emplacement. Onlapping relationships of sediments overlying these forced folds allow for dating of the intrusion where biostratigraphic data is available (Trude et al., 2003) . None of the intrusions in the Gippsland Basin have caused doming of overlying sediments, so no precise age of intrusion can be obtained.

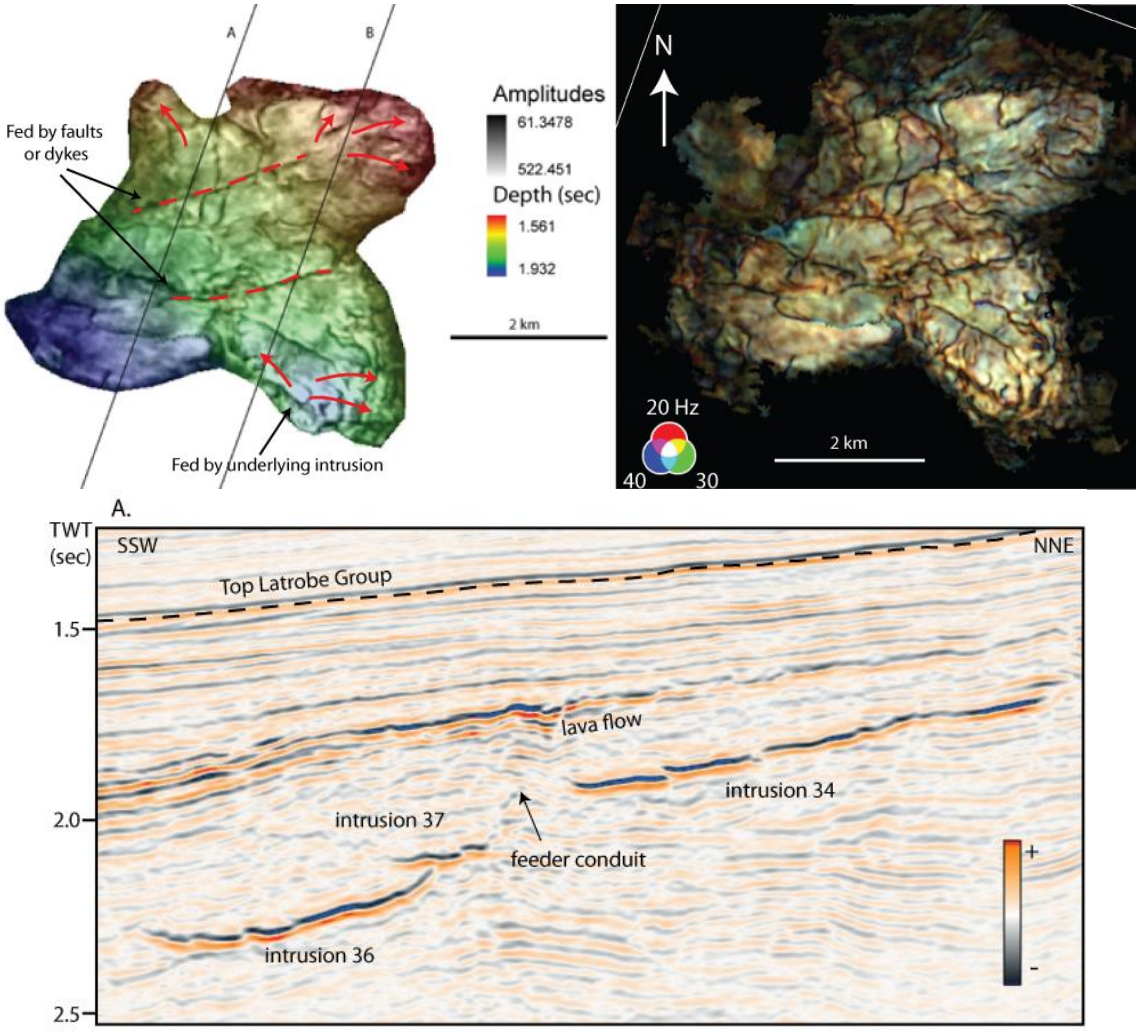

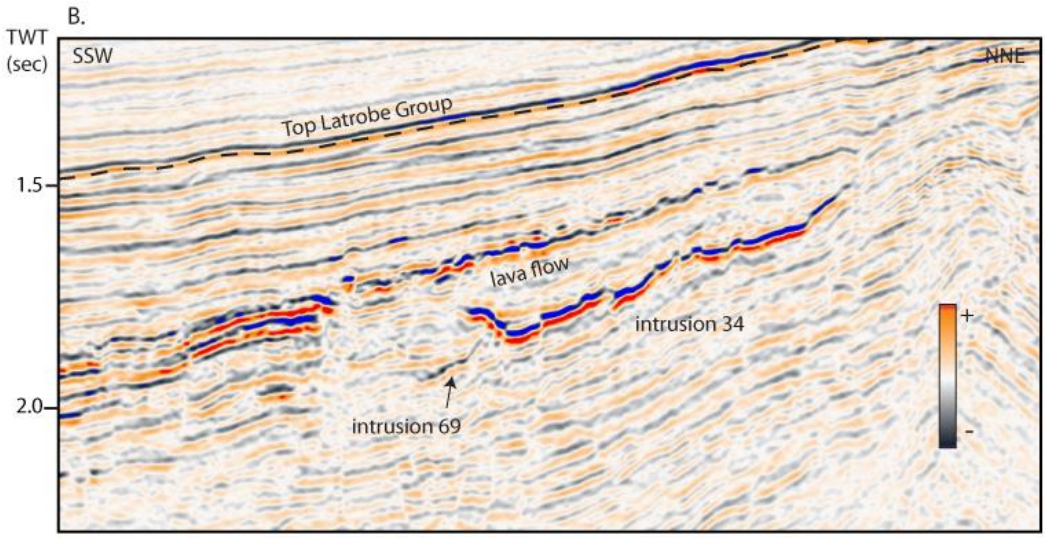

Figure 3: Example of an intrusion showing kinematic indicators of flow directions and possible feeding points, with locations of cross-sections A and B (dataset MAKO3D). Cross-section A shows an example of intrusions progressively shallowing (intrusion 36 to intrusion 37 and intrusion 34) and feeding overlying lava flows as indicated by feeders. Cross-section B shows a barely visible intrusion 69 feed intrusion 34, which in turn might have fed the overlying lava flow.

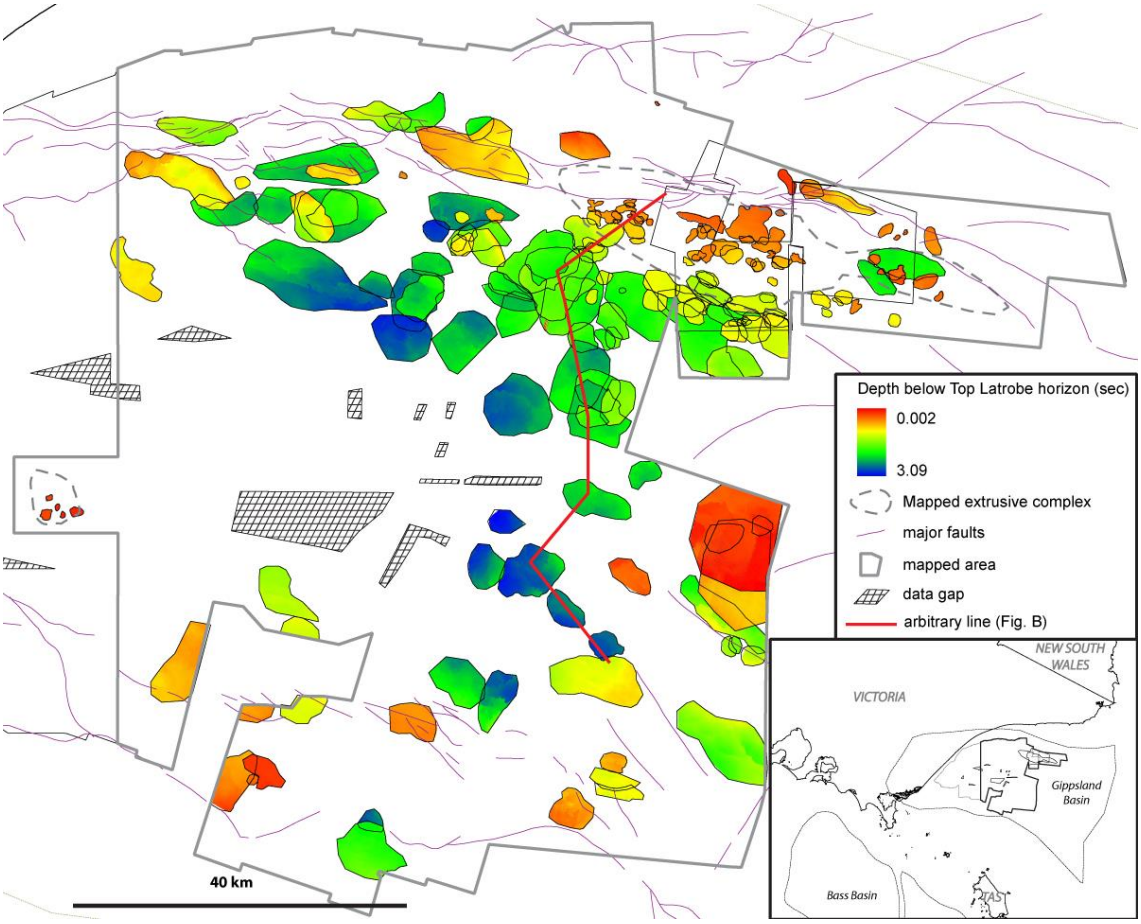

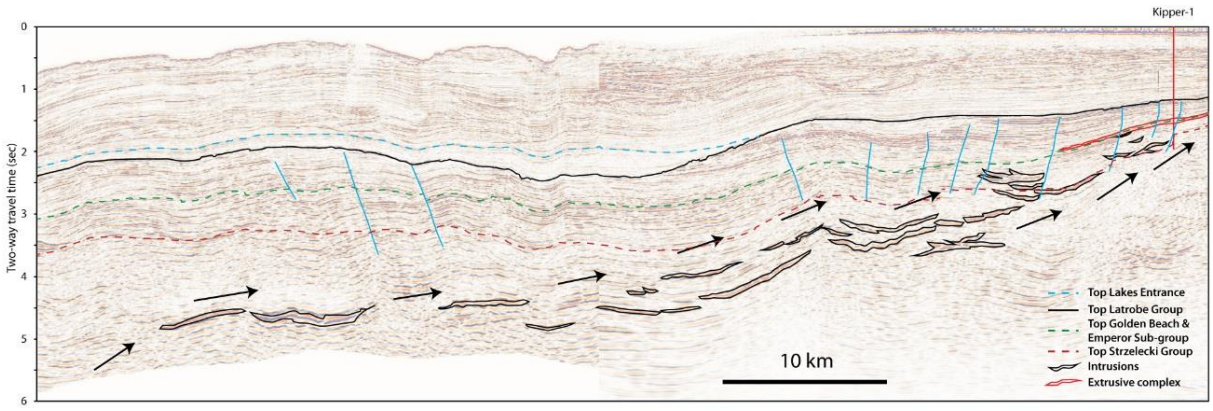

Figure 4: A: Depth in seconds below Top Latrobe horizon of mapped intrusions and location of arbitrary line showing a connected network of shallowing intrusions ultimately feeding the overlying lava flow (Figure 4B).

4.1.2 Extrusive units

The top of the Kipper extrusive sequences has been mapped in a single horizon with a surface area of ~422 km². The extent of the extrusive sequences has been confirmed by wells Admiral-1, Basker-1 to -5, Basker South-1, Chimaera-1, East Pilchard-1, Judith-1, Kipper-1, Kipper-2, Kipper-2A, Kipper-4A, Scallop-1, Manta-1, Manta-2A, Scallop-1, Shark-1 and Stonefish-1 (Table 2). The seismic expression of the extrusive sequences consists of a hard reflection with an irregular reflector on top. Separate lava flows can be picked in the western and southern part of the basin e.g. near wells Perch-1 and Garfish-1, but these were not mapped in detail in this study. The timing of extrusive activity was constrained using reported palynology results of surrounding sedimentary rocks obtained from well completion reports (WCR) (Table 2).

In addition to the Kipper extrusive sequences, multiple volcanic vents with a total area of 23.5 km² were identified near the Bream Field (west). The largest (main) vent has a diameter of ~2 km. The igneous origin of this cone was confirmed by core and ditch cutting samples (Bream-2 and Bream-A15 WCR). The vents are located above coal layers which are represented by strong reflectors in the seismic. Due to the reported weathered state of the cones (WCR) and due to the strong amplitude reflectors of the coal layers, the amplitudes of the vents do not stand out strongly from surrounding sediments and the location of sills and possible plumbing systems beneath the vents are masked (Figure 5). The top of the vents

complex coincides with the top of the Latrobe Group sediments (lower *N. asperus*), indicating a Middle Eocene age.

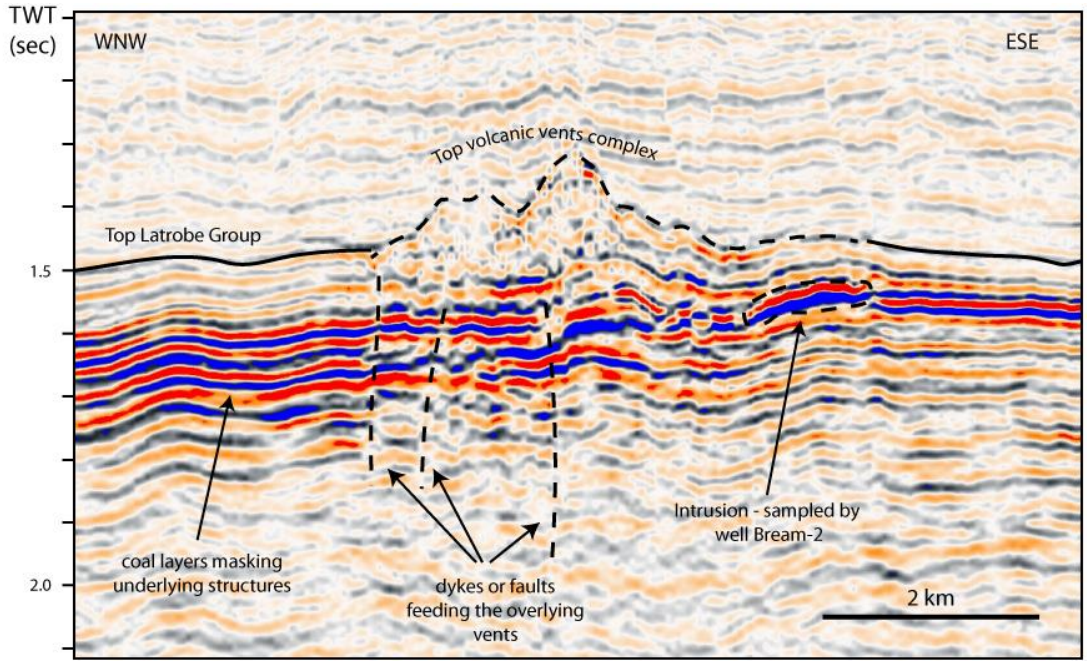

Figure 5: Interpreted crossline 1679 of the 3D Geo megasurvey through the volcanic vents near the Bream Field showing the top of the volcanic vents complex, top of the Latrobe Group sediments, high amplitude coal layers masking underlying structures, the location of the intrusion sampled by well Bream-2 and dykes or faults feeding the overlying vents.

4.2 Frequency decomposition and colour blending of seismic data

An RGB blend frequency decomposition map was constructed of the picked horizon of the top extrusive sequences to help delineate the extruded extrusive sequences. This spectral decomposition map shows several bright areas caused by frequency anomalies (Figure 6). Due to their brightness and texture, these bright areas are interpreted as extrusive sequences. A main extrusive sequence (extrusive sequence 1: Figure 6) can be identified which is intersected by the Kipper wells. A second extrusive sequence (extrusive sequence 2: Figure 6) can be identified towards the east, but it is not clear if both extrusive sequences are or were connected at one stage as the extrusive sequence may be too thin to resolve in the seismic data. Within these lava flows several high frequency anomalies can be discerned. Further analyses of cross-sections through these bright spots has confirmed that these bright spots are shallow intrusions that may have fed the extrusive sequences (Figure 6C). Faults are observed intersecting and offsetting the top of the extrusive sequences. Seismic data quality

does not appear detailed enough to identify kinematic indicators in these extrusive sequences, however 3D analyses has indicated at least part of the sequence in the NW is fed by a fault.

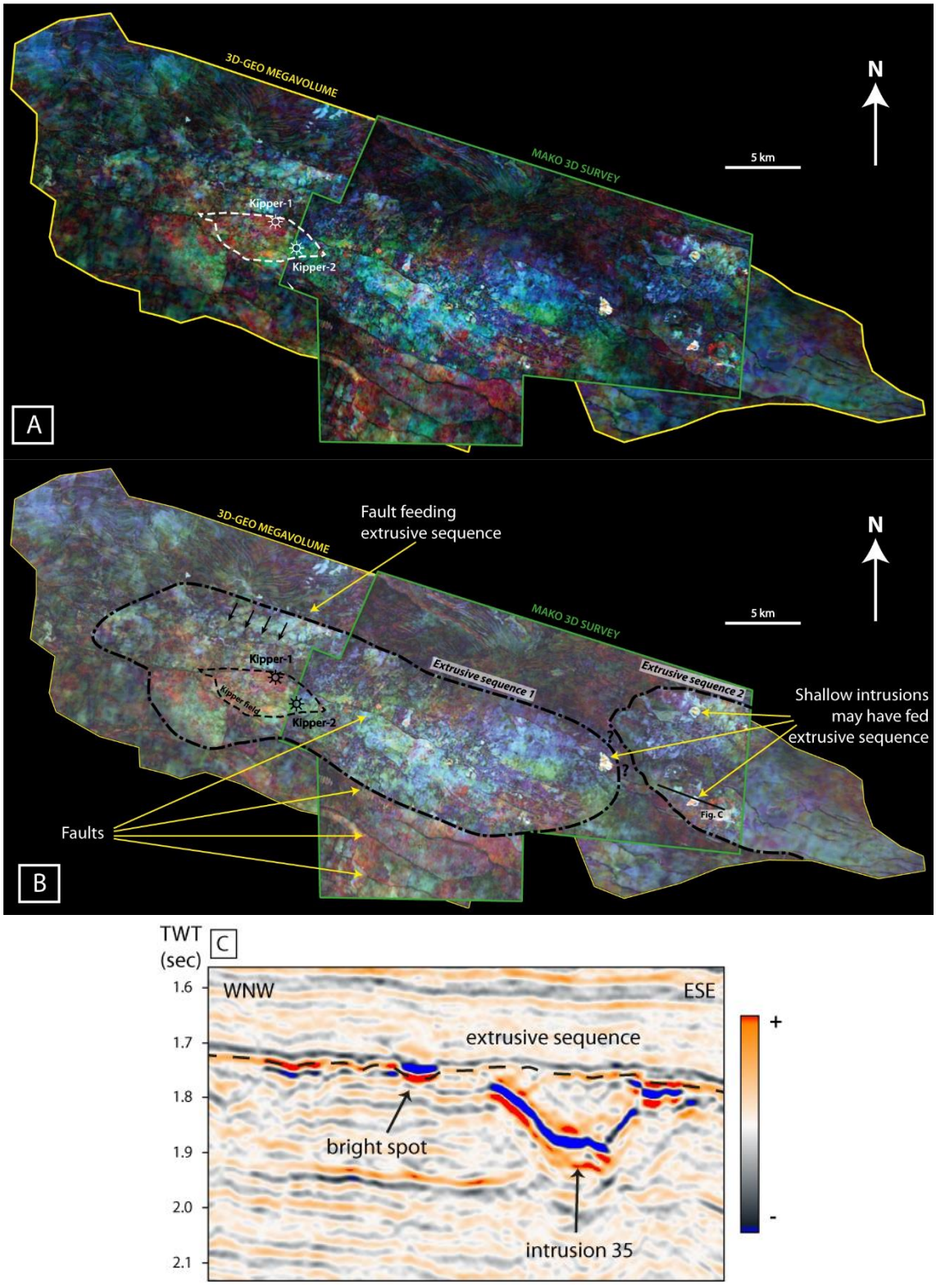

Figure 6: A: Spectral decomposition RGB blend (R: 10 Hz, G: 24 Hz, B: 52 Hz) image of the mapped horizon of the top of the Kipper extrusive sequences and location of the Kipper Field and wells Kipper-1

and -2. B: Interpreted spectral decomposition RGB blend of the mapped top of the Kipper extrusive sequences. C: Cross-section through one of the high frequency anomalies (location on Fig. 6B).

A HDFD frequency decomposition RGB blend volume (R: 20 Hz, G: 30 Hz, B: 40 Hz) which focusses on the coal layers was constructed of the area surrounding the western Bream field, to further identify magmatic features within the coal layers underlying the volcanic vents. Due to the slightly differing frequency responses of the coal layers and intrusions, several intrusions were identified within the coal layers. A plan view image of the mapped top of the volcanic vents complex (Figure 7A) shows the extent and main vents of the complex. A cross-section through the largest vent and an intrusion sampled by well Bream-2 illustrates the different frequency response of the intrusions within the coal layers. The coal layers show an overall bright response – a strong amplitude in all three frequencies, while the intrusions mainly show amplitudes in the 20 Hz (red) frequency range (Figure 7B). The portrayed intrusion has upward edges and is therefore saucer-shaped. The RGB blend of the intrusion shows slight doming in the centre of the intrusion. This is also observed in other intrusions in the Bream area.

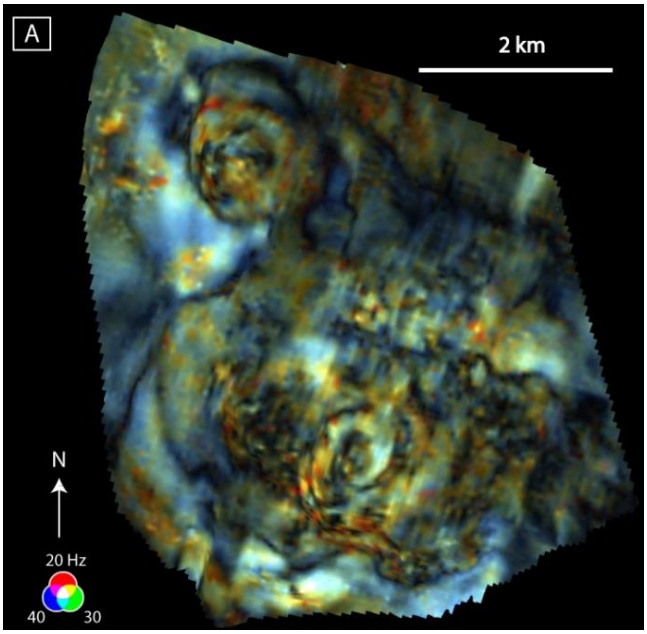

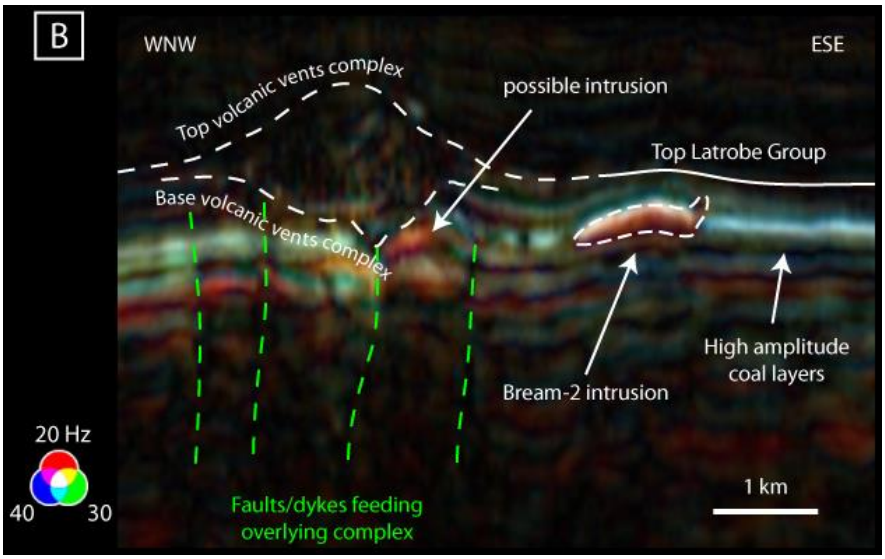

Figure 7: A: Plan view of RGB blend frequency decomposition (20, 30, 40 Hz) of the top of the volcanic vents complex near the Bream Field. B: Cross-section through intrusion sampled by well Bream-2, showing the different frequency response of the intrusion with regards to the coal layers.

4.3 Characterisation of wireline logs

Caliper (CALI), Gamma Ray (GR), Sonic (DT), Density (RHOB), Resistivity (LLD and LLS) and Photo-electric absorption factor (PEF) wireline logs for wells Kipper-1, Kipper-2, Kipper-2A and Kipper-4A, have been interpreted to characterise the petrophysical signatures of igneous rocks. Subaerially extruded basalts formed in a continuous outpouring of lava (i.e. resulting in lava flows), can consist of several packages of lava surrounded by a chilled crust, called flow lobes (Self et al., 1997). Typically, fresh subaerially extruded basalt presents a log signature characterised by high density (> 2.6 g/m³), high p-wave velocity (Vp > 5 km/s), high resistivity, low gamma ray (< 10 API) and low porosity (15%). Chilled margins surrounding the fresh basalt show lower Vp, density and resistivity and higher porosities, aiding identification of separate flow lobes (Boldreel, 2006).

Different extrusive facies have been interpreted for the different wells. Based on lower than average densities (2.4 – 2.7 g/m³) and wider than average caliper values (340 – 430 mm) due to washout or wall collapse, Kipper-1 has been interpreted to intersect a ~100 m section of hyaloclastite with high neutron values (up to 0.52) associated with clay bound water, whereas Kipper-2 is interpreted to intersect a mixture of lavas with higher, blockier densities than Kipper-1 and volcaniclastics. An example of log signature from well Kipper-1 and Kipper-2 is provided in Figure 8 with increased photoelectric absorption factors (PEF > 5 B/BE) as

indication for the presence of the volcanic rocks. Although PEF is extremely sensitive to washout and mudcake buildup (McPhail, 2000), it still gives a good indication of the presence of igneous rocks in these wells.

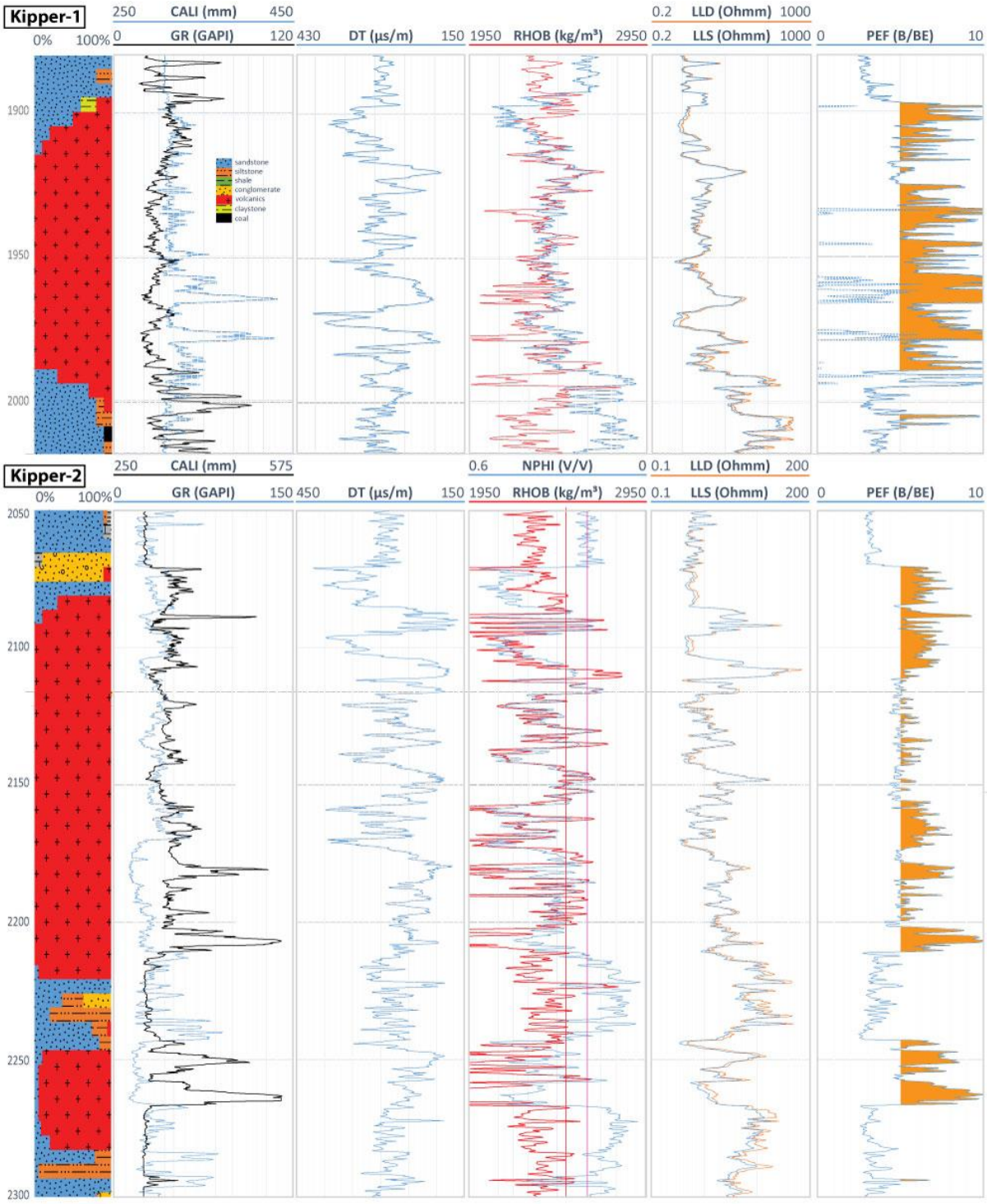

Figure 8: Examples of log signatures for Kipper-1 and Kipper-2.

4.4 Geochemistry

Table 1 (Appendix C) shows the major and trace element analyses of 24 newly acquired samples combined with a previous dataset acquired by McPhail (2000) (AM-sample names, 10 samples). Due to the weathered state of the samples, and in particular the cuttings, only major and trace elements have been analysed. All samples have been taken from within the Latrobe Group, except Garfish-1, which is the top of the Strzelecki Group. Petrographic analyses of core samples showed that the igneous lithologies recovered from the Bream-2, Bream-A15 and Tuna-4 wells are relatively fresh dolerites (also reflected in low Loss On Ignition (LOI), Appendix C - Table 1) and the Turrum-1 samples are basalts with varying degrees of alteration. Generally, a Nb/Y – Zr/Ti plot (Pearce, 1996) is less influenced by weathering than other plots as Zr/Ti remains constant during weathering (Nesbitt and Wilson, 1992). Although Nb/Y does increase slightly during weathering (Nesbitt and Wilson, 1992), the use of the plot in this case is still useful. This plot shows that the majority of the Gippsland Basin igneous samples fall within the alkali basalt field, with some samples in the basalt and andesite field (Figure 9). Due to the high SiO_2-content (>80 wt%) of the samples from well Garfish-1 and two of the West-Moonfish-1 samples (>74 wt%), these are discarded from any interpretation.

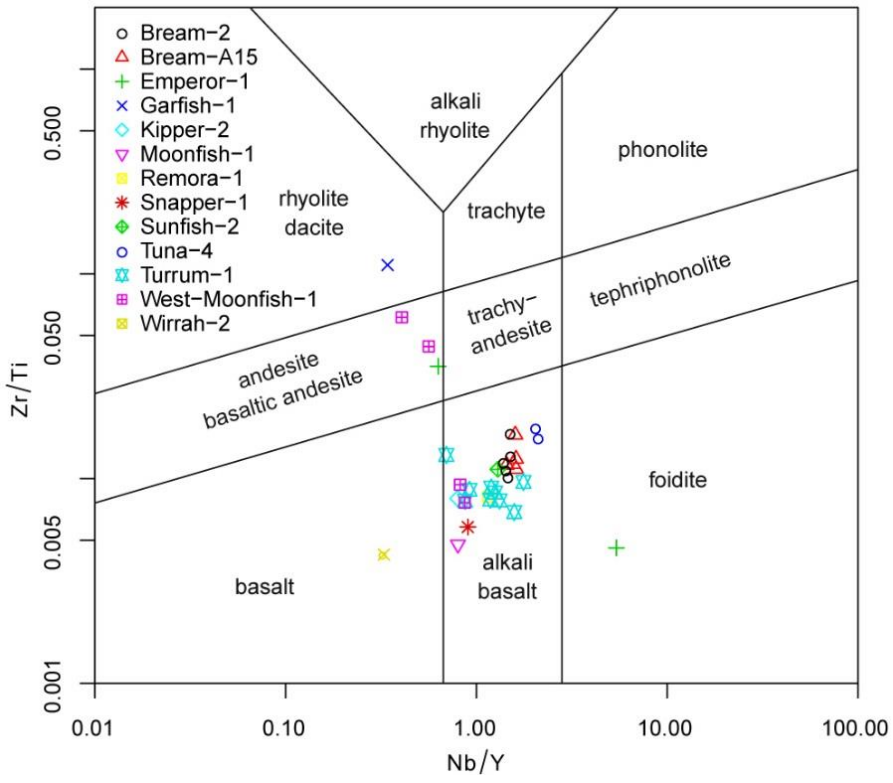

Figure 9: Nb/Y versus Zr/Ti plot (modified by Pearce, 1996) for analysed samples and samples from McPhail (2000)

Mantle-normalized incompatible element diagrams of intrusions show that dolerite samples from the Bream and Tuna wells have a typical Oceanic Island Basalt (OIB)-like trace element signature. They are relatively enriched in the LREE and incompatible elements such as Ce, Y and Zr (Figure 10a). The analysed extrusive rocks (Emperor, Garfish, Kipper, Remora, Snapper, Sunfish, Turrum, Moonfish and West Moonfish) show a trace element signature similar to the Upper Continental Crust (Rudnick and Gao, 2003; Taylor and McLennan, 1985) (Figure 10b). Primitive mantle-normalized rare earth element diagrams show a similar divide between the samples, with the Bream and Tuna intrusions showing an OIB signature and extrusive rocks showing an Upper Continental Crust signature (Figure 10c-d).

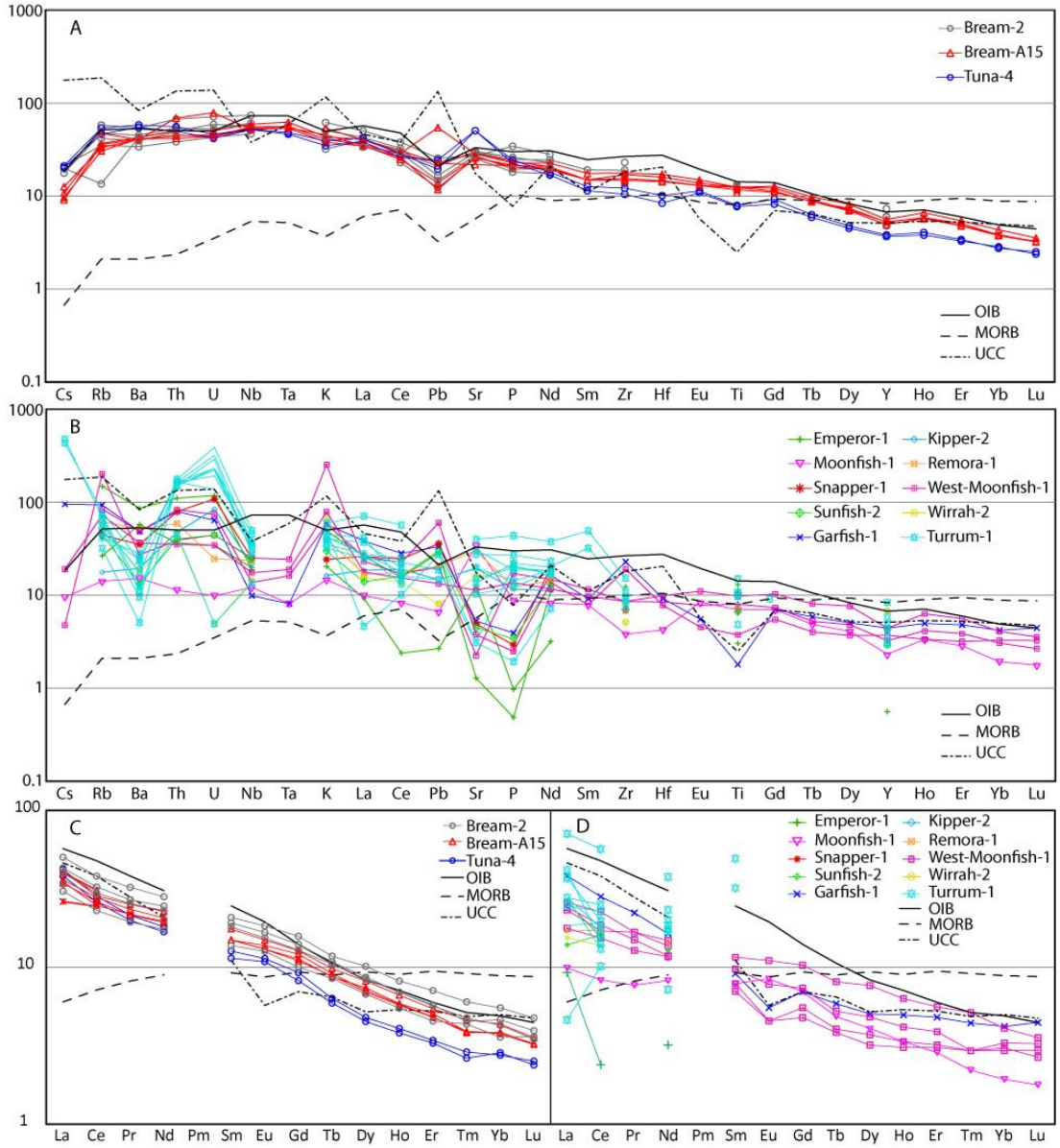

Figure 10: Mantle normalized incompatible trace element (A – B) and mantle normalized rare earth element plots (C – D) of sampled intrusive and extrusive rocks.

5. DISCUSSION

5.1 Previous work on Kipper volcanic sequence

Previous work on the Late Cretaceous Kipper volcanics has been conducted by O'Halloran and Johnstone (2001) and McPhail (2000). Using the G99A Kipper 3D seismic survey (acquired January 1999), O'Halloran and Johnstone (2001) were able to identify both extrusive and intrusive features near the Kipper field. They concluded that the extrusive lavas had variable thicknesses due to growth packages across west- to northwest-trending growth faults. O'Halloran and Johnstone (2001) proposed that these basaltic lava flows were fed through fissure-fed scoria cones and intrusive cone sheets feeding the overlying contemporaneous eruption centres. Samples taken from Campanian, Paleocene and Eocene volcanic intervals in exploration wells (Snapper-1, Bream-2, Bream-A15, Turrum-1, Remora-1, Kipper-2, Wirrah-2, Emperor-1, Sunfish-1) show that these igneous rocks consist of variably altered, fine-grained, glassy basaltic lavas (McPhail, 2000). The intrusive cone sheets described by O'Halloran and Johnstone (2001) are re-interpreted to be saucer-shaped sills, due to the sill radius exceeding sill height (H/R > 1: Haug et al. (2018)).

5.2 Magmatic plumbing system of the Gippsland Basin volcanics

Classic magmatic plumbing systems are generally portrayed as systems transporting magma from the earth's mantle through the crust through vertical dykes, to finally extrude onto the paleosurface. Through the use of 3D seismic reflection data (e.g. Magee et al., 2016) and field studies however, this idea has been expanded towards the possibility of lateral magma flow within individual plumbing systems. Shallow magmatic systems (<3 km depth), and particularly those within sedimentary basins, are often characterized by laterally extensive, interconnected sill complexes (Magee et al., 2016; Schofield et al., 2015). Studies in the Møre and Vøring Basins off the Norwegian coast have demonstrated that sill complexes can transport melt from lower to mid crustal levels to near surface over distances greater of 8-12 km, both vertically and laterally (Cartwright and Hansen, 2006).

The Kipper Field volcanic system has previously been interpreted as being fissure-fed where dilational faults have acted as magma conduits (O'Halloran and Johnstone, 2001). Our interpretations however, indicate that the magma travelled from the deepest part of the basin

(Central Deep) towards the basin-bounding faults through increasingly shallowing levels of intrusions (Figure 4). These intrusions form an extensive complex covering a significant lateral distance of ~40 km, which represents one of the longest potential plumbing systems described based on seismic reflection data. The intrusions or sills are interconnected through faults in some parts and fed the Kipper extrusive sequences through shallow saucer-shaped intrusions in places (Figure 6). Part of the extrusive sequences is fed by magma that exploited an E-W trending fault north of the complex (Figure 6).

The volcanic vents near the Bream Field however, do not share the same magmatic plumbing style as the Kipper Field volcanic system. Although seismic data quality is limited due to the presence of coal layers below the volcanic vents, a more vertical plumbing style is inferred. A few saucer-shaped sills, identified on RGB blends of frequency decomposition data and confirmed by core and cuttings samples, can be observed directly beneath the vents, however, delineation of these intrusions is difficult due to the coal layers (Figure 7B). Feeding of the sills and vents could have happened through dykes or faults acting as magmatic conduits, represented as vertical or near-vertical linear features on cross-sections. No evidence exists for an extensive sill complex implying lateral magma transport similar to the Kipper Field volcanic system.

5.3 Timing and duration of extrusive volcanic activity in the Gippsland Basin

Although the sampled core and cutting samples are not suitable for absolute age dating due to weathering, the age of extrusive activity can be constrained based on reported palynology (WCR) of sediments surrounding the intersected volcanic rocks in petroleum wells. Almost all of the sampled petroleum wells intersected extrusive rocks, with intrusive rocks limited to wells Whiting-1 and -2, Tuna-4 and Bream-2 and Bream-A15 among others. Palynology results of the intersected extrusive rocks indicate that the north-eastern part of the basin hosts the oldest extrusions of Turonian to Campanian age (*T. lilliei – N. senectus* palynomorphs – from WCR), whilst extrusive sequences appear to get younger along the fault system towards the west (Palaeocene to Eocene, *L. balmei* – lower *M. diversus* palynomorphs – from WCR) (Figure 11). Subsequent volcanism in the Eocene was located towards the centre of the basin, the Central Deep, with volcanic mounds and intrusions situated near the Bream field (upper *M. diversus – P. asperopolous*). This is in concordance with the riftward younging

of magmatism observed in other rift basins such as Baikal Rift (Kiselev, 1987) and the Ethiopian rift valley (Morton et al., 1979). Sailfish-1 intersects Miocene pyroclastic rocks in south-east of the basin (Figure 11). Due to its location and age, this volcanic activity is more likely to be related to Cenozoic magmatic activity in Tasmania (Meeuws et al., 2019) and Early Miocene basalts onshore Flinders Island (20 ± 2.7 Ma: Zwingmann et al. (2004)) rather than the Gippsland Basin.

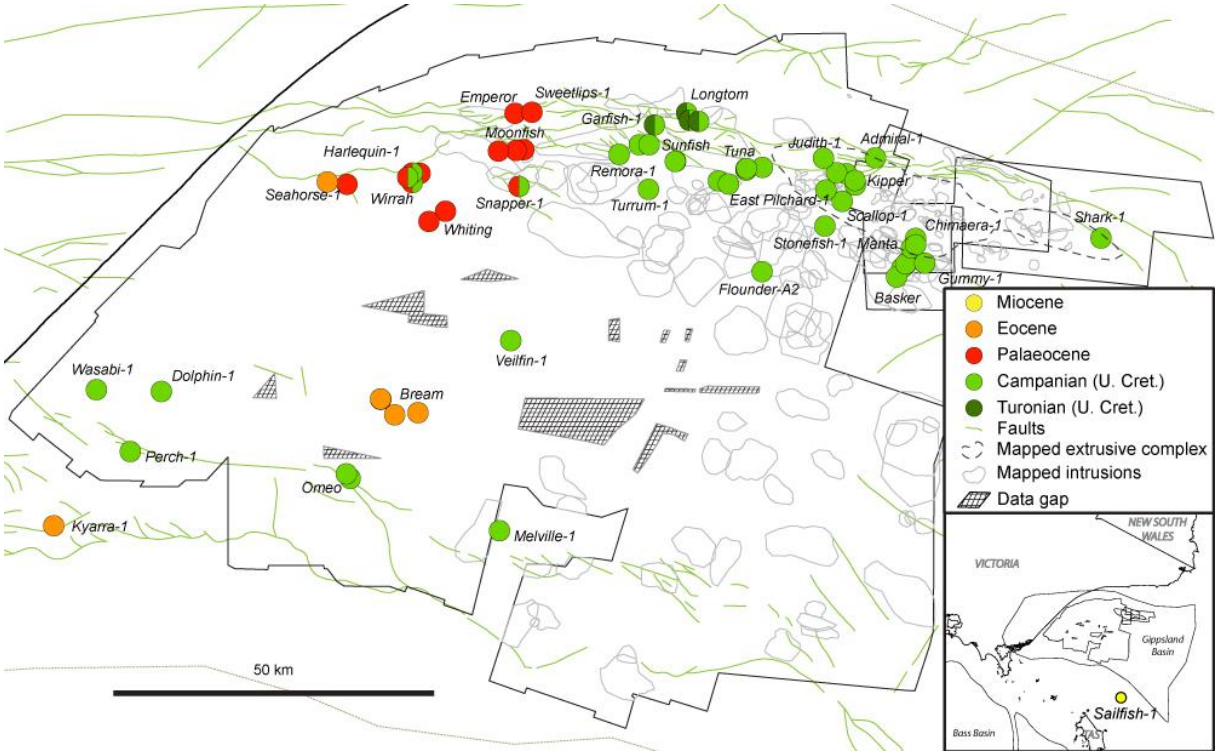

Figure 11: Age map of intersected extrusive rocks based on palynological dating of surrounding sedimentary rocks

5.4 Chemical variability of extrusive and intrusive rocks

All of the igneous samples analysed in this study fall within the 'within plate basalts' field of Pearce and Cann (1973), confirming a rift origin for the igneous rocks in the Gippsland Basin. A typical OIB-signature has been observed in the Bream and Tuna intrusions. This is in contrast to the UCC-signature observed in the extrusive samples from the remaining wells (Emperor-1, Kipper-2, Moonfish-1, Remora-1, Snapper-1, Sunfish-2, West-Moonfish-1, Wirrah-2 and Turrum-1). In order to fully understand the difference in trace element signature, any contamination or other issues due to the sampling of cuttings must be ruled out. Generally, interpretation of cutting samples can be problematic due to factors such as mixing of drill

cuttings from several depths, contamination by metal alloys used in drill bits and drill collars (e.g. Cu, Ni, Cr and Ta) and a bias towards the preservation of least altered primary igneous materials and more resistant alteration minerals and preferential loss of finer-grained and less resistant minerals (Fowler and Zierenberg, 2016). Whilst contamination is not observed in our samples, mixing of drill cuttings from several depths may obscure the true geochemical signature in some of the drill cutting samples. One possible explanation for the difference in signature between intrusive and extrusive samples is that the Bream and Tuna intrusions are significantly younger than the Campanian extrusions. The extrusive rocks penetrated by Bream-2 and Bream-A15 have been shown to be of Eocene age (Bream-2 and Bream-A15 Well Completion Report (WCR)), which most likely indicates a similar age for the intrusive bodies of this complex. However, for the intrusion penetrated by Tuna-4, which intruded into Campanian sediments, the age can only be constrained to be Campanian or younger. If the intrusion penetrated by Tuna-4 is younger than surrounding intrusions, then this would imply that the magmatic plumbing system has been established due to several magmatic pulses over time, where magma has travelled along existing and newly created pathways. Although this sample was relatively fresh (low LOI) compared to other sampled intrusions, additional analyses are needed to confirm this implied younger age of the intrusion penetrated by well Tuna-4.

5.5 Differences and similarities of magmatism in sedimentary basins

5.5.1 Meso-Cenozoic magmatism along the eastern Australian southern margin

The crustal trace element signatures observed in the sampled extrusive rocks, is also observed in the Jurassic dolerites and Cretaceous igneous rocks of Tasmania (Everard, 2014; Hergt et al., 1989; Meeuws et al., 2019), particularly the Cretaceous dykes from Cape Portland (north-east Tasmania) and the Cygnet Alkaline Complex (south Tasmania) (Everard, 2014). The Cape Portland dykes have been dated at 91 ± 1 Ma (K/Ar, minimum age) to 103 ± 23 Ma (Rb/Sr) (Sutherland and Corbett, 1974) and 102.3 ± 2.6 Ma and 101.3 ± 2.6 Ma (K/Ar on hornblende phenocrysts (McDougall and Green, 1982)) and the Cygnet Alkaline Complex has been dated at 101 Ma (K/Ar on sanidine and biotite; Evernden and Richards (1962)) and 97 and 100 Ma (K/Ar on hornblende; McDougall and Leggo (1965)). Although the Cretaceous Tasmanian magmatism is older than the Campanian extrusive rocks in the Gippsland Basin, there is some

palynological evidence for Turonian activity in the northern part of the offshore Gippsland Basin (Figure 11) and Aptian activity onshore the Gippsland Basin (116.04 ± 0.15 Ma dolerite dyke Samsu et al. (2019)). The Eocene Bream volcanics and Tuna intrusive show an OIB signature which coincides with geochemical trace element signature of undersaturated Cenozoic lavas found in onshore Tasmania (Meeuws et al., 2019). Additional isotope work is necessary to investigate potential similarities between the igneous rocks occurring in the Gippsland Basin and Tasmania.

The Bass Basin, adjacent to the Gippsland Basin, partly shares a similar rifting history with the Gippsland Basin but its magmatic plumbing network is quite different. Although some sills are present in the Bass Basin, most of them are not visible in seismic reflection data due to anomalously low acoustic impedance contrasts with surrounding sediments and the presence of coals within the EVCM in strata above many of the sills (Watson et al., 2019). The magmatic plumbing system of the Bass Basin has been interpreted to be sill- and or dyke-dominated (Reynolds et al., 2018b), whereas the Gippsland Basin is sill-dominated. The Bass Basin hosts several magmatic vents (e.g. near the Yolla gas field (Holford et al., 2012; Holford et al., 2017; Reynolds et al., 2018b)), whereas only one vent is recognized in the Central Deep of the Gippsland Basin (near the Bream Field). In addition to the Bream vent, a pyroclastic vent of Miocene age is located on the southern flanks of the Gippsland Basin and has been drilled by well Sailfish-1 (Figure 11). Technically outside of the Gippsland Basin, the area around the Sailfish-1 well hosts several extrusive vents and lava flows on the same horizon, indicating a similar Miocene age. Due to their location and age, these magmatic cones may be more closely related to the onshore Tasmanian magmatism and Flinders Island, rather than the Gippsland magmatism.

5.5.2 Magmatic plumbing system of rift basins along volcanic margins

The volcanic NW European Atlantic rifted margin and the sedimentary basins it hosts have been well studied with regards to their magmatic activity and makes a potential interesting comparison with the Gippsland Basin. One of the basins, the petroliferous Faroe-Shetland Basin (FSB), hosts a vast amount magmatic rocks and has been studied extensively (e.g. Boldreel, 2006; McLean et al., 2017; Schofield et al., 2015). In this basin, two trends have been observed in magmatic plumbing systems. In the Sissal sub-basin, the sills are fed away

from the NE-SW-trending bounding Sissal Basin fault, in a NW to SE direction. These sills climb mainly strata-bound towards the intra-basin high (Schofield et al., 2015). A second trend is observed within the northern Flett sub-basin, where magma flow directions diverge from the central axis of the basin and climb towards the bounding highs. This suggests that within the Sissal Basin, the magma input was located away from the Sissal Basin fault, whereas for the Northern Flett sub-basin, the magma input came from several zones running through the central axis of the basin (Schofield et al., 2015). Even though volcanic activity in the FSB post-dates rifting (break-up at 55 Ma, with main volcanic event occurring at 55 – 52 Ma (Schofield et al., 2015)), the latter trend can also be observed in the syn-rift magmatism in the Gippsland Basin, with magma input originating in the centre of the basin, travelling towards the basin bounding faults over a significant horizontal distance, and subsequent post-rift magma travelling vertically (e.g. Bream Field).

5.6 Implications for hydrocarbon exploration and development

The Kipper Field forms an example of a field where igneous rocks have formed an important element of the petroleum system. The top seal for the Kipper field consists of the extrusive sequences mapped in this work. It consists of mafic extrusive rocks, most likely basalt based on mineralogy (plagioclase and pyroxene) and has a thickness of 96 m in Kipper-1, 141 m in Kipper-2, 113.2 m in Kipper-A2 and 121 m in Kipper-A4, with Kipper-1 located closest to the crest of the trapping structure (from Kipper-1, -2, -A2 and –A4 WCR). Even though well log interpretations indicate that the extrusive rocks are more weathered and thinner in Kipper-1, they are still capable of holding a 328 gross gas column and a 14 m gross oil leg. Full closure is formed by a sealing fault to the north of the Kipper Field in addition to the top-sealing volcanics. Similar plays are possible in other areas such as East Pilchard-1 and Remora where basalt is overlying reservoir-quality sandstones containing hydrocarbons. Further investigations of the igneous rocks in the Gippsland basin could lead to additional successful sub-volcanic plays.

The reservoir for the main gas column and oil leg consists of the fluvio-deltaic sands of the Golden Beach Group, with an average porosity of 18% (from WCR). In Kipper-1, this reservoir is mainly sandy in nature while in Kipper-2, the reservoir consists of interbedded sandstone, siltstone and coal packages with a Net-to-gross of 34% (Sloan et al., 1992). Kipper-

1 has been interpreted to intersect fluvial channel systems while Kipper-2 has intersected the channel flanks and overbank deposits (Sloan et al., 1992). Vitrinite reflectance and Thermal Alteration Index (TAI) measurements on kerogens above and below the extrusive sequences suggest the presence of the extrusions has not caused any heating effects on the immediately underlying reservoir (from WCR). Reservoir quality decreases with depth, which is attributed to the increase of sedimentary matrix within the sandstone and not due to diagenetic cements (from WCR).

The effects of magmatic activity on hydrocarbon compositions is highly variable (e.g. Holford et al., 2013; Holford et al., 2012; Meeuws et al., 2016b). Large concentrations of CO_2 (some exceeding 30%) have been found in gas fields closely distributed along or immediately south of the Rosedale fault with concentrations increasing from west to east (O'Brien et al., 2008). Carbon isotopes of the CO_2 present indicate a magmatic origin (Boreham et al., 2001) and CO_2 concentrations seem to coincide with the higher concentration of igneous rocks along the Rosedale fault. The increase of CO_2 from west to east along the Rosedale fault gases coincides well with the observed increase of age and fractionation, where more fractionated and younger magmas contain lower concentrations of volatiles. In addition to CO_2, mercury (Hg) was found in the Kipper reservoir fluids (Black and Saunders, 2018) which may be of magmatic origin (Schutter, 2003).

6. CONCLUSIONS

Though the Gippsland Basin has been extensively studied for decades, the role of magmatism in the geological history of the basin has been largely overlooked. In this paper we have shown that the Gippsland Basin hosts a significant amount of igneous rocks, which have in places influenced the distribution of hydrocarbons. Of all 318 exploration wells drilled in the basin, 46 (~14.5%) have intersected both intrusive and extrusive mafic igneous rocks of Campanian to Middle Eocene age. The encountered igneous rocks consist mainly of basalts and dolerites with varying degrees of weathering. In this study we have mapped 181 intrusions and several lava flows near the Kipper Field and a volcanic cone complex overlying 5 intrusions near the Bream Field (west). Intrusions are mainly saucer-shaped while some are layer-parallel. Magma in the Gippsland Basin has been demonstrated to travel as sills from the Central Deep towards the basin bounding faults in the north and south, where it extruded onto the surface.

This magma travelled both vertically (3 sec TWT) and horizontally (> 40 km). This implies that magma sources are not necessarily situated directly below the end product of the magmatism as is commonly believed. The magmatic plumbing network observed here has been established over several magmatic pulses starting from the Campanian to the Eocene, with extrusive activity getting younger and more fractionated along the Rosedale fault towards the west. A second magmatic plumbing style has been observed near the Bream Field (west), where a Middle Eocene volcanic cone complex can be observed. This complex is fed by underlying intrusions and vertical to near-vertical faults or dykes.

Trace elements of sampled Cretaceous extrusive rocks show an upper continental crust signature similar to Cretaceous volcanics onshore Tasmania. An Eocene-age dolerite sill near the Bream Field (Bream-2) and a dolerite sill near the Tuna Field (Tuna-4) show an Oceanic Island Basalt signature similar to the Cenozoic basalts onshore Tasmania. Further geochemical analyses such as Sr-Nd-Pb isotopes and absolute age dating techniques are needed to fully unravel this geochemical signature.

ACKNOWLEDGEMENTS

This research forms part of a PhD project supported by the ASEG Research Foundation (RF14P05) and Australian Government Research Training Program Scholarship for which funding is greatly acknowledged. Geoscience Australia is thanked for providing the three dimensional seismic data. IHS are thanked for access to seismic interpretation software The Kingdom Suite. Foster-Findlay Associates' is thanked for the use of the GeoTeric software.

REFERENCES

Bernecker, T., Partridge, A.D. (Eds.), 2001. Emperor and Golden Beach Subgroups: The onset of Late Cretaceous sedimentation in the Gippsland Basin, SE Australia. Eastern Australasian Basins Symposium: a refocused energy perspective for the future, Special publication. Petroleum Exploration Society of Australia.

Birch, G.F., 1987. Igneous rocks of the Gippsland Basin. Esso Australia Ltd.

Birmingham, P.J., Grieves, K.R.A., Spring, D.E., 1985. Depth conversion techniques in the Gippsland Basin. Exploration Geophysics, 16(3): 172-174.

Black, A., Saunders, G., 2018. Offshore gas field development – the ripple effect. The APPEA Journal, 58(2): 695-699.

Blevin, J.E., Cathro, D.L., 2008. Australian southern margin synthesis, project GA707. Client Report to Geoscience Australia by FrOG Tech Pty Ltd.

Boldreel, L.O., 2006. Wireline log-based stratigraphy of flood basalts from the Lopra-1/1A well, Faroe Islands. In: Chalmers, J.A., Waagstein, R. (Eds.), Scientific results from the deepened Lopra-1 borehole, Faroe Islands, Geological Survey of Denmark and Greenland Bulletin, pp. 7-22.

Boreham, C.J., Hope, J.M., Hartung-Kagi, B., 2001. Understanding source, distribution and preservation of Australian natural gas: A geochemical perspective. The APPEA Journal, 41(1): 523-547.

Cartwright, J., Hansen, D., 2006. Magma transport through the crust via interconnected sill complexes. Geology, 34(11): 929-932.

Everard, J.E., 2014. Geological evolution of Tasmania / editors, Keith D. Corbett, Patrick G. Quilty, Clive R. Calver ; designer/compiler, June Pongratz. Special publication (Geological Society of Australia) ; 24. 0072-1085. Geological Society of Australia (Tasmanian Division), Sydney, NSW.

Evernden, J.F., Richards, J.R., 1962. Potassium-argon ages in eastern Australia. Journal of the Geological Society of Australia, 9(1): 1-49.

Featherstone, P., Aigner, T., Brown, L., King, M., Leu, W., 1991. Stratigraphic modelling of the Gippsland Basin. The APEA journal, 31(part 1): 105-114.

Fowler, A., Zierenberg, R.A., 2016. Geochemical bias in drill cutting samples versus drill core samples returned from the Reykjanes Geothermal System, Iceland. Geothermics, 62: 48-60.

Haug, Ø.T. et al., 2018. Shear Versus Tensile Failure Mechanisms Induced by Sill Intrusions: Implications for Emplacement of Conical and Saucer-Shaped Intrusions. Journal of Geophysical Research: Solid Earth, 123(5): 3430-3449.

Hergt, J.M., Chappell, B.W., McCulloch, M.T., McDougall, I., Chivas, A.R., 1989. Geochemical and Isotopic Constraints on the Origin of the Jurassic Dolerites of Tasmania. Journal of Petrology, 30(4): 841-883.

Holford, S.P. et al., 2013. Impacts of igneous intrusions on source and reservoir potential in prospective sedimentary basins along the western Australian continental margin. In: Keep, M., Moss, S.J. (Editors), The Sedimentary Basins of Western Australia IV, Perth.

Holford, S.P., Schofield, N., Macdonald, J.D., Duddy, I.R., Green, P.F., 2012. Seismic analysis of igneous systems in sedimentary basins and their impacts on hydrocarbon prospectivity: examples from the southern Australian margin. APPEA Journal, 52: 229-252.

Holford, S.P., Schofield, N., Reynolds, P., 2017. Subsurface fluid flow focused by buried volcanoes in sedimentary basins: Evidence from 3D seismic data, Bass Basin, offshore southeastern Australia. Interpretation, 5(3): SK39-SK50.

Jackson, C.A.-L., Schofield, N., Golenkov, B., 2013. Geometry and controls on the development of igneous sill–related forced folds: A 2-D seismic reflection case study from offshore southern Australia. Geological Society of America Bulletin, 125(11-12): 1874-1890.

Kiselev, A.I., 1987. Volcanism of the Baikal rift zone. Tectonophysics, 143(1): 235-244.

Magee, C., Hunt-Stewart, E., Jackson, C.A.L., 2013. Volcano growth mechanisms and the role of sub-volcanic intrusions: Insights from 2D seismic reflection data. Earth and Planetary Science Letters, 373: 41-53.

Magee, C. et al., 2016. Lateral magma flow in mafic sill complexes. Geosphere, 12(3): 809-841.

McDougall, I., Green, D.C., 1982. Cretaceous K/Ar ages from north-eastern Tasmania., Geological Survey of Tasmania Bulletin.

McDougall, I., Leggo, P.J., 1965. Isotopic age determinations on granitic rocks from Tasmania. Journal of the Geological Society of Australia, 12(2): 295-332.

McLean, C.E., Schofield, N., Brown, D.J., Jolley, D.W., Reid, A., 2017. 3D seismic imaging of the shallow plumbing system beneath the Ben Nevis Monogenetic Volcanic Field: Faroe–Shetland Basin. Journal of the Geological Society.

McPhail, A., 2000. A petrographic and geochemical study of Gippsland Basin volcanics., BSc Honours thesis, University of Adelaide, unpublished.

Meeuws, F., Foden, J., Holford, S., Forster, M.A., under review. Geochemical constraints on Cenozoic intraplate magmatism and their relation to Jurassic dolerites in Tasmania, using Sr-Nd-Pb isotopes. Chemical Geology.

Meeuws, F.J.E., Foden, J.D., Holford, S.P., Forster, M.A., 2019. Geochemical constraints on Cenozoic intraplate magmatism and their relation to Jurassic dolerites in Tasmania, using Sr-Nd-Pb isotopes. Chemical Geology, 506: 225-273.

Meeuws, F.J.E., Holford, S.P., Foden, J.D., Schofield, N., 2016. Distribution, chronology and causes of Cretaceous – Cenozoic magmatism along the magma-poor rifted southern Australian margin: Links between mantle melting and basin formation. Marine and Petroleum Geology, 73: 271-298.

Morton, W.H., Rex, D.C., Mitchell, J.G., Mohr, P., 1979. Riftward younging of volcanic units in the Addis Ababa region, Ethiopian rift valley. Nature, 280: 284.

Nesbitt, H.W., Wilson, R.E., 1992. Recent chemical weathering of basalts. American Journal of Science, 292(10): 740-777.

Norvick, M.S., Smith, M.A., 2001. Mapping the plate tectonic reconstruction of southern and southeastern Australia and implications for petroleum systems. The APPEA Journal, 41: 15-35.

O'Brien, G.W. et al., 2008. First order sealing and hydrocarbon migration processes, Gippsland Basin, Australia: implications for CO2 geosequestration, Eastern Australian Basins Symposium III. Petroleum Exploration Society of Australia, Sydney Convention and Exhibition Centre, NSW, Australia, pp. 1-28.

O'Halloran, G., Johnstone, E., 2001. Late Cretaceous rift volcanics of the Gippsland Basin, SE Australia - New insights from 3D seismic. In: Hill, K.C., Bernecker, T. (Editors), Eastern Australasian Basins Symposium: a refocussed energy perspective for the future. Petroleum Exploration Society of Australia, Melbourne, Victoria, pp. 353-361.

Pearce, J.A., 1996. A user's guide to basalt discrimination diagrams. In: Wyman, D.A. (Ed.), Trace Element Geochemistry of Volcanic Rocks: Applications for Massive Sulphide Exploration. . Geological Association of Canada, pp. 79–113.

Pearce, J.A., Cann, J.R., 1973. Tectonic setting of basic volcanic rocks determined using trace element analyses. Earth and Planetary Science Letters, 19(2): 290-300.

Planke, S. et al., 2017. Igneous seismic geomorphology of buried lava fields and coastal escarpments on the Vøring volcanic rifted margin. Interpretation, 5(3): SK161-SK177.

Planke, S., Symonds, P.A., Alvestad, E., Skogseid, J., 2000. Seismic volcanostratigraphy of large-volume basaltic extrusive complexes on rifted margins. Journal of Geophysical Research-Solid Earth, 105(B8): 19335-19351.

Power, M.R., Hill, K.C., Hoffman, N., Bernecker, T., Norvick, M.S., 2001. The structural and tectonic evolution of the Gippsland Basin; results from 2D section balancing and 3D structural modelling. In: Hill, K.C., Bernecker, T. (Eds.), Eastern Australasian Basin Symposium, A refocused energy perspective for the future. Petroleum Exploration Society of Australia, Special Publication, 1, pp. 373-384.

Rahmanian, V.D., Moore, P.S., Mudge, W.J., Spring, D.E., 1990. Sequence Stratigraphy and the Habitat of Hydrocarbons, Gippsland Basin Australia. Classic Petroleum Provinces, 50: 525-544.

Reynolds, P., Holford, S., Schofield, N., Ross, A., 2017. Three-Dimensional Seismic Imaging of Ancient Submarine Lava Flows: An Example From the Southern Australian Margin. Geochemistry, Geophysics, Geosystems, 18(11): 3840-3853.

Reynolds, P., Holford, S., Schofield, N., Ross, A., 2018a. The importance of subsurface lithology in controlling magma storage v. eruption: an example from offshore southern Australia. Journal of the Geological Society.

Reynolds, P., Schofield, N., Brown, R.J., Holford, S.P., 2018b. The architecture of submarine monogenetic volcanoes – insights from 3D seismic data. Basin Research, 30: 437-451.

Rudnick, R.L., Gao, S., 2003. Vol. 3: The Crust, 3.01 - The composition of the continental crust. . In: Holland, H.D., Turekian, K.K. (Eds.), Treatise on geochemistry. Elsevier-Pergamon, Oxford, pp. 1-64.

Samsu, A., Cruden, A.R., Hall, M., Micklethwaite, S., Denyszyn, S.W., 2019. The influence of basement faults on local extension directions: Insights from potential field geophysics and field observations. Basin Research, 0(0).

Schofield, A., Totterdell, J., 2008. Distribution, timing and origin of magmatism in the Bight and Eucla Basins. Geoscience Australia, Record 2008/4: 19.

Schofield, N. et al., 2015. Regional magma plumbing and emplacement mechanisms of the Faroe-Shetland Sill Complex: implications for magma transport and petroleum systems within sedimentary basins. Basin Research: n/a-n/a.

Schutter, S., 2003. Hydrocarbon occurrence and exploration in and around igneous rocks. In: Petford, N., McCaffrey, K. (Eds.), Hydrocarbons in crystalline rocks. Geological Society London, London, pp. 7-33.

Self, S., Thordarson, T., Keszthelyi, L., 1997. Emplacement of Continental Flood Basalt Lava Flows, Large Igneous Provinces: Continental, Oceanic, and Planetary Flood Volcanism. American Geophysical Union, pp. 381-410.

Sloan, M.W., Moore, P.S., McCutcheon, A., 1992. Kipper - A unique oil and gas discovery, Gippsland Basin, Australia. The APPEA Journal, 32(1): 1-8.

Smallwood, J.R., Maresh, J., 2002. The properties, morphology and distribution of igneous sills: modelling, borehole data and 3D seismic from the Faroe-Shetland area. North Atlantic Igneous Province: Stratigraphy, Tectonic, Volcanic and Magmatic Processes, 197: 271-306.

Sutherland, F.L., Corbett, E.B., 1974. The extent of Upper Mesozoic igneous activity in relation to lamprophyric intrusions in Tasmania. Papers and proceedings of the Royal Society of Tasmania, 107: 175-190.

Taylor, S.R., McLennan, S.M., 1985. The continental crust: its composition and evolution.

Trude, J., Cartwright, J., Davies, R.J., Smallwood, J., 2003. New technique for dating igneous sills. Geology, 31(9): 813-816.

Watson, D., Holford, S., Schofield, N., Mark, N., 2019. Failure to predict igneous rocks encountered during exploration of sedimentary basins: A case study of the Bass Basin, Southeastern Australia. Marine and Petroleum Geology, 99: 526-547.

Zwingmann, H. et al., 2004. New K-Ar and Ar-Ar ages for Tasmanian basalts: implications for volcanic evolution following Tasman rifting, Geological Society of Australia, 17th Convention, Hobart 2004, pp. 141.

Chapter 5

Geochemical signatures and seismic expression of Cretaceous-Cenozoic magmatic plumbing systems in the Bass Basin

Statement of Authorship

Title of Paper	Geochemical signatures and seismic expression of Cretaceous-Cenozoic magmatic plumbing systems in the Bass Basin.
Publication Status	☐ Published ☐ Accepted for Publication ☐ Submitted for Publication ☑ Unpublished and Unsubmitted work written in manuscript style
Publication Details	Meeuws, F.J.E., Holford, S.P., Foden, J., Schofield, N. Geochemical signatures and seismic expression of Cretaceous-Cenozoic magmatic plumbing systems in the Bass Basin. Unsubmitted

Principal Author

Name of Principal Author (Candidate)	Fun Julie Ellen Meeuws		
Contribution to the Paper	Performed analyses on all seismic data, interpreted geochemistry and seismic data, wrote manuscript and acted as corresponding author.		
Overall percentage (%)	80		
Certification:	This paper reports on original research I conducted during the period of my Higher Degree by Research candidature and is not subject to any obligations or contractual agreements with a third party that would constrain its inclusion in this thesis. I am the primary author of this paper.		
Signature		Date	2/07/2019

Co-Author Contributions

By signing the Statement of Authorship, each author certifies that:

i. the candidate's stated contribution to the publication is accurate (as detailed above);

ii. permission is granted for the candidate in include the publication in the thesis; and

iii. the sum of all co-author contributions is equal to 100% less the candidate's stated contribution.

Name of Co-Author	Associate Professor Simon Holford		
Contribution to the Paper	Helped in seismic data interpretation, manuscript evaluation and editing.		
Signature		Date	2/07/2019

Name of Co-Author	Emeritus Professor John Foden		
Contribution to the Paper	Helped in geochemistry interpretation and helped with manuscript evaluation.		
Signature		Date	2/07/2019

Name of Co-Author	Dr Nick Schofield		
Contribution to the Paper	Helped in seismic data interpretation and helped with manuscript evaluation.		
Signature		Date	2/07/2019

Please cut and paste additional co-author panels here as required.

ABSTRACT

Magmatic activity in hydrocarbon-bearing basins has both detrimental and beneficial impacts on prospectivity. In order to mitigate risks associated with increased exploration along magma-poor continental margins such as the southern Australian margin, a good understanding of magma transport within sedimentary basins is imperative. The use of three-dimensional (3D) seismic data delivers the necessary insight in magma transport through sedimentary basins. This study uses a combination of 3D and 2D seismic data to describe the magma plumbing styles of the Bass Basin. Regional mapping indicates that in this basin at least 10 pulses of magmatic activity occurred spanning the Cretaceous to the Miocene. Older magmatic activity occurred near major faults at the basin edges, with younger activity focussed in the basin centre. A southward younging trend can be observed within the younger magmatic activity. This is in concordance with southward younging trends observed onshore mainland Australia, due to the northward movement of the Australian plate. Major and trace element geochemistry of sampled extrusions and intrusions show strong similarities with Cenozoic magmas found in onshore Tasmania and Victoria, with an Oceanic Island Basalt (OIB) signature present in the majority of the Bass igneous rocks.

1. INTRODUCTION

Increasing levels of hydrocarbon exploration along continental margins such as the southern Australian margin has led to growing recognition of the variably detrimental and beneficial impacts of magmatic activity on prospectivity (Holford et al., 2012; Rateau et al., 2013; Schutter, 2003), though the processes by which magma is transported through sedimentary basins are poorly understood (Schofield et al., 2015). The Bass Basin is located on the Australian southern passive margin, which originated due to Gondwana break-up and the separation of Australia and Antarctica (Norvick, 2005; Norvick and Smith, 2001). Although described as a ‘non-volcanic’ margin, the Bass Basin contains a substantial record of largely undescribed Cretaceous-Cenozoic magmatic activity (Meeuws et al., 2016b; Reynolds et al., 2018b). The presence of igneous rocks in petroliferous basins such as the Bass Basin represents a key uncertainty that must be quantified due to the detrimental effects that

magmatic activity poses to source and reservoir rock quality (e.g. Holford et al., 2012; Schutter, 2003).

Previous studies of magmatism in the Bass Basin have been largely local in nature, focussing mainly on the Miocene magmatism in the Yolla 3D and Labatt 3D seismic surveys (Holford et al., 2017; Reynolds et al., 2018b; Velayatham, 2019). These studies demonstrated that the Cape Wickham sub-basin of the Bass Basin hosts three separate phases of volcanic mound construction between approximately 20 – 16 Ma (Reynolds et al., 2018b). These volcanic mounds are interpreted to be monogenetic volcanoes composed of hyaloclastite and/or pyroclastic rocks emplaced during submarine volcanic eruptions (Reynolds et al., 2018b). Thirteen dykes with a roughly north-south direction have been identified in the Labatt 3D survey (Velayatham, 2019) which were previously interpreted as strike-slip structures (Cummings et al., 2004). Sills present in the Labatt 3D survey are associated with dykes (Velayatham, 2019), indicating a dyke-dominated plumbing system of igneous activity. To date, there have been no regional studies of the igneous activity in this basin. Here we will present seismic interpretation results from the Cape Wickham Sub-basin of the Bass Basin to determine the spatial and temporal distribution of Cretaceous-Cenozoic volcanism. Additionally, geochemical analyses of recovered igneous rocks allow for a comparison of trace element signatures with nearby magmatism in the Gippsland Basin, onshore Tasmania and onshore Victoria (Newer and Older Volcanic Provinces).

2. GEOLOGICAL SETTING

The Australian southern margin originated due to the separation of Antarctica and southern Gondwana. This separation created several east-west trending rift basins, such as the Bight Basin, Otway Basin, Bass Basin and Gippsland Basin along the Australian southern margin (Figure 1). Rifting commenced in the west during the Middle-Late Jurassic, progressed eastwards and finally resulted in break-up during the Campanian in the Bight Basin to the west and during the Maastrichtian in Otway Basin to the east (Blevin, 2003). Due to the locus of rifting shifting southwards towards the Sorell Basin, west of Tasmania, the Bass Basin experienced extensional deformation but did not evolve into a passive margin basin. The structural style of the Bass Basin ranges from a graben to half-graben, showing large scale offset along NE and SW dipping normal faults and with tilted Palaeozoic and Proterozoic

basement blocks (Blevin et al., 2005) (Figure 2). This graben and half-graben allow for a subdivision into the Durroon sub-basin in the east (series of half-grabens) and the Cape Wickham sub-basin in the west (graben).

The section below summarizes the stratigraphy of the Bass Basin. The Barremian to Albian *Otway Group* is composed of volcanolithic sandstone and slightly carbonaceous siltstone interbedded with rare conglomerate and thin coal seams (Williamson et al., 1985), which is overlain by the Eastern View Coal Measures (EVCM) successions. The *Lower EVCM* (*Durroon Formation* in the Durroon Sub-basin) contains slightly carbonaceous mudstones and shales in a fault-barred, deep-water lacustrine environment (Brincat, 1992). The *Middle EVCM* consists primarily of silty shales with thin sandstone interbeds, passing upward into coal-rich and then sand-rich sequences. The *Middle EVCM* developed in a major fluvial system with associated wave-dominated delta systems prograding out into a restricted embayment or large lake (Suttill, 1995). The *Upper EVCM* is deposited during of the lower Eocene and was controlled by thermal sag where the environment was dominated by tide-dominated delta systems consisting of a complex mixture of distributary channels, strandline sand bars, peat swamps and shallow lagoons (Baillie and Bacon, 1988). The *EVCM* is conformably overlain by the thin, but laterally extensive upper Eocene *Demons Bluff Formation*, which represents the first major transgressive marine unit, consisting of fine-grained carbonaceous shales and silts with abundant secondary pyrite and carbonate (Williamson et al., 1985). The *Demons Bluff Formation* grades into coarser facies of medium to coarse-grained sandstone units towards the Durroon Sub-basin. The Oligocene to Pliocene *Torquay Group* (~450-1000m thick) overlies the *Demons bluff Formation* and consists of a lower section of calcareous shales and marls, grading upwards into a sequence of bioclastic limestones, ranging in age from Miocene to Holocene (Williamson et al., 1985).

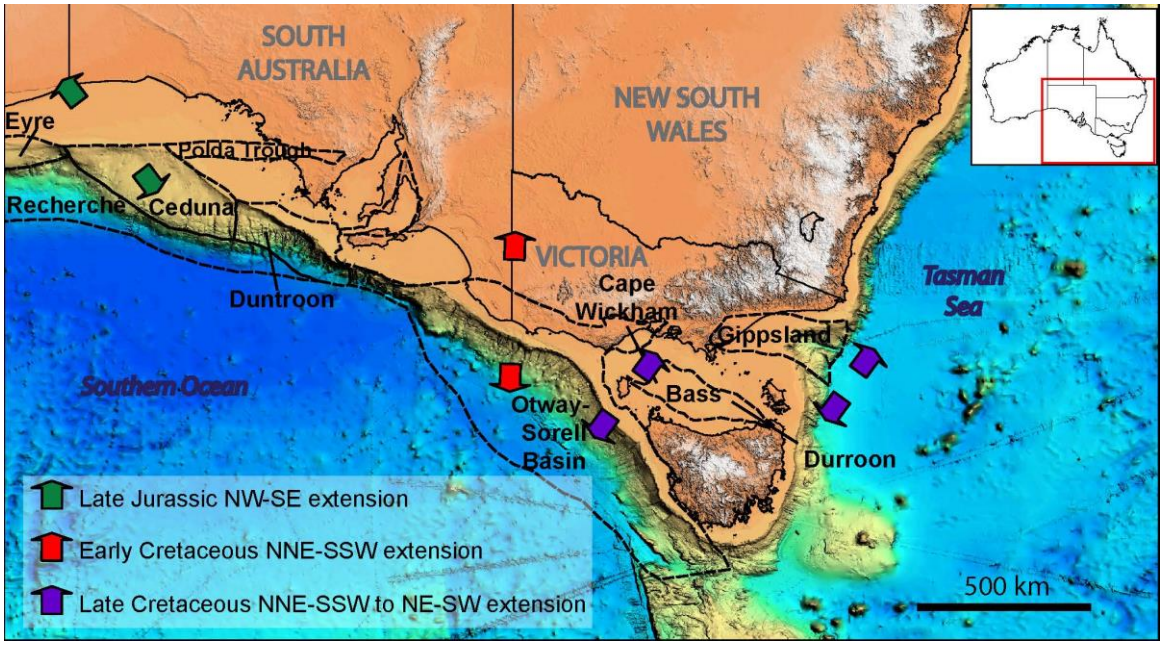

Figure 1: Digital Elevation Model of the Australian southern margin with location of the Bass and Gippsland Basin discussed in this paper and the orientation of extension. Green arrows indicate Late Jurassic (Callovian to early Berriasian), NW-directed extension. Red arrows indicate Early Cretaceous (early to mid-Berriasian to latest Barremian), NNE-directed extension. Purple arrows indicate Late Cretaceous (Turonian to Mid-Campanian), NNE- to NE- directed extension in the Gippsland and Bass Basins and Turonian to Late Maastrichtian, NNE- to NE-directed extension in the Otway, Sorell and Bass Basin (Meeuws et al., 2016b).

Although classified as a non-volcanic margin, magmatism was prevalent during the Meso-Cenozoic both onshore and offshore the southern Australian margin and the Bass Basin is no exception to this (e.g. Holford et al., 2012; Meeuws et al., 2016b and references therein) (Figure 3). Several episodes of magmatism are recognized within exploration wells and are linked to late-stage rifting processes (Ball et al., 2013), related to a mantle plume (Davies et al., 2015) or shear- and edge-driven mantle convection (Meeuws et al., 2016b). The volcanoes are mostly described as monogenetic in origin, and range from Jurassic to Holocene in age (Cas et al., 1993; Johnson, 1989). Apart from the volcaniclastic sediments in the Otway Group described earlier, the oldest igneous rocks have been found in the Middle Cretaceous Otway and Durroon Megasequences (Figure 3), consisting of highly weathered, amygdaloidal basalt, representing flows, mounds and cones, associated with large normal faults in the Durroon Sub-basin (Blevin, 2003). A following phase of Late Cretaceous to Palaeocene magmatism (Bass Megasequence, Figure 3), although poorly constrained due to overlying coal layers, is represented by lavas and intrusive rocks in the central and northeastern parts of the Bass

Basin (Blevin, 2003). The composition of these variably altered amygdaloidal basaltic flows ranges from alkali olivine basalt, to basanite and picrite (Blevin, 2003). Subsequent magmatism during the Oligocene to Miocene (Torquay Megasequence, Figure 3) was most extensive, expressed as volcanic mounds, vents, lava flows and intrusive sills and dykes (Blevin, 2003; Cummings et al., 2002; Lennon et al., 1999).

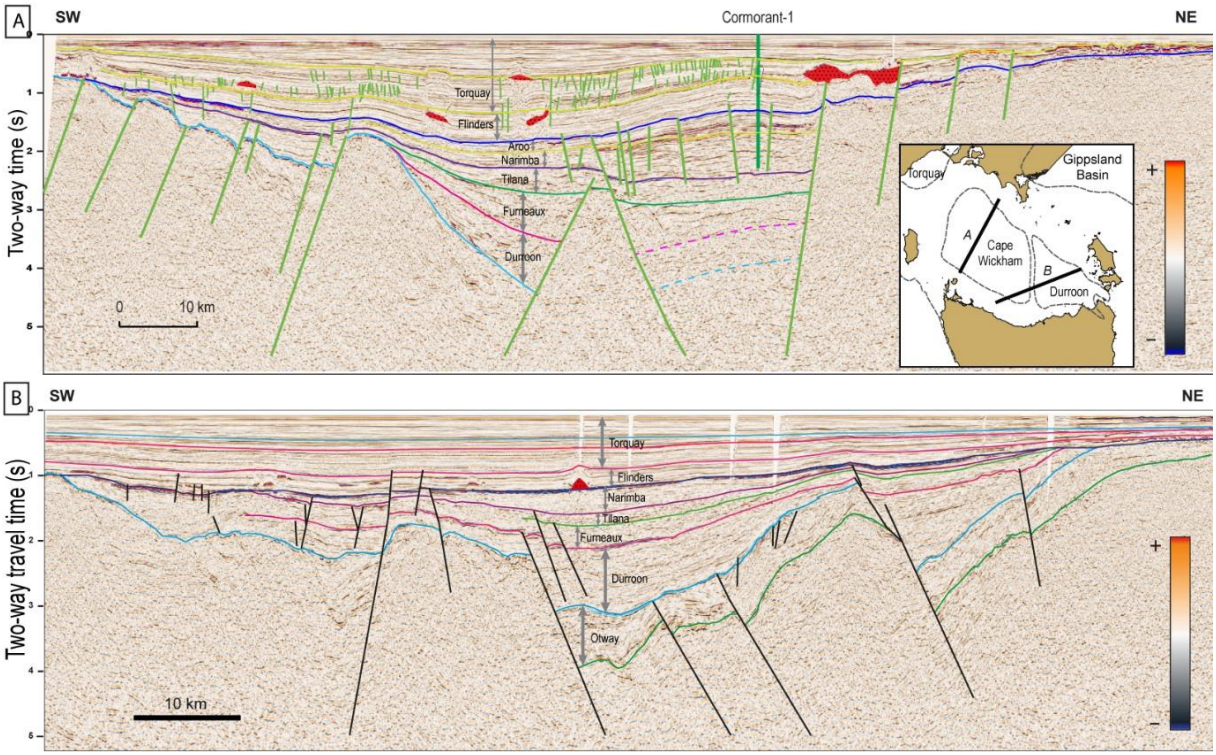

Figure 2: A: Seismic line 90-27 (normal SEG polarity. Bass Basin, Cape Wickham sub-basin regional cross-section with igneous features indicated in red. B: Seismic line 82-302 (normal SEG polarity). Bass Basin, Durroon sub-basin regional cross-section (from Meeuws et al. (2016b)). Location of seismic lines shown in inset

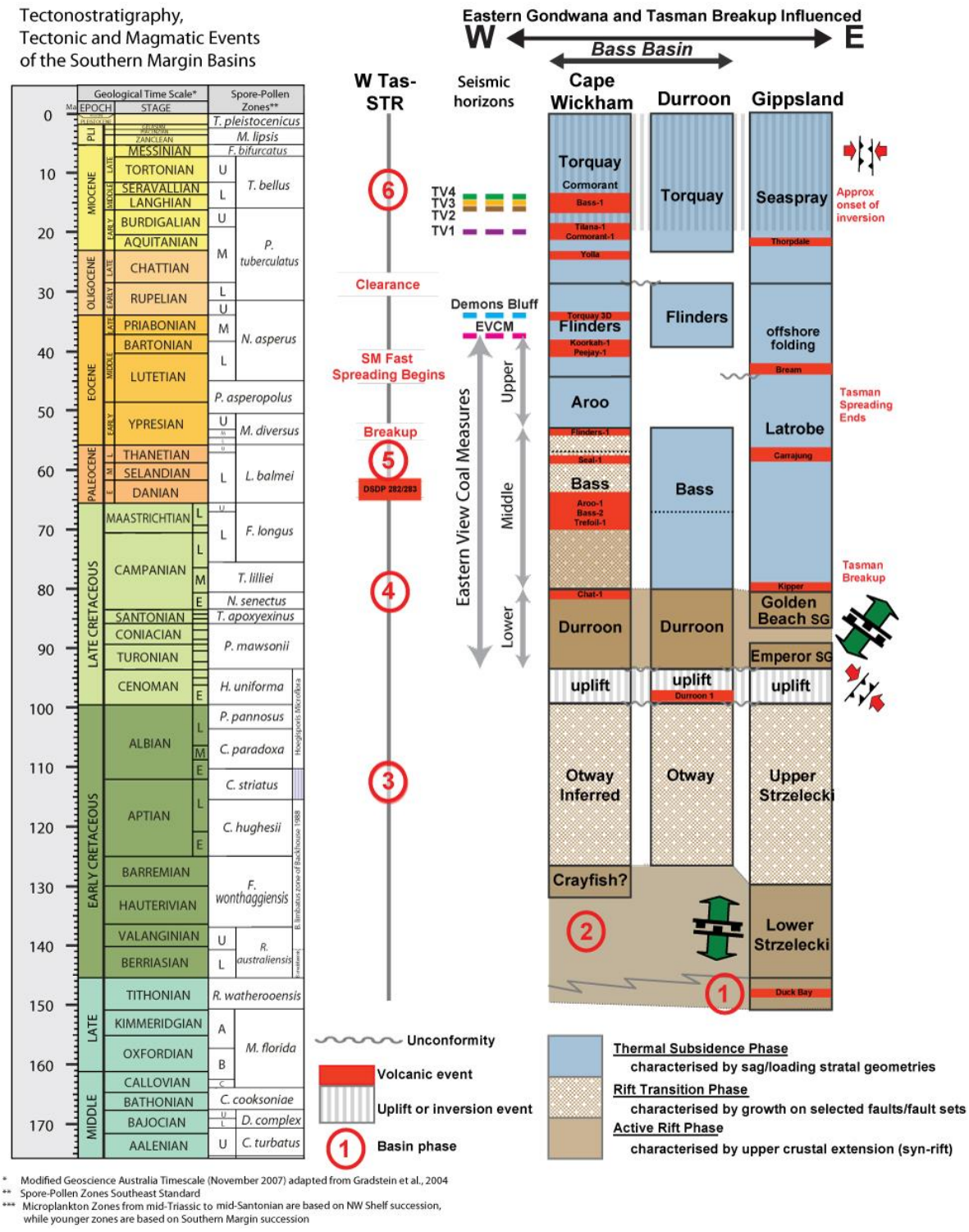

Figure 3: Mesozoic to recent tectonostratigraphic chart for the Bass and Gippsland Basin, with indications of magmatic events with corresponding sampled wells, picked seismic horizons (EVCM = Eastern View Coal Measures), and palynological zones discussed in the text (modified from Meeuws et al., 2016b)

3. DATA AND ANALYTICAL METHODS

3.1 Seismic data and resolution

This study uses several time-migrated 3D and 2D seismic reflection surveys which are mainly located in the Cape Wickham Sub-basin unless otherwise mentioned: 2D survey acquired by 3D Oil (TDOB08 – Durroon Sub-basin), Bass Strait 2D, Chappell 3D, Bass Cue 08 2D, Bass Strait Oil 2D (BOBS08 - Durroon Sub-basin), Dalrymple 3D, Peejay 2D and 3D, Shearwater 2D and 3D, Silvereye 3D, Targa 2D and Torquay 3D survey (Torquay Sub-basin of the Otway Basin) (Figure 4). These surveys cover approximately ~15000 km² and image down to 6 s TWT. 3D surveys have a bin spacing of 25 x 12.5 m with the exception of Peejay3D (25 x 25 m). Downwards increases of acoustic impedance (e.g. transition from a sedimentary rock into a high density volcanic rock) are generally visualised by a blue reflector unless otherwise indicated. Downwards acoustic impedance decreases (e.g. transition from a high density volcanic rock into a sedimentary rock) are visualised as a red reflector unless otherwise indicated.

Seismic resolution of the data changes greatly across and within the surveys. For example, in the Peejay3D survey the dominant frequency of the seismic data between 1.0 – 1.2 seconds TWT (Angahook Formation of the Torquay Group) is 36 Hz and drops down to 31 Hz between 1.6 – 1.7 seconds TWT (Middle EVCM). Sonic logs from the Peejay-1 well indicates that seismic velocity between 1.0 – 1.2 seconds TWT is approximately 2500 m/s, which gives a vertical resolution of approximately 17 m and a detectability of *ca.* 8.5 m and seismic velocity between 1.6 – 1.7 seconds TWT is 3300 m/s, resulting in a vertical resolution of 26 m and detectability of *ca.* 13 m. Frequencies in the Shearwater3D survey are 45 Hz between 0.5 – 0.6 s TWT, 42 Hz between 0.65 – 0.85 s TWT and 28 Hz between 1.7 – 1.9 s TWT, resulting in vertical resolutions of 11.4 m, 12.8 m and 21.6 m respectively.

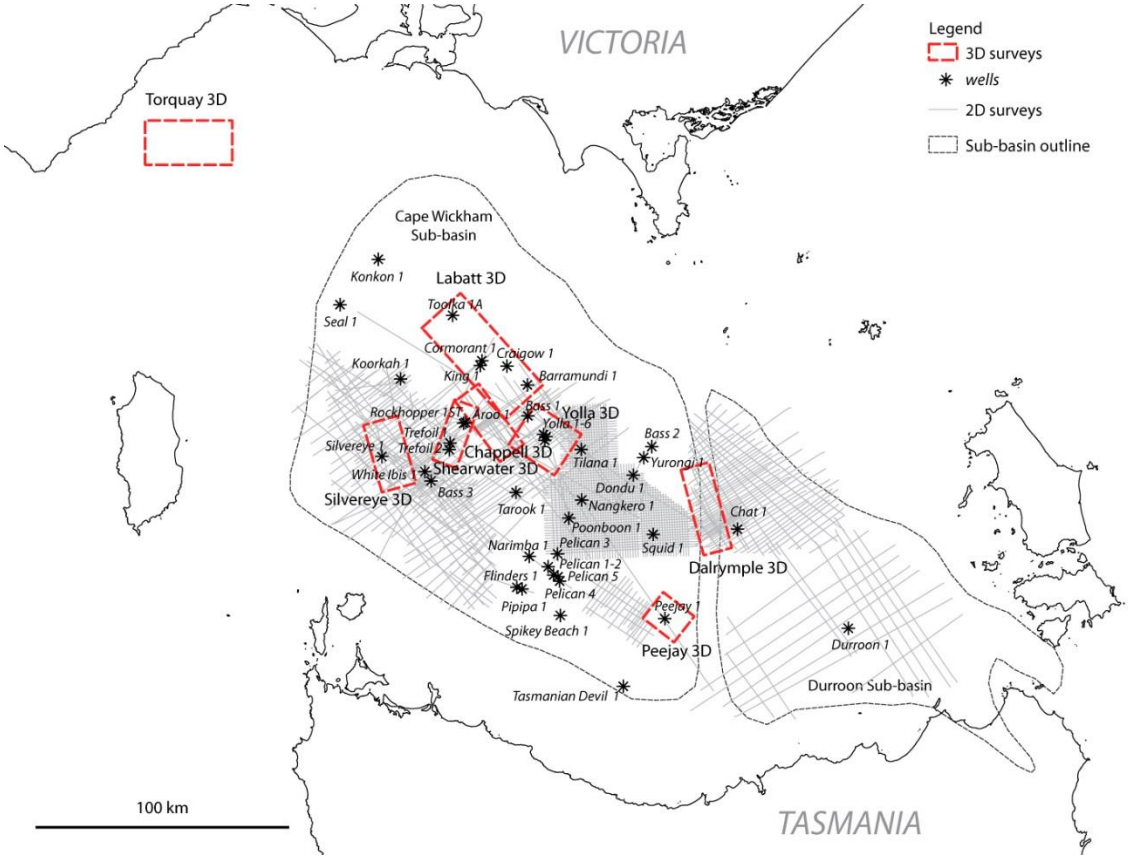

Figure 4: Overview of the Bass Basin with location of 3D and 2D seismic data surveys and locations of petroleum wells.

3.2 Seismic interpretation strategy

Seismic interpretation of extrusive and intrusive features is mainly focussed in the Cape Wickham Sub-basin of the Bass Basin. The interpretation of intrusive features is based on their tendency to cross-cut stratigraphy, their laterally discontinuous nature and high seismic amplitudes (Smallwood and Maresh, 2002).

Extrusive horizons were identified based on the seismic volcanostratigraphy and seismic geomorphology techniques of Planke et al. (2000) and Planke et al. (2017) respectively. Each top of the extrusive complex was picked, interpolated and smoothed. Conventional seismic attribute analyses, such as amplitude, time and envelope, were used to delineate the extent of the extrusives. Spectral decomposition frequency blends were created for some of the 3D surveys and High Definition Frequency Decomposition (HDFD) RGB blends were created to identify igneous rocks located within coal layers and aid better visualisation of intrusions and extrusions.

The extrusives mapped in this work occur at several stratigraphic levels within the Miocene to Eocene succession of the Bass Basin (Figure 5). Reynolds et al. (2018b) mapped three of these levels (TV1 – Top volcanic succession Yolla3D ca 20 Ma, TV2 – Top volcanic succession Labatt3D ca 16 Ma, TV3 – Top volcanic succession Bass-1 well ca 15 Ma) in the Yolla and Labatt 3D surveys. Expansion of the study area in this work has allowed for the recognition of additional levels: TV4 (Top volcanic succession Shearwater3D survey, ca 14 Ma) and levels coinciding with the Upper *N. asperus* (ca 34 Ma) zone, Top Demons Bluff formation (ca 36 Ma) and Top Eastern View Coal Measures (ca 38 Ma). Each of these horizons has been tied to palynological data available from Well Completion Reports (WCR) from petroleum wells Tilana-1, Cormorant-1, and Bass-1.

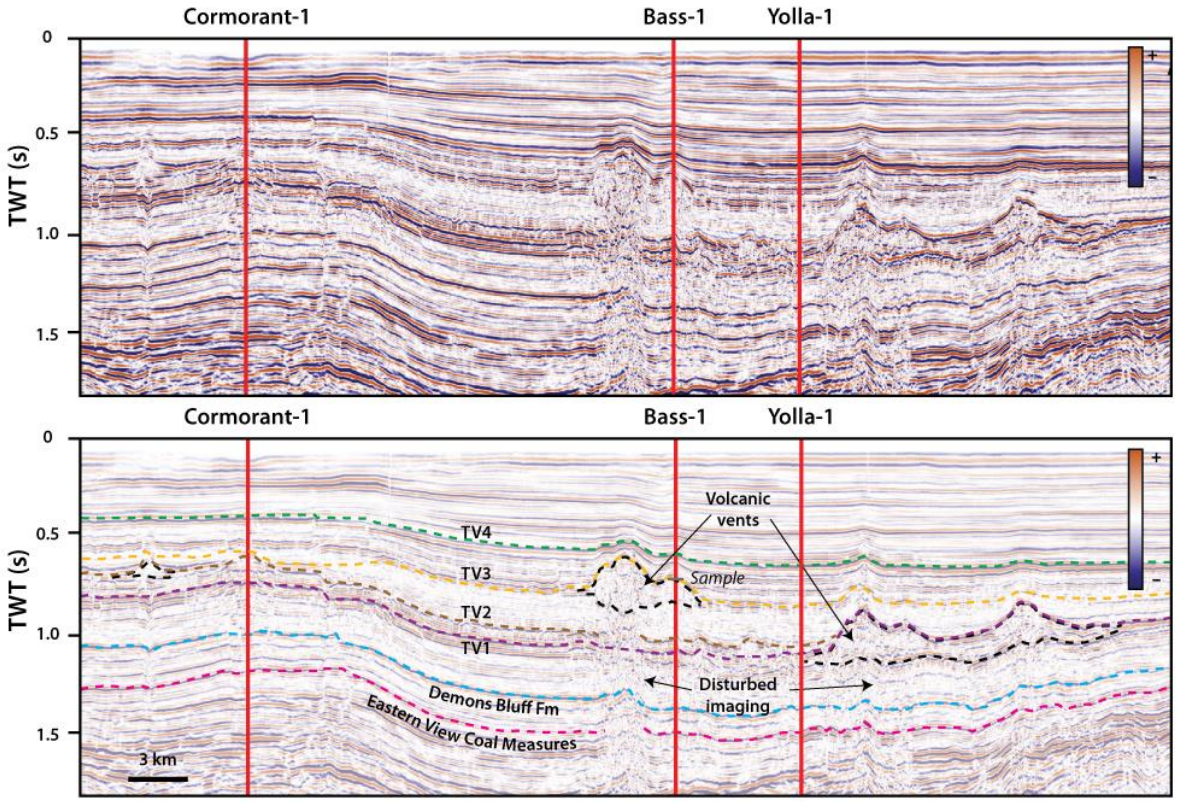

Figure 5: 2D seismic line through wells Cormorant-1, Bass-1 and Yolla-1, connecting the Labatt and Yolla 3D survey with indication of mapped horizons TV1-4 (modified from Reynolds et al. (2018b)).

3.3 Geochemical data

Cutting samples were collected from igneous rocks intersected by 17 exploration wells in the Bass Basin. Drill cutting samples have been ultrasonically washed and igneous lithologies have been separated and powdered using a mortar and pestle. These powders have then been

analysed using ICP on mixed acid digest using a lithium borate fusion at Bureau Veritas Adelaide (Appendix D - Table 1).

Unpublished geochemical data, analysed by Geoscience Australia (GA) in 2003, and geochemical data found in well completion reports (WCR) of corresponding petroleum wells have been added to this dataset. Analyses carried out by GA were performed on hand specimens (HS) and cutting samples. Samples were powdered and analysed for major and trace elements using X-ray fluorescence (XRF) at the Australian National University (ANU), Canberra.

4. RESULTS

4.1 Seismic interpretation of igneous features

4.1.1 Distribution and age of igneous rocks

A total of 126 igneous features have been mapped within the Bass Basin, with focus in the Cape Wickham Sub-basin. This magmatic activity is mainly focussed near major fault zones (Figure 6). However, this is likely an underestimate of the number of igneous bodies in the basin due to various factors including: gaps in seismic data coverage (e.g. near the Pelican wells), the increased difficulty of interpretation of igneous rocks in 2D seismic data compared to 3D seismic data, masking of igneous materials by overlying coal layers and or anomalously low acoustic impedance contrasts between igneous rocks and surrounding sedimentary sequences in the Bass Basin (Watson et al., 2019), and seismic resolution causing intrusions thinner than a certain thickness to be invisible (see section 3.1 for example numbers).

Of the 126 igneous features, 41 features were interpreted as extrusions, 58 as intrusions and a remaining 27 igneous bodies where the intrusive or extrusive nature is not clear due to their layer-parallel character and/or lack of 3D data. Extrusive features mainly consist of volcanic vents (33) with areas ranging between 0.5 - 316 km² and a few lava flows (6) with areas ranging between 23 – 804 km², with 28 extrusives smaller than 100 km². Intrusions are either layer-parallel or saucer-shaped and have an area of 1 – 90 km² with 53 intrusions smaller than 40 km². Within the interpreted 3D surveys, 6 out of 14 extrusions have been fed by underlying intrusions and 8 out of 15 have been fed by dykes.

Volcanic activity is not synchronous across the Bass Basin and volcanic vents occur at different stratigraphic levels. Igneous features mapped along the 10 interpreted igneous horizons allowed for a broad indication of spatial and temporal variation in extrusive activity in the basin (Figure 6). Although palynological data of sediments at the TV1 – TV4 depth is scarce as it does not intersect the main petroleum-bearing sequences, a rough age can be determined for the TV1 – TV4 horizons (Figure 3 and Table 2). According to these mapped ages, two trends can be observed in the distribution of the volcanic activity. The first trend observed is that the oldest magmatic activity is concentrated along the basin edges, near major faults (Teasdale, 2004). The second trend shows younger activity towards the centre of the basin, with a southward younging trend visible in the central area of the Cape Wickham sub-basin.

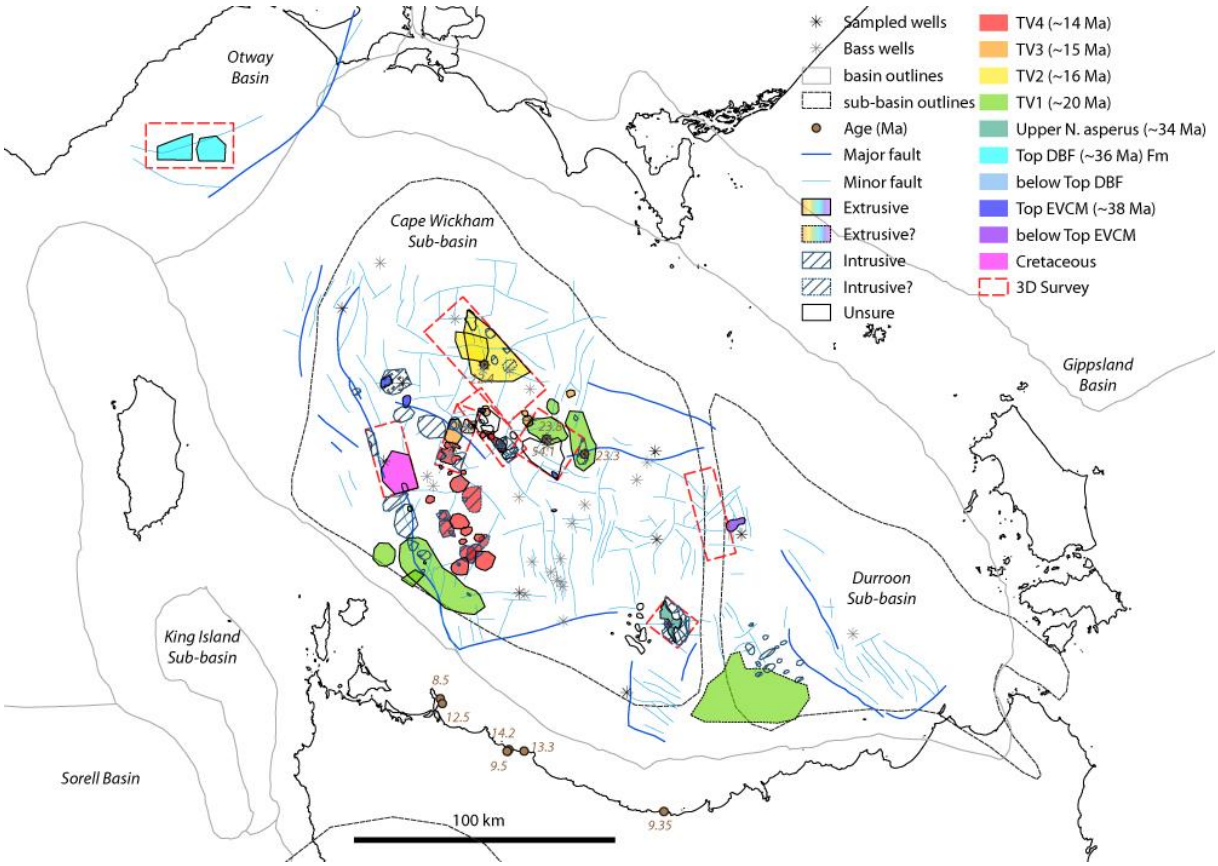

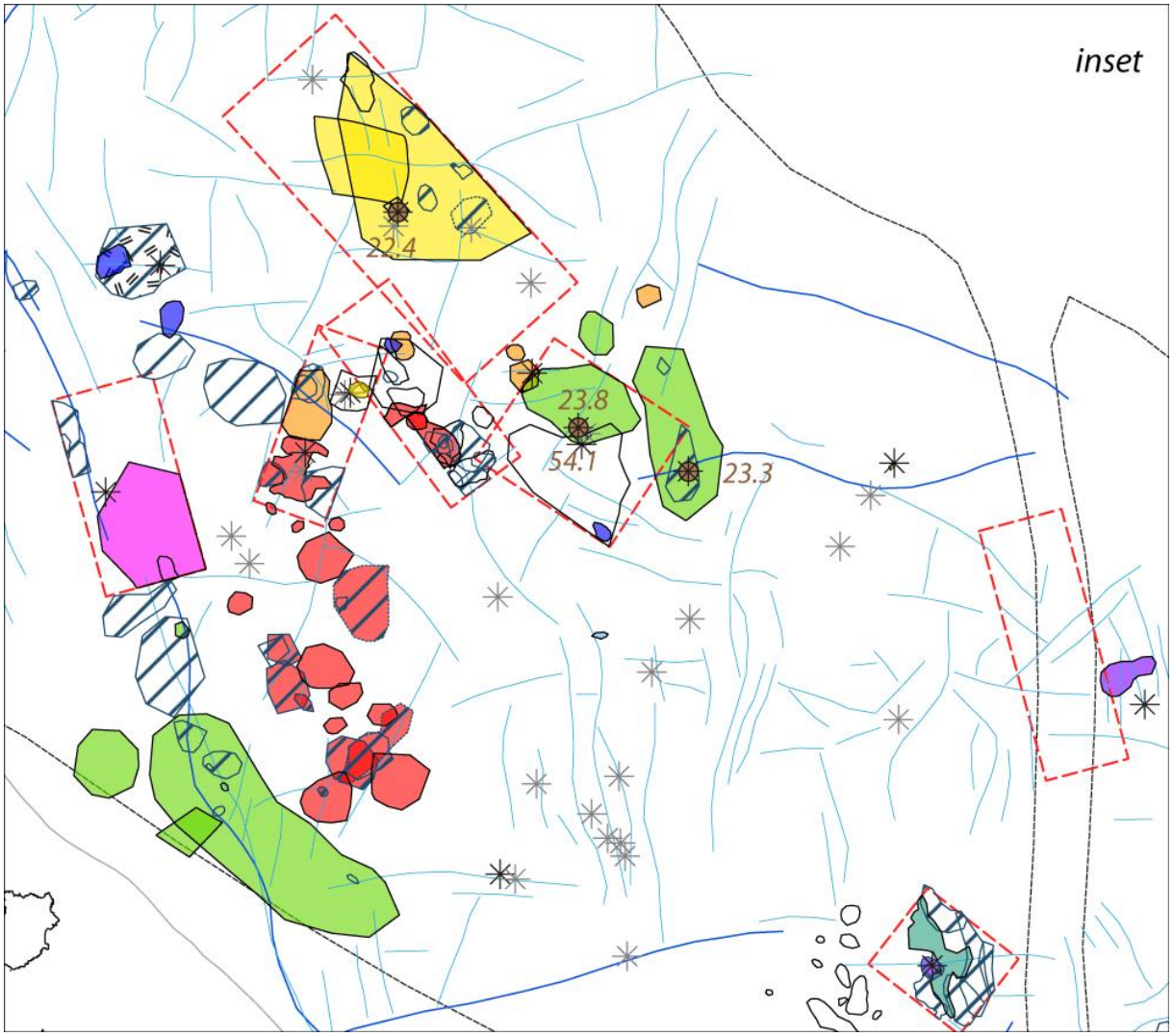

Figure 6: Mapped extrusions and intrusions in the Bass Basin and Torquay Sub-basin with indication of interpreted seismic ages and available K-Ar ages (Baillie, 1986; Cornell et al., 1986; Everard, 2014; Sutherland et al., 1996; Sutherland and Wellman, 1986; Wheeler and Kjellgren, 1986) and detailed inset showing southward younging trend in volcanic activity.

4.1.2 Magmatic styles of the Bass Basin

4.1.2.1 Examples of magmatic styles in the Shearwater3D survey

The Shearwater3D survey contains several magmatic features at different depths. It contains 16 magmatic vents and lava flows at levels TV4 and TV3, which are variably dyke-fed or fed by two underlying saucer-shaped sills. These two saucer-shaped sills have an area of ~8.9 km² with a diameter of 2.6 – 3.0 km and have each caused a forced fold within the overlying sedimentary rocks. A peak event defining the onlap surface of the forced folds coincides with

horizon TV4, indicating a TV4 age for these intrusions, which is the same as the age of the shallowest volcanic vents in this survey. The saucer-shaped intrusion in the north-west of the survey has been found to feed 4 vents, which are located above the edges of the intrusion. The intrusion in the south-west of the survey has been found to feed two overlying vents. An older sequence of extrusive vents in this survey coincides with horizon TV3 (± 0.15 s TWT deeper). Several dykes are identified in this survey based on their orientation, crosscutting relationships and the lack of evidence for vertically offset reflections across them. These dykes are likely feeding several volcanic vents in this survey (Figure 7). Forced folding is not limited to the intrusions present in the Shearwater 3D survey, with 6 intrusions of interpreted TV4 age, located south of Shearwater 3D.

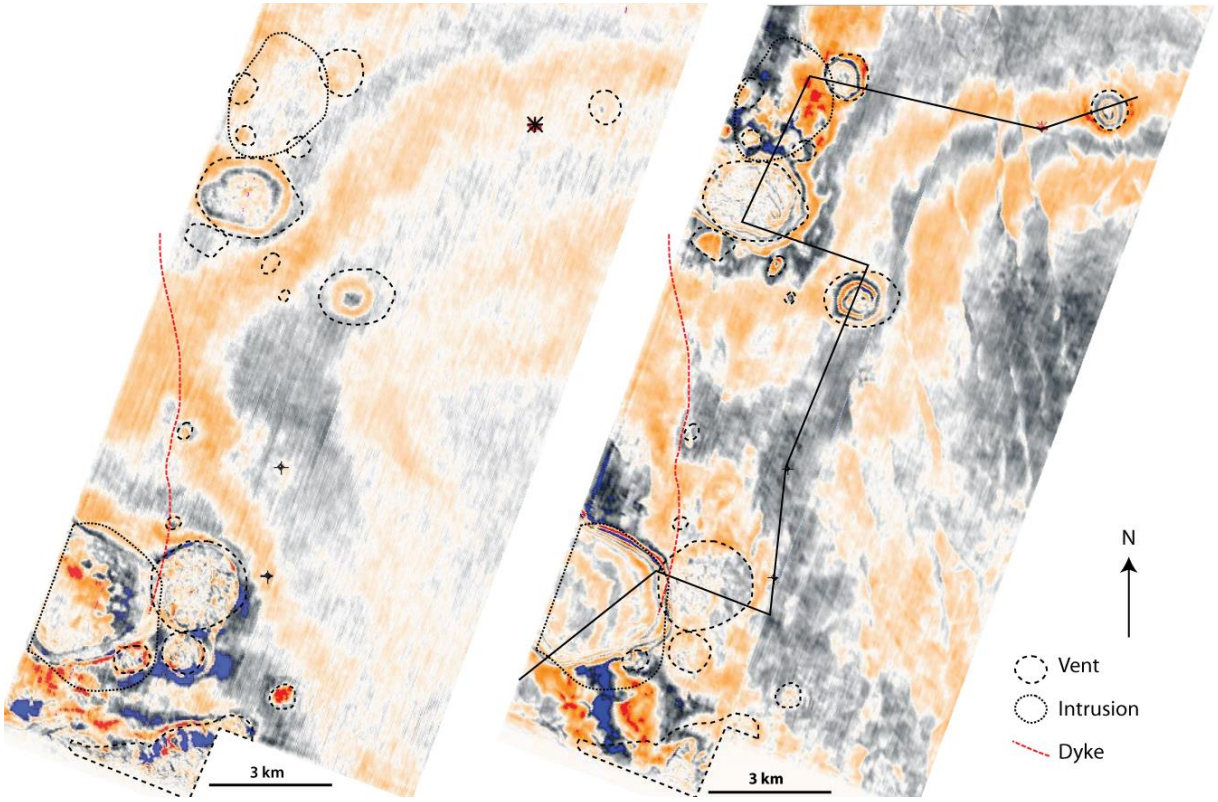

Figure 7: Left: Time slice at 0.5270 s TWT (± TV4 horizon) of survey Shearwater3D, showing volcanic vents (circular features) lined up with mapped dyke (red stipple line). Right: Time slice at 0.712 s TWT (± TV3 horizon) of survey Shearwater 3D, showing location of arbitrary line (Figure 8) through several circular magmatic features.

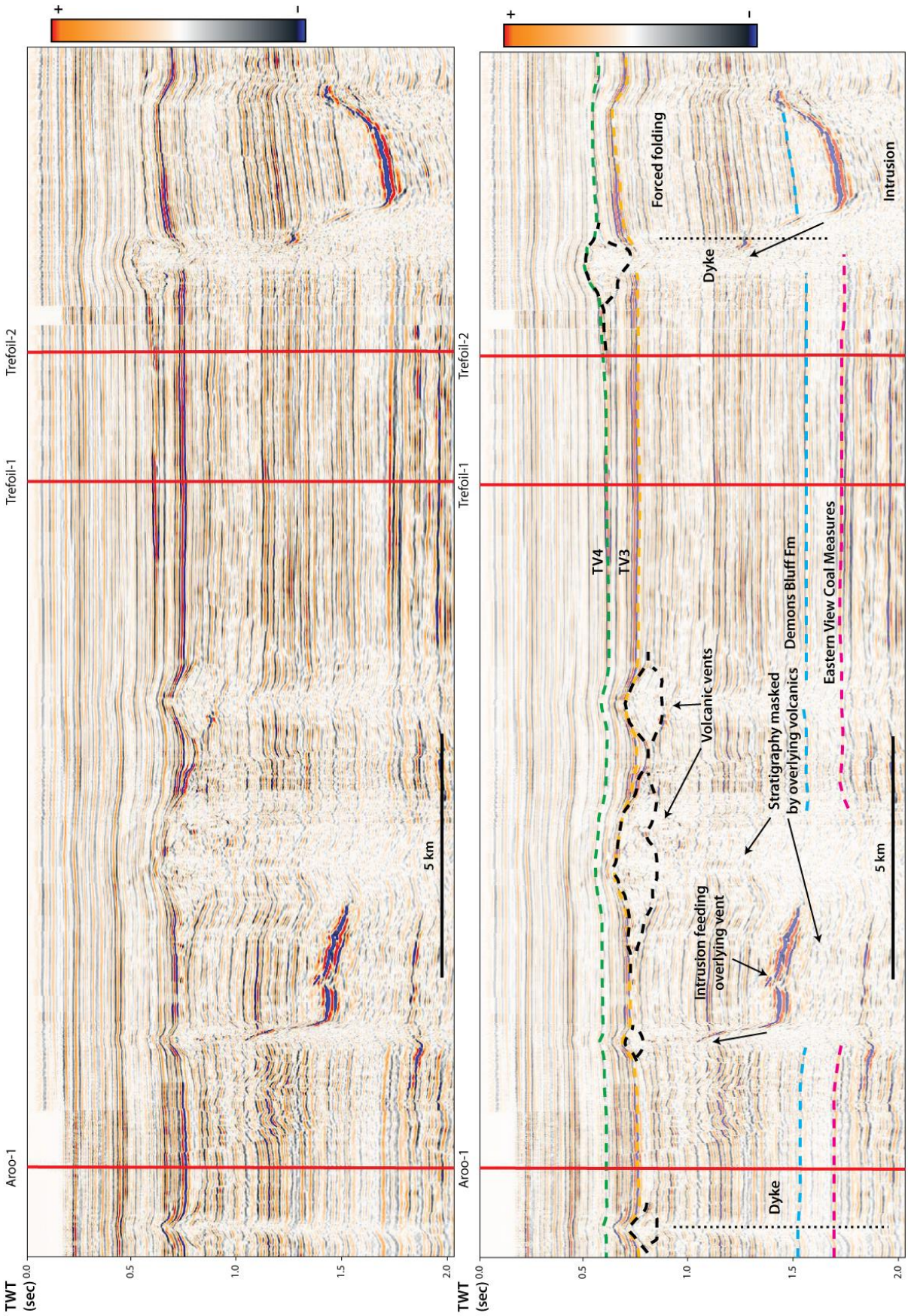
+
-
Aroo-1
Trefoil-1
Trefoil-2
TWT (sec)
0.0
0.5
1.0
1.5
2.0
5 km
Forced folding
Intrusion
Dyke
TV4
TV3
Volcanic vents
Stratigraphy masked by overlying volcanics
Demons Bluff Fm
Eastern View Coal Measures
Intrusion feeding overlying vent
Dyke

Figure 8: Arbitrary line through several magmatic features present in the Shearwater3D survey. Top: uninterpreted seismic line, bottom: interpreted seismic line. See Figure 7 for location.

4.1.2.2 Examples of magmatic styles in the Peejay3D survey

The Peejay3D survey contains an extremely shallow sill complex (50 - 100 m below paleo-seabed) which extrudes onto the paleo-surface as lava flows (Figure 9). Several smooth bodies, with convex-down and planar lobes in seismic cross-section (Figure 9 A-A' and B-B') are interpreted as compound intrusions as described by Reynolds et al. (2017). These intrusions have been intruded concordant to the country rock (Squid Sandstone within the Torquay Group) at a depth of roughly 50 - 100 m below the paleo-seabed. Similar compound sills have been observed in the Bight Basin towards the west of the Australian southern margin (Reynolds et al., 2017). A single elliptic feature with steep edges is observed in one of the larger sills (Figure 9, sill 2). This feature is interpreted as being a "maar", a shallow volcanic crater, with dimensions of 930 – 600 m for long axis. A 'broken bridge' (Schofield et al., 2012) can be observed between sill 1 and sill 2, where the two sills are joined together and the bridge of host rock in between underwent brittle failure during magma propagation and vertical inflation. Several lava flows can be identified and are characterised by their irregular or mottled appearance and smaller convex-down seismic reflections in cross-section (Figure 9 A-A'). The southernmost igneous body is interpreted as a sill (smooth seismic reflector) which travels northwards and surfaces as a lava flow (rough seismic reflector). A 600 – 550 m wide connection is present between the southern and northern lava flow. In seismic cross-section, this connection is characterised by convex-up reflections, indicating a dome structure (possible lava tube) and is covered by what looks like flow ridges (± 100 m spacing) in the RGB blend (Figure 9), indicating the direction of flow. Peejay-1, an exploration well in this survey does not intersect this complex but has however intersected a deeper sill present in the Eastern View Coal Measures in the Palaeocene L. balmei section (Figure 9 C-C'). Somewhat higher amplitudes than those of surrounding sediments suggest the location of the sill, however, without penetration of the well, it would have been difficult to predict due to the presence of overlying coal layers acting as a seismic transmission filter. Similar cases in the Bass Basin of coals masking underlying reflectors (e.g. Flinders-1) have been demonstrated by Watson et al. (2019). The strata above the sampled intrusive in the Peejay-1 well show doming

which could be caused by forced-folding due to the emplacement of the intrusion. Forced folding above the shallow intrusions is not observed in this dataset.

The seismic signature of the igneous rocks imaged in the Peejay 3D survey is very similar to igneous rocks mapped in the southwestern part of the Durroon Sub-basin, suggesting a similar shallow sill complex is present in this area.

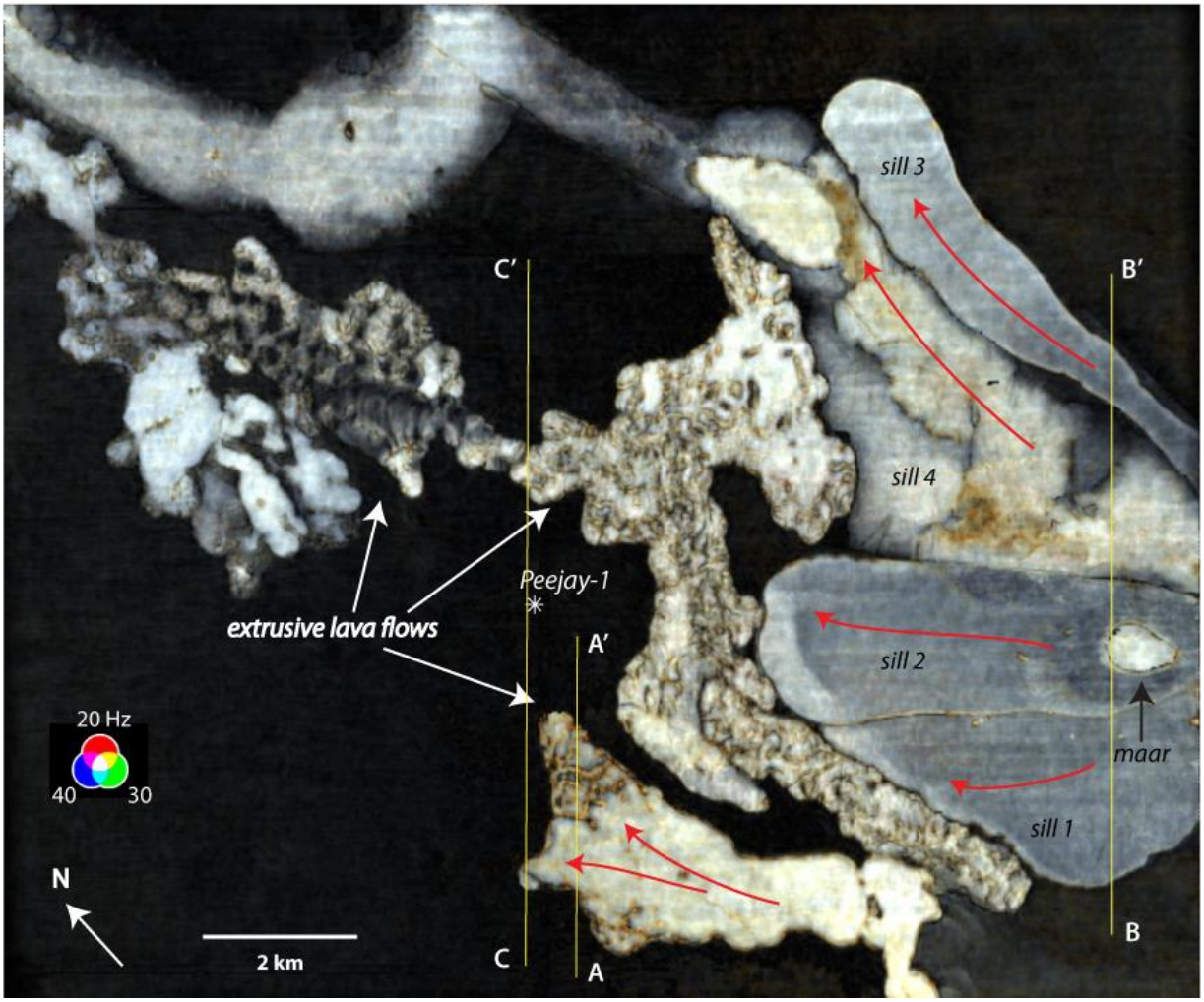

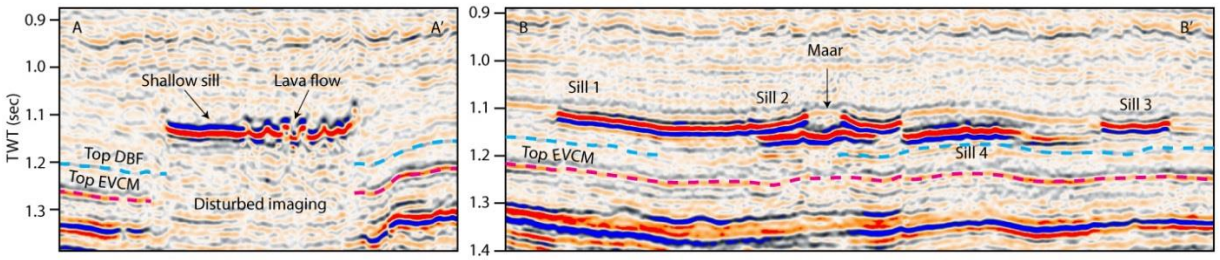

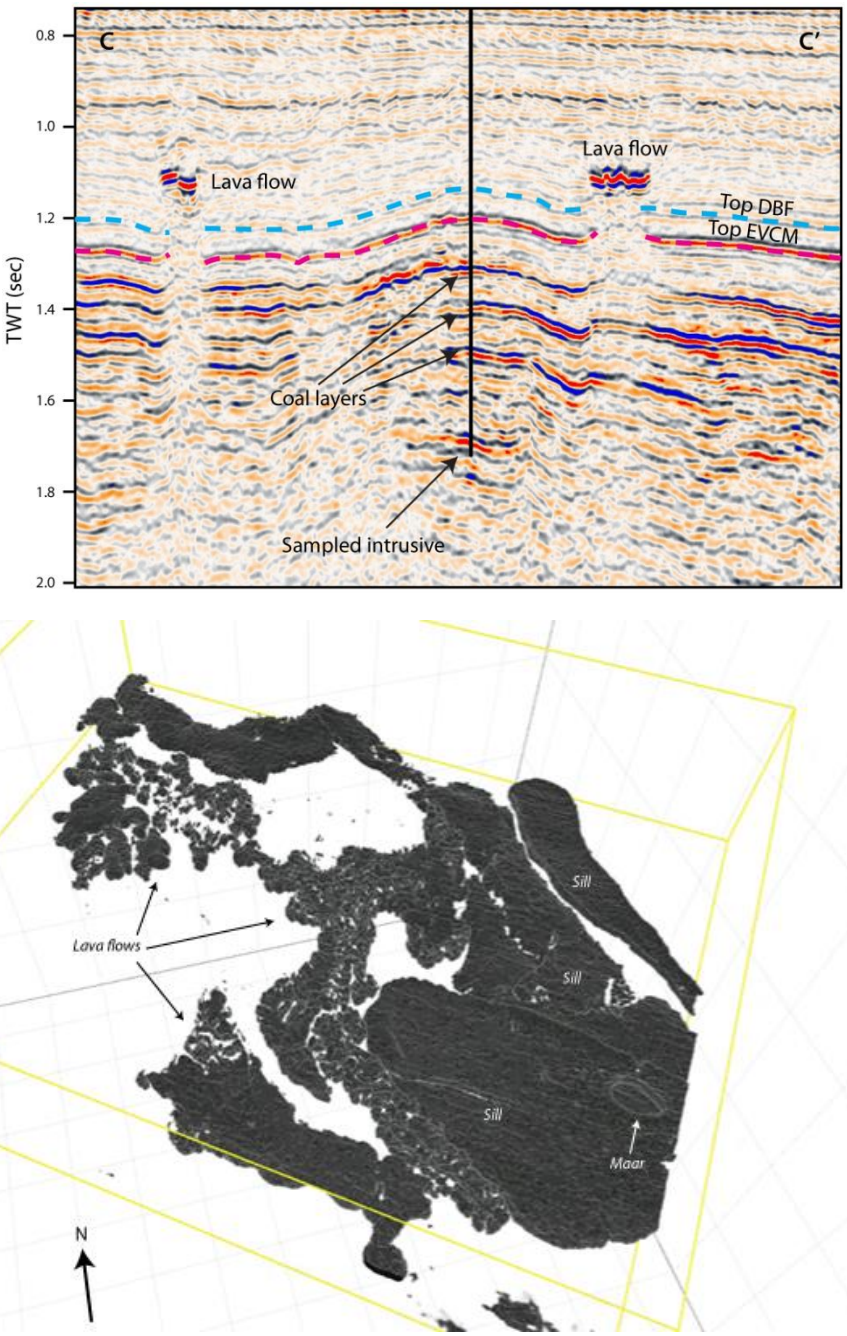

Figure 9: RGB blend of frequency decomposition map (R: 20 Hz, G: 30 Hz, B: 40 Hz) with direction of flow (red arrows) and location of cross sections A-A' and B-B' (top) and opacity rendered 3D view (bottom) of igneous rocks found in the Peejay3D survey, illustrating the shallow nature of the sills complex.

4.2 Geochemistry

Table 1 (Appendix D) shows major and trace element analyses of newly acquired samples (FM) combined with analyses conducted by Geoscience Australia (GA) and analyses found in well completion reports (WCR). Due to the varying weathered state of the samples,

a Nb/Y – Zr/Ti plot (Pearce, 1996) is used as Zr/Ti remains constant and Nb/Y increases only slightly during weathering (Nesbitt and Wilson, 1992) (Figure 10). This plot shows that igneous samples mainly fall within the alkali basalt field, with some occurrences in the basalt to basaltic andesite and trachyandesite field. Due to high SiO_2 content (> 80 wt%) samples from well Silvereye-1 have been excluded from any interpretations.

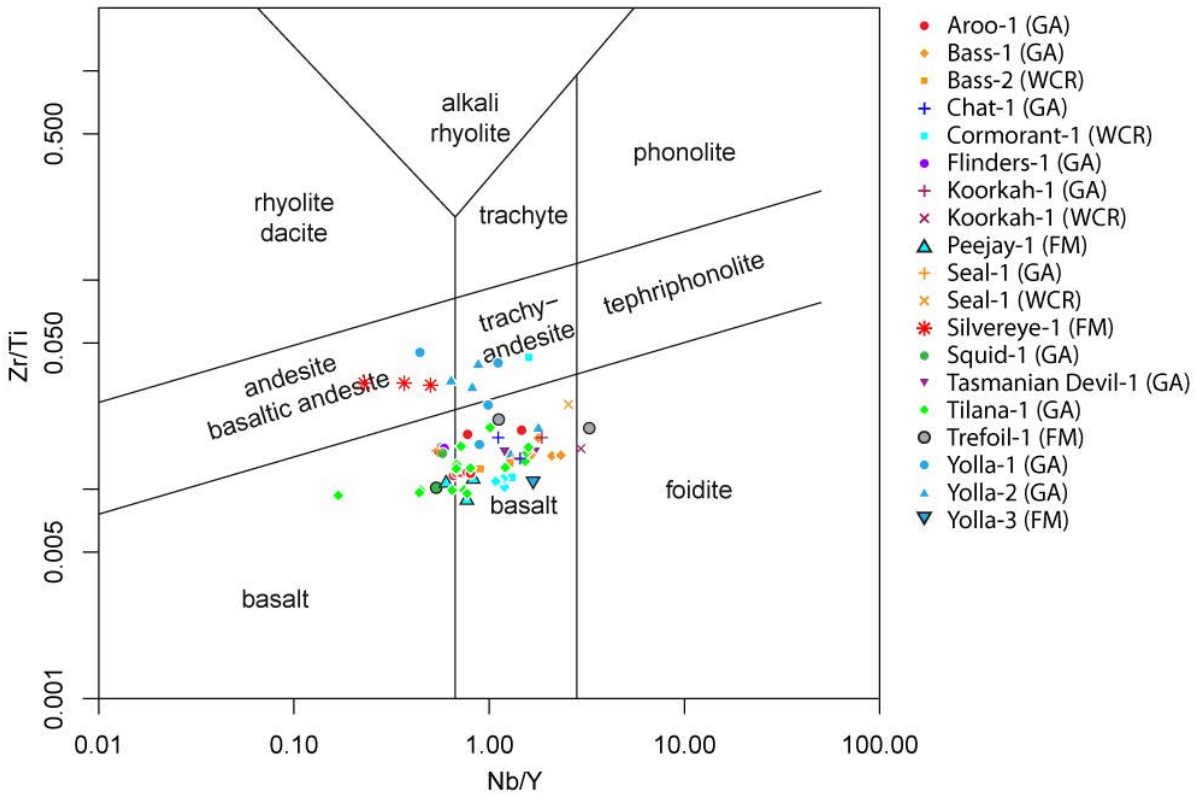

Figure 10: Nb/Y versus Zr/Ti plot of analysed samples for this study (FM) and previously analysed samples by Geoscience Australia (GA) and found in well completion reports (WCR).

Mantle-normalized incompatible element diagrams show large variability between samples (Figure 11). Due to the weathered state of the samples, mobile elements such as Cs, Rb, Ba, K, Pb and Sr have been removed from incompatible element diagrams to facilitate interpretation (Figure 11 C-D). Generally, samples show an Oceanic Island Basalt (OIB) signature, with some samples displaying an enrichment in heavy rare earth elements (HREE) (Figure 11 A, C and E). Samples from wells Yolla-1, Yolla-2, Yolla-3 and Silvereye-1 (> 80 wt% SiO_2) show a very distinct Upper Continental Crust (UCC) signature (Figure 11 B, D and F). This difference in trace element signature does not show any temporal variation.

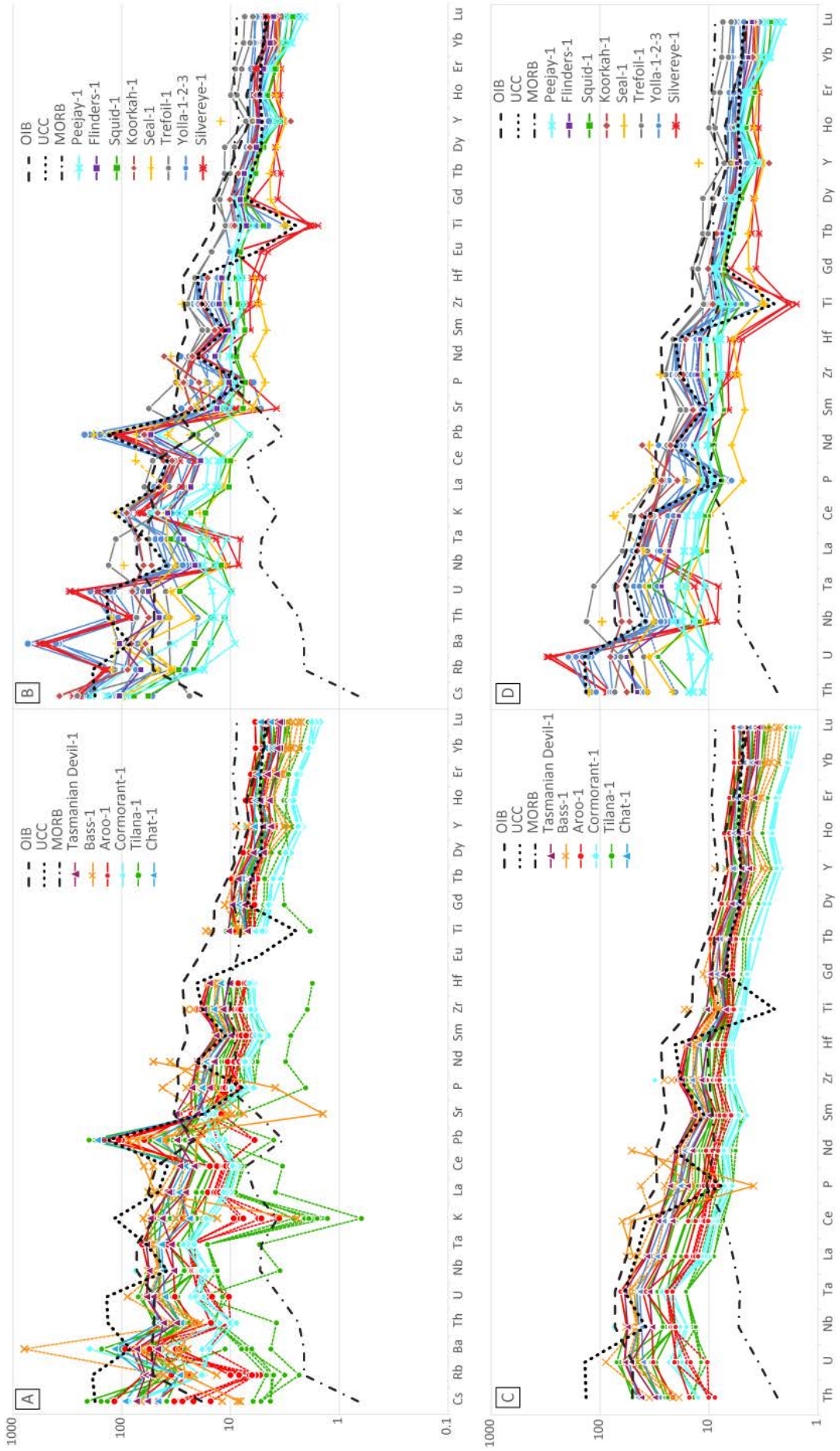
A
B
C
D
OIB
UCC
MORB
Tasmanian Devil-1
Bass-1
Aroo-1
Cormorant-1
Tilana-1
Chat-1
Peejay-1
Flinders-1
Squid-1
Koorkah-1
Seal-1
Trefoil-1
Yolla-1-2-3
Silvereye-1
Cs Rb Ba Th U Nb Ta La Ce Pb Sr P Nd Sm Zr Hf Eu Ti Gd Tb Dy Y Ho Er Yb Lu
1000
100
10
1
0.1

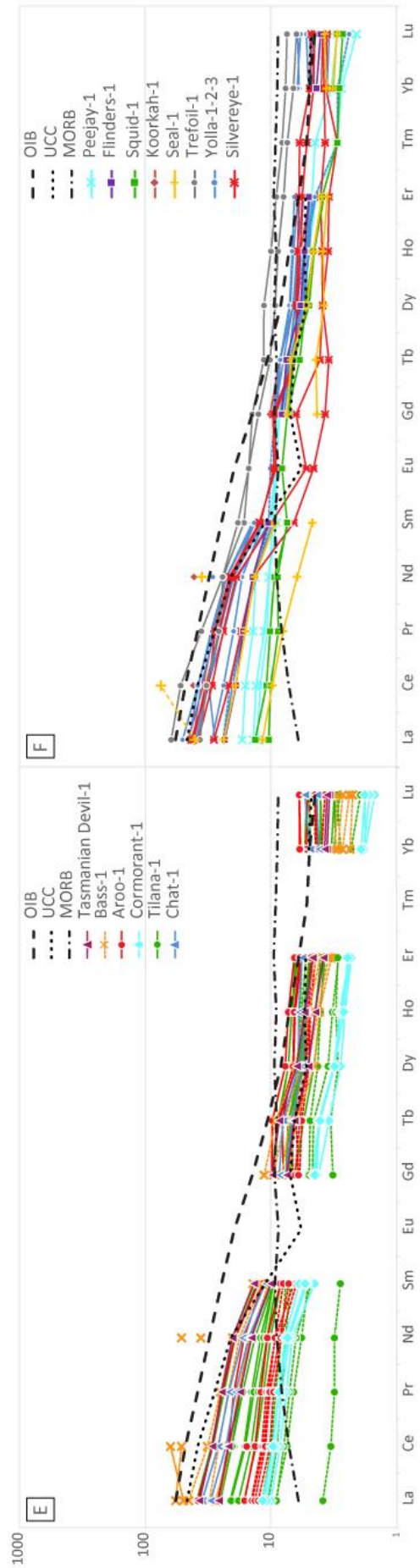

Figure 11: Primitive mantle normalized (McDonough and Sun, 1995) incompatible element diagrams with all elements (A-B) and mobile elements excluded (C-D) and primitive mantle normalized (McDonough and Sun, 1995) rare earth element diagrams (E-F) for analysed samples. Dashed lines represent samples analysed by Geoscience Australia. OIB and MORB values from Sun and McDonough (1989), UCC values from Rudnick and Gao (2003).

5. DISCUSSION

We have described a large number of igneous intrusions and extrusions of Cretaceous to Miocene age buried within the syn- and post-rift successions of the Bass Basin offshore south-eastern Australia. Findings are that Cretaceous to Eocene magmatic activity mainly occurred near major faults along the basin edges, whereas younger Miocene magmatic activity occurring in the centre of the Cape Wickham Sub-basin shows a southward younging trend similar to onshore volcanism in Eastern Australia.

5.1 Previous work on magmatic activity in the Bass Basin

Previous work by Reynolds et al. (2018b) in the Labatt 3D and Yolla 3D survey indicated the presence of volcanic vents of Miocene age which either form linear rows or occur as isolated vents. When occurring on a row, these vents onlap against each other in a northerly direction (Reynolds et al., 2018b), this would suggest a southward younging trend in agreement with the large scale younging trend observed in the Cape Wickham Sub-basin (Figure 6). Three quarters of the isolated vents are most likely fed by magma that has exploited normal faults and sills are only found beneath 8% of the isolated vents within the Labatt 3D survey (Reynolds et al., 2018b). These sills are either saucer or layer-parallel shaped with a diameter of 2 – 4 km and do not form interconnected complexes with adjacent sills. The remaining 92% of vents in the Labatt and Yolla survey do not show evidence for the presence of sills beneath the vents (Reynolds et al., 2018b). Velayatham (2019) identified 13 dykes within the Labatt 3D survey. All of the interpreted sills here in this study are associated with dykes interpreted by Velayatham (2019) and the vents interpreted by Reynolds et al. (2018b) seem to coincide with the presence of dykes (Figure 12).

Reynolds et al. (2018b) did not observe any evidence for forced folding above the sills in the Labatt and Yolla surveys, in the Shearwater 3D survey however, we have interpreted forced folding above two sills with TV4 age. Out of the 48 igneous bodies that have an assigned age, 22 (~45.8%) fall within the TV4 age group, compared to 6 for TV3, 4 for TV2 and 9 for TV1. This could indicate more numerous magmatism during this TV4 episode.

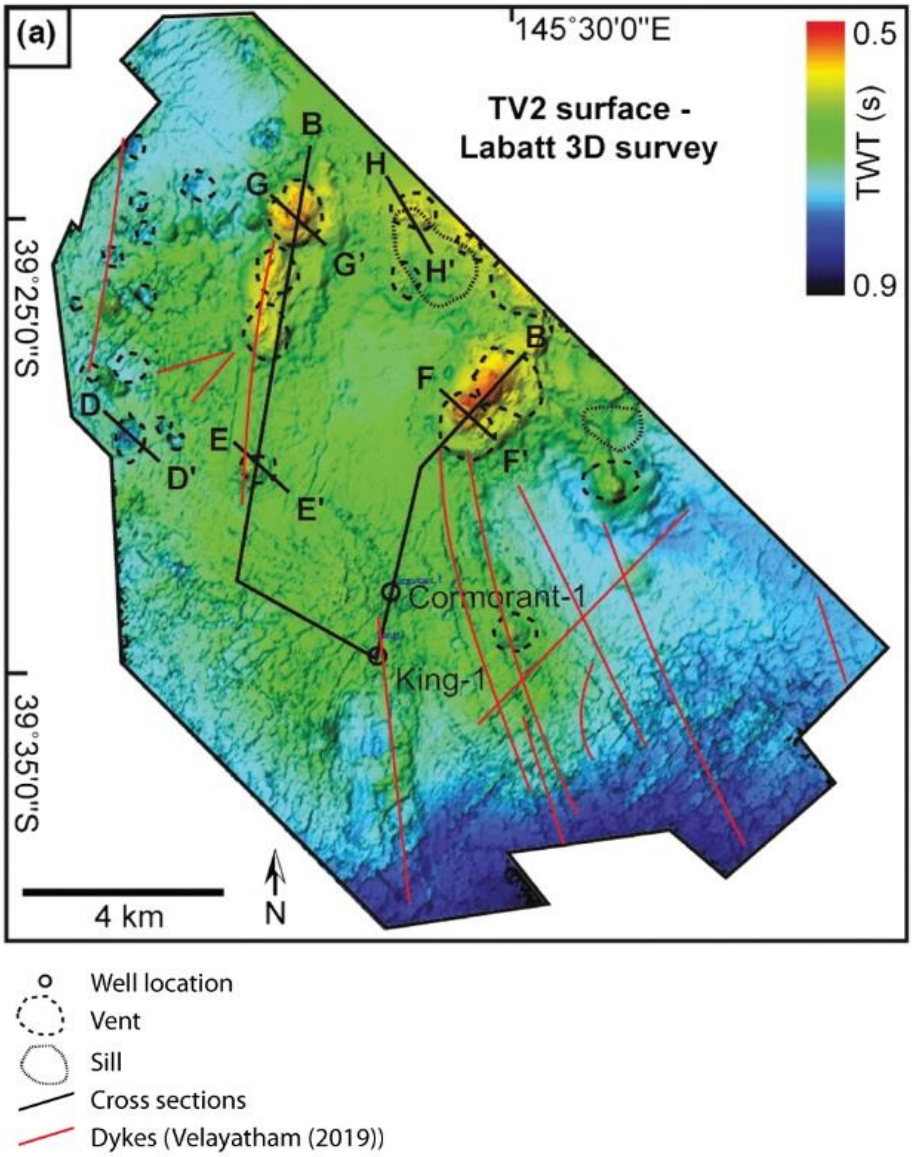

Figure 12: Overview of mapped vents on top of TV2 surface time map (from Reynolds et al. (2018b)), location of dykes (red lines) (from Velayatham (2019)) and sills mapped in this study.

5.2 Age of volcanic activity

The age progression of magmatism from the edges of basins towards their centres has been demonstrated in rift basins such as the Main Ethiopian Rift, the Baikal Rift or Chaine des Puys (Maccaferri et al., 2014 and references therein) and the nearby Gippsland Basin, where Cretaceous magmatism is mainly located near the basin bounding faults in the north and south and middle Eocene magmatism is observed in the centre near the Bream Field (Chapter 3). The southward younging trend in the centre of the Cape Wickham sub-basin however has not been observed in any of the nearby offshore basins, such as the Gippsland Basin (Chapter 3)

and the Bight Basin (Reynolds et al., 2018a). Interestingly, a similar southward younging trend is observed in the Central volcanoes and Leucitite provinces (Davies et al., 2015; Wellman and McDougall, 1974) of the Eastern Australian Volcanic Province. These southward younging trends have previously been explained by the Australian continent moving northwards over stationary hot mantle upwellings, or plumes, with activity occurring where lithospheric thicknesses are below 150 km (Davies et al., 2015). Using these hotspot trails and the age of magmatic activity, it has been derived that the Australian plate is moving northwards at a rate of 57 ± 4 km/Ma between 23 – 16 Ma (Cohen et al., 2013). Based on our rough calculations, the rate of southward younging in the centre of the Cape Wickham basin ranges between 35 – 50 km/Ma, which is slower than the quoted rate by Cohen et al. (2013). , however, due to the great uncertainty on the age of the extrusive activity using seismic data and palynology, no firm conclusion can be made. It is worth noting that the youngest igneous rocks in onshore Tasmania are located at the Nut or Circular Head, a porphyritic basaltic volcanic neck (8.5 Ma: Baillie (1986)), which is located exactly south of the mapped southward younging trend (Figure 6), so it is possible that this location forms the last representation of this hotspot trail.

5.3 Magmatic plumbing styles of the Bass Basin

The magmatic plumbing style of the Bass Basin is mainly dominated by dykes and either by large saucer-shaped sills which have caused forced-folding of overlying sediments as seen in the Shearwater 3D survey (section 4.1.1) or sills which do not exhibit any forced folding. Smaller size sills are difficult to recognize due to several facts such as anomalously low acoustic impedance contrast between igneous rocks and surrounding sedimentary sequences, and the occurrence of masking coal-layers above the igneous rocks (Watson et al., 2019). The extrusive component of igneous activity in the Bass Basin mainly consists of volcanic vents and lava flows (see section 4.1.2 for an example).

5.3.1 Comparison of magmatic styles to the neighbouring Gippsland Basin

Although adjacent to each other, the Bass and Gippsland Basin only partly share their geological history. The eastern Cape Wickham Sub-basin is geologically more closely related to the nearby Otway Basin as they have been subjected to stresses associated with the final stages of separation between Australia and Antarctica and therefore the opening of the

Southern Ocean, while the western Durroon Sub-basin is more closely related to the Gippsland Basin due to stresses associated with the break-up of eastern Gondwana and opening of the Tasman Sea (Meeuws et al., 2016). Both basins contain a mixture of both extrusive and intrusive igneous rocks, however the observed magmatic style and age are quite different, with igneous activity in the Bass Basin generally being much younger. Before comparing the magmatic plumbing styles of both basins, it should be noted that large-scale interpretations of the Gippsland Basin are possible due to the availability of the large merged 3D seismic cube (Chapter 3) which covers the main part of the Gippsland Basin. The Bass Basin however, only has a few 3D seismic surveys available with 2D seismic data filling the gaps, which hinders a full 3D understanding of possible large-scale plumbing networks in the basin.

Table 3 shows the main magmatic differences and similarities between the Bass and Gippsland Basin. Magma transport in the Bass Basin is dyke-dominated whereas faults and sills are responsible for the transport in the Gippsland Basin. Seismic data in the Bass Basin has shown that magma is mainly transported through dykes without evidence of a large interconnected sill network, which is in contrast to the Gippsland Basin, where a large sill complex spans a lateral distance of over 40 km (see Chapter 4) and is most likely responsible for magma transport in the shallow crust. The extrusive component of the magmatic activity in the Bass Basin consists of volcanic vents with occasional lava flows, however, the occurrence of lava flows might be underestimated due to the more straightforward interpretation of vents over lava flows in 2D seismic data. The Gippsland Basin however, predominantly contains lava flows and has only a single reported volcanic vent complex near the Bream Field in the centre of the basin and a Miocene volcanic vent on the south-eastern edge of the basin (Chapter 4). Though the density of sills is different, the intrusive features of both basins are quite similar, with both saucer-shaped and layer-parallel sills occurring. In addition, the Bass Basin contains several shallow sills which have caused forced folding of overlying sediments, whereas the Gippsland Basin does not show forced folding above any of its sills. Cretaceous and Cenozoic magmatic activity has been observed in both basins. Magmatic activity in the Gippsland Basin is more numerous during the Cretaceous, with 54 out of 84 wells intersecting Cretaceous extrusive rocks and minor magmatism occurring during the Eocene (near Bream Field) and Miocene (near Sailfish-1) (Chapter 4). Although Cretaceous igneous activity has been reported in the Durroon as a basalt flow intersected by the Durroon-

1 well in the Durroon Sub-basin, the location and extent is less well known in the Cape Wickham Sub-basin due to the lack of well control and poor seismic resolution at depth (Blevin, 2003). Eocene to Miocene magmatic activity is more numerous in the Cape Wickham Sub-basin, with at least 31 igneous features mapped within this period (Figure 6).

Table 3: Overview of magmatic plumbing style of the Bass Basin compared to the Gippsland Basin

	Bass Basin	Gippsland Basin
Mode of magma transport	- Dykes: many dykes have been recognized throughout the data and especially the Labatt3D survey	- Sills and faults, no dykes visible in seismic data: sills have been shown to form a large connected sill complex, travelling a lateral distance of over 40 km (see Chapter 4)
Extrusive features	- Volcanic vents with occurrences of lava flows	- Predominantly lava flows with a single Eocene volcanic vent near the Bream Field in the centre of the basin and a Miocene volcanic vent on the edge of the basin towards the southeast near well Sailfish-1
Intrusive features	- Saucer-shaped and layer-parallel sills, voluminous enough to cause forced-folding in some cases	- Saucer-shaped and layer-parallel sills, no forced-folding observed
Age of magmatic activity	- Although Cretaceous activity has been observed within the Bass Basin, magmatic activity mainly occurred during the Cenozoic.	- Predominantly Cretaceous magmatic activity with minor activity during the Eocene (Bream Field) and Miocene (Sailfish-1)

5.4 Geochemistry compared with Bass Strait Cenozoic igneous rocks

Cenozoic magmatism is widespread in the Bass Strait with occurrences in Victoria to the north (Older and Newer Volcanic Provinces), Gippsland Basin to the east and Tasmania to the south of the Bass Basin. Compared with these provinces a number of observations can be made.

Fractionation - Generally, the Bass Basin volcanics are geochemically very similar to the Gippsland Basin volcanics. Cr and Ni contents are similar for the same mg# in the two basins, indicating these magmas have undergone similar amounts of fractionation. Sc is slightly higher (30 - 20 ppm) in the Bass Basin versus (22 – 10 ppm) in the Gippsland Basin for the same mg#. Compared to the Tasmanian Cenozoic mafic rocks, Cr, Ni and Sc concentrations are similar to the concentrations found for the basalts and basaltic andesites found in Tasmania (Meeuws et al., 2019). A Sc versus mg# plot suggests that the Bass Basin samples are more defined by

fractionation, with an inflection point occurring around a mg# of 60, where olivine fractionation gets replaced by pyroxene/ilmenite fractionation (Figure 14). This is in contrast to the Tasmanian and Victorian samples, which do not show a similar inflection point, suggesting they have been dominated by olivine fractionation only.

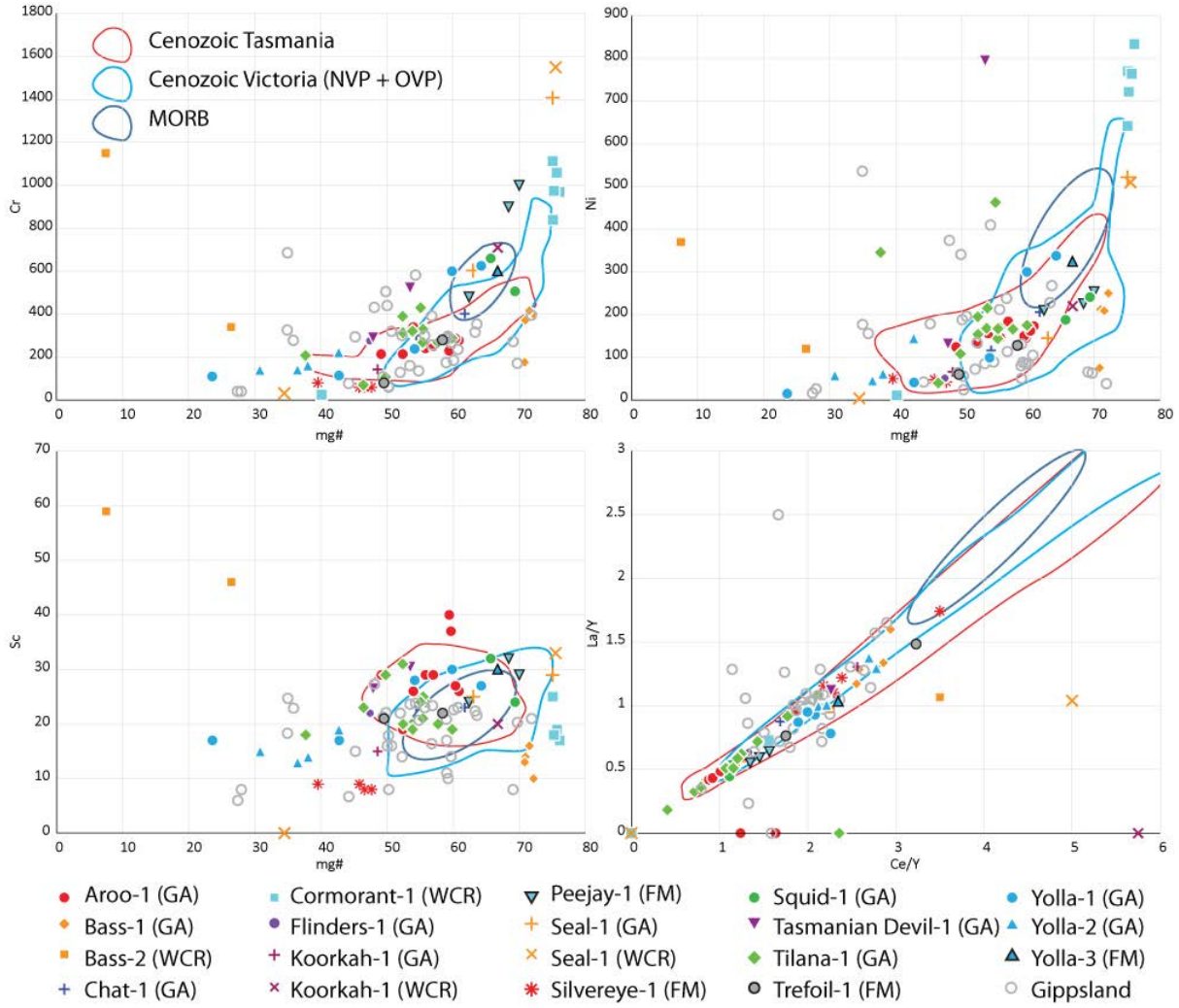

Figure 14: Cr, Ni and Sc versus mg# and La/Y versus Ce/Y for Bass Basin samples compared to Gippsland Basin (Chapter 3), Cenozoic Tasmanian (Meeuws et al., 2019) and Cenozoic Victorian (Older and Newer Volcanic Province) samples.

Partial melting - La/Y versus Ce/Y again show a similar overlap between the igneous rocks found in the Bass and Gippsland Basin, indicating similar amounts of partial melting. The Bass Basin mafics extend a little further towards higher and lower degrees of partial melting, whereas the Gippsland Basin mafics are more scattered around La/Y ~ 1 and Ce/Y ~ 1.8. Scatter of the Gippsland Basin mafics in this graph is mainly caused by the very altered Turrum-1

samples (see Chapter 4). Compared to the Tasmanian Cenozoic mafics, the Bass Basin magmas overlap the basaltic andesite and basalt range, whereas the Gippsland Basin samples fall within the basalt field (Meeuws et al., 2019). This indicates that the range of depths at which partial melting has occurred is a lot smaller and towards the shallow end of the Tasmanian magmas. In comparison, the Victorian samples, similar to the Tasmanian ones, show a much larger spread, indicating a larger range of partial melting depths than the more shallowly generated Bass and Gippsland Basin magmas.

Source enrichment – Ti versus mg# indicates a slightly higher Ti concentration and similar Zr and Nb concentrations in the Gippsland Basin samples for similar mg#. Compared to the Tasmanian Cenozoic mafics, the samples fall within the range of basalt and basaltic andesites (Meeuws et al., 2019). The Bass Basin and Victorian samples overlap slightly for Ti, Zr and Nb concentrations per mg#, however the Victorian samples span a much larger range towards higher concentrations for each of these elements.

The majority of the Gippsland volcanics are considerably older (Cretaceous) than the studied volcanics in the Bass Basin. The Cretaceous igneous rocks encountered in the Gippsland Basin show a clear upper continental crust (UCC) influence, in contrast to the Cenozoic Bass Basin volcanics. Younger, Eocene volcanism in the Gippsland Basin (Bream and Tuna area, Chapter 4) shows an OIB signature comparable to the Tasmanian Cenozoic basalts (Meeuws et al., 2019) and the igneous rocks observed in the Bass Basin.

5.5 Unusual silicic intrusions or effects of weathering?

Watson et al. (2019) identified an unusual zone in the upper third section of intrusions intersected by Seal-1, Toolka-1A and Flinders-1. Based on well logs, Watson et al. (2019) propose that a rise in gamma response (48-74 API) and marginally lower densities (2.62-2.72 g cm^{-3}) in wells Toolka-1A, Seal-1 and Flinders-1, are due to the occurrence of a silicic intrusion within mafic dolerite intrusions. Watson et al. (2019) used major element geochemistry from Seal-1 as evidence for their conclusion, however, weathering may have greatly affected major element concentrations and may have artificially raised SiO_2 and $Na_2O + K_2O$ contents, which would explain the increase in gamma ray response. Trace element plots such as Nb/Y versus Zr/Ti (Pearce, 1996) are more reliable in these cases and show that the Seal-1 sample plots

within the alkali basalt field. Additionally, increased neutron porosities at the level of the proposed silicic intrusion indicate that the weathering might be more likely than the presence of silicic rocks as these generally have low neutron porosities, while weathered basalts would show higher neutron porosity values due to the presence of H_2O.

6. CONCLUSIONS

This study of seven 3D and numerous 2D seismic reflection datasets has shown that the Cape Wickham Sub-basin of the Bass Basin hosts a large number of igneous features of Late Cretaceous to Cenozoic age, consisting mainly of basalts and dolerites with varying degrees of alteration. Peaks in magmatic activity are observed in the Paleocene syn-rift and Oligocene-Miocene post-rift successions. Here we have mapped 58 intrusions and 41 extrusions which mainly consist of volcanic cones and few lava flows. Intrusions are mainly saucer-shaped or layer-parallel and can be voluminous enough to cause folding of overlying sediments as has been demonstrated in the Shearwater3D survey. Seismic interpretation has demonstrated that magma is transported through dykes to form sills and volcanic vents in the Cape Wickham Sub-basin. This is in contrast to the neighbouring Gippsland Basin, which contains a large network of interconnected sills allowing magma to travel from the centre of the basin towards the basin edges. Magmatism in the Cape Wickham Sub-basin is not synchronous and at least 10 episodes of magmatic activity, ranging from Cretaceous to Middle Miocene, have been identified. Within the Cape Wickham Sub-basin, two age trends can be observed in magmatic activity, with older episodes focussing near basin edges and southward younging magmatism occurring in the centre. The observed southward younging trend of magmatism is in concordance with southward magmatic younging trends observed on the Australian mainland and seamount chains offshore eastern Australia.

Major and trace element geochemical analysis of igneous samples generally shows an Oceanic Island Basalt signature with samples from the Yolla wells trending towards an Upper Continental Crust signature. Bass Basin and Gippsland Basin igneous rocks are geochemically very similar and have formed under similar shallow partial melting conditions and underwent similar amounts of fractionation. Compared to Cenozoic igneous rocks in onshore Tasmania and Victoria, the offshore Bass and Gippsland Basin have formed at shallower depths and are

comparable to the basalts and basaltic andesites found in onshore Tasmania and Victoria. Although the Bass and Gippsland Basin igneous rocks show similar trace element signatures to the Cenozoic basalts and basaltic andesite groups found onshore Tasmania and Victoria (Older and Newer Volcanic Provinces), Sr-Nd-Pb isotope analyses should be conducted to further constrain similarities or differences of magmatic sources of these provinces.

ACKNOWLEDGEMENTS

This research forms part of a PhD project supported by the ASEG Research Foundation (RF14P05) and Australian Government Research Training Program Scholarship for which funding is greatly acknowledged. Geoscience Australia is thanked for providing the three dimensional seismic data and geochemical data. IHS are thanked for access to seismic interpretation software The Kingdom Suite. Foster-Findlay Associates' is thanked for the use of the GeoTeric software.

REFERENCES

Baillie, P.W., 1986. Radiometric ages for Circular Head and the Green Hills basalt, north-western Tasmania, Tasmania Department of Mines.

Baillie, P.W., Bacon, C.A., 1988. Integrated sedimentological analysis: the Eocene of the Bass Basin. APEA Journal, 29(1): 312-327.

Ball, P., Eagles, G., Ebinger, C., McClay, K., Totterdell, J., 2013. The spatial and temporal evolution of strain during the separation of Australia and Antarctica. Geochemistry, Geophysics, Geosystems, 14(8): 2771-2799.

Blevin, J.E., 2003. Petroleum geology of the Bass Basin, interpretation report, an output of the Western Tasmanian Regional Minerals Program.

Blevin, J.E., Trigg, K.R., Partridge, E.D., Boreham, C.J., Lang, S.C., 2005. Tectonostratigraphy and potential source rocks of the Bass Basin. APPEA Journal, 45: 601-622.

Brincat, M.P., 1992. Seismic interpretation of structural and stratigraphy, permit T-15-P, Durroon Sub-basin, off-shore northeastern Tasmania, University of Adelaide.

Cas, R., Simpson, C., Sato, H., 1993. Newer volcanics province - processes and products of phreatomagmatic activity.

Cohen, B.E., Knesel, K.M., Vasconcelos, P.M., Schellart, W.P., 2013. Tracking the Australian plate motion through the Cenozoic: Constraints from 40Ar/39Ar geochronology. Tectonics, 32(5): 1371-1383.

Cornell, C.D., Cowan, W.C., Mosness, T.L., Rankin, J.G., Walla, R.J., 1986. Appendix 10: Petrology and Geochronology of Tilana-1. In: Tilana-1 Final Well Report, pp.267-273. Sydney.

Cummings, A.M., Hillis, R., Tingate, P.R., 2004. New perspectives on the structural evolution of the Bass Basin: implications for petroleum prospectivity. In: Boult, P.J., Johns, D.R., Lang, S.C. (Editors), Eastern Australasian Basins Symposium II, 19-22nd November 2004, Adelaide, South Australia. Petroleum Exploration Society of Australia, pp. 133-149.

Cummings, A.M., Hillis, R.R., Tingate, P.R., 2002. Structural evolution and thermal maturation modelling of the Bass Basin. APPEA Journal, 42(2): 175-191.

Davies, D.R., Rawlinson, N., Iaffaldano, G., Campbell, I.H., 2015. Lithospheric controls on magma composition along Earth/'s longest continental hotspot track. Nature, 525(7570): 511-514.

Everard, J.E., 2014. Geological evolution of Tasmania / editors, Keith D. Corbett, Patrick G. Quilty, Clive R. Calver ; designer/compiler, June Pongratz. Special publication (Geological Society of Australia) ; 24. 0072-1085. Geological Society of Australia (Tasmanian Division), Sydney, NSW.

Faustmann, C., 1995. The seismic expression of volcanism in the Bass Basin referring to western Victorian analogues, University of Adelaide, unpublished.

Holford, S.P., Schofield, N., Macdonald, J.D., Duddy, I.R., Green, P.F., 2012. Seismic analysis of igneous systems in sedimentary basins and their impacts on hydrocarbon prospectivity: examples from the southern Australian margin. APPEA Journal, 52: 229-252.

Holford, S.P., Schofield, N., Reynolds, P., 2017. Subsurface fluid flow focused by buried volcanoes in sedimentary basins: Evidence from 3D seismic data, Bass Basin, offshore southeastern Australia. Interpretation, 5(3): SK39-SK50.

Johnson, R.W. (Ed.), 1989. Intraplate volcanism in eastern Australia and New Zealand. Intraplate volcanism in eastern Australia and New Zealand. Cambridge University Press, in association with Australian Academy of Science.

Lennon, R.G., Suttill, R.J., Guthrie, D.A., Waldron, A.R., 1999. The renewed search for oil and gas in the Bass Basin: Results of Yolla-2 and White Ibis-1. The APPEA Journal, 39: 248-262.

Maccaferri, F., Rivalta, E., Keir, D., Acocella, V., 2014. Off-rift volcanism in rift zones determined by crustal unloading. Nature Geoscience, 7: 297.

McDonough, W.F., Sun, S.S., 1995. Composition of the Earth. Chemical Geology, 120: 223-253.

Meeuws, F.J.E., Foden, J.D., Holford, S.P., Forster, M.A., 2019. Geochemical constraints on Cenozoic intraplate magmatism and their relation to Jurassic dolerites in Tasmania, using Sr-Nd-Pb isotopes. Chemical Geology, 506: 225-273.

Meeuws, F.J.E., Holford, S.P., Foden, J.D., Schofield, N., 2016. Distribution, chronology and causes of Cretaceous – Cenozoic magmatism along the magma-poor rifted southern Australian margin: Links between mantle melting and basin formation. Marine and Petroleum Geology, 73: 271-298.

Nesbitt, H.W., Wilson, R.E., 1992. Recent chemical weathering of basalts. American Journal of Science, 292(10): 740-777.

Norvick, M.S., 2005. Plate tectonic reconstructions of Australia's southern margins.

Norvick, M.S., Smith, M.A., 2001. Mapping the plate tectonic reconstruction of southern and southeastern Australia and implications for petroleum systems. The APPEA Journal, 41: 15-35.

Pearce, J.A., 1996. A user's guide to basalt discrimination diagrams. In: Wyman, D.A. (Ed.), Trace Element Geochemistry of Volcanic Rocks: Applications for Massive Sulphide Exploration. . Geological Association of Canada, pp. 79–113.

Planke, S. et al., 2017. Igneous seismic geomorphology of buried lava fields and coastal escarpments on the Vøring volcanic rifted margin. Interpretation, 5(3): SK161-SK177.

Planke, S., Symonds, P.A., Alvestad, E., Skogseid, J., 2000. Seismic volcanostratigraphy of large-volume basaltic extrusive complexes on rifted margins. Journal of Geophysical Research-Solid Earth, 105(B8): 19335-19351.

Rateau, R., Schofield, N., Smith, M., 2013. The potential role of igneous intrusions on hydrocarbon migration, West of Shetland. Petroleum Geoscience, 19(3): 259-272.

Reynolds, P., Holford, S., Schofield, N., Ross, A., 2017. The shallow depth emplacement of mafic intrusions on a magma-poor rifted margin: An example from the Bight Basin, southern Australia. Marine and Petroleum Geology, 88: 605-616.

Reynolds, P., Holford, S., Schofield, N., Ross, A., 2018a. The importance of subsurface lithology in controlling magma storage v. eruption: an example from offshore southern Australia. Journal of the Geological Society.

Reynolds, P., Schofield, N., Brown, R.J., Holford, S.P., 2018b. The architecture of submarine monogenetic volcanoes – insights from 3D seismic data. Basin Research, 30: 437-451.

Rudnick, R.L., Gao, S., 2003. Vol. 3: The Crust, 3.01 - The composition of the continental crust. . In: Holland, H.D., Turekian, K.K. (Eds.), Treatise on geochemistry. Elsevier-Pergamon, Oxford, pp. 1-64.

Sayers, J., Symonds, P.A., Direen, N.O., Bernardel, G., 2001. Nature of continent-ocean transition on the non volcanic rifted margin of the central Great Australian Bight. In: Wilson, R.C.L., Whitmarsh, R.B., Taylor, B., Froitzheim, N. (Eds.), Non-volcanic rifting of oceanic margins; a comparison of evidence from land and sea. Geological Society of London, pp. 51-76.

Schofield, N. et al., 2012. Seismic imaging of 'broken bridges': linking seismic to outcrop-scale investigations of intrusive magma lobes. Journal of the Geological Society, 169(4): 421-426.

Schofield, N. et al., 2015. Regional magma plumbing and emplacement mechanisms of the Faroe-Shetland Sill Complex: implications for magma transport and petroleum systems within sedimentary basins. Basin Research: n/a-n/a.

Schutter, S., 2003. Hydrocarbon occurrence and exploration in and around igneous rocks. In: Petford, N., McCaffrey, K. (Eds.), Hydrocarbons in crystalline rocks. Geological Society London, London, pp. 7-33.

Smallwood, J.R., Maresh, J., 2002. The properties, morphology and distribution of igneous sills: modelling, borehole data and 3D seismic from the Faroe-Shetland area. North Atlantic Igneous Province: Stratigraphy, Tectonic, Volcanic and Magmatic Processes, 197: 271-306.

Sun, S.-s., McDonough, W.F., 1989. Chemical and isotopic systematics of oceanic basalts: implications for mantle composition and processes. Geological Society, London, Special Publications, 42(1): 313-345.

Sutherland, F.L., Forsyth, S.M., Zwingmann, H., 2002. Bassian basalts: dating, Cenozoic biogeohistory and a new model for Tasmanian volcanism. Geological Society of Australia Abstracts, 67(251).

Sutherland, F.L., Hendry, D.F., Barron, B.J., Matthews, W.L., Hollis, J.D., 1996. An unusual Tasmanian tertiary basalt sequence, near boat Harbour, northwest Tasmania. Records of the Australian Museum, 48(2): 131-162.

Sutherland, F.L., Wellman, P., 1986. Potassium-argon ages of Tertiary volcanics rocks, Tasmania. Papers and proceedings of the Royal Society of Tasmania, 120: 77-86.

Suttill, R.J., 1995. Palaeogeographic study of the Paleocene and Early Eocene sequences of the Eastern View Coal Measures in T/23P.

Teasdale, J., 2004. Southern Australian Margin SEEBASE® Compilation, April 2004, Geoscience Australia, Canberra.

Velayatham, T., 2019. Subsurface fluid flow in Australian sedimentary basins, The University of Adelaide, unpublished.

Watson, D., Holford, S., Schofield, N., Mark, N., 2019. Failure to predict igneous rocks encountered during exploration of sedimentary basins: A case study of the Bass Basin, Southeastern Australia. Marine and Petroleum Geology, 99: 526-547.

Wellman, P., McDougall, I., 1974. Cainozoic igneous activity in eastern australia. Tectonophysics, 23(1–2): 49-65.

Wheeler, B.F., Kjellgren, G.M., 1986. Yolla-1 Final Well Report (Amoco Australia Petroleum Company (unpubl.).

Williamson, P.E. et al., 1985. Pre-Eocene stratigraphy, structure, and petroleum potential of the Bass Basin. APEA Journal, 25(1): 362-81.

Chapter 6

Thesis conclusions

CONCLUSIONS

This thesis examines the temporal and spatial distribution of Cenozoic magmatism along the south-eastern Australian margin, with focus on Tasmania and the Bass and Gippsland Basins. This is achieved through detailed mapping of 3D and 2D seismic reflection data and major and trace element and isotope geochemistry on available rock samples onshore Tasmania, and from wells in the Bass and Gippsland Basins. Within this thesis, several research aims/objectives have been investigated:

1. Accurately constrain the distribution and chronology of Cenozoic intraplate magmatism in the Bass and Gippsland Basins.
2. Determine the nature of subvolcanic 'plumbing systems' and provide insights into the modes of Cenozoic magma transport through sedimentary basins in south-eastern Australia.
3. Explain the geodynamic origins of anomalous Cenozoic intraplate magmatism in south-eastern Australia at basin-to-mantle scales.

Both the Bass and Gippsland Basin host a voluminous record of mafic magmatic activity of Late Cretaceous to Miocene age in their syn- and post-rift sedimentary successions. Despite only being separated by the Bassian Rise, these basins only share part of the tectonic evolution and therefore the distribution and chronology of igneous events differs significantly. Within the Gippsland Basin, magmatism mainly occurred in several phases ranging from the Late Cretaceous (Campanian) to Middle Eocene, with the most abundant activity occurring during the Late Cretaceous. Through detailed mapping of available 3D seismic reflection datasets, we have shown that in the upper crust, magma travelled from the centre of the Gippsland Basin (Central Deep) towards the basin-bounding major faults in the north (Rosedale Fault System) and south (Darriman Fault System). This magma travelled through an extensive interconnected network of sills, spanning over 40 km laterally and several kilometres vertically, to finally extrude onto the paleo-surface as lava flows near the basin edges. This network has been established over several magmatic pulses starting from the Campanian to the Middle Eocene, with extrusive activity and fractionation progressing from east to west along the northern Rosedale fault. Subsequent magmatism is represented by a Middle Eocene volcanic

cone complex, located in the Central Deep near the Bream Field. In contrast to the Late Cretaceous magmatism, these volcanic cones are fed by underlying intrusions and vertical to near-vertical faults or dykes. A small area in the south-east of the basin, near the Sailfish-1 well, hosts several pyroclastic cones of Miocene age. Based on the age and location of this magmatic activity, it is more likely to be related to the Tasmanian Cenozoic magmatism. The Bass Basin on the other hand hosts a large number of igneous rocks with ages ranging from the Cretaceous to the Miocene, with the magmatic activity mainly occurring during the Miocene. Cretaceous to Eocene magmatic activity is mainly focussed at major faults near the basin edges. In contrast to the Gippsland Basin, no lateral network of sills has been observed and magma transport through the upper crust inhibits a more vertical nature through vertical to near-vertical dykes and faults. Miocene magmatic activity is constrained to the centre of the Cape Wickham Sub-basin and is expressed as volcanic cones and few sills. This phase of magmatic activity shows a remarkable age trend, with younger, Miocene, magmatic activity trending towards the south. This trend is in concordance to magmatic activity observed on the Australian mainland and seamount chains offshore eastern Australia. Figure 1 illustrates an overview of the distribution and timing of magmatism in the researched areas.

Cenozoic magmatism in Tasmania has a complex origin, with igneous compositions spanning a wide range from highly silica-undersaturated olivine melilitites and nephelinites to basanites, ne-hawaiites, olivine basalts and quartz-tholeiites. Major and trace element and isotope geochemistry has shown that this wide range of compositions is controlled by variable degrees of melting during decompression melting of a peridotite source and contamination by a residual source responsible for the Jurassic dolerites. More specifically, a thermal upwelling with a HIMU signature traversed a Pacific MORB-like asthenosphere and released small degree melts generated within the garnet-lherzolite stability field, and interacted with the mantle lithosphere. Further lithospheric heating caused low degree melts to rapidly rise to the surface producing alkaline melts with Oceanic Island Basalt (OIB) trace element signatures. Higher degree melts were created by more extensive heating and were mixed with remnants of a source responsible for the Jurassic dolerites where it was still residing in the lithosphere. This mixing component can be recognized in the Upper Continental Crust (UCC) signature observed in trace element patterns. Major and trace element and isotope

geochemistry of the limited Cretaceous magmatism in Tasmania shows intermediate compositions and isotope ratios in between those of the Jurassic and Cenozoic igneous rocks.

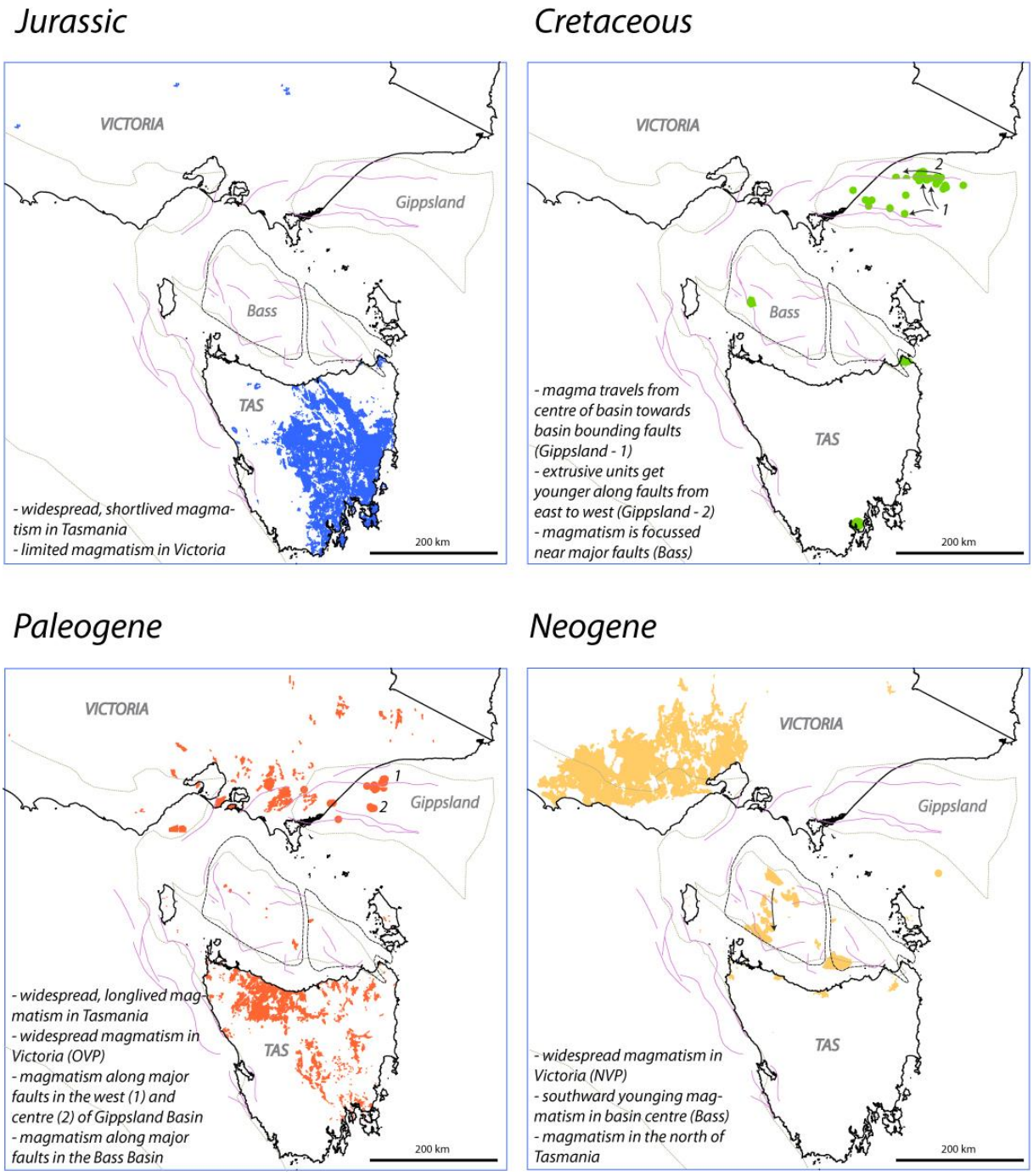

Figure 1: Overview of the distribution and timing of magmatism in Tasmania, the Gippsland and Bass Basins and Victoria.

Major and trace element geochemistry of Bass and Gippsland Basin igneous rocks have shown that compositions fall within the alkali basalt to basalt field. Cretaceous to Eocene sampled lavas occurring along the northern Rosedale Fault system in the Gippsland Basin show a UCC trace element signature similar to the silica-oversaturated samples from Tasmania. Middle Eocene intrusions and extrusions sampled in the centre of the Gippsland Basin (near the Bream Field) exhibit an OIB trace element signature, similar to the silica-undersaturated igneous rocks of Tasmania. The igneous rocks sampled in the Bass Basin show a similar OIB trace element signature, with the exception of the igneous rocks sampled by Yolla-1, Yolla-2 and Yolla-3. Major and trace element geochemistry indicate that the Bass and Gippsland Basin melts have been formed at similar shallow depths and similarly high degrees of melting as the basalt and basaltic andesite groups of the Tasmanian Cenozoic igneous rocks.

Future directions

Due to the weathered state and minimal sample size of the igneous samples recovered by petroleum wells in the Bass and Gippsland, no isotope geochemistry has been attempted, however, to fully unravel the geochemical signature of the offshore igneous rocks, isotope geochemistry is necessary. Sr, Nd and Pb isotope geochemistry will allow to better constrain the differences and or similarities with the Jurassic, Cretaceous and Cenozoic magmatism observed onshore in Tasmania and Victoria. It would be interesting to test if the offshore samples which show an UCC trace element signature show Sr and Nd isotope ratios trending towards those of the Tasmanian Jurassic dolerites and if there is a HIMU component present in the samples with an OIB trace element signature. To achieve this, targeted drilling and coring of igneous rocks is necessary to provide good samples. Igneous rocks are often deemed not interesting by petroleum companies and are therefore often skipped during coring and wireline logging, even though the analyses of igneous rocks present can provide better insights in the history of the basin, and allow for more accurate thermal and subsidence models. This is especially the case where intrusions are present as it is often quite difficult to determine the timing of intrusion using seismic data alone.

Increased knowledge of the timing of magmatic activity is also crucial to better understand the offshore magmatism. Although some absolute ages have been obtained previously, the weathered state of the offshore samples hinders the absolute dating of the offshore igneous rocks as weathering of feldspars to sericite will provide an age that is younger than the crystallisation age of the igneous rocks (Verati and Jourdan, 2013). Pyroxene is generally more resistant to weathering and may be a better candidate to provide with absolute ages of intrusive events in the offshore basins (Ware and Jourdan, 2018). This will allow to better understand the signatures observed in the trace element data.

The seismic reflection surveys used in these studies are of varying quality and improved data quality can improve the interpretation of igneous rocks in sedimentary basins. Re-processing of older seismic surveys can already have a significant effect on data quality and therefore identification of igneous rocks. We have shown that the use of spectral decomposition images can aid the identification of igneous rocks in amongst other high amplitude reflections. Further development of similar frequency decomposition techniques will provide us with much more information of already available datasets.

References

Verati, C., Jourdan, F., 2013. Modelling effect of sericitization of plagioclase on the 40K/40Ar and 40Ar/39Ar chronometers: implication for dating basaltic rocks and mineral deposits. Geological Society, London, Special Publications, 378.

Ware, B., Jourdan, F., 2018. 40Ar/39Ar geochronology of terrestrial pyroxene. Geochimica Et Cosmochimica Acta, 230: 112-136.